Development of sustained and tunable release of antiretrovirals with polymeric prodrugs synthesized *via* RAFT polymerization

Shin-Tian (Peter) Chien

A dissertation submitted in partial fulfillment of the
Requirements for the degree of

Doctor of Philosophy

University of Washington

2025

Reading Committee:

Kim A. Woodrow, Chair
Ayokunle Olanrewaju
James Lai

Program Authorized to Offer Degree:

Bioengineering

University of Washington

Abstract

Development of sustained and tunable release of antiretrovirals with polymeric prodrugs synthesized *via* RAFT polymerization

Shin-Tian (Peter) Chien

Chair of the Supervisory Committee:
Kim A. Woodrow

Department of Bioengineering

Antiretroviral therapy (ART) is highly effective in treating and preventing human immunodeficiency virus (HIV), but its success relies on strict adherence to dosing regimens to suppress viral replication. Long-acting formulations (LAFs) address this challenge by reducing dosing frequency. However, the diverse physicochemical properties of antiretrovirals make some drugs incompatible with traditional diffusion- and dissolution-based delivery systems. To overcome the limitations associated with the physical properties of individual antiretrovirals that prevent sustained delivery, we propose the chemical modification of drugs to obtain prodrug monomers, and the subsequent reversible addition-fragmentation chain-transfer (RAFT) polymerization of said prodrug monomers to obtain "drugamers". Drugamers have been demonstrated to have an extended duration of action when subcutaneously injected to obtain an *in situ* forming depot. Despite their promise, the broader applicability of this approach to other antiretrovirals with varying properties has not been fully investigated. Here, we synthesized raltegravir (RAL) and atazanavir (ATV) polymeric prodrugs, or drugamers, to evaluate their potential for sustained release. Drugamers were dissolved in dimethylsulfoxide (DMSO) and

subcutaneously injected as *in-situ* forming implants in murine models. The release profile was tunable by adjusting the hydrophilicity by modification of the polymer composition with distinct comonomers. Furthermore, co-injections of different copolymers of RAL drugamers could achieve summations of release profiles of individual RAL drugamers to sustain the release of RAL for 42 days, which is the longest duration that has been reported. RAL drugamers were well-tolerated and are excreted renally after drug release without the need for surgical removal. This study demonstrates the versatility of RAFT polymeric prodrugs for the sustained delivery of hydrophilic drugs, highlighting the tunability and broad applicability of the drugamer platform to improve adherence to antiretroviral regimen.

TABLE OF CONTENTS

TABLE OF FIGURES

LIST OF SCHEMES

LIST OF TABLES

ACKNOWLEDGEMENTS

First and foremost, I would like to thank my advisor and mentor, Dr. Kim A. Woodrow. Kim, thank you for giving me the opportunity to work in the Woodrow Lab on such a unique project while simultaneously allowing me the freedom to explore my scientific questions. I am a better writer and communicator today because you mentored me. Beyond the scientific mentoring, I sincerely appreciate you teaching me that there is life outside of science and helping me become the man I am today.

I would like to thank all the members of my committee: Dr. Patrick S. Stayton, Dr. James Lai, Dr. Ayokunle Olanrewaju, and Dr. Rodney JY Ho. Thank you all for all the advice and feedback on my project; I appreciate all the insight you all have given me. Pat, I thoroughly enjoyed working with you and appreciate all the chemistry and PK discussions we had. Thank you also for teaching me to handle criticism with grace. James, thank you for always reminding me to focus on the scientific method; the advice has shaped how I tackle and communicate my research. Furthermore, thank you for believing in that 22-year-old Taiwanese kid with the American Dream, as I would not be at UW had I not met you in 2017. Ayo, I truly appreciate you going out of your way to get to know me and always treating me with such warmth. Rodney, it is such an honor to have worked with you and I appreciated your invaluable insight on long-acting HIV formulations.

I would also like to thank Dr. Ian T. Suydam for all the guidance you gave me throughout my project. Ian, it was so much fun working with you and developing the chemistry with you. Your ability to parse out my ideas even in their fuzzy stages, as well as teaching in general, is unparalleled.

I would like to thank NIH/NIAID (R01AI145483 and R01AI150325) for providing the grants to Kim to support my work. In addition, I would like to thank the Ministry of Education of

my home country of Taiwan for awarding me Government Scholarship to Study Abroad (教育部留學獎學金).

Thank you to all past and present members of the Woodrow Lab; my work would not be possible had it not been for the scientists who paved the way first. Thank you, Hannah F., Rachel, Jae, Hannah V., and Jamie, for being my mentors when I joined the lab. Jamie, thank you especially for teaching me all I know today about animal work. I will never forget you recruiting Meilyn to help train me on handling mice for tail pricks; it no longer takes me half an hour to sample 3 μL of blood. Thank you, Hannah V., My-Anh, Ioana, Duru, Joyce, Vivi, Teri, and Emily for being my peers and, most of all, my friends throughout this journey. Thanks for all the science and life discussions we've had in N507. Hannah, it's amazing to see how much you've excelled since our first meeting during the UW campus visit in the winter of 2018. Ioana, your hardworking personality always inspires me (sweaty palm high-five). Duru, thank you for giving me the opportunity to mentor you and all the fun conversations we've had on history, philosophy, and sports. Joyce, thank you for being a source of encouragement, especially in these past months for my job search.

To the UW Bioengineering community, thank you for your support and friendship. Thank you to the Stayton Lab, especially Roy, Selvi, and Takuma, for the opportunity to work with such talented scientists. Thank you to the members of the Pun Lab that worked in MolES, especially Ben, Alex P., and Trey, who I can bounce ideas off or just have good conversations. Thank you, Cara, Kerry, and Kevin, for the friendship and the fun times. Thank you, Phuong, Ayumi, Alex N., and My-Anh (tree stump gang), for all the fun we've had since we started the PhD journey together. Ayumi, your warmth and kindness are unlike any other, and I hope to visit you and Kyler in San Diego soon. My-Anh, I am so fortunate to have worked with you and learned

analytical skills from you. More importantly, I am blessed to have experienced your selflessness and friendship.

Thank you to the friends who were my family away from home during this journey. Thank you, Bobo, Caroline, Johnny, Patrick, Yvonne, Morgan, Larissa, and Neil, for your wonderful company in Seattle. Thank you, Avery, Meaghan, and Ginger, for being my roommates and family and for all the weekends we spent cooking. Thank you, Jason and John, for the support from the East Coast and the Christmas miracles we strangely have year-round. Thank you, Phil and Albert, for being my close friends since sixth grade and continuing to encourage me to this day. 亮国 and Mars, 很開心有你們兩個好朋友，天神見! 正皓，感謝你當年陪我一起來西雅圖念研究所，我會懷念之前室友的時期，以及哲鋼社的笑話。

爸爸媽媽，感謝你們把我和我兄弟帶到大時讓我們出國，也是透過你們不斷的支持，才會有我現在所有的經歷。Adam, thanks for being the older brother I've always admired. Sid, it's always a joy seeing you become so independent and capable. I am fortunate to have the support my family gives me.

Now, onto the next chapter.

Chapter 1. SUMMARY AND SPECIFIC AIMS

Combination antiretroviral therapy (cART) significantly prolongs the lifespan of those who are living with HIV/AIDS by reducing HIV-related morbidity and mortality[1]. However, the rigid drug regimen for daily oral medication can lead to poor adherence in certain populations as low as 16.4%[2]. Poor adherence to antiretrovirals is now the main barrier to successful therapy[3,4]. Pre-exposure prophylaxis (PrEP) is also highly dependent on drug adherence to be effective, as one study demonstrated PrEP effectiveness increased from 58.0% to 83.5% when adherence rate increased from 75% to 97.5%[5]. Poor adherence to antiretroviral (ARV) therapy may result in insufficient plasma or intracellular concentrations of ARV and result in failure in suppressing viral replication[6]. While adherence has been correlated with decreased HIV infection, existing practices measuring adherence rely on subjective metrics, such as self-reported adherence[7]. To this end, many groups have developed improved models to identify the critical drug levels required to inhibit HIV, as well as developing real-time assays to determine drug levels as opposed to [7–9]. Major reasons for nonadherence include lack of education on HIV, access to cART, and stigma associated with HIV[10]. Not all factors of nonadherence apply to all populations and reasons for nonadherence requires a more nuanced understanding of users of ARVs, but less frequent dosing of ARVs can potentially improve patient outcome. These challenges in drug adherence have led to increased interest in long-acting formulations for preventing or treating HIV.

Several drug delivery systems (DDS) have been developed for long-acting or sustained delivery for PrEP or treatment[11,12]. For example, dapivirine vaginal rings (DVR) is a silicone ring that sustains the release of dapivirine, a non-nucleoside reverse transcriptase inhibitor (NNRTI), locally in the vagina, and protects users for one month[13]. However, DVR is

restricted to usage in women only, which excludes approximately 47% of HIV patients worldwide in 2022[14]. In addition, studies have shown users removing the vaginal ring during menses, as well as not being significantly more effective than oral PrEP, which makes it less effective than other long-acting modalities[15,16]. Nanosuspensions of solid drug nanocrystals have been developed for intramuscular injectables with cabotegravir (CAB-LA) and rilpivirine (RPV-LA) that can be dosed every 1 or 2 months[17,18]. Compared to their daily oral antiretrovirals, long-acting injectables (LAI) of cabotegravir have demonstrated 66-89% decreased HIV infection rate in clinical studies, demonstrating improved outcome of users with LAI[19,20]. More recently, twice-yearly injections of LA lenacapavir developed by Gilead were proven to be 100% effective in a phase 3 clinical trial as HIV PrEP [21].

Although the US FDA has approved CAB-LA, RPV-LA, and subcutaneous lenacapavir as LA products, there are still several shortcomings (highlighted in Table 1.1). One such shortcoming includes high volumes required for dosage (3 mL)[22]. The volume of dosage prevents administration as a subcutaneous injection (max recommended volume is 1.5 mL), which is the less painful route when compared to intramuscular[23]. Furthermore, the long PK tail of cabotegravir has also suggested potential integrase inhibitor resistance due to long-term exposure[24]. Despite the significantly extended duration of action, subcutaneous injections of lenacapavir require oral lead-in with different dosages for the initial 14 days to reach therapeutic concentrations[25]. Lastly, long-acting cabotegravir/rilpivirine and lenacapavir are formulations that depend on the low aqueous solubility of the antiretroviral, and thus are not compatible with more hydrophilic antiretrovirals[26,27]. In a review on LA delivery of ARVs, the recommended log P of suitable ARVs for LA delivery was 2-5, which precludesss approximately 15/31 of the current FDA approved ARVs[26]. Alternative strategies to sustain the delivery of hydrophilic

ARVs can expand the "toolbox" to prevent or treat HIV infection. Thus, these limitations associated with DVR, CAB-LA, RPV-LA, and LA-lenacapavir necessitate new DDS that address the various needs of patients with HIV. Moreover, alternative formulations can potentially allow for sustained delivery of more hydrophilic ARVs with approved safety profiles. Beyond working with drugs with known safety profiles, the repurposing of old drugs for long-acting release can save up to 300 million USD of investment in development of new drugs[28]. Therefore, it can be beneficial to explore alternative long-acting formulation strategies from an economic and patient outcome standpoint.

Table 1. 1. Limitations of Current Long-acting Modalities

Long-acting Modality	***Dosing Frequency***	***Limitations***
Dapivirine Vaginal Ring	4 weeks	• Restricted to usage in biological females[29] • Nonadherence during menses[15,16] • Not more effective than daily oral PrEP in HIV prevention[15]
Long-acting Intramuscular Cabotegravir/Rilpivirine	1-2 months	• High volume of injection (3 mL) [22] • Formulation currently not compatible with more hydrophilic ARVs [26,27] • Development of drug resistance from PK tail [30]
Long-acting Subcutaneous Lenacapavir	6 months	• Require oral lead-in to reach therapeutic concentration[25] • Formulation currently not compatible with other ARVs [26,27]

Effort has been made in the lab to develop DDS that sustain release of a combination of ARVs with mixed results, with different shortcomings for each DDS. The Woodrow Lab

investigated sustained delivery with a combination shown to have high synergy in inhibiting viral replication in DDS for sustained delivery[31]. In this combination, Raltegravir (RAL) was especially intriguing due to the high penetration in the female genital tract and male seminal compartment[32,33]. The potential of RAL to be used in PrEP alone or in combination with lamivudine has been investigated in a clinical trial due to the high penetration in vaginal and gut tissue[34]. The Woodrow Lab has attempted to formulate nanosuspensions of solid RAL nanocrystals, but failed to sustain release for more than 14 days. In addition, we have fabricated several PLGA implants wherein the release of drugs was driven by the slow diffusion of drug across PLGA. One such implant include the solvent-cast poly(lactic-*co*-glycolic acid) (PLGA) films loaded with RAL, which sustained release of RAL for 37 days, but required a long lead-in period of 28 days[35]. RAL-loaded PLGA electrospun fiber mats achieved sustained release for 37 days, but they failed to address the issue of delayed release, despite the increased total surface area relative to solvent-cast films. The DDS designed by the lab relied on diffusion- or dissolution-based drug release mechanisms and ultimately demonstrated incompatibility with antiretrovirals with insufficient hydrophobicity, such as RAL, to achieve sustained release (shown in **Fig 2.2**)[36].

Thus, we propose the development of polymeric prodrugs synthesized by reversible addition-fragmentation chain transfer (RAFT) polymerization as an alternative method to achieve sustained release of antiretrovirals. RAFT polymerization enables the synthesis of polymers with well-defined architecture and low molar mass dispersity[37]. Polymeric prodrugs that sustain release can also be synthesized by RAFT polymerization, as Ho *et al.* have demonstrated sustained delivery of tenofovir alafenamide (TAF) for 60 days with TAF "drugamers"[38]. RAFT polymeric prodrugs were coined "drugamers" due to the conversion of

drug into polymerizable prodrug monomers, wherein the drug itself becomes the drug delivery material after polymerization of the monomers. Following the successful synthesis of drugamers, we propose to formulate drugamer solutions in biocompatible organic solutions. When drugamer solutions are subcutaneously injected, drugamers will undergo a phase inversion due to the drugamer's inherent insolubility in water, and form a depot at the injection site *in situ*[39]. The translatability of the drugamer platform as *in situ* forming implants (ISFIs) has not been fully investigated. We envision the development of ARV polymeric prodrugs that sustain release for timescales of weeks to months. Release of ARVs can be tuned by adjusting the polymer comonomer compositions of the drugamer, which controls the degree of water penetration in drugamer depots when subcutaneously injected.

The goal of this proposed thesis work is to develop RAFT polymeric prodrugs for subcutaneous injectable *in situ* forming depots to achieve sustained release of antiretrovirals. Research for the thesis will investigate the following:

1.1. AIM 1: To investigate the synthesis of drugamers by RAFT polymerization with high drug loading and for sustained delivery of ARVs.

Polymeric prodrugs synthesized by RAFT polymerization will be developed for sustained release of ARVs. ARVs with free hydroxyl groups will be conjugated to a methacrylate promoiety by a cleavable ester linkage to obtain monomers for RAFT polymerization. Drugamers with different comonomer compositions will be synthesized for potential sustained delivery of ARVs. Discussion of current data for aim 1 can be found in Chapter 3. The investigation of the synthesis of drugamers will be conducted with the following subaims:

Subaim 1.1: Synthesize prodrug monomers of Raltegravir and Atazanavir

Synthesis of ARV prodrug monomers will be conducted by a series of coupling routes to obtain a cleavable ester linkage. Specifically, coupling routes utilizing uronium reagent, carbodiimide, and acyl chlorides will be attempted to couple the hydroxyl groups of drugs to methacrylate promoieties to obtain polymerizable prodrug monomers. Characterization of the synthesized monomers will be performed with a series of instrumental analyses to confirm successful synthesis.

Subaim 1.2: Obtain ARV homopolymer drugamers via *RAFT polymerization.*

RAFT polymerization will be conducted on synthesized prodrug monomers to obtain well-defined drugamers. RAFT polymerization will be initially carried out with just the prodrug monomer itself to assess the polymerizability of prodrug monomers. RAFT polymerization conditions will be selected based on what is available in the literature and consulting collaborating scientists (Stayton Lab). Drugamers may also be polymerized with a rhodamine monomer (methacryloxyethyl thiocarboamoyl rhodamine B, RhMA) with a target degree of polymerization of 1, or theoretically, one RhMA per polymer chain. Successful polymerization will be assessed by a series of proton nuclear magnetic resonance (^{1}H-NMR) to determine the conversion, molecular weight, and drug loading.

Subaim 1.3: Modification of polymer comonomer composition to obtain RAL and ATV copolymer drugamers.

Comonomer composition of drugamers will be adjusted by copolymerizing the prodrug monomers with other comonomers. Specifically, prodrug monomers will be copolymerized with 2-(methylthio)ethyl methacrylate and/or butyl methacrylate by random copolymerization to control the hydrophilicity of the drugamer. Like the homopolymers synthesized in subaim 1.2, ^{1}H-NMR experiments will assess the conversion, molecular weight, drug loading, and final comonomer ratio.

Subaim 1.4: In vitro assessment of RAL drugamers of different physical properties due to different comonomer compositions.

For a given ARV, a series of drugamers with different comonomer compositions will be analyzed with *in vitro* experiments to compare differing physical properties. Precipitation of drugamers will be used to assess hydrophilicity and depot-forming ability of drugamers. Precipitation behavior will be utilized to construct ternary plots to compare the physicochemical properties of

Innovation: Polymeric prodrugs, or drugamers, synthesized in this research are novel polydisperse molecules that can sustain release of ARVs. This aim explores synthesizing drugamers with ARVs not previously chemically modified for RAFT polymerization. This aim serves as a framework for synthesizing drugamers for sustained release of drugs with hydroxyl groups that can be utilized for conjugation. Furthermore, this aim explores the tunability of physical properties of drugamers by adjusting the polymer comonomer composition.

Impact: Drugamers provide a method to sustain the release of RAL, ATV, and potentially other ARVs with functional groups that can be chemically modified to obtain a prodrug monomer. Drugamers serve as a DDS capable of sustained release of ARVs for timescales of months, which can offer protection from HIV.

1.2. AIM 2: To measure the pharmacokinectics and safety of single subcutaneous injection of *in-situ* forming implants of RAL and ATV drugamers

Pharmacokinetic curves of subcutaneous injections of RAL and ATV drugamers will be established to evaluate sustained release of such ARVs. RAL and ATV homopolymer and copolymer drugamers will be subcutaneously injected either as single polymer injections or as combinations of homopolymer and copolymer drugamers. The modification of comonomer composition can tune the hydrophilicity of the drugamer polymer chains. The varying hydrophilicity of drugamers can drives differences in water penetration in the precipitated drugamer depots when administered *in vivo*. The tunability of drug release rate achieved by modification of comonomer composition in the polymer backbone will be investigated. Serum concentrations of RAL will be analyzed with LC-MS/MS. In addition to tracking serum concentration and depot quality, tolerability to drugamer depots will be determined by histology.

Subaim 2.1: Establish the pharmacokinetic profile of single subcutaneous injections of RAL and ATV drugamers.

RAL and ATV drugamers will be formulated as solutions in organic solvent (DMSO) and subcutaneously injected in the right flank of mice. Blood will be collected at certain timepoints by either tail-prick method or submental bleeds to establish the pharmacokinetic profile of homopolymer and copolymer drugamers. Serum concentration of RAL and ATV will be quantified by LC-MS/MS. Longitudinal tracking of the fluorescent depots *in vivo* using IVIS will allow for a qualitative assessment of the state of the depot. IVIS data will also elucidate the dissolution kinetics of drugamer depots. *In vivo* studies will be terminated when ARVs are no

longer detectable. Release profiles of ARVs from single injections of different drugamers will be compared using Pharmacokinetic Non-Compartmental Analysis (PKNCA) package on R-Studio.

Subaim 2.2: Assess the tolerability and safety after treatment with subcutaneous injections of antiretrovirals

After subcutaneous administration of ARV drugamers, mice weight and activity will be tracked longitudinally for the duration of the study. To characterize the local response to the implant, the injection site was excised following animal sacrifice. The injection site will be stained with hematoxylin & eosin (H&E) and Masson's Trichrome (MT) stain to investigate for lymphocyte infiltration, foreign giant cell formation, and collagen deposition.

Innovation: Subcutaneous injectables of RAL drugamers can sustain the release of RAL for weeks to a month. ISFIs of RAFT polymeric prodrugs has not been studied outside of one example with TAF, and thus the strategies utilized to tune release has not been fully demonstrated to apply to all drugs. Furthermore, previous strategies to achieve tunable release focused on linker chemistry, which is not compatible with RAL due to its unique physicochemical properties, which is further discussed in Chapter 3 and 4. This aim focused on investigating the degree of tunability in drug release afforded by the copolymerization approach.

Impact: Drugamers potentially provide sustained release of RAL with facile administration of subcutaneous injection without needing surgery to insert long-acting implants. Compared to CAB-LA and RPV-LA, injections with drugamers would require significantly smaller volumes, which would increase the acceptability of injectable treatment among people living with

HIV[40]. Extended duration of action enabled by drugamers can potentially address hurdles associated with adherence to HIV treatment and PrEP.

1.3. Aim 3: To investigate the extent of sustained release of RAL by co-injection of unique RAL drugamers

Despite the potential of RAL as an ARV for pre-exposure prophylaxis, RAL release has not been observed to be sustained above the 4 x PA-IC90 for more than 18 days, thus limiting its usage in long-acting formulations [34,41,42]. This was due to the hydrophilicity of RAL that makes drug encapsulation and sustained release difficult [43]. Due to the hydrophilicity of RAL, RAFT polymeric prodrugs (drugamers) were synthesized with high loading and demonstrated tunable release. In the effort to extend the duration of release, RAL drugamers with different release profiles will be co-injected to achieve a summation of their release. Furthermore, we will investigate the admixing different drugamers as one single formulation and its effect on RAL release. The investigation on co-injection to achieve sustained release will be achieved through the following subaims:

Subaim 3.1: Investigate the effect of subcutaneous co-injection of different RAL drugamers on the sustained release of RAL

RAL drugamers developed in Aim 1 (RAL homopolymer and the relatively hydrophilic and hydrophobic copolymer) will be formulated as separate solutions, then co-injected in mice at opposite flanks for a total of two depots. After subcutaneous injection, blood samples will be collected at certain timepoints by either tail-prick method or submental bleeds, and then analyzed

by LC-MS/MS to establish the pharmacokinetic profile. The depot dissolution kinetics will be analyzed by IVIS imaging. Tolerability to a greater injection of drug will be analyzed by longitudinal tracking of weight and histological analysis.

Subaim 3.2: Investigate the effect of co-injecting admixed formulations of different RAL drugamers on the sustained release of RAL

RAL drugamers will be admixed as one single formulation, and then injected in mice at opposite flanks for a total of two depots. Similarly to subaim 3.1, blood samples will be collected and analyzed by LC-MS/MS to establish the pharmacokinetic profile. Depot dissolution kinetics will also be monitored by IVIS imaging. The release profile will be compared to the co-injection investigated in subaim 3.1 to determine whether admixing affects depot formation, and subsequently affect the sustained release of RAL.

Innovation: This study represents the first instance of co-injection to modulate the release of ARVs from drugamer ISFIs, which is simultaneously sustains the longest duration of RAL release to our best knowledge. Furthermore, this study explores the complexity of depot formation and its effect on drug release from drugamer depots

Impact: The extended duration of sustained release with polymeric prodrugs of RAL exceeded sustained release with previous diffusion- and dissolution-based DDS previously developed by the Woodrow Lab. Polymeric prodrugs can serve as an alternative DDS to achieve sustained release with drugs that are incompatible with diffusion- and dissolution-based DDS.

Furthermore, this study demonstrates the potential for prior admixing of different drugamers and the possibility to deliver drugamer co-injections as one single injection.

Chapter 2. INTRODUCTION TO RESEARCH

2.1. ABSTRACT

Antiretroviral therapy is highly effective in suppressing viral replication of the human immunodeficiency virus, but effective therapy requires adherence to a strict drug regimen. Multiple barriers prevent the adequate adherence required to achieve viral suppression. Long-acting formulations may address the hurdles associated with the strict drug regimen of antiretroviral therapy and would be welcomed by certain populations among people living with HIV and those who take antiretrovirals for pre-exposure prophylaxis. However, not all ARVs can be formulated as long-acting formulations, particularly with diffusion- and dissolution-based drug delivery systems due to inadequate loading or rapid release. Synthesis of long-acting prodrugs may serve as an alternative method to obtain long-acting formulations that can help address the barriers to adherence. Long-acting prodrugs are an umbrella term for a variety of molecules, wherein different promoieties are selected to achieve different purposes. A variety of antiretrovirals have been synthesized as long-acting prodrugs. Polymeric antiretroviral prodrugs synthesized by RAFT polymerization are well-defined and show great promise in achieving long-acting release, with examples of drugs other than antiretrovirals.

2.2 GAPS IN TREATMENT AND PREVENTION OF HIV

2.2.1. Introduction to HIV

The human immunodeficiency virus (HIV) invades host immune cells, which leads to an immune-deficient state and ultimately demise over a period of ~2-10 years [44]. There are 39 million people globally infected with HIV in 2022, and 1.3 million people became newly infected in the last year [14]. The HIV infection pandemic is generalized in sub-Saharan

countries, particularly Swaziland, Lesotho, Botswana, and South Africa [45]. In the past decade, regions historically less affected by HIV, such as Eastern Europe and Central Asia, have also seen an increase of HIV infection incidence [46]. However, in some regions, including Zimbabwe, Malawi, and Tanzania, disease burden has decreased by measure to reduce the risk of sexually transmitted infections [45,47]. In many regions of the world, the populations most at-risk are men who have sex with men, intravenous drug users, people in prisons, sex workers and transgender people [45]. Other studies have also shown that most infections occur through heterosexual transmission, and women, particularly young women and adolescent girls (aged 15-24 years) are more at risk of HIV infection [48,49]. Given the widespread incidence of the HIV pandemic, it is urgent to develop pre-exposure prophylaxis (PrEP) that suit patients' needs and curb the spread of the disease.

HIV predominantly infects CD4+ T cells, thereby preventing the effective regulation of the immune response to pathogens [50]. This weakening of the immune system and the replication cycle of HIV has been thoroughly studied over the past four decades (**Fig 2.1**). HIV is a retrovirus and replicates by integrating its DNA into the host genome [51]. Transmission of HIV occurs through contact with infected bodily fluids with mucosal tissue, blood, or broken skin, which is usually during unprotected sexual activities [52,53]. Subsequently, the infection of host cells is initiated by the envelope glycoprotein (gp120 and gp41) of HIV binding to the target CD4 receptor [54]. After fusion with the host cell, single-strand RNA is released into the host cell cytoplasm and reverse transcribed into HIV DNA, and subsequently integrated into the host DNA [44,51]. The HIV DNA is then transcribed into viral RNA and mRNA, assembled into new virus particles that bud from the host and infect uninfected immune cells [44]. The reverse transcription of the virus DNA is also highly prone to error, resulting in the emergence of drug

resistance and immune evasion [55]. The rapid replication and recombinant nature of HIV replication make it challenging to develop diagnostic tests, biomedical prevention and treatment, and vaccines [56].

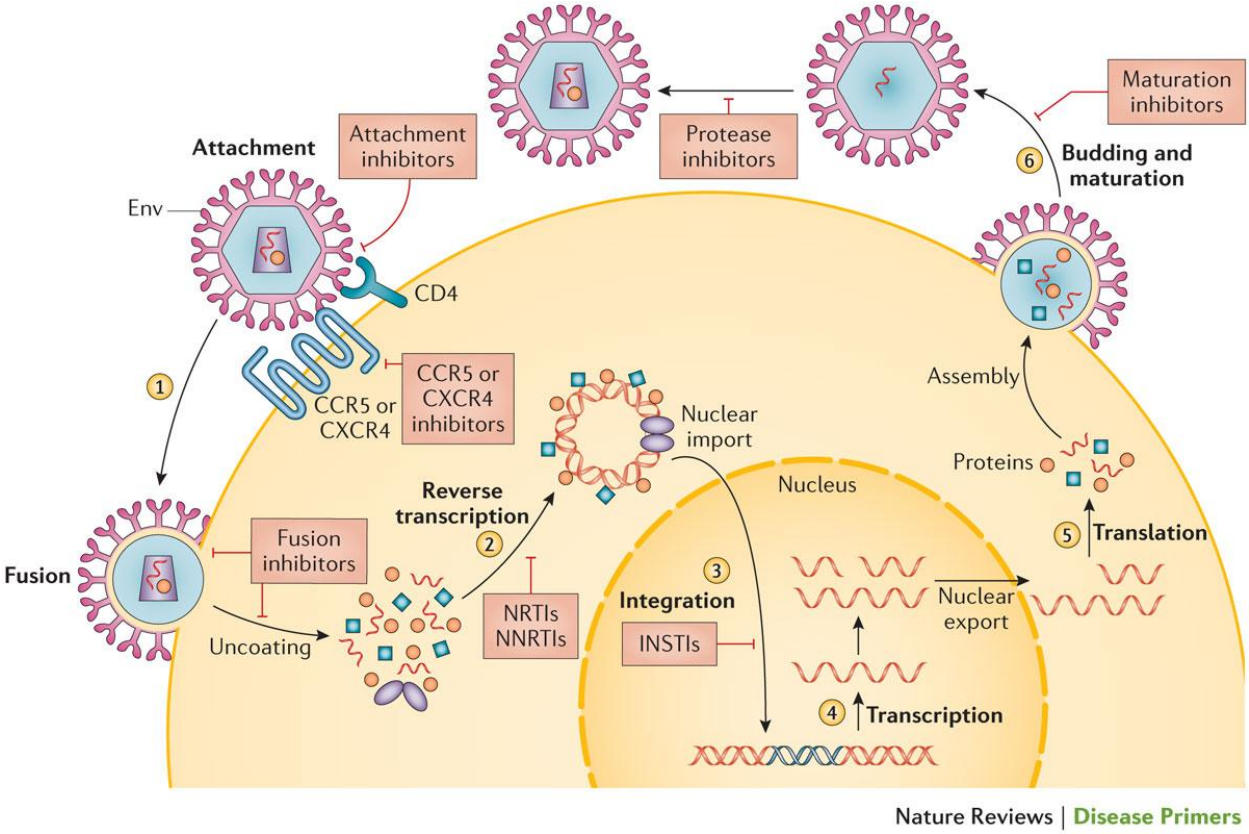

Fig 2. 1. The HIV "life cycle"

The HIV replication cycle is initiated by the virus docking onto CD4 receptor of the host cell, and the CCR5 and/or CXCR4 interacting with the envelope HIV proteins. After fusion, HIV RNA is unpacked and reverse transcribed into DNA, and subsequently integrated into the host DNA. The HIV DNA is then transcribed to mRNAs, which is then translated to synthesize viral proteins and eventually mature virions. The peach-shaded boxes indicate the step in the replication cycle inhibited by a specific class of ARVs. Figure borrowed from HIV review by Deeks *et al* [51].

2.2.2. Treatment of HIV with ARVs and associated adherence hurdles

Antiretroviral (ARV) drugs have been developed and inhibit specific steps of the viral life-cycle and have been demonstrated to suppress viral replication completely or nearly completely when drug regimen was followed [51]. As mentioned above, HIV virus can develop drug resistance to ARVs due to rapid mutation. However, this can be addressed with the co-administering of ARVs with several unique mechanisms of action, which can inhibit the replication of viruses with resistance to ARVs of one mechanism. ART also prevents transmission of HIV among people who have not yet contracted HIV [57]. However, ART is not curative, and the cessation of ART results in rapid viral rebound in a matter of weeks [58]. This is due to the fact that ART does not "eradicate" HIV, and the subset of replication-competent latent reservoirs can cause viral rebound [59,60]. ART requires high levels of adherence to the drug regimen, which would otherwise result not only in viral rebound but also resistance development, disease progression, and death [6,61].

Barriers to adherence to ART are highly multifaceted in developing and developed countries, owing to complex behavioral, cognitive, and structural barriers that prevent proper ART adherence [62,63]. Barriers can be classified as patient-related, wherein adherence to ART was affected by the patient. Examples include patients not wanting to take medication in public, forgetting to take medication at a specified time, or lack of understanding the treatment instructions [61]. Barriers can also be associated with daily schedules, wherein daily schedules of patients prevent adherence to ART. Examples include lack of access due to distance or scheduling, sleeping through dosages, or simply being too busy or distracted [61]. Overall, the most frequent reasons for nonadherence to ART are "forgetting doses" (35-52%), "being away from home" (46%), and "change in daily routine" (45%) [64].

Significant efforts have been made to address the hurdles of adherence to ART. Supportive strategies have been developed to improve adherence, such as peer support, text messaging, and counseling [65]. Therapy can enable greater engagement of patients with their ART and thus improve adherence [51]. Although these interventions demonstrated improved adherence, the rate of adherence still waned after the cessation of intervention [65]. Alternative strategies are being explored to improve adherence to ART, such as long-acting (LA) formulations to decrease the pill burden associated with ART [66]. LA strategies have demonstrated improved adherence and therapy effectiveness in the field of contraception and biophosphonate therapy, suggesting the potential of improving adherence and efficacy of ART with LA options [67]. Current LA strategies, such as long-acting cabotegravir and rilpivirine and dapivirine vaginal rings, show promise in improving adherence and reduction in clinical interventions [11,13,68]. More recently, twice-yearly injections of LA lenacapavir developed by Gilead were proven to be 100% effective in a phase 3 clinical trial as HIV PrEP [21]. Several clinical studies have demonstrated LAI to be superior to daily oral PrEP in preventing HIV infection, in particular decreasing the risk of HIV acquisition by 66% [69,70]. Another clinical study demonstrated an 88% lower risk of HIV infection when LA cabotegravir was used in place of oral tenofovir disoproxil fumarate plus emtricitabine [71]. In addition to the improved patient outcome of LA formulations delivering ARVs, providing LA treatment options allows patients to select treatment options that best suit their respective lifestyles.

2.2.3. Attitudes towards long-acting injectables of ARVs

Patient acceptance of LA formulations is critical for the success of the technology and patient perspective is useful for future directions in development. Certain groups of individuals are receptive towards LA injectables (LAI) as ART, in particular young people and individuals

struggling with adherence [40]. Some individuals even noted that once-a-week shots were greatly superior to daily pills in maintaining adherence [40]. In some populations, LAI also are preferable compared to oral ARV. For example, in a group of men who have sex with men in China, the number of men who would probably be or are willing to use LAI-PrEP is 40.74% greater than the number of men who would probably be or are willing to use oral PrEP [72]. Preference for LAI can also increase as patients use it for longer as it is integrated in their daily lives[73]. Key factors in acceptance of LAI are efficacy and side effects [40]. Therefore, as long as long-acting formulations are demonstrated to be just as effective as oral drugs and have minimal side effects, patients will be willing to try LA formulations. The expansion of LAI for patients to select from can promote usage to treat or prevent HIV infection and can decrease the incidence of infection.

2.2.4. Diffusion and dissolution-based DDS and their limitations

LA delivery can be achieved with diffusion- and dissolution-based DDS to release drugs, wherein release is usually driven by diffusion across a polymer matrix or membrane [74,75]. Most designs of LA formulations are dissolution-based, biodegradable or non-biodegradable implants, or hydrogels [75]. Examples of successful diffusion-based DDS include drug encapsulation into polylactide-co-glycolide (PLGA)/polylactic acid (PLA) based microspheres in formulations for octreotide acetate (Sandostatin® LAR, Novartis) and leuprolide acetate (Lupron®, Takeda) to achieve dosing frequencies of 4-12 weeks [76]. Other examples of commercialized diffusion-based implants are nonbiodegradable ethylene vinyl acetate (EVA) copolymer implants that release loaded etonogestrel for up to three years (Nexplanon, Merck) [77,78]. Despite the achievement of long-acting release of other drugs, ARVs have relatively lower potency, and thus usually require a significantly greater release rate that is not yet

achievable by diffusion and dissolution-based implants [79]. Nevertheless, there have been significant efforts to sustain the release of ARVs in the treatment and prevention of HIV infections with diffusion- and dissolution-based implants and injections that have extended the duration of action. One example of diffusion-based nonbiodegradable implants loaded with drugs is dapivirine encapsulated in a silicone elastomer, wherein drug is released by diffusion across the elastomer [80]. Examples of dissolution-based DDS include nanosuspensions of nanocrystals. Cabotegravir and rilpivirine have also been successfully formulated as nanosuspensions for LA delivery to treat and prevent HIV [18,81]. Biodegradable, subdermal polymeric implants loaded with islatravir also extended release of ARVs for up to 12 weeks. Significant progress have also been made in the preclinical development of ARV implants [82]. Other LA-DDS delivering ARVs in preclinical development include nonbioerodable silicone tube implants loaded with nevirapine, refillable nonpolymer nanochannel delivery implant loaded with tenofovir alafenamide and emtricitabine, biodegradable matrix implants loaded with islatravir [83–85]. Despite the success of some diffusion- and dissolution-based DDS in delivering ARVs, the physicochemical properties and potency make many ARVs incompatible with such DDS.

These approaches are most successful for hydrophobic and insoluble drugs where high drug loading and slow dissolution from the hydrophobic matrix drives extended duration of action [86]. In contrast, hydrophilic drugs typically have low drug loading and rapid dissolution from these same DDS [43,76]. Even when ARVs are not highly hydrophilic, release from hydrophobic carriers may not be sustained. For example, ARVs like bictegravir (log P=1.45) were loaded in PLGA nanoparticles, but the release was sustained for approximately 20 days above the 4 x PA-IC90 (protein adjusted-90% inhibitory concentration), which is a significantly

shorter duration compared with state-of-the-art ARV LA formulations[87–89]. Furthermore, although some drugs that can be formulated as nanocrystals, finely dispersed particles can eventually aggregate and settle over time during storage [90]. Various classes of ARVs with different physicochemical properties were developed to suppress HIV, and not all are inherently suitable for diffusion- and dissolution-based DDS [91,92]. In particular, many nucleoside reverse transcriptase inhibitors and some integrase inhibitors and protease inhibitors are relatively hydrophilic.

Efforts have been made by the Woodrow Lab to develop diffusion- and dissolution-based DDS to sustain the release of ARVs. The Woodrow Lab has attempted to formulate nanosuspensions of solid RAL nanocrystals with a top-down approach. These RAL nanocrystals achieved rapid onset at high concentrations, however, they failed to sustain release for more than 14 days. In addition, solvent-cast poly(lactic-*co*-glycolic acid) (PLGA) films loaded with RAL sustained release of RAL for 37 days, but only after a lag period of 28 days [93]. Electrospun fiber implants were thought to address the issue with drug release lag due to the greater surface area [94]. RAL-loaded PLGA electrospun fiber mats achieved sustained release for 37 days but failed to address the issue of delayed release, despite the increased total surface area relative to solvent-cast films. The release profiles ultimately do not meet the criteria of "long-acting" release in the field of HIV [11]. The DDS designed by the lab relied on diffusion- or dissolution-based drug release mechanisms and ultimately demonstrated incompatibility with antiretrovirals with insufficient hydrophobicity, such as RAL, to achieve sustained release for up to 1 month to allow for monthly administrations (**Fig 2.2**)[36]. The lack of sustained release of RAL from nanocrystals was also observed by Kovarova *et al.*, wherein plasma concentration of RAL remained above four times the protein-adjusted 90% inhibitory concentration (4 x PA-IC90) for

only 18 days [42]. Thus, alternative approaches should be explored to achieve LA formulations to treat and prevent HIV.

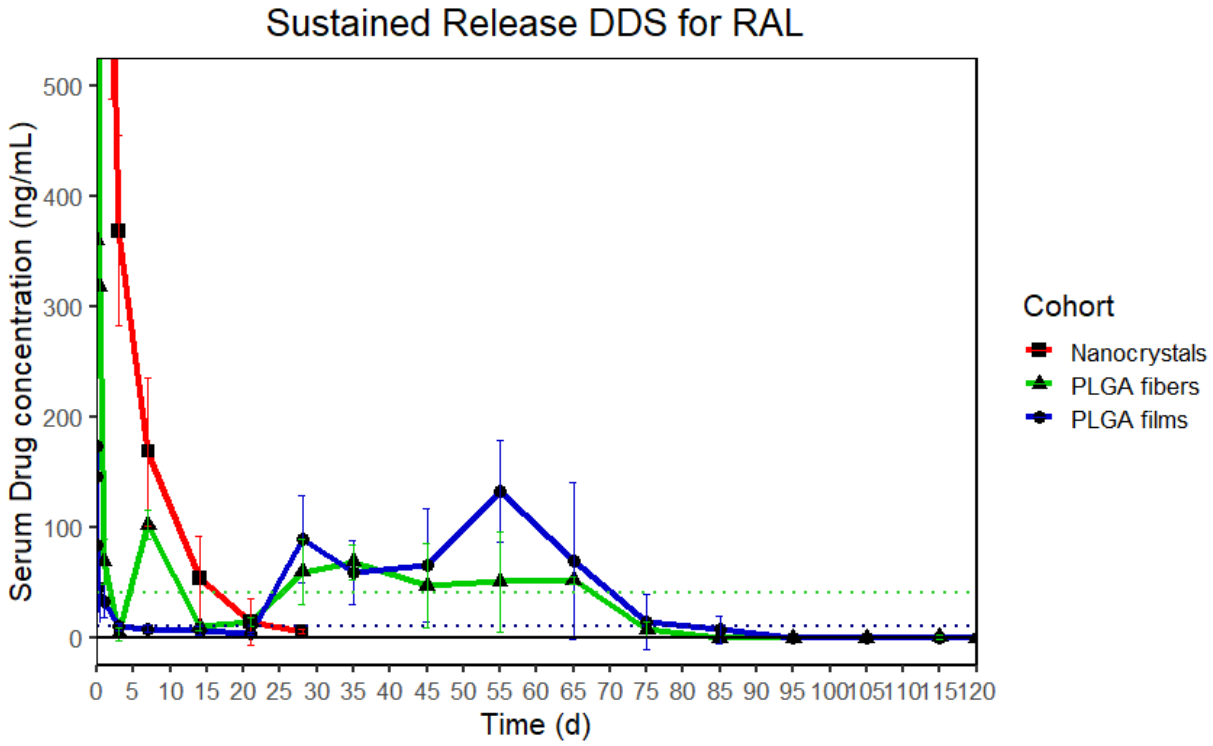

Fig 2. 2. Diffusion- and dissolution-based DDS for sustained release of RAL developed in the Woodrow Lab

The three DDS developed by the Woodrow Lab either did not sustain release for sufficiently long, or a long lag period was observed. The green dotted line indicates the target concentration (4x protein associated 90% inhibitory concentration). The blue dotted line indicates the 90% inhibitory concentration.

2.3. PRODRUGS FOR SUSTAINED DELIVERY

LA-prodrug DDS is a subcategory of LA formulation (LAF) where the prodrug design facilitates the DDS to achieve extended duration of action [36]. LA-prodrug DDS are different

from conventional prodrugs; conventional prodrugs typically described as a single molecular entity composed of the API, a promoiety of variable complexity, and a cleavable covalent linkage between the API and promoiety. Following uptake and distribution the covalent linkage is cleaved enzymatically or hydrolytically to release the API, with the timing and location of cleavage largely determined by the structure of the linkage [95]. Depending on the available functional groups for modification, a wide range of chemistries can be employed to obtain cleavable linkers such that the API can revert back to its bioactive form (**Fig 2.3**). Conventional prodrugs focus on optimizing ADME properties of APIs and are not necessarily long-acting [95]. For example, conversion of the reverse transcriptase inhibitor tenofovir into tenofovir alafenamide reversibly masks a phosphate group, resulting in significantly enhanced cell permeation that leads to higher intracellular drug concentrations [96]. Conventional prodrugs can offer prolonged duration of action since ADME properties directly impact pharmacokinetics, and can be considered "long-acting" in certain cases, such as opioid delivery, where the target dosing frequency is 72 h [97]. In contrast, for LA-prodrugs, the promoiety and linker are selected to enable a drug delivery strategy to promote the extended duration of action. The key distinction between conventional prodrugs versus LA-prodrugs is the criteria used to select promoieties and linkers. Various strategies of LA-prodrugs are discussed in the following sections; the first section (2.3.1) discusses small molecular weight (MW<1000 Da) promoieties, and the second section (2.3.2) discusses macromolecular/polymeric promoieties.

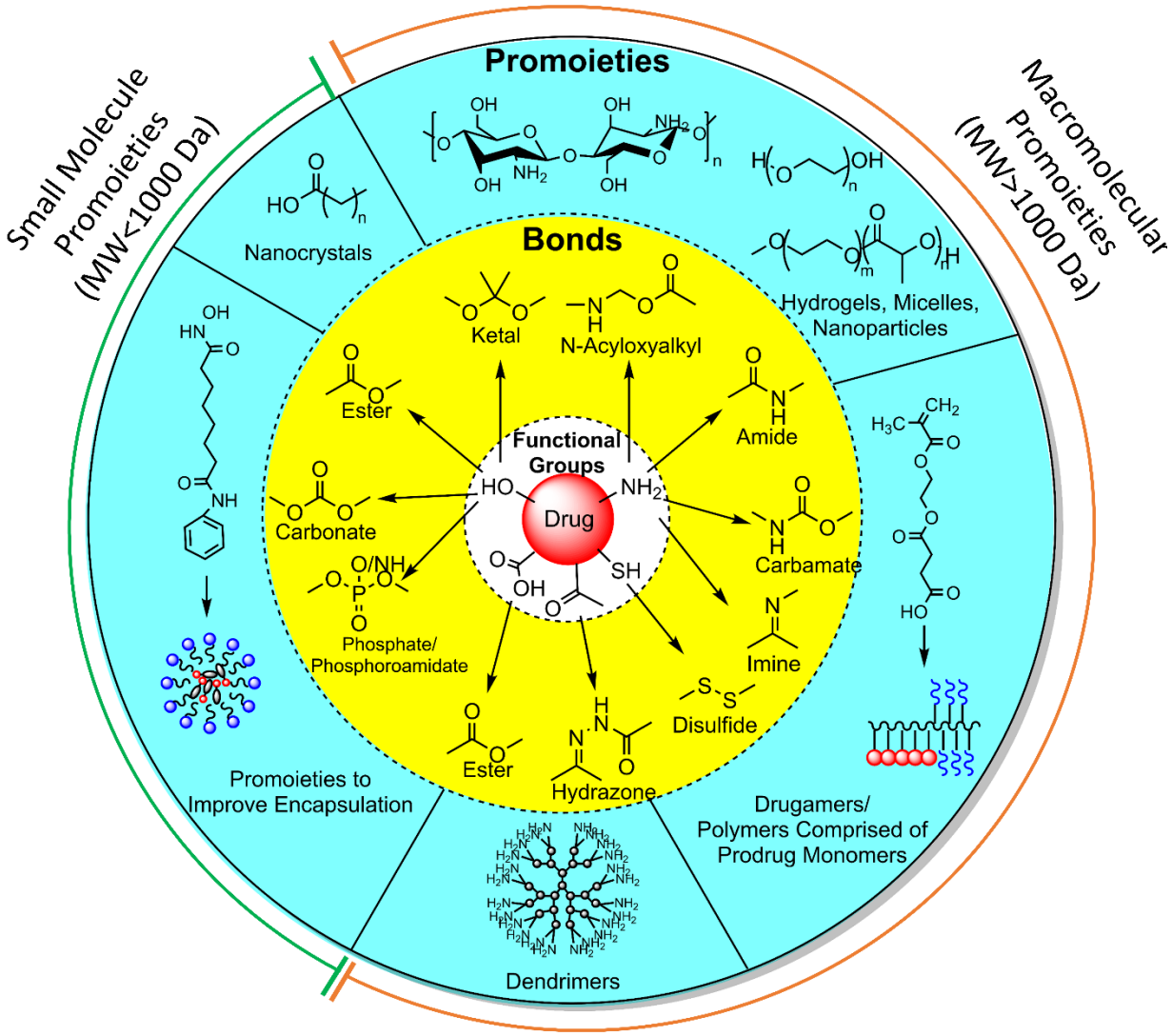

Fig 2. 3. Cleavable bonds used in LA prodrugs

ARVs with free functional groups potentially be modified to obtain LA prodrugs. Several of these cleavable bonds have been utilized for conventional prodrugs, such as the phosphate bond in tenofovir disoproxil fumarate. The outer light blue area highlights LA-prodrug DDS strategies.

2.3.1. Long-acting prodrugs with small molecular weight (MW<1000 Da) promoieties

In this section, we review LA-prodrugs employing small molecule promoieties (typically MW<1000 Da), where the promoiety structure is a well-defined chemical entity that leads to LA-prodrugs with defined chemical structure and molecular weight. Strategies of this type are further organized by how the LA-prodrug is used to achieve extended duration of action. The first subsection focuses on tuning the physiochemical properties of LA-prodrugs using different promoieties in order to promote encapsulation and slow dissolution from various drug delivery systems. The second subsection focuses on lipophilic prodrugs and how their high-order assembly yields slow dissolution and sustained bioavailability.

2.3.1.1. Small MW Promoieties to Improve Encapsulation in Drug Carriers

Drug carriers are biocompatible tools used to transport APIs for pharmaceutical applications, such as nanoparticles, micelles, hydrogels, dendrimers, etc. [98]. Drug carriers entrap APIs, then release drug by diffusion through biodegradation or erosion of the carrier, swelling, or osmotically induced events [75]. Various carriers can be used to improve the delivery of drugs to achieve extended duration of action. One of the main challenges for passive encapsulation via noncovalent interactions is poor drug loading [99]. Small hydrophilic drugs with molecular weight <1000 Da and logP or logD <3.0 are particularly difficult to encapsulate in hydrophobic carriers [100]. The weak interaction between drug and carrier in these systems leads to rapid partitioning into the aqueous phase under physiological conditions, limiting the duration of action [101,102]. In certain cases, drug encapsulation of hydrophilic drugs in carriers such as PLGA microspheres is poor due to the rapid partitioning into the external aqueous phase during the formulation step [103]. Likewise, insufficient drug loading is one of the major hurdles preventing widespread clinical usage of polymeric micelles, despite their potential to treat

tumors in a long-acting manner due to the improved solubility and bioavailability of chemotherapeutic drugs [104]. Long-acting prodrugs designed to enhance non-covalent interactions with the carrier can improve encapsulation efficiency and loading while sustaining release by minimizing partitioning to plasma or tissue.

Several research groups have applied LA-prodrug strategies to improve the loading and release of hydrophilic drugs with polymeric carriers, often focusing on the effect of promoiety lipophilicity. Creighton *et al.* investigated various acyl ester prodrugs of raltegravir (RAL) that were designed to prevent ionization and increase lipophilicity. LA-prodrug modifications of RAL increased encapsulation in poly(lactic-glycolic acid) (PLGA) nanoparticles by as much as 20-25 folds when compared to free RAL [105]. Creighton *et al.* attributed the greater encapsulation efficiency of RAL prodrugs to the enhanced non-covalent interactions with the polymer/solvent oil phase of the emulsion. While increased octanol:water partition coefficients (P_{ow}) were necessary for high loading a direct correlation with P_{ow} values was not observed, likely due to prodrug specific interactions in 1-octanol compared to the polymer/solvent oil phase of the emulsion. *In vitro* results demonstrated release was sustained with a heptanoate RAL-prodrug (approximately 100% cumulative release just under 80 h) and a benzoate RAL-prodrug (approximately 100% cumulative release just under 100 h). Although the duration of action is shorter compared with other formulations for HIV treatment, this study demonstrates a strategy to minimize burst release from PLGA nanoparticles.

Prodrugs to improve drug encapsulation in the carrier are typically conjugated to a lipophilic promoiety due to the increased affinity to the drug carrier. This is because polymers for drug carriers tend to be hydrophobic to lower the water ingress to slow drug release [106]. However, increasing lipophilicity of a prodrug is not a prerequisite for increasing affinity with

the drug carrier; phosphates (triphosphate and monophosphate) have been used as promoieties for nucleoside reverse transcription inhibitors (NRTI) [107]. For example, Agostoni *et al*. noted that the triphosphorylation of zidovudine (AZT) increased the loading in MIL-100 Fe metal-organic frameworks from 1.4 wt% to 24.4 wt% [108]. The increased encapsulation was attributed to the formation of interactions between the phosphate groups of the NRTI with the coordinatively unsaturated iron(III) metal sites. Release of the AZT triphosphate prodrug was sustained for approximately 3 days, whereas the half-life of oral free AZT was approximately 1 h[109]. One thing to note is that despite the conjugation to phosphates significantly improving encapsulation, this was not the original intention of the researchers when designing triphosphorylated-AZT, as phosphorylation is a key step to be in the drug's active form, hence why some experts may argue this is not the definition of a prodrug [110]. Nevertheless, it can be considered as a strategy to improve encapsulation in addition to preemptive conversion to the drug's active form.

Conversion of drugs into LA-prodrugs with acyl esters and other lipophilic promoieties have also demonstrated sustained *in vitro* and *in vivo* effects. In treatment of other diseases, the prodrug approach also improved encapsulation in micelles [111], NPs [112], dendrimers [113], liposomes [114–116]. Xing *et al.* demonstrated the moeixitican-loaded liposomes inhibited tumor growth for up to 15 days with an inhibition rate of 66.86%, whereas the corresponding inhibition for CPT11 loaded liposomes was 46.06%. The authors attributed the increased *in vivo* antitumor activity to the sustained drug release of moeixitican-loaded liposomes, improved systemic circulation, and tumor accumulation via the enhanced permeability and retention.

In summary, in this section we discussed how drugs with poor compatibility to the carrier can result in poor encapsulation and lead to rapid partitioning out of the carrier, limiting

opportunities for slow dissolution. Conversion of free drugs into more lipophilic prodrugs improves encapsulation for a variety of carriers, but additional promoiety properties could result in improved loading and release for specific drugs and carriers. As stated above, the promoieties selected are to increase the affinity for the drug carrier and do not necessarily require a lipophilic promoiety. For example, promoieties that introduce specific hydrogen bonding functional groups or hydrophobic interactions may be useful in improving encapsulation. Despite these prodrugs increasing the encapsulation efficiency (80-100%) in drug carriers, they still result in poor loading, thus limiting their application for long-acting drug delivery [107].

2.3.1.2. Fatty acyl promoieties for solid drug dispersions

Solid drug dispersions (SDD) are an important class of LAF for poorly water-soluble drugs that naturally self-assemble into amorphous or semicrystalline solids and are used for treatment in several diseases [117]. Most pharmaceutical nano/micron-sized SDDs result from top-down approaches for bulk drug comminution by milling or homogenization. Drug release from SDD is mediated by the slow dissolution of drug from the surface of these nanosized solids (**Fig 3)**. By reducing the particle size of solids, the solubility and dissolution rate of poorly water-soluble drugs are greatly increased due to the increased surface area and decreased diffusion layer thickness [118]. As defined by the Nernst-Brunner equation, the diffusion coefficient is directly proportional to the dissolution rate [119,120]. The desired release rate of a drug from an SDD can be obtained by tuning the dissolution rate according to the desired particle size and drug aqueous solubility. A lipophilic promoiety conjugated to a drug can decrease its aqueous solubility and dissolution rate from an SDD. SDDs are almost entirely drug with minimal amounts of excipients to offer a "carrier-free" LAF [121]. This is especially advantageous compared with oil depots of fatty acyl prodrugs where the drug partitioning limits dissolution.

SDD are formulated as suspensions stabilized with surfactants and injected subcutaneously or intramuscularly to form depots at the injection site. Drugs such as cabotegravir (CAB, logP=0.16 [122]) and rilpivirine (RPV, logP=5.47 [123]) have poor aqueous solubility, which makes it amenable for formulation as an SDD that has been successfully translated to clinical products[18,124]. For APIs with high aqueous solubility, conjugation to a fatty acyl promoiety generates a LA-prodrug that may facilitate formulation as SDD with tunable dissolution rates for extended duration of drug action. SDD formulated from LA-prodrugs have demonstrated clinical efficacy and are advantageous for long-term treatment of diseases [125,126]. For example, paliperidone palmitate (PP) is a prodrug of paliperidone conjugated with palmitic acid that results allows formulation as an SDD and results in slower dissolution in a LAF (Invega Sustena, Invega Trinza, Janssen Pharmaceuticals) [127]. Aripiprazole lauroxil (AL) is an N-acyloxy methyl prodrug of aripiprazole with decreased aqueous solubility due to its conjugation with lauric acid, which facilitates formulation as an LAF to treat schizophrenia (Aristada, ALKERMES®)[128]. Oral formulations of paliperidone and aripiprazole are dosed daily, whereas the SDD formulations are dosed once every 1-3 months[129–132]. The success of long-acting antipsychotic prodrug formulated as SDD has been a paradigm for other APIs, such as antiretroviral (ARV) drugs. In addition, fatty acyl prodrug modifications of hydrophilic drugs have been successfully formulated as SDD.

Gendelman and Edagwa *et al.* have chemically modified ARV drugs with various physiochemical properties into LAFs, which they have termed LASER-ART (long-acting slow effective release ART). LASER-ART entails the dissolution of the LA-prodrug ARV from the SDD followed by hydrolysis of the prodrug from the promoiety to release the active pharmaceutical ingredient (API) [133]. Conversion of LA-prodrug into the active species can be

mediated by carboxyesterases enzymes that hydrolyze ester, carbamate, and amide linkages[134]. Long-acting prodrug strategies enable successful formulation of many available hydrophilic ARV drugs as nanocrystalline SDD to extend duration of drug action. For instance, abacavir (ABC), a relatively hydrophilic ARV drug (logP=1.20) [135], was successfully formulated as a LA-prodrug by conjugating it to myristic acid via an ester linkage. The poorly water-soluble LA-prodrug (MABC) could be formulated into a nanocrystal SDD that prolonged therapeutic levels of ABC in plasma and reduced dosing frequency [136]. Myristic acid, a 14-carbon fatty acid, is a recurring promoiety used in LASER-ART to enable nanocrystal formulation and inhibiting enzymes necessary for HIV replication [136]. Tuning the fatty acid chain length offers a design lever to control dissolution rate by tuning aqueous solubility and hydrolysis rate of the LA-prodrug and release of the active drug. Deodhar *et al.* investigated the effect of fatty acyl promoiety carbon lengths (C14, C18, C22) on duration of action of dolutegravir (DTG). They found that C18-DTG prodrug SDDs afforded the longest duration of action as measured by plasma concentration levels remaining above PA-IC90 (*in vitro* protein associated-90% inhibition concentration) for 367 days [137]. The C14-DTG prodrug SDD also provided a long duration above PA-IC90 for at least 112 days, whereas C22-DTG prodrug SDDs maintained PA-IC90 levels for only about 7 days. The authors noted that the dissolution rate is driven primarily by the LA-prodrug aqueous solubility rather than the carbon length of the fatty acyl chain. To confirm the role of solubility, Deodhar *et al.* synthesized a C18-DTG prodrug and a C18 dimer DTG prodrug comprised of two DTG conjugated together via a C18 diester. The C18 dimer DTG prodrug exhibited a shorter duration of action as indicated by plasma concentrations dropping below PA-IC90 after <140 days. This is due to the significantly greater octanol solubility of the C18 DTG prodrug, indicating change in drug release rate was driven by

solubility instead of solely the alkyl carbon length. LASER-ART have also been successfully applied to synthesize LA-prodrugs of lamivudine, tenofovir, emtricitabine, darunavir, and other ARV drugs for formulation as SDD with extended duration of action, thus demonstrating the wide variety of drugs suitable to this LAF strategy [138–140].

LASER-ART has also been applied to APIs that have been formulated as conventional SDDs and shown to result in promising attributes such as reducing injection-site reactions, large injection volumes, and frequent dosing [141–143]. For example, CAB is already clinically approved as a long-acting injectable SDD, and was used for LASER-ART by Kulkarni *et al.* They showed that a single intramuscular injection of C18-CAB prodrug SDD in mice yielded concentrations above the PA-IC90 for at least 364 days [122]. These data along with favorable administration and manufacturing properties suggest that a C18-CAB prodrug SDD may be promising as a once-yearly injectable. These data also suggest that different acyl chain lengths may be suitable to tune the desired drug dissolution rate depending on the inherent aqueous solubility of the parent API. Hilaire *et al.* also applied LASER-ART to RPV where they developed a library of N-acyloxyalkyl RPV prodrugs with varying alkyl carbon lengths (6-18 carbons) [144]. N-acyloxyalkyl RPV prodrugs undergo bioconversion into N-hydroxymethyl RPV in the presence of esterases *in vivo* and is further converted into the parent drug after hydrolysis. Following intramuscular injections in BALB/cJ mice (45 mg/kg RPV), a single intramuscular injection of C14-RPV (NM3RPV) SDD maintained RPV concentrations above PA-IC90 (12 ng/mL) over 4, 12, and 25 weeks depending on the injection dose of 45, 75, 100 mg/kg, respectively. In contrast, nanoformulation of the parent drug (NRPV) displayed faster decay in plasma concentrations and maintained RPV plasma concentration above PA-IC90 for only 7 weeks at the highest dose (100 mg/kg). When comparing the duration of action of the

two formulations, NM3RPV exhibited 13- and 26-fold increases in plasma RPV apparent half-life and mean residence time compared to NRPV. This study demonstrates that, even for highly hydrophobic and insoluble APIs that are readily formulated as SDD, synthesizing LA-prodrugs with altered solubility can further tune dissolution rates promote longer durations of drug action in tissue and plasma. In addition to promoiety architecture (alkyl carbon length, linker selection, etc.), other parameters have been shown to influence the duration of action of LASER-ART. For example, particle size and choice of surfactant can influence cellular uptake of nanocrystals and generate intracellular drug depots [145]. Intracellular depots of nanocrystals provide a secondary depot within cells and have been observed to offer greater antiretroviral activity for a longer duration than a depot formed at the injection site [136,146]. Poloxamers used as coatings to stabilize solid dispersions have also been functionalized with folic acid (FA) to facilitate folate-receptor targeted endocytosis and increase intracellular depots within macrophages [147]. In contrast to simple oil vehicles, LASER-ART and nanocrystal formulations offer multiple levers to tune to achieve the desired release rate depending on the inherent aqueous solubility of the API.

Here we summarize LA-prodrug modifications formed by the addition of a lipophilic promoiety to various APIs that will enable formulation of nano/micron-sized solid drug dispersions and micelles for extended duration of action. A wide range of release behavior can be achieved depending on the physiochemical properties of the prodrug and the DDS formulation employed. For example, ABC LA-prodrug SDD resulted in extended duration of action on the order of days and weeks, whereas C18-DTG and C18-CAB LA-prodrug SDDs extended duration of drug action up to one year. The use of fatty acyl prodrugs is an effective method to enable formulation as LAF for many drugs, and it is amenable to different types of linkers. This strategy

has also demonstrated tunability by adjusting the carbon length of the conjugated hydrocarbon chain from C6-C22. However, the degree of tunability of release rate by modifying carbon length has not been fully explored despite exhibiting significantly extended durations of release. The generalizability of this approach to other hydrophilic ARV drugs and the ability of carbon length alone to achieve the longer release duration has not been fully demonstrated.

2.3.2. *Long-acting prodrugs with macromolecular (MW>1000 Da) promoieties*

In this section, we discuss long-acting prodrugs employing macromolecular promoieties (typically MW > 1000 Da). These strategies typically involve drugs directly conjugated to a reactive macromolecular entity (post-modification) and the direct polymerization of polymerizable prodrug monomers [148]. Macromolecular entities include natural (chitosan, dextran) and synthetic polymers (polyethylene glycol, poly(N-(2-hydroxypropyl) methacrylamide). By using different polymers and polymer architecture, polymeric promoieties can act as the drug carrier to achieve controlled release [149]. As discussed in the previous sections, conjugation of a hydrophilic drug to a macromolecular promoiety can minimize the rapid dissolution due to the low affinity the drug has to the carrier. In the case of polymeric prodrugs, the burst release of drugs is suppressed by covalently conjugating the drug to the polymeric carrier, where the release is governed by cleavage of linkers [150]. Furthermore, conjugation to a polymeric promoiety can facilitate the formation of higher-order structures for the long-acting delivery of antiretrovirals, such as gels, micelles, and nanoparticles [36]. By using polymeric promoieties, polymeric prodrugs can tune the sustained delivery of

antiretrovirals with unique polymeric carriers, adjusting the molecular weight of polymer chains, utilizing different linkers, and achieving targeted delivery with targeting ligands [151].

2.3.2.2 Backbone Polyprodrugs

Polymeric prodrugs, such as polyanhydrides (PA), polyanhydride esters (PAE), polycarbamates, and polycarbonates, with the drug incorporated as monomers in the polymer backbone, which is released as the backbone degrades. These polymeric prodrugs are sometimes referred to as backboned polyprodrugs[152]. As mentioned in the previous section, prodrug made from postmodification of polymeric promoieties suffer from lower drug loading content, as well as difficulty in controlling conjugation sites, and thus difficulty in efficient and sustained drug release[152,153]. Backboned polyprodrugs are synthesized by step-growth polymerization, wherein difunctional prodrug/drug monomers are covalently linked to obtain a high molecular weight polymer prodrug[154]. One example of backboned polyprodrugs for long-acting delivery of antiretrovirals is the backboned polymer prodrug synthesized by Shakil *et al* by using the difunctional emtricitabine (FTC) as the monomer[155]. The difunctional nature of FTC is due to the free amine and hydroxyl group, which was conjugated to hexamethylene bis(chloroformate) by cleavable carbonate and carbamate linkages to obtain poly(hexyl-FTC) with a drug loading up to 57%. The release of FTC was sustained over three days by the gradual cleavage of carbamate and carbonate linkages. Formulation as backbone polyprodrugs enables the long-acting release of hydrophilic NRTIs which are incompatible with non-prodrug LA formulations.

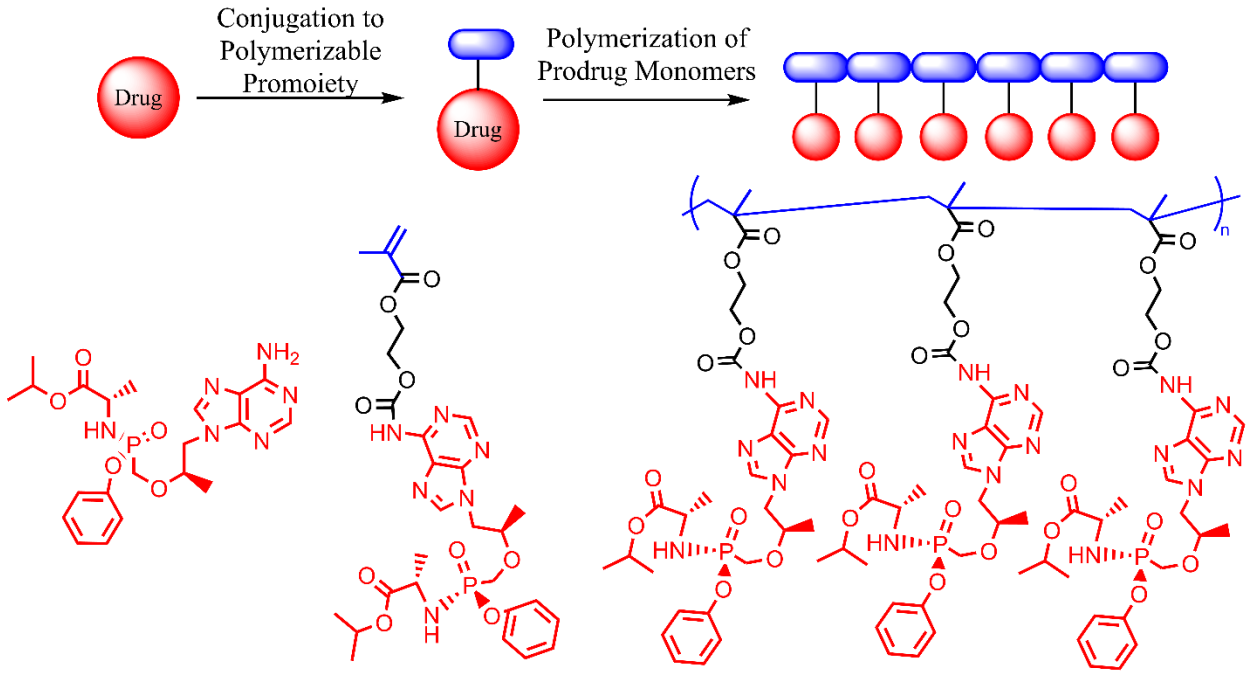

Fig 2. 4. General scheme of drugamer or polymers comprised of polymerizable prodrug monomers

The scheme (top) describes the conversion of a drug into a prodrug monomer that is subsequently polymerized to obtain a "drugamer". An example drugamer (bottom) synthesized by RAFT using a TAF monomer *[38]*.

2.3.2.3. Polymeric Prodrugs Synthesized from RAFT Polymerization

Polymerizable prodrug monomers can be used to obtain well-defined block copolymers to formulate micellar polymeric prodrug with improved encapsulation and drug stability. Polymerizable prodrug monomers are obtained by modifying the drug with moieties such as acrylamide and methacrylate that promote drug polymerization to the pendant groups of the polymer backbone (scheme shown in **Fig 2.4**)[156,157]. RAFT polymerization is especially useful in obtaining polymer prodrugs with low polydispersity and precise control of molecular mass relative to other polymerization techniques[158]. Control over molecular weight can

provide more uniform physicochemical properties[159]. Furthermore, prodrugs synthesized by RAFT polymerization can be obtained in relatively mild synthesis conditions, wherein harsh reagents are not required[160]. In addition, RAFT polymers are amenable to a wide range of functionalization and the formation of advanced architectures (such as star or bottlebrush polymers), self-assembled nanostructures, and stimuli-responsive systems[160]. In this subsection, we specifically discuss examples of polymer prodrugs obtained via RAFT polymerization and exclude other RAFT polymer prodrugs if the drug was conjugated to the polymer by post-modification techniques which has been discussed in other reviews[158]. In contrast to strategies discussed in subsection 3.5.1, RAFT results in polymer prodrugs conjugated to pendant groups instead of integrated in the polymer backbone. For example, Hasegawa *et al.* used RAFT to polymerize ibuprofen-acrylamide (IBUAAm) prodrugs for micelles[156]. IBUAAm was obtained by conversion of the carboxylic acid of IBU into an acyl chloride group, and linked to acrylamide by an ester bond. Block copolymerization of IBUAAm using RAFT was facilitated with a PEG macromolecular chain-transfer agent (PEG-CTA, MW=10k Da). Hasegawa *et al.* successfully polymerized IBU polymers with the number average molecular weight (Mn) ranging from 9706-26410 Da and PDI ranging from 1.15-1.20. IBU polymers improved the stability of ibuprofen within the micelle compared to physically encapsulated drug and resulted in release of days to months depending on the length of the hydrophobic drug segments of the copolymer (≤20 and 53 units). Interestingly, the use of longer hydrophobic segments resulted in the formation of worm-like micelles rather than spherical micelles, which may also affect drug release kinetics.

Das *et al.* used RAFT polymerization to synthesize various polymeric prodrugs of ciprofloxacin (cipro) with different polymeric architecture and linkers[161]. Cipro prodrug

monomers were copolymerized with poly(ethylenegylcol methacrylate) (950 Da) (O950) as diblock copolymers and random copolymers to observe the effect on micelle self-assembly. The diblock copolymer self-assembled into micelles in aqueous conditions where the hydrophilic corona of O950 encapsulated the hydrophobic polymer segments of the prodrug. The diblock polymer architecture was observed to have reduced ester hydrolysis rates relative to the random copolymer prodrug, which was claimed to be a result of hindered water penetration into the hydrophobic core and demonstrated the importance of polymer architecture on sustained release. Das *et al.* also ussed a fast-hydrolyzing phenyl ester (CPM) linker and slow-hydrolyzing aliphatic ester (HBC) linker to further modulate cipro release. Copolymers containing CPM and HBC linkers show that 50% of drug was released over 120 h and 21 d, respectively. An inhalable version of the polymer prodrug was also developed where the cipro methacrylate monomer was conjugated to a protease-cleavable valine-citrulline (VC) linker with either a self-immolative spacer or phenyl ester (CTM) linker. Copolymerization via RAFT was carried out with the prodrug monomers with different linkers and a hydrophilic mannose comonomer, which acts as both the hydrophilic component to improve solubility and a targeting ligand for alveolar macrophages[162]. Mannose receptors on the drugamer induced receptor-mediated endocytosis by alveolar macrophages, which is followed by cleavage of the VC linker by intracellular cathepsins to release the active cipro compound[163]. After intratracheal aerosolization of drugamers in mice, both the VC and CTM-drugamer exhibited sustained concentration of cipro within the lung at concentrations greater than the minimum inhibitory concentration (0.065 μg/g), whereas free cipro was quickly cleared from the lungs within 2 h. VC-drugamer also exhibited superior AUC over 48 h compared to CTM-drugamers and free cipro (25.6x and 74.8x, respectively), and sustained intracellular delivery to alveolar macrophages at >3 magnitudes

greater than the minimum inhibitory concentration. In a challenge study with *Burkholderia thilandensis*, 100% of the mice administered the VC-drugamer survived 14 days after bacteria inoculation compared with only 25% survival of mice administered free cipro[163]. The sustained delivery of cipro up to 7 days improved biodistribution, and resulted in a dose-sparing regimen that illustrates the drugamer platform as promising candidate for further clinical development.

Ho *et al.* also used polymer prodrug comprised of polymerizable prodrug monomers to formulate injectable depots to achieve long-acting delivery of ARV drugs[38]. The authors synthesized a library of tenofovir alefanamide (TAF) drugamers with drug wt% of 34-73%. TAF-drugamers were subcutaneously injected to form a depot capable of sustaining release over an order of months. The mechanism of depot formation is shown in **Fig 2.5**. A single subcutaneous injection of the TAF drugamer sustained release of TAF, which accumulated intracellularly as the active metabolites (tenofovir diphosphate) for up to 50 days. Gradually, polymer chains in the depot are shed after sufficient drug is released, and depot dissolution eventually occurs as the polymer chains are excreted renally (**Fig 2.6**).

The release rate of TAF was tuned by using a faster-releasing carbamate linker (p(benzyl-TAFMA)) or slower-releasing carbamate linker (p(alkyl-TAFMA). In addition to controlling release rates with different linker chemistry, local environments in the depot may result in differential water and enzyme activity that will affect hydrolysis of the carbamate linkers. The authors describe that TAF is released from the polymer backbone upon hydrolysis of the carbamate linkers and results in hydration of the pendant functionalized hydrophilic chains that are shed from the depot. Diblock designs of p(glycerolmonomethacrylate)-*b*-p(alkyl-TAF-methacrylate) and p(glycerolmonomethacrylate)-*b*-p(benzyl-TAF-methacrylate) incorporate

glycerol segments to increase hydrophilicity of the copolymer, which may effect depot structure and stability in a way that promotes faster dissolution. The drugamers developed by Stayton *et al.* were also amenable to further encapsulation in other drug delivery carriers. Drugamers have also been integrated with delivery systems other than micelles and depots. For example, Dart *et al.* formulated these same TAF drugamers in PCL electrospun fibers via blend electrospinning[164]. Sustained release of the active metabolite from these electrospun fiber patches was observed over a 2-month period under *in vitro* conditions.

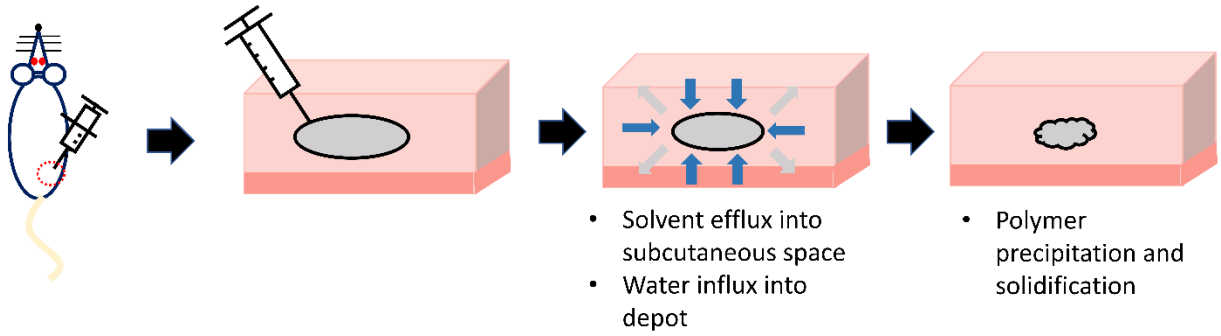

Fig 2. 5. Depot formation in situ following subcutaneous injection of drugamers

Drugamers were formulated as an organic solution (e.g. dimethylsulfoxide) and injected in the subcutis. Upon injection, the organic solvent effluxes into the subcutis as water diffuses into the polymer solution. At a critical concentration of water and organic solvent, the polymer precipitates, forming a depot in the subcutis.

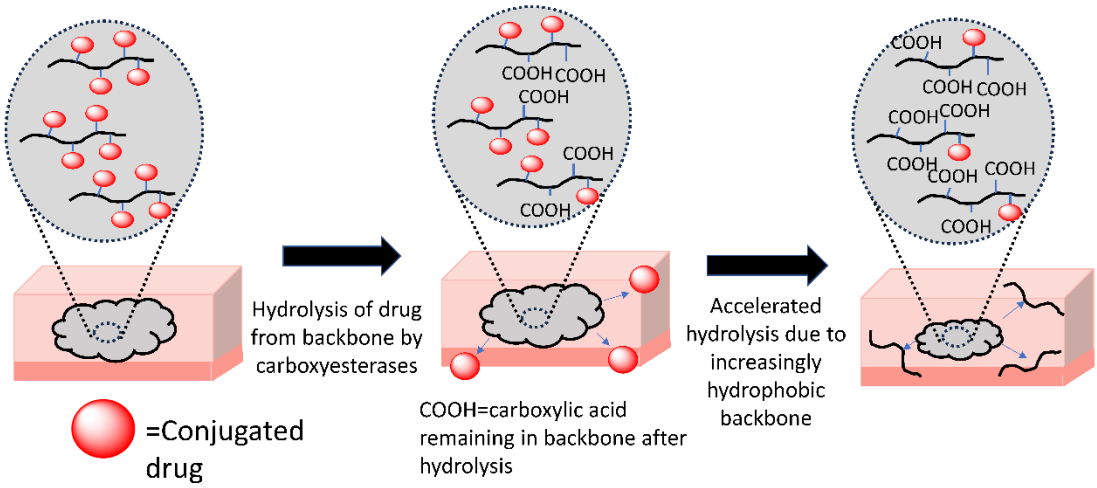

Fig 2. 6. Drug release mechanism from drugamer depot

Drugamers form depot *in situ* when injected subcutaneously. Drug is released when cleavage occurs to polymer chain. At a critical amount of drug released, polymer chains are shed from the depot and cleared by renal clearance[38].

2.4 CONCLUSION

HIV treatment and prevention with ART is highly effective but is dependent on strict adherence to the drug regimen to suppress viral replication. Poor adherence can be attributed to a variety of reasons, such as forgetting dosages or lack of understanding of ART. Although current interventions involving counseling is beneficial in increasing rate of adherence, there is a need for other methods to aid in increasing adherence to ART. LAFs can potentially address the hurdle of adherence with less frequent administration, and have demonstrated improved patient outcome. However, not all ARVs were compatible with diffusion- and dissolution-based DDS. Thus, the prodrug approach was considered due to the promising results observed in literature. We discuss two main categories of LA-prodrugs: small molecular promoieties and macromolecular polymeric prodrugs comprised of prodrug monomers. Small molecular promoieties can be conjugated to drugs for multiple reasons, either for improved encapsulation

efficiency for greater loading in DDS or to enable fabrication as crystals which can subsequently be formulated as LA nanosuspension. Macromolecular polymeric prodrugs can also be synthesized with polymerizable prodrug monomers, wherein the drug itself becomes the material that enables LA delivery. In some cases, ARVs can be polymerized by step-condensation, where drug release is sustained through degradation of the backbone. In other cases, RAFT polymerization can be utilized to obtain well-defined polymeric prodrugs by polymerizing the methacrylate promoiety. RAFT polymerization allows for a great degree of tunability in release by adjusting the polymer architecture or polymer composition of the polymeric prodrug. Current results demonstrate sustained release of ARVs with a subcutaneous injection of "drugamers" of TAF. Therefore, the thesis will focus on the development of polymeric prodrugs of ARVs synthesized by RAFT polymerization and explore the potential sustained release, and compare with previous DDS formulated in the Woodrow Lab.

Chapter 3. SYNTHESIS AND INVESTIGATION OF PHYSICAL PROPERTIES OF ARV DRUGAMERS

3.1. ABSTRACT

Drugamers offer the potential to reduce antiretroviral (ARV) dosing frequency due to their high drug loading and sustained release as in situ forming implants (ISFIs). To develop ARV drugamers for use as long-acting formulations (LAFs), raltegravir (RAL) and atazanavir (ATV) were chemically modified into prodrug monomers and polymerized via RAFT polymerization. Unlike tenofovir alafenamide (TAF), which was modified at the amine group to generate a carbamate linker, RAL and ATV were modified at their hydroxyl groups to form ester linkers. The lower pKa of RAL (pKa = 6.67) accelerated ester cleavage, highlighting critical design considerations for drugamers with rapid-release drugs. Prodrug monomers of RAL and ATV were synthesized via the acyl chloride and carbodiimide routes, respectively, and polymerized with varying comonomer compositions, including 2-methylsulfinyl ethyl methacrylate (MSEMA) and butyl methacrylate (BMA). The resulting drugamers were synthesized with high drug loading, ranging from 51.88-74.60 wt%, depending on the design of the polymer composition. The drug loading observed in the resulting drugamers exhibited greater drug loading than commercial, noncovalent polymeric formulations used for *in situ* forming implants (ISFIs, 2-29 wt%). In addition, copolymerization with comonomers demonstrated the tunable physical properties of the drugamer platform, as shown in precipitation studies. Notably, RAL-MSEMA copolymers demonstrated greater hydrophilicity than RAL homopolymers and RAL-BMA copolymers. These findings illustrate the adaptability of the drugamer platform to different ARVs, paving the way for novel LAF development.

3.2. INTRODUCTION

LAF of ARVs can potentially improve adherence to ART among patients with less frequent dosing and less stigma [165]. LAFs have demonstrated improved patient outcome and decreased rates of infection by removing critical adherence barriers to oral ARVs [69–71]. Despite the approval of CAB-LA, studies show mutations conferring to CAB resistance can occur in macaques treated with LA-CAB, demonstrating the need for other LA formulations with different antiretrovirals [166]. This chapter investigates the sustained released of RAL and ATV afforded by the use of polymeric prodrugs synthesized in the previous chapter. These polymeric prodrugs are coined as “drugamers”, which has high loading of drug and tunable properties by changing the cleavable linker, targeting moiety, and enables the delivery of a range of hydrophilic and lipophilic antiretrovirals [38,161,162].

By using a polymeric prodrug approach, sustained release could potentially be achieved with drugs that were previously incompatible with DDS relying on noncovalent interactions. More specifically, the hydrophilicity of RAL can result in incompatibility with certain DDS to achieve sustained release, as demonstrated in the previous experiments in the Woodrow Lab. RAL has been formulated as nanocrystals, in solvent-cast films, and electrospun fibers, which all have drawbacks preventing usage as LAFs, as discussed in subsection 2.2.2. However, the limitations associated with the physical properties of the ARV become minimally important after synthetic conjugation[38]. In this study, RAL and ATV were synthetically conjugated to a methacrylate group to obtain polymerizable prodrug monomers. Drugamers are synthesized by RAFT polymerization of the respective prodrug monomers. These drugamers have been studied extensively in other contexts, but only one publication has been published for subcutaneous depots [38,167,168].

RAL and ATV were selected due to their potency and different mechanisms of action compared to TAF, as well as the potential for combination delivery due to the predicted synergy [31]. RAL is an integrase inhibitor that inhibits the integration of viral DNA into the host DNA[169]. ATV is an azapeptide inhibitor of protease of HIV-1 and prevents the formation of mature virion [170]. RAL and ATV both contain free hydroxyl groups available for chemical modification downstream to obtain cleavable ester linkages, which contrasted TAF, which is modified with the amine group to generate a carbamate linker. In addition to the utilization of a different functional group, RAL and ATV both offer a range of clinical advantages. For example, RAL demonstrated desirable mucosal penetration in the female genital tract [32]. RAL also demonstrated high penetration in the seminal compartment [33]. Studies have shown ATV to be safe for long-term use and high efficacy in the absence of boosting with ritonavir [171]. Lastly, the Woodrow Lab have synthesized RAL prodrugs, as discussed in Chapter 2, indicating the feasibility of making RAL prodrugs with other promoieties [105].

3.3 MATERIALS AND METHODS

3.3.1. Materials and reagents

Raltegravir was purified from Isentress® (400 mg RAL, Merck). Atazanavir was purified from commercial ataznavir sulfate capsules (300 mg ATV, Northstar Rx). The total synthesis of monomers used thionyl chloride (Sigma-Aldrich), triethylamine (TEA, Sigma-Aldrich), mono-2-(methacryloyloxy)ethyl succinate (SMA, Sigma-Aldrich), 1-ethyl-3-(3-dimethylaminopropyl)carbodiimide hydrochloride (EDC HCl, Sigma, Aldrich), 4-dimethylaminopyridine (DMAP, Acros Organics), dichloromethane (DCM, anhydrous, Sigma-Aldrich), toluene (Sigma-Aldrich), sodium bicarbonate (NaHCO3, Fisher Scientific), glacial acetic acid (Acros Organics), diethyl ether (Sigma-Aldrich), hexanes (Sigma-Aldrich), ethyl

acetate (Sigma-Aldrich), acetone (Thermo Fisher Scientific), magnesium sulfate anhydrous (MgSO4, Millipore Sigma), 2-(methylthio)ethyl methacrylate (MTEMA, Sigma-Aldrich), hydrogen peroxide (H2O2, 30% in water, Fisher Scientific). The total synthesis of polymers by RAFT polymerization used butyl methacrylate (BMA, Sigma-Aldrich), methacryloxyethyl thiocarbamoyl rhodamine B (RhMA, Polysciences Inc.), 4-(((ethylthio)carbonothioyl)thio)-4-cyanopentanoic acid (ECT, Sigma-Aldrich), 2,2'-azobis(4-methoxy-2,4-dimethylvaleronitrile) (V70, Wako Fujifilm), N,N-dimethylformamide (DMF, extra dry, with molecular sieve, Fisher Scientific), diethyl ether (Sigma-Aldrich), acetone (Thermo Fisher Scientific). Fasudil monohydrochloride (eNovation Chemicals) was used for drug weight percent quantification. Regenerated cellulose dialysis membranes (Spectrum Laboratories) were used for polymer purification.

3.3.2. Isolation of Raltegravir from Isentress tablets

Raltegravir was isolated as a neutral compound from ISENTRESS® tablets (400 mg per tablet, Merck & Co.). Crushed Raltegravir tablets were incubated in dichloromethane (DCM, 400 mL) with glacial acetic acid (10 mL) overnight at room temperature. The resulting slurry was then filtered through a frit packed with celite. The filtrate was then concentrated under reduced pressure. The crude material was then recrystallized with the addition of isopropanol (initially 70 °C and cooled to room temperature) overnight, and then placed in the -20 °C freezer overnight to continue recrystallization. The product was then dried over high vacuum overnight to provide pink solids (1150 mg, Yield=57.5%). The full ^{1}H-NMR and ^{13}C-NMR spectra are shown on **Fig S1** and **Fig S2**, respectively. ^{1}H-NMR (300 MHz, DMSO-*d*6) δ 12.21 (s, 1H), 9.85 (s, 1H), 9.11 (s, 1H), 7.39 (dd, J=6, 3 Hz, 2H), 7.17 (t, J=9 Hz, 2H), 4.51 (d, J=6 Hz, 2H), 3.48 (s, 3H), 2.56 (s, 3H), 1.74 (s, 6H). ^{13}C NMR (101 MHz, DMSO-*d*6) δ 169.38, 166.67, 163.45, 161.04, 159.52,

159.02, 153.52, 152.73, 146.68, 135.82 (d, $J_{F,C}$=3.03) 130.47 (d, $J_{F,C}$=8.08), 125.36, 116.10 (d, $J_{F,C}$=21.21), 58.49, 42.58, 33.93, 27.97, 11.66.

3.3.3. Molecular weight determination of synthesized prodrug monomers

Molecular weight determination was carried out by UW Mass Spectrometry Center. Accurate mass was determined by LC-MS/MS with tandem quadrupole Time-of-Flight (AB Sciex TripleTiOF 5600+). The MS was coupled with an I-Class Acquity UPLC, direct infusion syringe pump to isolate the analyte. MultiQuant™ Software was used to analyze the data to obtain the accurate mass.

3.3.4. Synthesis of RAL-SMA prodrug monomers by two-step esterification via *acid chlorides*

Commercial mono-2-(methacryloyloxy)ethyl succinate (SMA, 1036 mg, 4.50 mmol) was added to neat thionyl chloride ($SOCl_2$, 1.74 mL, 23.9 mmol) under argon and stirred at room temperature for 30 minutes and reacted at 50 °C for 1 h. The excess $SOCl_2$ was removed by evaporation under reduced pressure and co-evaporated with additional benzene twice to remove residual $SOCl_2$, yielding a clear oil. The oil was dissolved in anhydrous DCM (50 mL), then slowly added to a solution of RAL (1000 mg, 2.25 mmol) and triethylamine (TEA, 0.88 mL, 6.30 mmol) in anhydrous DCM purged with argon gas. Stir the reaction mixture and react at room temperature for 3 h. Quench the reaction by diluting the reaction mixture with DCM (50 mL), and wash with saturated sodium bicarbonate (NaHCO3, 2x, 100 mL) and brine (1x, 100 mL). The organic phase was dried over magnesium sulfate and concentrated under reduced pressure. The crude product was purified by flash chromatography using 5:1 ethyl acetate: acetone, then precipitated using 1:1 hexane: diethyl ether (2x, 40 mL) to obtain the RAL-SMA. The product was then dried over high vacuum overnight to provide dark blue or brown amorphous solids. Yield = 357.8 mg (24.18%). The full ^{1}H-NMR and ^{13}C-NMR spectra are

shown on **Fig S3** and **Fig S4**, respectively. ^{1}H NMR (500 MHz, DMSO) δ 10.00 (s, 1H), 8.91 (s, 1H), 7.34 (s, 2H), 7.15 (s, 2H), 6.02 (d, J = 0.7 Hz, 1H), 5.66 (s, 1H), 4.42 (d, J = 6.4 Hz, 2H), 4.29 (s, 4H), 3.50 (s, 3H), 2.83 (s, 2H), 2.64 (s, 2H), 2.57 (s, 3H), 1.85 (t, J = 1.3 Hz, 3H), 1.76 (s, 6H). ^{13}C NMR (126 MHz, DMSO) δ 171.26, 169.34, 166.41, 165.76, 162.19, 161.92, 160.26, 159.23, 158.73, 157.97, 152.70, 140.40, 135.59, 135.31, 135.29, 133.75, 129.18, 129.11, 126.05, 115.09, 114.92, 62.37, 62.09, 57.89, 41.50, 33.16, 28.51, 28.48, 26.62, 17.87, 10.66. ESI=MS for $C_{30}H_{34}N_6O_{10}F$ [M]: 657.2, [M+Na^+]: 679.2.

3.3.5. Stability testing of RAL-SMA in polar aprotic solvents to determine polymerization conditions

Stability of monomers was measured by using high-performance liquid chromatography (HPLC, Shimadzu Prominence). Simultaneous detection of RAL and RAL-SMA was performed by using reversed phase HPLC employing a Kinetex® 5 μm C18 column (100 Å, 250 x 4.6 mm). The mobile phases used were acetonitrile (ACN) as mobile phase A and 25 mM KH_2PO_4 dissolved in water as mobile phase B. Samples were eluted with a isocratic flow of 45:55 A:B at 1 mL/min for 12 min measuring the absorbance at 300 nm.

RAL-SMA was dissolved in DMF or DMSO and incubated at a water bath (Thermo Scientific Precision) at designated temperatures (35, 45, 70 °C) to determine the stability of RAL-SMA over time. Approximately 25-50 μL of the incubated solution was drawn up at given timepoints, diluted 10-fold, filtered through a 0.22 μm PTFE filter, and analyzed by the HPLC. Samples were measured with an injection volume of 10 μL with an isocratic flow of 45% A:55% B at 1 mL/min for 12 min measuring the absorbance at 300 nm. RAL and RAL-SMA had an approximate retention time of 4.8 min and 9.0 min, respectively.

3.3.6. Synthesis of 2-(methylsufinyl)ethyl methacrylate

2-(methylthio)ethyl methacrylate (MTEMA, 1 g, 5.99 mmol) was added to a round-bottom flask in an ice bath and, sealed with a rubber septum, and purged with argon gas. 20% Hydrogen peroxide (H_2O_2, 0.72 g, 4.23 mmol) solution was added to the round-bottom flask *via* a syringe pump at 50 µL/min. The solution was allowed to react in an ice bath. After 24 h, the reaction was quenched by adding deionized water. The aqueous solution was extracted with dichloromethane (25 mL, 3x). The organic phase was dried with magnesium sulfate and concentrated under reduced pressure. The concentrated sample was purified with flash chromatography using 5% (v/v) methanol (MeOH) in DCM as the mobile phase. The product was then dried over high vacuum overnight to provide white amorphous solids. Yield (41.55%). The full ^{1}H-NMR spectrum is shown on **Fig S6**. ^{1}H NMR (300 MHz, DMSO) δ 6.04 (d, J = 0.8 Hz, 1H), 5.70 (s, 1H), 4.26 (s, 2H), 2.75 (s, 2H), 2.11 (s, 3H), 1.96 – 1.82 (m, 3H). ESI=MS for $C_7H_{13}O_3S$ [M]: 177.6, [M+Na^+]: 199.0.

3.3.7. Reversible addition-fragmentation chain-transfer (RAFT) polymerization of RAL homopolymer drugamers (p(RAL-SMA-co-RhMA))

RAFT polymerization of RAL-SMA and one Rhodamine monomer (methacryloxyethyl thiocarboamoyl rhodamine B, RhMA) per polymer chain was conducted in anhydrous dimethylformamide (DMF) under inert argon atmosphere. 4-cyano-4-[(ethylstuflanylthiocarbonyl)sulfanyl]pentanoic acid (ECT) and 2,2'-azobis(4-methoxy-2,4-dimethylvaleronitrile) (V70) were used as the chain-transfer agent (CTA) and radical initiator, respectively. The initial monomer/CTA/initiator ($[M]_0$:$[CTA]_0$:$[I]_0$) ratio was 40:1:0.25, respectively. RAL-SMA (425 mg, 0.647 mmol), RhMA (13.3 mg, 0.020 mmol), ECT (4.39 mg, 0.017 mmol), and V70 (1.29 mg, 0.004 mmol) were added to a 10 mL round-bottom flask and

dissolved in anhydrous DMF (1.02 mL). Once a homogeneous solution was obtained, the flask was sealed with a rubber septum and purged with argon gas for 35 minutes. Subsequently, the flask was transferred to a preheated oil bath at 45 °C and allowed to react for 8 hours. The reaction was quenched by exposure to atmospheric air and crude product was precipitated in diethyl ether. The precipitant was redissolved in DMF and dialyzed against dimethylsulfoxide (DMSO) for 48 h to remove unreacted reactants using dialysis tubing (MWCO=3500 Da), switching the dialysis solvent once at 24 h. After dialysis against DMSO, the polymer solution was dialyzed against water at 4 °C for 24 h, switching the dialysis solvent three times. The resulting drugamer was frozen and lyophilized for 72 h. ^{1}H-NMR was used to characterize the purified drugamer in DMSO-*d*6. RAL drug wt% was calculated by spiking the sample with a known concentration of Fasudil HCl as the internal standard. The ratio of integration of polymer RAL proton peaks at 7.06 and 7.29 ppm to the Fasudil HCl proton peak at 9.5 ppm was used to obtain the drug wt% (74.60 wt%). A full ^{1}H-NMR spectrum of a spiked sample is shown on **Fig S7**. The approximate molecular weight was calculated using monomer conversion by comparison of the vinyl peak integration before and after the polymerization (24000 Da). The polymer synthesized with the protocol described in this subsection was referred to as pRAL.

3.3.8. RAFT polymerization of RAL-SMA MSEMA comopolymer drugamers (p(RAL-SMA-co-MSEMA-co-RhMA))

RAFT polymerization of RAL-SMA and MSEMA and one RhMA per polymer chain was conducted in anhydrous DMF under inert argon atmosphere. ECT and V70 were used as the CTA and radical initiator, respectively. The initial monomer/CTA/initiator ($[M]_0$:$[CTA]_0$:$[I]_0$) ratio was 25:1:0.2, respectively. The initial feed ratio of RAL-SMA/MSEMA was roughly 1:1. RAL-SMA (400 mg, 0.609 mmol), MSEMA (98.8 mg, 0.560 mmol), RhMA (32.5 mg, 0.049

mmol), ECT (12.8 mg, 0.049 mmol), and V70 (3.01 mg, 0.010 mmol) were added to a 10 mL round-bottom flask and dissolved in anhydrous DMF (1.21 mL). Once a homogeneous solution was obtained, the flask was sealed with a rubber septum and purged with argon gas for 35 minutes. Subsequently, the flask is transferred to a preheated oil bath at 42 °C and allowed to react for 24 hours. The reaction was quenched by exposure to atmospheric air and the crude product was precipitated in diethyl ether. The precipitant was redissolved in DMF and dialyzed against DMSO for 48 h to remove unreacted reactants using dialysis tubing (MWCO=3500 Da), switching the dialysis solvent once at 24 h. After dialysis against DMSO, the polymer solution was dialyzed against water at 4 °C for 24 h, switching the dialysis solvent three times. The resulting drugamer was frozen and lyophilized for 72 h. ^{1}H-NMR was used to characterize the purified drugamer in DMSO-*d*6. RAL drug wt% was calculated by spiking the sample with a known concentration of Fasudil HCl as the internal standard. The ratio of integration of polymer RAL proton peaks at 8.89 and 9.99 ppm to the Fasudil HCl proton peak at 9.5 ppm was used to obtain the drug wt% (51.88 wt%). Final comonomer ratio in purified drugamer of RAL:MSEMA was calculated by comparing the ratio of integration of the RAL proton peaks at 7.12 and 7.32 ppm with MSEMA proton peaks at 4.23 and 4.42 ppm after subtracting the contribution to the integration from the overlapping RAL peaks (53:47, RAL:MSEMA, respectively). The approximate molecular weight was calculated using monomer conversion by comparison of the vinyl peak integration before and after the polymerization (8300 Da). The polymer synthesized with the protocol described in this subsection was referred to as pRAL-MSEMA.

3.3.9. RAFT polymerization of RAL-SMA Butyl-MA (BMA) comopolymer drugamers (p(RAL-SMA-co-BMA-co-RhMA))

RAFT polymerization of RAL-SMA and BMA and one RhMA per polymer chain was conducted in anhydrous DMF under inert argon atmosphere. ECT and V70 were used as the CTA and radical initiator, respectively. The initial monomer/CTA/initiator ($[M]_0$:$[CTA]_0$:$[I]_0$) ratio was 40:1:0.25, respectively. The initial feed ratio of RAL-SMA/BMA was roughly 0.85:0.15 RAL-SMA (400 mg, 0.609 mmol), BMA (12.7 mg, 0.090 mmol), RhMA (11.9 mg, 0.018 mmol), ECT (4.72 mg, 0.018 mmol), and V70 (1.38 mg, 0.004 mmol) were added to a 10 mL round-bottom flask and dissolved in anhydrous DMF (0.867 mL). Once a homogeneous solution was obtained, the flask was sealed with a rubber septum and purged with argon gas for 35 minutes. Subsequently, the flask is transferred to a preheated oil bath at 42 °C and allowed to react for 24 hours. The reaction was quenched by exposure to atmospheric air and the crude product was precipitated in diethyl ether. The precipitant was redissolved in DMF and dialyzed against DMSO for 48 h to remove unreacted reactants using dialysis tubing (MWCO=3500 Da), switching the dialysis solvent once at 24 h. After dialysis against DMSO, the crude product was dialyzed against water at 4 °C for 24 h, switching the dialysis solvent three times. The resulting drugamer was frozen and lyophilized for 72 h. ^{1}H-NMR was used to characterized the purified drugamer. ^{1}H-NMR was used to characterize the purified drugamer in DMSO-*d*6. RAL drug wt% was calculated by spiking the sample with a known concentration of Fasudil HCl as the internal standard. The ratio of integration of polymer RAL proton peaks at 7.07 and 7.29 ppm to the Fasudil HCl proton peak at 9.5 ppm was used to obtain the drug wt% (66.23 wt%). Final comonomer ratio in purified drugamer of RAL: BMA was calculated by comparing the ratio of integration of the RAL proton peaks at 7.12 and 7.32 ppm with MSEMA proton peaks at 4.15

and 4.39 ppm after subtracting the contribution to the integration from the overlapping RAL peaks (84:16, RAL:BMA, respectively). The approximate molecular weight was calculated using monomer conversion by comparison of the vinyl peak integration before and after the polymerization (18000 Da). The polymer synthesized with the protocol described in this subsection was referred to as pRAL-BMA.

3.3.10. Isolation of Atazanavir from Reyataz tablets

Atazanavir (ATV) was isolated as a neutral compound from Reyataz tablets (300 mg per tablet). Crushed Atazanavir tablets were incubated in DCM (120 mL) with TEA (3 mL) overnight at room temperature. The incubated suspension was extracted with deionized water (100 mL, 3x), and then with brine (100 mL, 2x). The organic layer was subsequently collected and dried with magnesium sulfate, and then filtered by vacuum filtration. The filtrate was then concentrated under reduced pressure, yielding white amorphous solids. The product was then dried over high vacuum overnight to provide white amorphous solids (yield=71.17%). The full ^{1}H-NMR spectrum is shown on **Fig S8**. ^{1}H NMR (300 MHz, DMSO) δ 9.10, 8.65, 8.64, 7.96, 7.44, 7.18, 5.01, 3.96, 3.95, 3.51, 2.80, 2.79, 2.78, 2.76, 0.76, 0.62. ^{13}C NMR (126 MHz, DMSO) δ 170.49, 156.47, 149.95, 139.44, 139.07, 137.98, 137.59, 129.51, 129.25, 128.43, 126.59, 126.27, 122.83, 120.42, 68.63, 52.15, 51.87, 40.57, 40.40, 40.24, 40.07, 39.90, 39.73, 39.57, 38.24, 34.04, 33.86, 27.14, 26.73.

3.3.11. Synthesis of ATV-SMA prodrug monomers by esterification via *1-Ethyl-3-(3'-dimethylaminopropyl) carbodiimide*

ATV (1000 mg, 1.42 mmol) was added to a to a 100 mL round flask and dissolved in anhydrous DCM (25 mL). In a separate 100 mL round flask, SMA (980 mg, 4.26 mmol), 1-ethyl-3-(3'-dimethylaminopropyl)carbodiimide (EDC, 1360 mg, 7.09 mmol), and 4-

dimethylaminopyradine (DMAP, 867 mg, 7.09 mmol) were dissolved in anhydrous DCM (25 mL). ATV solution was transferred to the other round flask via syringe and needle. The solution was allowed to react for 24 hours under argon gas at room temperature. The reaction was quenched by diluting in DCM (200 mL) and extracted with brine (2x, 100 mL), $NaHCO_3$ (1x, 100 mL), followed by brine (2x, 100 mL). The crude product was then purified by flash chromatography with a 3:1 mixture of DCM:acetone as the mobile phase. The desired fractions were then collected and concentrated under reduced pressure, yielding a yellow wax-like substance. The wax-like substance was redissolved in DCM and then precipitated with hexanes (40 mL). Precipitated solids were then dried overnight under high vacuum to yield white solids (yield=70.13%). The full ^{1}H-NMR spectrum is shown on **Fig S9**. ^{1}H NMR (300 MHz, DMSO) δ 8.96 (s, 1H), 8.64 (s, 1H), 7.93 (s, 5H), 7.34 (m, 3H), 7.18 (m, 5H), 6.67 (t, 2H), 6.03 (d, *J* = 0.7 Hz, 1H), 5.67 (t, 1H), 5.04 (s, 1H), 4.48 (d, *J* = 12.3 Hz, 1H), 4.30 (s, 4H), 3.95 (d, *J* = 9.0 Hz, 3H), 3.66 (d, *J* = 9.5 Hz, 1H), 3.54 (s, 3H), 3.43 (s, 3H), 3.04 (m, 1H), 2.89 (m, 1H), 2.68 (m, 6H), 1.86 (d, *J* = 0.6 Hz, 3H), 0.77 (d, *J* = 15.1 Hz, 18H). ^{13}C NMR (126 MHz, DMSO) δ 171.97, 171.14, 169.99, 168.90, 166.33, 155.98, 149.40, 138.39, 137.27, 137.02, 135.54, 129.14, 129.03, 127.78, 125.98, 125.88, 125.81, 122.25, 119.85, 72.40, 62.36, 61.96, 59.23, 57.75, 51.34, 51.21, 40.02, 39.85, 39.78, 39.69, 39.52, 39.35, 39.19, 37.59, 33.60, 33.54, 30.58, 28.85, 28.54, 26.46, 26.36, 17.84. ESI=MS for $C_7H_{13}O_3S$ [M]: 917.46.

3.3.12. RAFT polymerization of ATV homopolymer drugamers (p(ATV-SMA-co-RhMA))

RAFT polymerization of ATV-SMA and one RhMA per polymer chain was conducted in anhydrous DMF under inert argon atmosphere. ECT and V70 were used as the CTA and radical initiator, respectively. The initial monomer/CTA/initiator ($[M]_0$:$[CTA]_0$:$[I]_0$) ratio was 15:1:0.22, respectively. ATV-SMA (256 mg, 0.279 mmol), RhMA (13.9 mg, 0.021 mmol), ECT (5.27 mg,

0.020 mmol), and V70 (1.35 mg, 0.004 mmol) were added to a 10 mL round-bottom flask and dissolved in DMSO-*d*6 (0.798 mL). Once a homogeneous solution was obtained, the flask was sealed with a rubber septum and purged with argon gas for 35 minutes. Subsequently, the flask was transferred to a preheated oil bath at 42 °C and allowed to react for 8 hours. The reaction was quenched by exposure to atmospheric air and was isolated by precipitation in diethyl ether. The precipitant was redissolved in DMSO and dialyzed against DMSO for 48 h to remove unreacted reactants using dialysis tubing (MWCO=3500 Da), switching the dialysis solvent once at 24 h. After dialysis against DMSO, the crude product was dialyzed against water at 4 °C for 24 h, switching the dialysis solvent three times. The resulting drugamer was frozen and lyophilized for 72 h. ^{1}H-NMR was used to characterize the purified drugamer in DMSO-*d*6. ATV drug wt% was calculated by spiking the sample with a known concentration of Fasudil HCl as the internal standard. The ratio of integration of polymer ATV proton peaks at 7.06 and 7.29 ppm to the Fasudil HCl proton peak at 9.5 ppm was used to obtain the drug wt% (70 wt%). The molecular weight was calculated using monomer conversion by comparison of the vinyl peak integration before and after the polymerization (12000 Da). The polymer synthesized with the protocol described in this subsection was referred to as ATV.

3.3.13. RAFT polymerization of ATV-SMA MSEMA comopolymer drugamers (p(ATV-SMA-co-MSEMA-co-RhMA))

RAFT polymerization of RAL-SMA and MSEMA and one RhMA per polymer chain was conducted in DMSO-*d*6 under inert argon atmosphere. ECT and V70 were used as the CTA and radical initiator, respectively. The initial monomer/CTA/initiator ($[M]_0$:$[CTA]_0$:$[I]_0$) ratio was 25:1:0.2, respectively. The initial feed ratio of ATV-SMA/MSEMA was roughly 25:75. ATV-SMA (150 mg, 0.164 mmol), MSEMA (81.9 mg, 0.465 mmol), RhMA (17.4 mg, 0.026

mmol), ECT (11.5 mg, 0.044 mmol), and V70 (2.96 mg, 0.010 mmol) were added to a 10 mL round-bottom flask and dissolved in DMSO-*d*6 (0.847 mL). Once a homogeneous solution was obtained, the flask was sealed with a rubber septum and purged with argon gas for 35 minutes. Subsequently, the flask was transferred to a preheated oil bath at 42 °C and allowed to react for 24 hours. The reaction was quenched by exposure to atmospheric air and the crude product was precipitated in diethyl ether. The precipitant was redissolved in DMF and dialyzed against DMSO for 48 h to remove unreacted reactants using dialysis tubing (MWCO=3500 Da), switching the dialysis solvent once at 24 h. After dialysis against DMSO, the crude product was dialyzed against water at 4 °C for 24 h, switching the dialysis solvent three times. The resulting drugamer was frozen and lyophilized for 72 h. ^{1}H-NMR was used to characterize the purified drugamer in DMSO-*d*6. ATV drug wt% was calculated by spiking the sample with a known concentration of Fasudil HCl as the internal standard. ATV drug wt% was calculated by spiking the sample with a known concentration of Fasudil HCl as the internal standard. The ratio of integration of polymer ATV proton peaks at 7.06 and 7.29 ppm to the Fasudil HCl proton peak at 9.5 ppm was used to obtain the drug wt% (53.80 wt%). Final comonomer ratio in purified drugamer of ATV: MSEMA was calculated by comparing the ratio of integration of the ATV proton peaks at 8.95 ppm with MSEMA proton peaks at 4.23 and 4.42 ppm after subtracting the contribution to the integration from the overlapping RAL peaks (26:74, ATV: MSEMA, respectively). The approximate molecular weight was calculated using monomer conversion by comparison of the vinyl peak integration before and after the polymerization (5800 Da). The polymer synthesized with the protocol described in this subsection was referred to as pATV-MSEMA.

3.3.14. Cloud point determination of RAL drugamers

Solutions of drugamers in DMSO were prepared by dissolving drugamer in DMSO as a stock solution. The stock solution was diluted serially to obtain solutions with different concentrations of drugamer (300, 75, 37.5, 9.38, 4.69, 0.23 mg/mL). Initial solutions (10 µL) were titrated with 0.5-1 µL of water as the nonsolvent to induce precipitation. After every addition of water, 2 µL of the sample was analyzed using the Nanodrop. Cloud point was determined to be when the transmittance decreased by more than 2% (700, 750, and 800 nm, where minimal absorption occurs) for three wavelengths relative to the transmittance of a drugamer solution where no precipitation occurred. Transmittance decrease by greater than 2% was selected as the threshold due to the accuracy of the instrument reported to be typically within 2%; thus when the transmittance decreases by more than 2%, it can no longer be attributed to random error of the instrument. Once precipitation is achieved, the final water content in the solution is calculated to determine the water wt% required to induce drugamer precipitation. A complete summary of all cloud points determined is shown in **Table S1**.

3.4 RESULTS AND DISCUSSION

3.4.1. Synthesis of polymerizable prodrug monomer RAL-SMA

RAL-SMA was synthesized using a bottom-up approach wherein the drug was chemically modified to obtain prodrug monomers, which can then be polymerized as a homopolymer or copolymer drugamer. The hydroxyl group on the pyrimidine ring of RAL was considered to be a functional group amenable to functionalization without the need for protective groups. The RAL-SMA prodrug monomer with a hydrolyzable ethyloxysuccinyl (alkyl ester) linker was synthesized by a two-step esterification *via* an acyl chloride group, as shown in

Scheme 1. The ethyloxysuccinyl linker was intentionally selected due to the lesser steric bulk with greater spacing between the polymerizable moiety and drug, which can result in improved polymerization downstream [172]. Furthermore, despite phenyl ester linkers exhibiting greater hydrolizability than alkyl ester linkers, the ethyloxysuccinyl ester linker was expected to be cleavable due to the relatively low pK_a of RAL (pK_a=6.63), which is discussed in section 3.4.2 [105,161].

In the synthesis of RAL-SMA, a series of instrumental analysis was used to confirm successful esterification and preservation of the necessary moiety for polymerization and the pharmacophore. The hydroxyl proton of RAL (**Fig 3.1**) was no longer detected in the ^{1}H-NMR spectrum of RAL-SMA (**Fig 3.1**), indicating the esterification from the reaction of an alcohol with an acyl chloride. The RAL peaks as shown in **Fig 3.1A** were preserved in the ^{1}H-NMR of RAL-SMA in **Fig 3.1C**, indicating the preservation of the pharmacophore. The formation of an alkyl ester linkage is confirmed by the comparison of ^{13}C-NMR spectrum. The disappearance of the hydroxyl carbon (δ =124.88 ppm) of RAL and appearance of downstream signals (δ =160-175 ppm) in the ^{13}C-NMR spectra of RAL-SMA demonstrated the successful esterification of RAL and SMA. The formation of RAL-SMA was further confirmed by LCMS, where the observed signal has a m/z ratio of 657.2, which matches the calculated exact mass (656.2 Da). The purity of RAL-SMA was assessed with ^{19}F-NMR. ^{19}F-NMR is a sensitive nucleus that shows a wide range of chemical shifts. The fluorine on the fluorophenyl group of RAL and RAL-SMA exhibit peaks with unique and resolved chemical shifts in their respective spectra. The ^{19}F-NMR spectrum of RAL-SMA shown in **Fig S5** shows just one singlet peak with a unique chemical shift compared to the ^{19}F-NMR of RAL. Due to the wide range of chemical

shift associated with ^{19}F-NMR, the singlet arose solely from the fluorine of RAL-SMA, as the fluorine signal of RAL was resolved from RAL-SMA, thus indicating a pure product.

Despite the low yield obtained *via* coupling with acid chloride, it was the most optimal coupling route in all the esterification routes that were explored. For example, coupling with hexafluorophosphate benzatriazole tetramethyl uronium (HBTU) was also explored, which have been used in esterification of phenolic and primary aliphatic esters[173]. However, the yield (8.99%) was far lower compared to the yield of the acid chloride route (24.18%). Furthermore, esterification via the HBTU route yielded unwanted side products that could be detected with ^{19}F-NMR despite rigorous purification, which was likely a hexafluorophosphate salt. Other studies have demonstrated the limited applicability of HBTU coupling due to formation of side-products[174]. Esterification via the acid chloride route had a greater yield due to the greater, which offered good yield when reacting with extremely hindered groups[175].

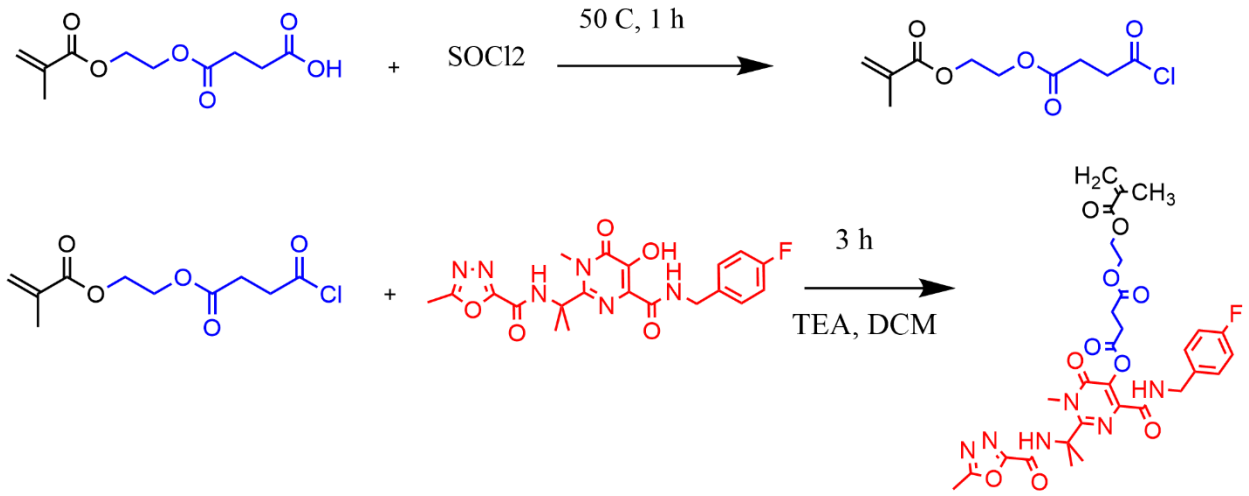

Scheme 3. 1. Synthesis of polymerizable prodrug RAL-SMA by acid chloride

RAL: raltegravir; SMA: mono-2-(methacryloyloxy)ethyl succinate; SOCl2: thionyl chloride; TEA: triethylamine; DCM: dichloromethane. Black corresponds to the methacrylate group that is

reacted to obtain the polymer backbone. Blue corresponds to the linker/spacer. Red corresponds to the drug.

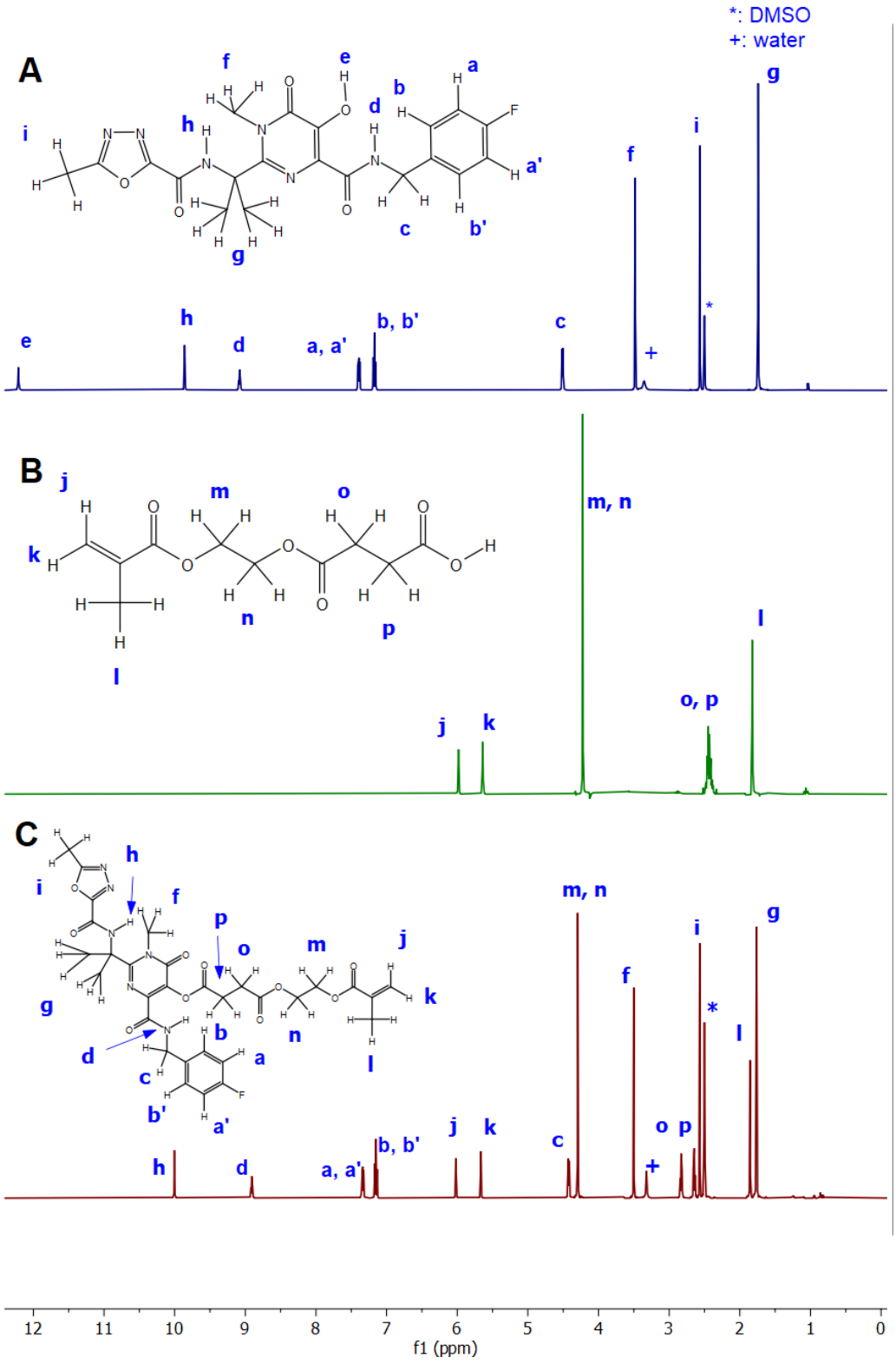

Fig 3. 1. Stacked ^{1}H-NMR spectra in DMSO-*d*6 of the reactants used in the esterification to obtain RAL-SMA and the final product

(A) RAL. (B) SMA. (C) RAL-SMA. Protons were assigned based on the splitting patterns and integration. Protons from the same moiety were annotated in the same way in the reactant and product. The disappearance of the hydroxyl peak (annotated as "e") and downfield shift of methylene peaks of SMA (annotated as "o, p") indicated the successful esterification, which was further confirmed with LCMS and ^{13}C-NMR analysis (**Fig S4**).

3.4.2. Stability of RAL-SMA in polar aprotic solvents

To confirm the stability of the cleavable alkyl ester bond throughout the duration of polymerization, RAL-SMA was incubated at elevated temperatures and the degree of hydrolysis was tracked longitudinally. The use of thermal initiators have been explored thoroughly in RAFT polymerization, and thus was selected as the source of radicals for polymerization downstream [176,177]. Polar aprotic solvents have been used in free radical polymerization to a greater success compared with other organic solvents [178]. RAL-SMA was dissolved in DMSO or DMF, and the percentage of hydrolysis was measured by analyzing the ratio of RAL to RAL-SMA at designated time points. Fitting timepoints determined the half-life of RAL-SMA to a nonlinear (weighted) least-squares model fit and determined the time at which 50% of the hydrolysis occurred based on the model. The alkyl ester linking RAL to SMA was easily cleavable, which has been attributed to the low pK_a of RAL (pK_a=6.63±0.02), making RAL an excellent leaving group and the alkyl ester easily hydrolysable [105,179].

The half-lives of RAL-SMA in selected conditions are summarized in **Table 3.1**. RAL-SMA demonstrated shorter half-lives in higher temperatures, as shown by comparing the half-lives (18.5 and 8.4 h) in 45 and 70 °C in DMSO, respectively. A similar trend could be observed

in the half-lives (110.8 and 57.5 h) of RAL-SMA when comparing 35 and 45 °C in DMF, respectively. RAL-SMA also exhibited greater stability in DMF as opposed to DMSO. The driving mechanism to prodrug instability in the different solvents and at different temperatures was outside the scope of this dissertation, but nevertheless provided optimal conditions to conduct polymerization of the prodrug monomer, while allowing drug to still be conjugated to the polymer backbone throughout the duration of polymerization. Polymerization was ultimately chosen to be conducted in DMF at 45 °C due to the greater monomer stability. Furthermore, 45 °C was greater than the thermal decomposition (30 °C) of V70 to initiate polymerization [180]. Polymerization in DMF at 35 °C was attempted but will not be discussed in this dissertation due to the low monomer conversion.

Table 3. 2. Half-lives of RAL-SMA in DMSO and DMF

Solvent	***Temperature (°C)***	$t_{1/2,\ RAL\text{-}SMA}$ ***(h)***
DMSO	70	8.4
DMSO	45	18.5
DMF	45	57.5
DMF	35	110.8

3.4.3. Synthesis of polymerizable prodrug ATV-SMA

In the effort to design polymerizable prodrugs of antiretrovirals with different mechanisms of action, we synthesized a prodrug monomer of a protease inhibitor, ATV. Protease inhibitors are potent drugs and have the potential for monotherapy in long-term therapy [181]. ATV was selected because it contained a secondary hydroxyl group that can be used for esterification. Like RAL-SMA, SMA was selected due to an ethylene glycol spacer for better

polymerization. Greater yield was obtained with ATV-SMA than RAL-SMA, which might be attributed to the higher pK_a of the hydroxyl group of ATV (pK_a=11.92) compared to RAL (pK_a=6.63), making ATV a poorer leaving group and likely with fewer synthesized prodrugs converting back to the unconjugated drug during prodrug synthesis [105,182]. ATV was successfully conjugated to SMA such that the methacrylate moiety could be utilized for polymerization downstream.

ATV was conjugated to SMA via one-step EDC/DMAP route by coupling the secondary hydroxyl group with the carboxylic acid of SMA to obtain a reversible alkyl ester linkage (**Scheme 3.2**). Confirmation of successful synthesis was confirmed through a series of instrumental analysis. The disappearance of the peak (δ=~3.95 ppm, annotated as "u" in **Fig 3.2A**) of ATV indicated successful esterification. The downfield shift of the proton adjacent to the secondary hydroxyl group (δ=4.49 ppm, multiplet annotated as "i" in **Fig 3.2C**) further confirmed the formation of ATV-SMA. Characteristic peaks of ATV and SMA were observed in the ^{1}H-NMR spectrum of ATV-SMA. Vinyl peaks (δ=5.67 and 6.03 ppm) observed in ATV-SMA suggested polymerizable promoiety, or the methacrylate group, was preserved in the coupling reaction. Lastly, the formation of ATV-SMA was confirmed by LCMS, where the observed signal has a m/z ratio of 917.4, which matches the calculated exact mass (916.4 Da).

Esterification with EDC/DMAP was selected when synthesizing ATV-SMA due to the greatest yield obtained. Esterifications via HBTU and acyl chloride were explored but resulted in poor yields (0% and 12.59% for HBTU and acyl chloride coupling, respectively). Poor yield with HBTU might be attributed to the poor sterics hindering the reaction of the activated ester of SMA with ATV [183]. Coupling with acyl chlorides may have resulted in poor yields due to the numerous side reactions occurring simultaneously [183]. The *O*-acylisourea intermediate may be

less sterically hindered from reacting with the hydroxyl group compared to the activated ester obtained with HBTU coupling.

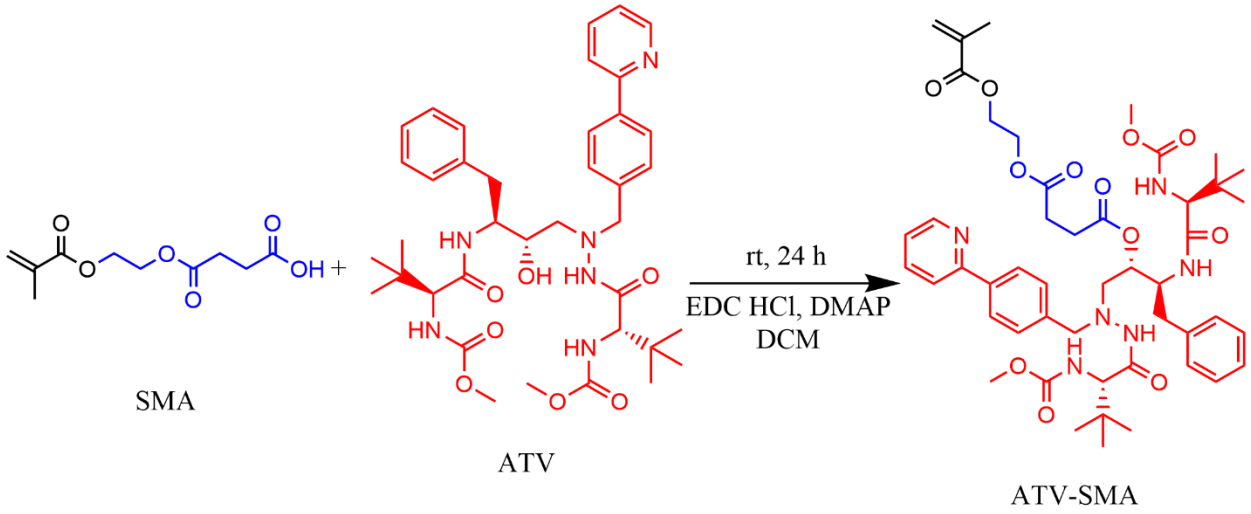

Scheme 3. 2. Synthesis of polymerizable prodrug ATV-SMA by EDC/DMAP

ATV: atazanavir; SMA: mono-2-(methacryloyloxy)ethyl succinate; EDC HCl: 1-ethyl-3-(3-dimethylaminopropyl) carbodiimide hydrochloride; DMAP: 4-dimethylaminopyridine; DCM: dichloromethane. Black corresponds to the methacrylate group that is reacted to obtain the polymer backbone. Blue corresponds to the linker/spacer. Red corresponds to the drug.

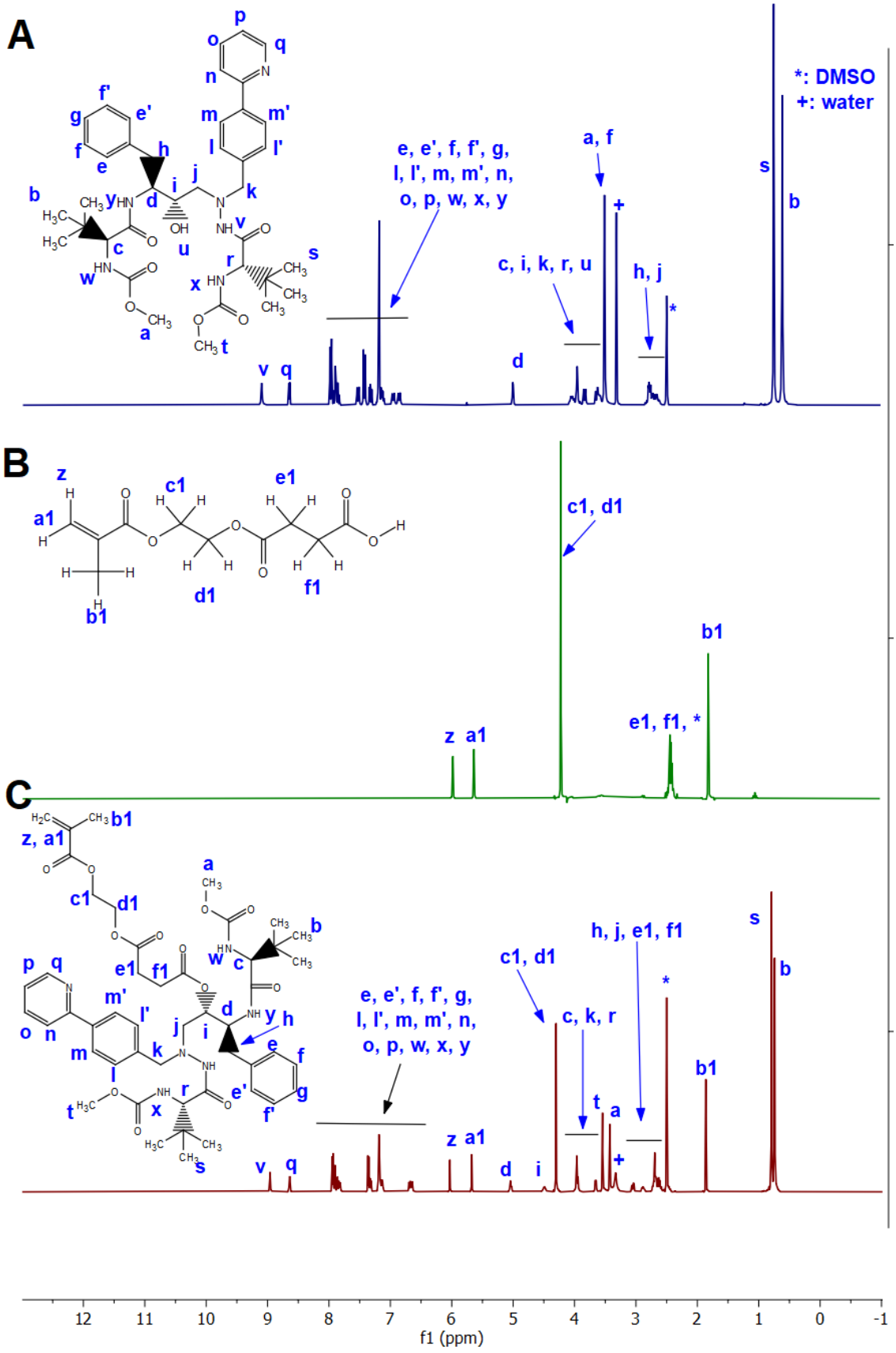
A
*: DMSO
+: water
e, e', f, f', g, l, l', m, m', n, o, p, w, x, y
a, f
c, i, k, r, u
h, j
B
c1, d1
b1
e1, f1, *
z a1
C
h, j, e1, f1
c1, d1
c, k, r
e, e', f, f', g, l, l', m, m', n, o, p, w, x, y
12 11 10 9 8 7 6 5 4 3 2 1 0 -1
f1 (ppm)

Fig 3. 2. Stacked ^{1}H-NMR spectra in DMSO-d6 of the reactants used in the esterification to obtain ATV-SMA and the final product

(A) ATV. (B) SMA. (C) ATV-SMA. Protons were assigned based on the splitting patterns and integration. Protons from the same moiety were annotated in the same way in the reactant and product. The disappearance of the hydroxyl peak (annotated as "u") and the downfield shift of the proton adjacent to the hydroxyl group (annotated as "i") indicate the successful esterification.

3.4.4. Design and synthesis of RAL homopolymer drugamer

RAL homopolymers (pRAL) were synthesized by RAFT polymerization to obtain a polymeric prodrug using RAL as the building blocks of the polymer. RAL homopolymers were designed to maximize the mass fraction or loading of RAL within the polymer. RhMA was copolymerized with both copolymers with a degree of polymerization of 1 for imaging and tracking purposes for studies downstream. Polymerization of RAL-SMA was carried out with ECT as the CTA and V70 as the thermal initiator in DMF at 45 °C over 8 h, with a resulting monomer conversion of 87.44% (**Scheme 3.3**). RAL content was calculated to be 74.60 wt%. RAL homopolymer drugamer was purified with a series of dialysis to remove unreacted prodrug monomers and organic solvents. Characterization of pRAL was summarized in **Table 3.2**.

A series of ^{1}H-NMR analysis confirmed successful polymerization (**Fig 3.3**). Monomer conversion was confirmed by comparing the integration of the vinyl peaks at δ=5.67 and 6.03 ppm at the beginning and end of the reaction. Drug content could be measured by spiking polymer with known amounts of Fasudil HCl as the internal standard. By comparing the integration of the singlet peak of the internal standard at δ=9.95 ppm with integration of peaks of the drug, the molar amount of drug could be calculated, which could be further calculated to obtain the drug content in mass.

In summary, homopolymers of RAL prodrug monomers were synthesized with high drug loading. A key challenge in long-acting technologies treating HIV is the need for medicines with maximum drug loading to keep administration volume at a minimum [11]. RAL drugamers offer the advantage of very high drug loading, as the building blocks of the polymer are the drugs itself.

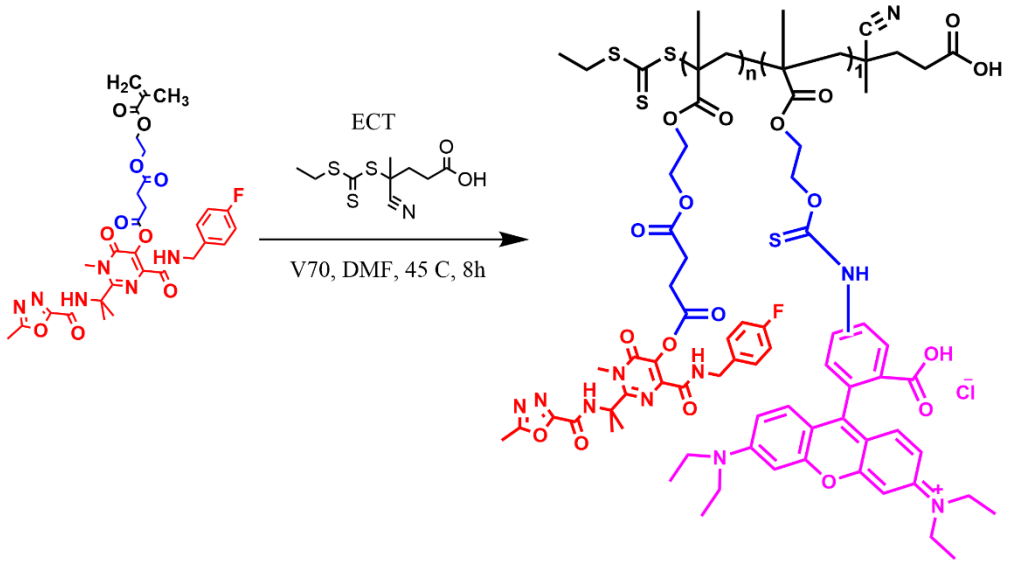

Scheme 3. 3. Polymerization of RAL-SMA to obtain RAL homopolymer drugamer

Black corresponds to the methacrylate group that is reacted to obtain the polymer backbone. Blue corresponds to the linker/spacer. Red corresponds to the drug. Pink corresponds to the rhodamine monomer unit with a theoretical DP of 1 in each polymer chain. ECT: 4-cyano-4-[(ethylsuflanylthiocarbonyl)sulfanyl]pentanoic acid. V70: 2,2'-azobis(4-methoxy-2,4-dimethylvaleronitrile). DMF: dimethylformamide.

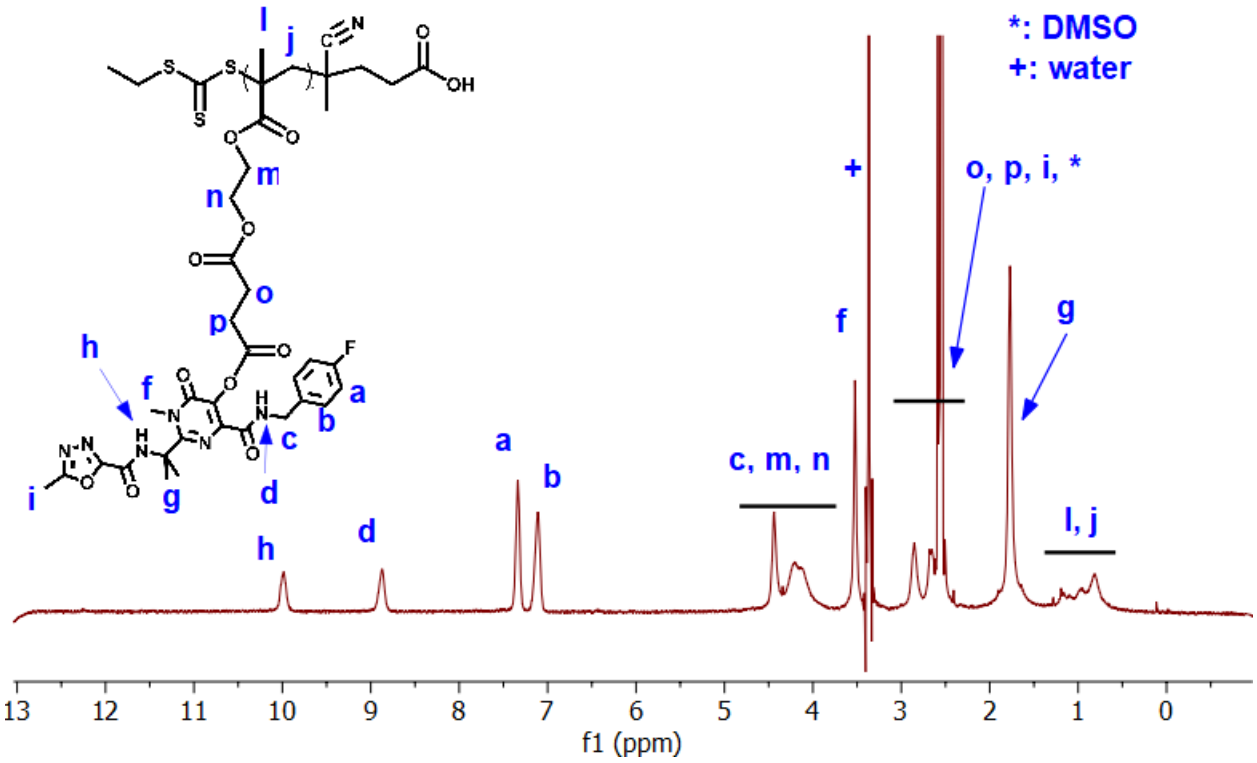

Fig 3. 3. Representative ^{1}H-NMR spectra of RAL homopolymer drugamer with assigned protons

3.4.5. Design and synthesis of RAL copolymer drugamers with MSEMA and BMA

In order to modulate the sustained release of RAL, a family of RAL random copolymer drugamers were synthesized with tunable hydrophilicity. We selected the random polymerization of RAL-SMA with hydrophilic or hydrophobic comonomers to tune the hydrophilicity of the drugamer, and thereby varying the degree of water penetration to tune release rate *in vivo*. In the effort to synthesize a more hydrophilic RAL drugamer, RAL-SMA was copolymerized with 2-(methylsulfinyl)ethyl methacrylate (MSEMA), a biocompatible DMSO-analogue methacrylate monomer[184]. MSEMA was synthesized in-house by a typical oxidation procedure with 2-(methylthio)-ethyl methacrylate (MTEMA). RAL-SMA was copolymerized with MSEMA at a molar feed ratio of 50:50, respectively, with a target degree of polymerization of 25 (**Scheme**

3.4A). We also hypothesized that the release of RAL can be slowed by copolymerizing with a lipophilic monomer to decrease water penetration. Thus, to obtain a more hydrophobic RAL drugamer, butyl methacrylate (BMA) was selected as monomer due to the commercial availability, as well as other studies demonstrating the biocompatibility and usage as drug delivery coating and primers of poly(*n*-butyl methacrylate (PBMA)[185–187]. RAL-SMA was copolymerized with BMA at a molar feed ratio of 85:15, with a target degree of polymerization of 40 **(Scheme 3.4B**). Like the RAL homopolymer, RhMA was copolymerized with both copolymers with a degree of polymerization of 1 for imaging and tracking purposes for studies downstream.

RAL-MSEMA copolymer drugamers (pRAL-MSEMA) were synthesized by RAFT polymerization and resulted in a monomer conversion of 80.52% with RAL content of 51.88 wt%. RAL-BMA copolymers (pRAL-BMA) were synthesized by RAFT polymerization and resulted in a monomer conversion of 77.73% and RAL content of 66.23 wt%. Characterization of RAL copolymer drugamers was summarized in **Table 3.2**. Successful polymerization was also analyzed with ^{1}H-NMR (**Fig 3.4**), with similar characterization as described in subsection 3.4.3. Ratio of comonomers could be calculated by comparing characteristic peaks of RAL with that of the comonomer at δ=4.15 and 4.23 ppm for BMA and MSEMA, respectively. Experimental molar ratios of monomers were comparable with feed molar ratios of monomers. The characterization results of pRAL-MSEMA and pRAL-BMA were summarized in **Table 3.2**.

We aimed to change the polymer comonomer composition in order to tune the release of RAL from the polymer backbone. Different linkers could be employed to modulate the release rate of RAL, such as phenolic ester linkers and enzyme cleavable linkers[161,168]. Aliphatic alkyl ester linkers are relatively more stable towards hydrolysis, as shown by the work of Das *et*

al. comparing alkyl and phenyl ester linkers. However, as subsection 3.4.2 has demonstrated, the alkyl ester linker is particularly susceptible to hydrolysis due to the low pK_a of RAL (pK_a=6.63±0.02), indicating tuning the release with different linkers could only accelerate release instead of tuning for both slower and faster release. Thus, a copolymerization approach was taken to modulate the degree of water penetration. We hypothesize that the release of RAL can be tuned by copolymerization of RAL prodrug monomers (RAL-SMA) with a water soluble comonomer to increase water penetration within the polymer. Block copolymerization has been studied extensively regarding self-assembling capabilities for drug delivery [188–190]. However, self-assembled structures were not necessary to the design of the polymeric prodrug, thus random copolymerization was employed for the more facile synthesis.

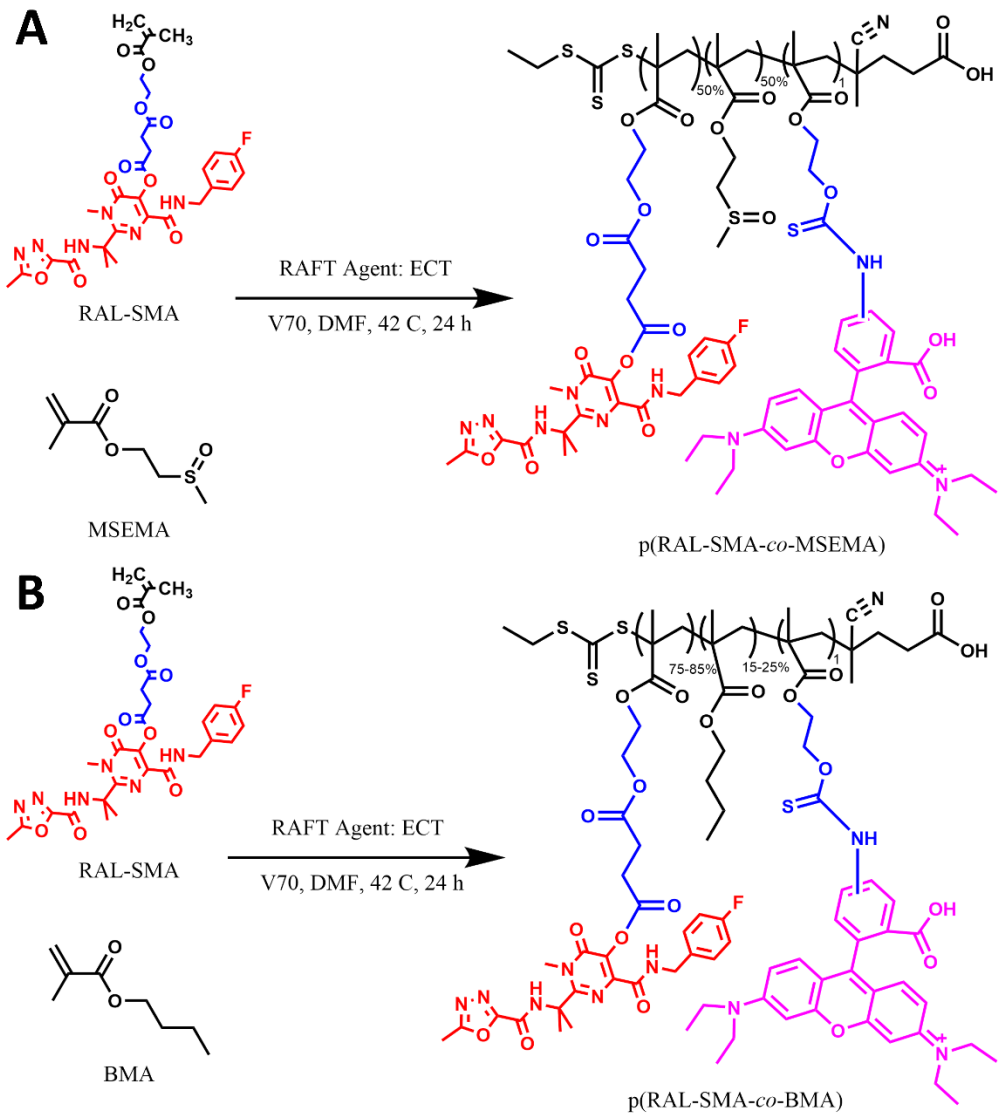

Scheme 3. 4. Copolymerization of RAL-SMA copolymer drugamer with tunable release

Black corresponds to the methacrylate group that is reacted to obtain the polymer backbone. Blue corresponds to the linker/spacer. Red corresponds to the drug. Pink corresponds to the rhodamine monomer unit with a theoretical DP of 1 in each polymer chain. (A) Polymerization of RAL-MSEMA copolymer (p(RAL-SMA-*co*-MSEMA)). (B) Polymerization of RAL-BMA copolymers (p(RAL-SMA-*co*-BMA)).

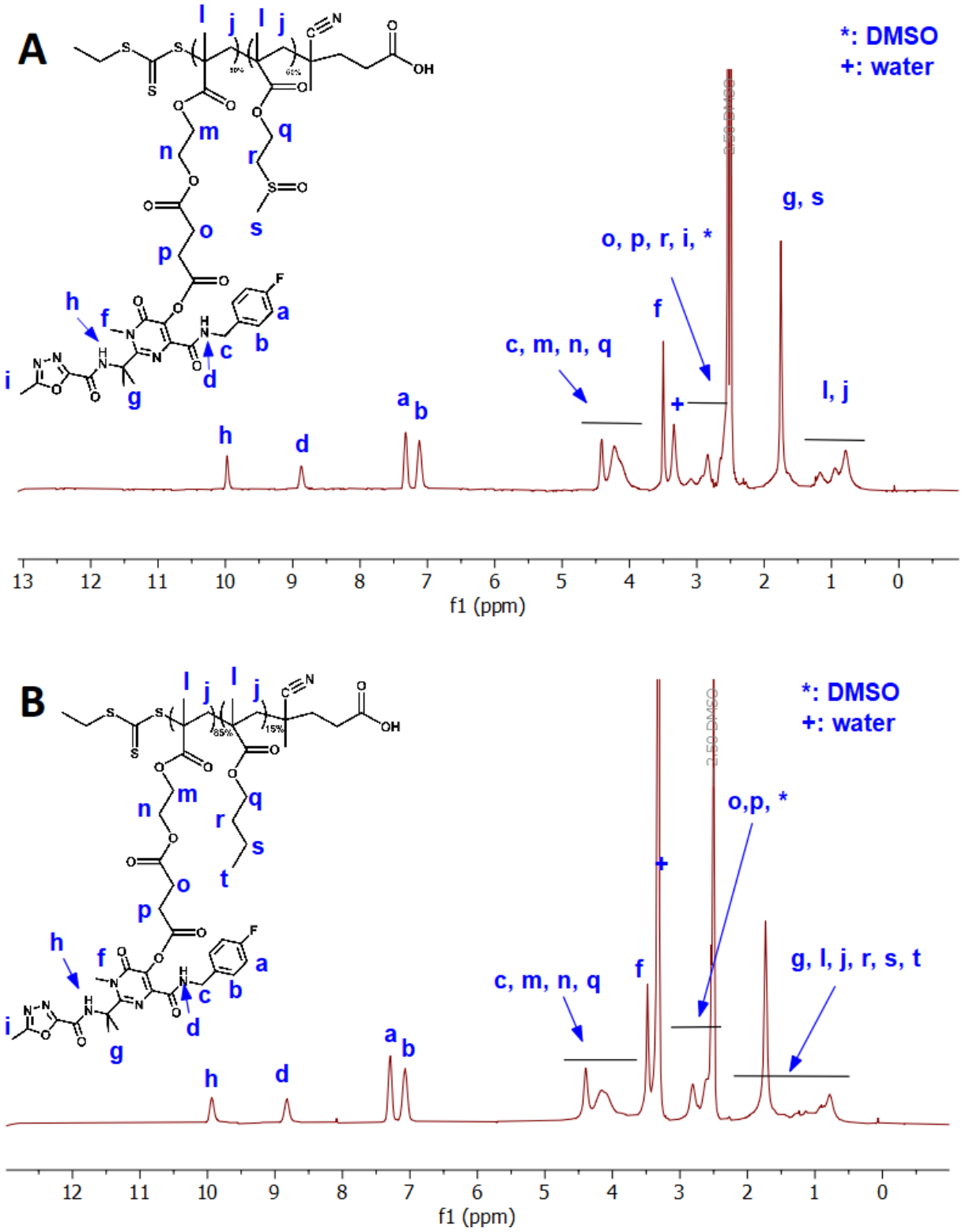

Fig 3. 4. Representative ^{1}H-NMR spectra of RAL copolymer drugamer with assigned protons

(A) RAL-MSEMA copolymer. (B) RAL-BMA copolymer.

Table 3. 3. Summary of characterization of drugamers detailing polymer composition, molecular weight, and RAL content.

Polymer	***RAL-SMA (feed) mol%***	***RAL-SMA (exp) mol%***	***Co monomer (feed) mol%***	***Co monomer (exp) %***	***M_n [a] (kDa)***	***RAL wt%[b]***
pRAL	100	100	N/A	N/A	24	74.60
pRAL-MSEMA	50	53.32	50[c]	46.67[c]	8.3	51.88
pRAL-BMA	85	84.21	15[d]	15.79 [d]	18	66.23

[a]As determined by ^{1}H-NMR using the conversion and initial feed ratio of monomer and CTA.
[b]As determined by ^{1}H-NMR with DMSO-*d*6 as the solvent using Fasudil HCl as the internal standard and known mass of polymer.
[c]MSEMA was the comonomer.
[d]BMA was the comonomer.

3.4.6. Design and synthesis of ATV homopolymer and copolymer drugamers

In the effort to make LA formulations of protease inhibitors, a family of ATV drugamers for tunable release of ATV was synthesized by RAFT polymerization. A homopolymer drugamer of ATV (pATV) with alkyl ester linkers was synthesized in order to maximize the total drug content. RAFT polymerization of the ATV homopolymer drugamer was carried out at 42 °C in DMSO-*d*6 over 23 h. The polymerization conditions were selected due to the stability of ATV-SMA in these conditions (section **S1** and **Fig S10**). The target degree of polymerization was 12 ATV monomers and 1 monomer of RhMA for imaging purposes downstream. A monomer conversion of 86% was achieved, which was obtained by comparing change in peak integration of vinyl peaks in the ^{1}H-NMR spectra of the sample before and after the polymerization (**Fig 3.5A**). Drug loading was calculated by spiking samples with a known

amount of Fasudil HCl, which was determined to be 70.42 wt%. A copolymer with MSEMA was also carried out by RAFT polymerization to obtain a more hydrophilic drugamer. The target degree of polymerization was also 12 with 1 monomer of RhMA for imaging purposes. The feed molar ratio of ATV and MSEMA was 25:75, respectively. Monomer conversion and drug loading was calculated in the same way as the ATV homopolymer with ^{1}H-NMR (**Fig 3.5B**). Copolymerization of ATV-SMA and MSEMA achieved a monomer conversion of 99.36%. Drug loading was calculated to be 53.80 wt%. The characterization results were summarized in **Table 3.3**.

In the effort to increase the release rate of ATV, the polymer comonomer composition was changed to increase the hydrophilicity of ATV drugamers to increase water penetration as a drug depot *in vivo*. With increased water penetration, hydrolysis of ATV from the polymer backbone would likely accelerate. Like the copolymers of RAL drugamers, MSEMA was chosen to increase the hydrophilicity of the drugamer, such that greater water penetration could be achieved after the formation of a depot *in vivo*. However, unlike the pRAL-MSEMA, the ATV-MSEMA copolymer drugamer (pATV-MSEMA) contained a much higher proportion of MSEMA to drug (50:50 versus 25:75 of drug:MSEMA for RAL and ATV drugamers, respectively). As discussed in subsection 3.4.3., the hydroxyl group of ATV has a high pK_a (pK_a=11.92), thus making it a poor leaving group, and thus ATV prodrugs are expected to have a slower release than RAL due to the inherent characteristic of the drug itself [191]. The greater MSEMA content in the polymer backbone can provide a greater degree of water penetration to achieve the desired drug release rate. This hypothesis will be further tested with *in vivo* studies in murine models.

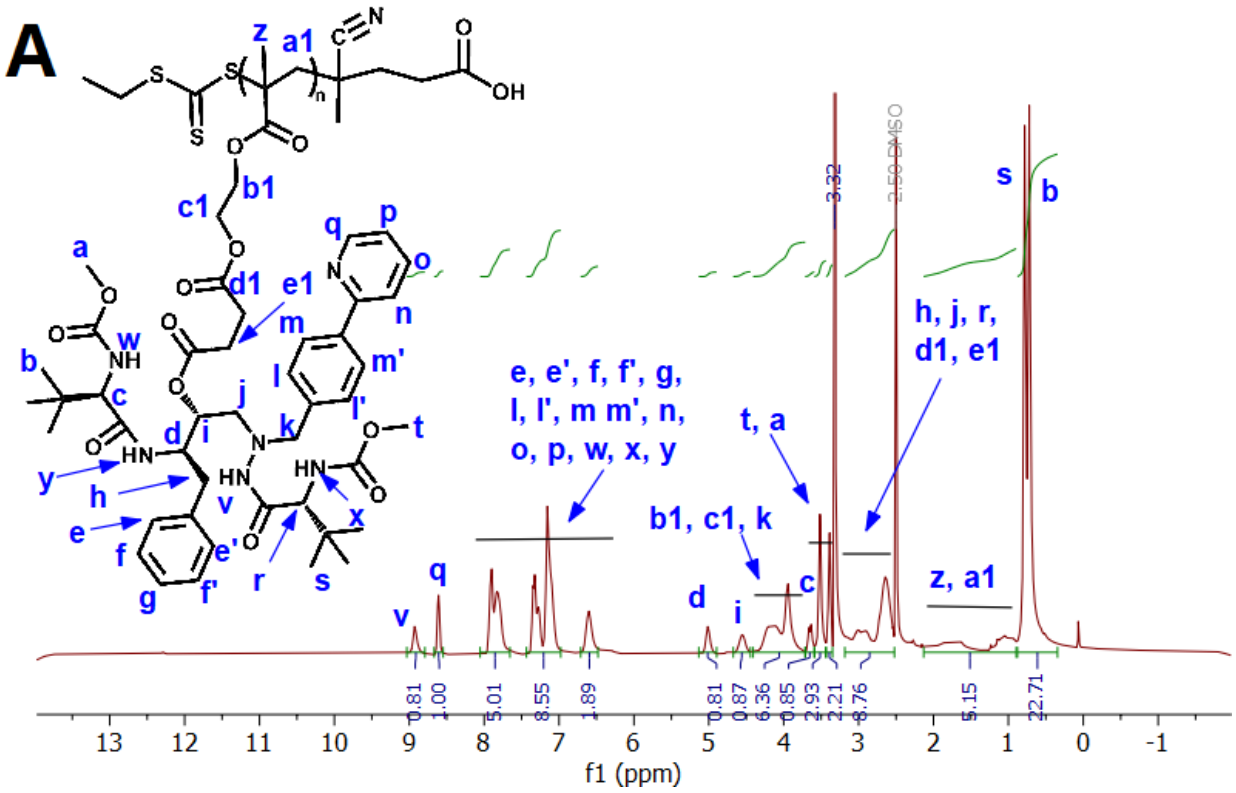
A
z
a1
n
OH
c1
b1
d1
e1
m
m'
l
l'
j
k
i
d
h
y
e
f
g
f'
e'
r
s
v
x
t
w
a
b
c
q
p
o
n
3.32
2.50 DMSO
s
b
h, j, r,
d1, e1
e, e', f, f', g,
l, l', m m', n,
o, p, w, x, y
t, a
b1, c1, k
z, a1
0.81
1.00
5.01
8.55
1.89
0.81
0.87
6.36
0.85
2.93
2.21
8.76
5.15
22.71
13 12 11 10 9 8 7 6 5 4 3 2 1 0 -1
f1 (ppm)

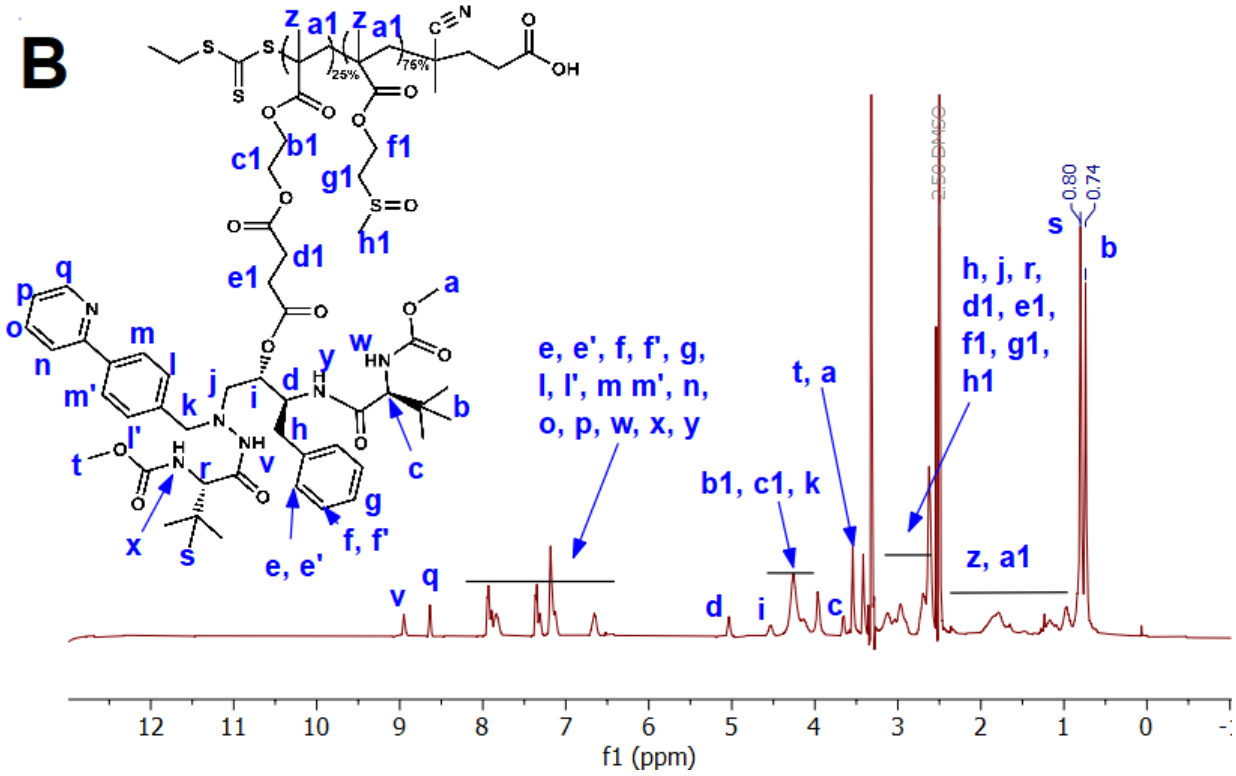
B
z
a1
25%
75%
OH
c1
b1
f1
g1
h1
d1
e1
a
w
y
x
s
t
l'
m'
n
o
p
q
m
l
k
j
i
d
h
v
r
g
f, f'
e, e'
c
b
2.50 DMSO
0.80
0.74
h, j, r,
d1, e1,
f1, g1,
h1
e, e', f, f', g,
l, l', m m', n,
o, p, w, x, y
t, a
b1, c1, k
z, a1
12 11 10 9 8 7 6 5 4 3 2 1 0
f1 (ppm)

Fig 3. 5. Representative ^{1}H-NMR spectra of ATV homopolymer and copolymer drugamer with assigned protons

(A) pATV. (B) pATV-MSEMA.

Table 3. 4. Summary of characterization of drugamers detailing polymer composition, molecular weight, and ATV content.

Polymer	***ATV-SMA (feed) mol%***	***ATV-SMA (exp) mol%***	***Co monomer (feed) mol%***	***Co monomer (exp) %***	***M_n [a] (kDa)***	***ATV wt%[b]***
pATV	100	100	N/A	N/A	12	70.42
pATV-MSEMA	25	75	26.11[c]	73.89[c]	5.8	53.80

[a]As determined by ^{1}H-NMR using the conversion and initial feed ratio of monomer and CTA.
[b]As determined by ^{1}H-NMR with DMSO-*d*6 as the solvent using Fasudil HCl as the internal standard and known mass of polymer.
[c]MSEMA was the comonomer.

3.4.7. Assessment of different physical properties of RAL drugamers with varying polymer comonomer compositions.

It was hypothesized that the hydrophilicity of the RAL drugamers could be tuned by changing the comonomer composition, and thus controlling the degree of water penetration that drives drug release [38]. Based on the composition in the polymer backbone, our RAL drugamers were expected to have the following relative release rate from fastest to slowest: pRAL-MSEMA > pRAL > pRAL-BMA. The hydrophilicity of RAL drugamers was compared by observing the critical nonsolvent (water) content necessary to induce polymer precipitation from an organic solution. Drugamers undergo a phase inversion due to the drugamer's inherent

hydrophilicity/hydrophobicity and form a depot at the injection site *in situ*, therefore, it is critical to investigate the precipitation behavior of RAL drugamers. To test for varying hydrophilicity, RAL drugamer solutions formulated in DMSO at different concentrations (4.69-300 mg/mL) were prepared by serial dilution and titrated with water until precipitation was observed. Following the addition of water droplets into polymer solutions, an exchange between DMSO and water occurs, which drives the polymer into a thermodynamically unstable state, wherein the chemical potential of the solid phase is lower (i.e., at a more stable state), resulting in the solidification of the polymer once a critical amount of DMSO effluxes to the aqueous phase [39,192]. Precipitation was observed by measuring the transmittance change, indicating the formation of a suspension, which was defined as the cloud point. We observed RAL drugamers with polymer backbones that include hydrophobic monomers exhibited cloud points with lower water mass fractions.

Over the range of concentrations, a lower water mass fraction was required to induce precipitation in pRAL-BMA, while a greater water mass fraction was required for pRAL-MSEMA. The ternary component system (drugamer, DMSO, and water) was represented in the ternary plot shown in **Fig 3.6**. The binodal curve divides the possible compositions yielding a monophasic or multiphasic mixture, which can be determined experimentally with the cloud point measurements mentioned above [193,194]. The shift of the binodal curve in the ternary phase diagram (RAL drugamer/DMSO/water, **Fig 3.6**) towards the polymer-nonsolvent axes further represented the greater affinity to water (nonsolvent) in the following order: pRAL-MSEMA > pRAL > pRAL-BMA. When comparing the different RAL drugamers, the shift of binodal curve could be observed in the general translation along the bottom axis towards lower water mass fraction. The shift of the binodal curve was due to the affinity towards water, which

was reflected in the range of compositions of polymer/solvent/nonsolvent remains in a thermodynamically stable state in a singular phase. The greater affinity to water reflected the range of hydrophilicity in RAL drugamers, which was in agreement with the comonomers incorporated in the polymer backbone. Thus, the hydrophilicity of the pRAL-MSEMA required a greater amount of water to induce precipitation. In contrast, the pRAL-BMA is more hydrophobic, and reaches thermodynamic instability with less water, resulting in polymer precipitation with a lower water fraction in the ternary system. As mentioned earlier, this result would suggest to have the following relative release rate from fastest to slowest: pRAL-MSEMA > pRAL > pRAL-BMA. This is due to the water penetration being dependent upon the contact angle, as illustrated previously by Choi and Liang [195]. One may argue that a contact angle experiment would be a more appropriate measurement to predict the relative release rate, but it was critical to determine the precipitation behavior of the drugamers to evaluate the ability to form depots *in situ* when injected into animal models. In addition, given that only two ATV drugamers were synthesized, the precipitation behavior of ATV drugamers was not studied, as well as the significantly greater MSEMA content in pATV-MSEMA compared to pRAL-MSEMA. Thus, the precipitation behavior between ATV drugamers were expected to follow a similar trend as RAL drugamers. In summary, RAL drugamers were confirmed to have varying degrees of hydrophilicity and should exhibit different release profiles when administered as a subcutaneous injection.

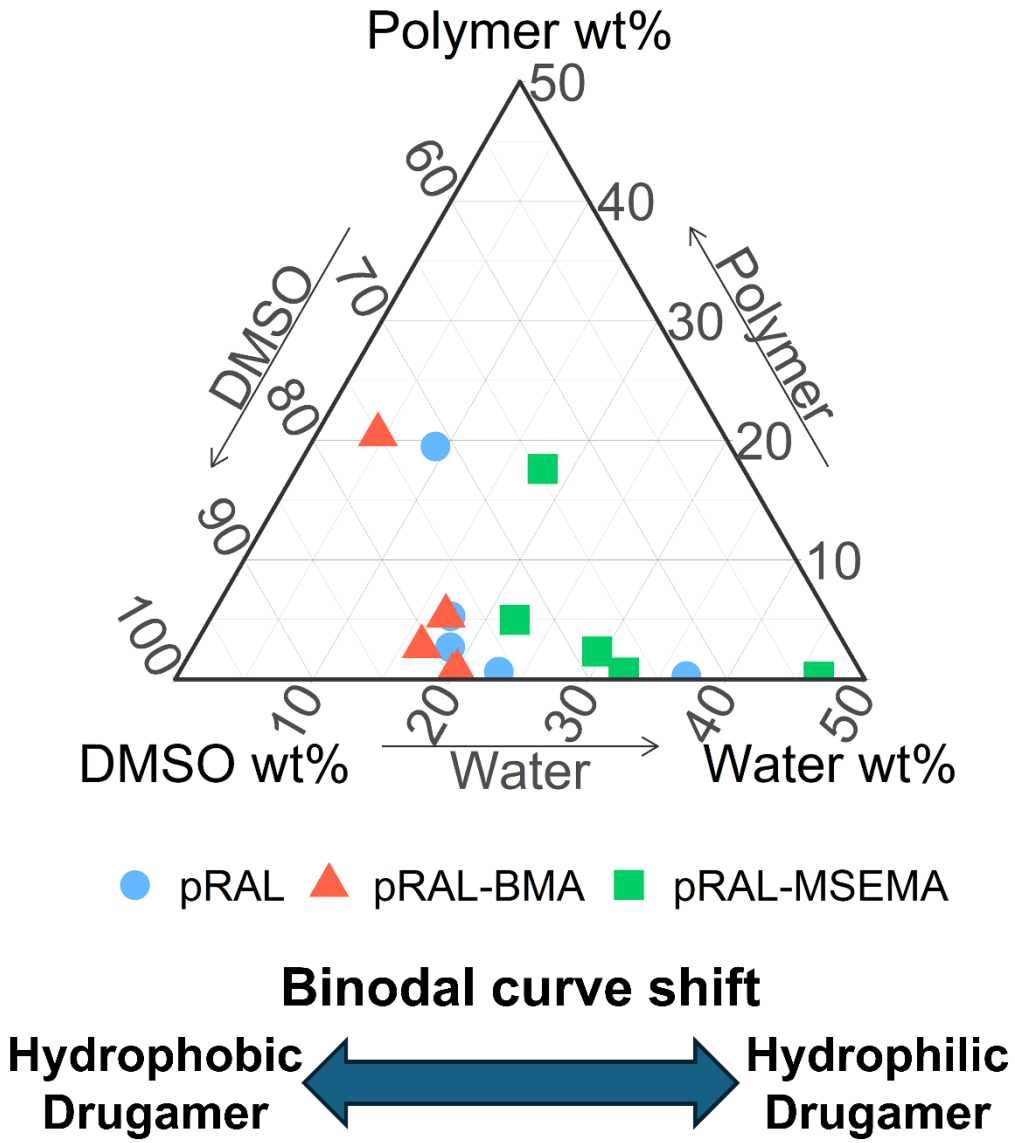

Fig 3. 6. Nonsolvent induced precipitation of RAL homopolymer and copolymer drugamers

A ternary phase diagram of different RAL drugamers. Cloud points were determined by titration of polymer solutions prepared in DMSO with water as the nonsolvent. The plotted points on the ternary phase diagram correspond to the points on the binodal curve of a specific RAL drugamer, wherein red triangles correspond to pRAL-BMA, blue circles to pRAL, and green squares to pRAL-MSEMA.

3.5 CONCLUSIONS

In this chapter, ARV drugamers were synthesized by polymerizing polymerizable antiretroviral prodrugs. Building on previous work in the lab focused on developing RAL prodrugs for improved nanoparticle encapsulation, this study advanced the conjugation chemistry of RAL's hydroxyl group [105]. RAL prodrug monomers were synthesized through a two-step process, linking RAL to a methacrylate group via an alkyl ester linker (RAL-SMA). These monomers were then polymerized using RAFT polymerization to produce a family of well-defined polymeric prodrugs, termed drugamers. The drugamer platform was extended to ATV, a protease inhibitor, demonstrating its potential for combination antiretroviral delivery. The successful synthesis of ATV drugamers highlights the platform's translatability to other drugs with free hydroxyl groups. However, the synthetic process may require adjustments for drugs with distinct chemical properties, as exemplified by the low pK_a of RAL's hydroxyl group versus ATV's hydroxyl group, thus different esterification routes were utilized when synthesizing prodrug monomers of the two ARVs. The resulting drugamers achieved high drug loading (51.88–74.60 wt%), significantly exceeding the drug loading of commercial, noncovalent polymeric formulations for *in situ* forming implants (ISFIs, 2–29 wt%) [196]. Additionally, RAL drugamers with tunable physical properties were obtained by varying the comonomer composition via random copolymerization. This tunability was validated by the distinct precipitation behaviors observed among different RAL drugamers. In the following chapter, *in vivo* experiments with the synthesized drugamers will be discussed, focusing on their potential to sustain drug release over extended durations.

Chapter 4. PHARMACOKINECTICS OF SINGLE SUBCUTANEOUS INJECTION OF ARV DRUGAMERS

4.1 ABSTRACT

A series of RAL and ATV drugamers were subcutaneously injected into into mice to establish the pharmacokinetic curves of drugamers and determine the extension of duration of action afforded by the drugamer platform. Following administration, drugamers precipitated *in situ* and formed "tight" depot in the subcutis. By tuning the degree of water penetration into the depot, hydrolysis of the drug from polymer backbones of RAL homopolymer and copolymers drugamers (pRAL-MSEMA, pRAL, and pRAL-BMA) exhibited a range of release profile from 14 to 28 days above 4 x PA-IC90. Conversely, minimal drug release was observed from ATV drugamer depots, and hydrophilic ATV copolymers was insufficient in increasing the release of drugs. Given both drugs utilizing alkyl ester linkages and copolymerization with hydrophilic comonomers (MSEMA), the lack of release of ATV was attributed to the high pK_a (pK_a=11.92), causing ATV to be a poor leaving group. The findings of this section demonstrate the importance of optimization of linker chemistry for drugs with higher pK_a prior to modification of polymer composition. In addition to providing sustained release of RAL, drugamer depots were demonstrated to be well-tolerated by mice, as no significant weight loss was observed. Furthermore, histological analyses confirmed mild and reversible foreign body response to drugamers following depot dissolution, indicating the safety of the drugamer platform.

4.2 INTRODUCTION

LAF injectables have demonstrated improved patient outcomes and decreased HIV infections when compared with oral drug regimens [69–71]. One class of LAF injectables is *in situ* forming implants (ISFI), wherein a liquid formulation generates a solid or semisolid depot *in situ* following injection [197]. This can be achieved with water-insoluble polymers that are formulated in organic solutions that precipitate upon administration without requiring surgical implantation. ISFIs enabling long-acting release of drugs have been studied for the treatment of periodontitis, opioid use disorder, cancer, schizophrenia, and HIV[198–203]. However, a key limitation of these ISFI formulations was the low drug loading, as the polymer often constitutes a large portion of the implant mass, with current commercially available ISFIs having drug loading from 2-29 wt% [196]. Preclinical ISFIs designed to deliver anti-HIV ARVs have similar drug loading (10-30 wt%) [203].

As described in chapter 2, polymeric prodrugs of TAF synthesized by RAFT polymerization achieved long-acting release with a drug loading - up to 73 wt% [38]. Following injection, the water-insoluble drugamer undergoes a phase-inversion: DMSO effluxes outwards into the subcutaneous space, and water influxes to the depot [39]. At a critical water content, the drugamer precipitates and forms a solid depot *in situ*. Drug release results in ionized carboxylate groups on the polymer backbone, increasing hydrophilicity and ultimately leading to depot degradation [38]. Concurrently, the molecular weight of the polymer decreases below the glomerular filtration cutoff, facilitating its clearance [204]. Tuning drugamer hydrophilicity and the degree of water penetration into the depot enables control of linker cleavage, and consequently, the release rate of RAL or ATV. To this effort, we have synthesized a series of

ARV drugamers and their copolymers with varying degrees of water penetration for tunable release rate of ARVs.

To evaluate the tunability of ARV drugamer release profiles, a series of RAL and ATV drugamers were synthesized and formulated into solutions in organic solvent for subcutaneous injection. We hypothesize that differences in polymer composition and hydrophilicity will result in varying degrees of water penetration, ultimately leading to distinct release profiles for RAL and ATV.

4.3 MATERIALS AND METHODS

4.3.1. Materials and reagents

Formulations of drugamer injections were prepared in 0.65 μL microcentrifuge tubes (Corning Costar). Formulation of drugamer injections were prepared with DMSO-*d*6 (Acros Organic). RAL and RAL-d6 standards (Alsachim, Inc.) and ATV and ATV-d15 standards (Axon Medchem) were used for LC-MS/MS analysis. Millipore water, acetonitrile (ACN, Fisher Scientific), formic acid (Fisher Scientific), and methanol (MeOH, Fisher Scientific) were used to prepare mobile phases for LC-MS/MS analysis. Solvents used for LC-MS/MS were all Optima LC/MS grade. ACN (Fisher Scientific) was used for the extraction of serum to prepare samples for LC-MS/MS analysis. Polyvinyledene fluoride (PVDF) membrane syringe filters (Fisher Scientific) were used to prepare samples for LC-MS/MS analysis.

4.3.2. Animal procedure and ethics statement

All animal procedures and handling were performed with the approval of the Institutional Animal Care and Use Committee and kept in accordance with federal and state policies on animal research at the University of Washington. Female BALB/cJ mice, aged 6-8 weeks, were obtained from Jackson Laboratory. Mice were housed in specific pathogen-free conditions

(mouse hepatitis virus, mouse parvovirus, minute virus of mice, reovirus-3, pneumonia virus of mice, rotavirus, Theiler mouse encephalomyelitis virus, lymphocytic choriomeningitis virus, ectromelia virus, Sendai virus, *Mycoplasma pulmonis*, pinworms, and fur mites). Mice were provided ad libitum access to food and water. Light-dark cycles of 12 h were maintained.

At designated timepoints, blood was collected from mice via tail prick or subcutaneous bleed. Tail prick was employed such that volume of blood collected stayed below the blood collection limits of 10% of mouse weight within any 2-week period as mandated by the animal protocol. Tail prick samples were obtained by pricking the tail with a $23^{3}/_{4}$ G needle. Volume of blood collected via tail prick were quantified by using a pipette. Blood was then diluted in 15 µL of PBS such that there was sufficient volume of sample for downstream processing. Submental bleeds were performed using 5 mm lancets weekly after the initial 2-week period where tail prick was employed. At the study endpoint, terminal blood collection was performed using cardiac puncture. To isolate serum, all blood samples (diluted and non-diluted) were allowed to clot at 4 °C overnight. Samples were centrifuged at 2.3 kG for 10 min and the supernatant was collected. The supernatant was centrifuged once more at 2.3 kG and the supernatant was collected again to yield the final serum samples for downstream processing and analysis.

4.3.3 Solution formulation for subcutaneous injection for single drugamer injections

Drugamer solutions were prepared by adding the desired amount of drugamer to a 0.65 mL microcentrifuge tube and then adding the appropriate amount of DMSO-*d*6 to achieve the desired concentration. The mixture was mixed by a vortex mixer for 5-20 minutes until a viscous homogeneous solution was obtained. The solutions were centrifuged until no pellet formation could be observed by the naked eye. Drugamer solutions were prepared such that each mouse

received 5 mg of the drug in a 30 µL injection. The solutions were prepared at a concentration of 223.41, 321.25, 251.65, and 271.98 mg/mL for pRAL, pRAL-MSEMA, pRAL-BMA 85:15, pRAL-BMA 75:25, respectively.

4.3.4. Subcutaneous injection of mice with drugamer solution

Female 6-8 weeks old BALB/cJ mice were anesthetized using isoflurane delivered via a precision gas vaporizer. The injection site, the right flank, was shaved and sterilized by swabbing with an alcohol prep pad. Drugamer solutions (30 µL) were subcutaneously injected using insulin syringes with $29^{1}/_{2}$G needles. To determine the accurate dosage of drugamers in each mouse, microcentrifuge tubes containing drugamer solutions were weighed prior to the addition of the drugamer solution, before, and after the subcutaneous injections. The change in weight equated to percentage of the solution injected, which could be used to calculate the total mass of drugamer injected in mice. The drug dosage per animal could be calculated given the drug wt% of the drugamer.

4.3.5. Post-injection drugamer stability assessment

Due to RAL drugamers demonstrating a relatively faster rate of hydrolysis, the amount of hydrolysis that occurred during the preparation of the drugamer solution was measured using ^{19}F-NMR (470 MHz, DMSO). Immediately after subcutaneous injection, the remaining drugamer solution was stored on ice. Subsequently, the frozen drugamer solution was thawed and diluted with 600 µL of DMSO-*d*6. Hydrolysis% was calculated by comparing the integration of free RAL peak (δ=-115.72 ppm) with integration of RAL drugamer (δ=-115.93 ppm) and using the equation (Eq (4.1)) shown below.

$$Hydrolysis\% = \frac{(Integration\ of\ hydrolyzed\ RAL)}{(Total\ integration)} \times 100 \quad (4.1)$$

4.3.6. In vivo *imaging of drugamer depot and excised organs by IVIS*

After mice were subcutaneously injected with drugamer solutions, mice were anesthetized with isoflurane gas and placed in the IVIS in vivo imaging system (Caliper Xenogen, PerkinElmer). Mice were laid in the lateral position. Depots were monitored using fluorescent mode (Ex/Em: 500/620 nm). The fluorescence intensity emitted from the depot in each mouse was quantified using Xenogen Living Image software. Mice were imaged prior to treatment to determine the lower and upper bounds of the scale of fluorescence to be used throughout the experiment. The lower bound of the scale of fluorescence (radiant efficiency, $(\frac{p/sec/cm^2/sr}{\frac{\mu W}{cm^2}})$) was determined to be the maximum fluorescence emitted by the mouse fur, while the upper bound of the scale was determined arbitrarily to be 1-2 orders of magnitude greater than the lower bound value. The region of interest of a specific mouse was identified at t=0 d by using an ellipse that encapsulated the drugamer depot, which was a primarily continuous region wherein the fluorescence exceeded the lower bound of the scale of fluorescence. The total radiant efficiency (TRE) was tracked longitudinally to quantifiably estimate the elimination rate of the drugamer depot. Normalized radiance efficiency was calculated by normalizing the total radiant efficiency to the minimum total radiant efficiency to account for the background signal. The equation (Eq. (4.2)) used to calculate was described by Ho *et al.* and is shown below[38].

$$Normalized\ Radiant\ Efficiency\ (\%) = \frac{TRE_{detected} - TRE_{min}}{TRE_{max} - TRE_{min}} \times 100 \quad (4.2)$$

Depot area is measured by analyzing fluorescence images with ImageJ. To automatically select the area, a threshold analysis was performed. First, the image was scaled given the size of the image (23.1 x 23.1 cm). Then, a copy of the blue channel was created, and a representative area of the depot was manually selected to correspond to a fluorescent region, such that the

threshold was identified. Then the thresholded areas were identified by ImageJ by analyzing areas of all sizes (0-Infinity) and circularities (0.00-1.00). Areas were calculated by counting the number of pixels in the region, given each pixel was a known area based on the established scale. A representative image of the calculation of depot area is shown in the Appendix (**Fig S13**).

Select organs were also excised to investigate the elimination route of the drugamer depot. Lymph nodes (inguinal), the female reproductive tract (FRT), spleen, lungs, kidneys, and liver were collected. The FRT, spleen, lungs, kidney, and liver were imaged on black paper (Strathmore) with Caliper Xenogen IVIS (Ex/Em: 500/620).

4.3.7. Serum sample preparation for LC-MS/MS analysis

Serum samples were thawed and centrifuged at 10000 G for 10 min. Serum samples were then added to cold ACN spiked with internal standard (RAL-*d*6) to induce precipitation. Samples in ACN were vortexed thoroughly, centrifuged at 10000 G for 10 min, and the supernatant was filtered using a 0.22 μm PVDF filter, then added to a 200 μL HPLC vial.

4.3.8. Quantification of drug concentration in serum by LC-MS/MS analysis

The liquid chromatography system comprised of an I-Class Acquity UPLC, Direct Infusion Syringe Pump as the inlet system. Samples were separated using ACQUITY UPLC BEH C18 columns (130 Å, 1.7 μm, 2.1 mm X 50 mm). The LC system was coupled to a Waters Xevo TQ-S tandem quadrupole mass spectrometer with a Micromass Zspray™ Atmospheric Pressure Ionisation (API) Source. Data analysis was conducted using MassLynx® software (v4.1).

Stock solutions of RAL and RAL-*d*6 were prepared at 1 mg/mL in DMSO. RAL-*d*6 was selected as the internal standard. Working solutions of RAL and RAL-*d*6 were prepared at 10000, 1000, 10, 1 ng/mL and 10000, 1000, 15 ng/mL, respectively. Calibration standards were

prepared by diluting working solutions in appropriate volumes of neat ACN to obtain a calibration range of 0.1-100 ng/mL of RAL and a fixed concentration of 10 ng/mL of RAL-*d*6. Quality control standards (QCs) were prepared at 3.33 (low), 33.33 (medium), and 333.33 (high) ng/mL of RAL in neat ACN. Spiked serum QCs were prepared with the addition of blank serum to neat ACN resulting in the final concentration of 33.33 ng/mL of RAL. Samples were prepared within 72 hours prior to analysis and stored at -20 °C until analysis.

Stock solutions of ATV and ATV-*d*15 were prepared at 1 mg/mL in DMSO. ATV-*d*15 was selected as the internal standard. Working solutions of ATV and ATV-*d*15 were prepared at 20000, 2000, 20, 2 ng/mL and 20000, 2000, 30 ng/mL, respectively. Calibration standards were prepared by diluting working solutions in appropriate volumes of neat ACN to obtain a calibration range of 0.2-200 ng/mL of ATV and a fixed concentration of 20 ng/mL of ATV-*d*15. The calibration standards were then diluted with Millipore water (1:1 (v/v) ACN:water) to obtain final concentrations of 0.1-100 ng/mL of ATV and 10 ng/mL of ATV-*d*15. Quality control standards (QCs) were prepared by the same method to obtain concentrations at 3.33 (low), 33.33 (medium), and 333.33 (high) ng/mL of ATV in 1:1 (v:v) ACN:water. Spiked serum QCs were prepared with the addition of blank serum to neat ACN resulting with a concentration of 66.66 ng/mL of ATV, and then diluted with water to obtain a final concentration of 33.33 ng/mL. Samples were prepared within 72 hours prior to analysis and stored at -20 °C until analysis.

Mobile phase A was composed of 10 mM of formic acid in ultrapure water and mobile phase B was composed of 10 mM formic acid in 50:50 ACN: MeOH. Solvents were prepared before each set of analyses. The flow rate of the mobile phase was fixed at 0.5 mL/min. Injection volumes were fixed at 2 μL. The mobile phase gradient was initially fixed at 98% A:2% B for 1 minute. Over the next 5 minutes, the ratio of mobile phase B was increased such that the ratio

was 0% A:100% B; this ratio was held for the following 2 minutes. The following mobile phase method was to minimize carryover in between analysis of different samples. Over the following 0.10 minute, the ratio of B was decreased such that the ratio of mobile phase was 98% A:2% B. The ratio of B was increased once more such that the ratio of mobile phase was 0% A:100% B over 1 minute, and then held for 1 minute. This cycle was repeated twice more. Lastly, ratio of mobile phase was returned to 98% A:2% B over 0.10 minute and then held for 1.70 minutes.

The mass spectrometer was operated in positive ion mode. The ionization parameters were as follows: capillary voltage of 3 kV, cone voltage of 40 V, source temperature of 350 ° C, desolvation gas flow of 800 L/h, cone gas flow of 150 L/h, and collision gas flow of 0.15 L/min. The mass spectrometer was engaged in between 2.5-12.1 minutes for each run. The *m/z* transitions and retention times for RAL and RAL-*d*6 were as follows: 445.35→109.10, 4.10 min and 451.35→115.10, 4.11 min, respectively. The C_{max}, T_{max}, and AUC_{all} were determined by using the PKNCA R package by Denney *et al* [205].

4.3.9. Histological assessment of subcutaneous injection site

At the termination of the animal study, mice were sacrificed, and the injection site was excised for histological assessment. For single injection studies, the skin distal to the injection site was excised and acted as the control. Following tissue excision, the skin was cut into strips of the subcutaneous space and placed in histology cassettes. The skin was washed twice with PBS and then fixed in formalin overnight. Fixed tissue was embedded in paraffin, sectioned in 4 µm cross-sections of the subcutaneous space, and then stained with Masson's trichrome and hematoxylin and eosin (H&E) stains. Sectioning, embedding, and staining were conducted by the Histology and Imaging Core at the University of Washington.

4.4. RESULTS AND DISCUSSION

4.4.1. Formulation of ARV drugamer solutions for subcutaneous injections

Drugamer solutions for subcutaneous injections were formulated in DMSO-*d*6 to obtain a homogeneous solution, which forms a depot *in situ* as water (nonsolvent) influxes and DMSO (solvent) effluxes. RAL drugamers were determined to have an experimental solubility of at least 642 and 322 mg/mL for pRAL and pRAL-MSEMA, respectively. As discussed in Chapter 3, pRAL and pRAL-MSEMA were RAL homopolymer drugamers and relatively hydrophilic RAL-MSEMA copolymer drugamer, respectively. Similarly, pATV was determined to have an experimental solubility of at least 620 mg/mL as well. The above concentrations were not defined as the maximum solubilities of polymers in DMSO, but was utilized to empirically determine concentrations of drugamer solutions where drugamers are completely soluble, while ensuring the volume of DMSO injected into mice was tolerable. Drugamer solutions prepared for subcutaneous injections were formulated at concentrations such that approximately 5 mg of RAL or ATV was delivered in a 30 µL injection. The formulation of drugamer solutions and dosage of animals in each *in vivo* experiment are summarized in **Table 4.1**.

Table 4. 1. Drugamer solution formulation and drug dosage

Entry	**Study**	**Drugamer Solution Concentration (mg/mL)**	**Drug Dosage (mg)**
1	pRAL	223.41	4.78±0.16
2	pRAL-MSEMA	321.25	4.82±0.16
3	pRAL-BMA	251.68	4.64±0.51
4	pATV	204.09	4.15±0.19
5	pATV-MSEMA	309.80	4.44±0.64

4.4.2. Post-injection stability of RAL drugamer

RAL drugamer subcutaneous injectables were designed to sustain the release of RAL by slow hydrolysis of drug from the backbone, and premature hydrolysis and burst release of RAL would be undesirable. The alkyl ester of RAL-SMA has demonstrated cleavability when incubated in DMSO-*d*6 at room temperature over a span of days, thus the amount of hydrolysis that occurred during the preparation of drugamer solution needed to be measured to ensure that drug is not prematurely cleaved during formulation, which could lead to "burst release" upon injection. The hydrolysis of RAL during the formulation step was measured with ^{19}F-NMR. Free hydrolyzed RAL and RAL conjugated to drugamer exhibited resolved peaks (δ=-115.72 and δ=-115.93 ppm, respectively), and amount of hydrolysis was quantified using **Eq. (4.1)**. ^{19}F-NMR spectrum with the peaks of interest used to calculate hydrolysis can be seen in **Appendix A** (**Fig S11**). RAL homopolymer drugamers showed negligible hydrolysis (0.15±0.16 % hydrolysis), demonstrating the increased stability of the alkyl ester linker when RAL-SMA was polymerized. It could be concluded that RAL drugamer solutions do not contain free RAL when solutions are prepared at most one day before administration, and would not cause burst release due to the presence of free RAL.

4.4.3. Characterization of single RAL homopolymer drugamer subcutaneous injectable depots

The sustained release profile of RAL provided by *in-situ* forming homopolymer drugamer was investigated with *in vivo* experiments in murine models. Following subcutaneous injection, the organic solvent (DMSO-*d*6) diffuses outwards of the system and into the subcutaneous space, while the nonsolvent (water) ingresses *via* diffusion, thereby causing the water-insoluble drugamer to precipitate and thus forming the semi-solid depot that controls drug

delivery[192,206]. The pharmacokinetic profile of RAL homopolymer drugamer was assessed by analyzing serum concentration of RAL over 60 days, as shown in **Fig 4.2A**.

Following a single injection, RAL was immediately detectable and reached a local maximum of 180.74 ng/mL in serum, before dropping below the 4 x PA-IC90 at t=1-3 d. On t=7 d, serum concentration of RAL increased significantly and persisted above the target concentration up to t=28 d. Following t=28 d, serum concentration decreased below the 4 x PA-IC90, and was no longer detectable at t= 56 d. In summary, pRAL exhibited an AUC_{all}=4091 d ng mL^{-1}, T_{max}=7 d, and a C_{max}=193.76 ng/mL with sustained release above the 4 x PA-IC90 for 21 days.

The depot could be observed by using IVIS due to the rhodamine monomer conjugated to each polymer chain, allowing the visualization of a "tight" and localized depot in each mouse. Depot area (not the surface area) obtained by analysis with ImageJ was measured to be 0.580 ± 0.330 cm^2. The fluorescence intensity was tracked longitudinally (shown in **Fig 4.2B**) to estimate the dissolution and clearance rates of the depot from the injection site. The fluorescence intensity maintains an approximately constant value from the day of administration up to t=35 d, followed by a sharp decrease in fluorescence intensity, which was due to polymer chains being cleared from depot, which was then excreted renally (shown in **Fig S15**). The trend of the IVIS data was in agreement with the serum concentration of RAL. However, the decline observed in IVIS was approximately one week later than the decline in the serum concentration. This decline in systemic RAL delivery prior to bulk drugamer depot dissolution suggests that a critical amount of hydrolysis of the polymer backbone was necessary to achieve critical hydrophilicity to increase the water penetration, which in turn resulted in bulk drugamer depot dissolution. Following drugamer dissolution, limited amounts of RAL would be delivered systemically.

Furthermore, the addition of a rhodamine unit to the polymer backbone was shown to not influence the release profile significantly. This was confirmed by a separate study where mice were subcutaneously injected with pRAL without a rhodamine unit, and the release profile was similar (**Fig S12**).

A single subcutaneous injectable of pRAL offered sustained release of 21 days above the target concentration. However, a "lag" phase could still be observed from t=1-7 d wherein the serum concentration of RAL was below the target concentration. In a clinical setting, this "lag" phase would warrant oral supplementation until the serum concentration reaches the target concentration[6,207]. Furthermore, despite the sustained release afforded by pRAL being longer than previously observed in literature, a single injection of pRAL does not offer significantly extended duration of action and cannot be administered as a monthly injection. Therefore, the release of RAL must be tuned to release at a slower rate to achieve a longer duration of action.

4.4.4. Characterization of single RAL-MSEMA or RAL-BMA copolymer drugamer subcutaneous injectable depots

Polymer composition and hydrophilicity can be rationally designed to control water penetration and drug release profiles. We pursued a copolymer strategy to modulate the release profile observed for pRAL. First, to minimize the "lag" in serum concentration on t=1-7 d after subcutaneous injections of pRAL, we designed a polymer incorporating monomers to increase hydrophilicity, thereby increasing water penetration and drug release. By modifying the comonomer composition of the polymer chain to include more hydrophilic monomers (MSEMA) to increase water penetration, a faster release of RAL in serum was achieved such that serum concentration of RAL was above the target from the day of administration. The greater amount of water required to induce precipitation in pRAL-MSEMA suggested greater hydrophilicity and

water penetration. Conversely, in order to achieve a longer duration of action , we incorporated more hydrophobic monomers (BMA) in the polymer backbone slowed the release of RAL by slowing water penetration. The tunability of RAL release by modifying the comonomer in the backbone was investigated *in vivo*.

As hypothesized, RAL drugamers demonstrated tunable release by using a copolymerization approach. Inclusion of MSEMA to obtain the more hydrophilic pRAL-MSEMA exhibited faster release, effectively eliminating the previously observed "lag". Following a single subcutaneous injection of pRAL-MSEMA, serum concentration of RAL was above the target concentration immediately after administration and remained above the 4 x PA-IC90 until t=14 d. After t=14 d, the serum concentration of RAL drops below the PA-IC90 and persists until the termination of the study. In summary, pRAL-MSEMA exhibited a T_{max}=14 d, C_{max}=269.97 ng/mL, and AUC_{all}=3415 ng d mL^{-1} and sustained release above the 4 x PA-IC90 for 14 days.

Conversely, pRAL-BMA exhibited slower release of RAL. Due to the hydrophobicity decreasing water penetration and slowing release, subcutaneous depots of pRAL-BMA exhibited a more delayed and sustained release. As observed with pRAL, the serum concentration of RAL was not immediately above the target concentration and dropped below the 4 x PA-IC90 for t=1-7 d. After t=14 d, serum concentration of RAL persisted above the 4 x PA-IC90 until t=42 d. To summarize, pRAL-BMA exhibited a T_{max}=14 d, C_{max}=202.43 ng/mL, and AUC_{all}=5057 d ng mL^{-1}, and sustained release above the 4 x PA-IC90 for 28 days.

Depot dissolution was also estimated by longitudinally tracking depot fluorescence after administration *via* IVIS imaging. Depots formed by pRAL-MSEMA showed a slightly larger spread in area (0.699 ± 0.193 cm^2), compared to pRAL depots (0.580 ± 0.330 cm^2). However, this

may be an artefact as the depot area of pRAL-BMA (0.990 ± 0.277 cm^2) was larger than both RAL drugamer depots. The observation differed from what Ho *et al* saw in TAF drugamer depots, wherein the homopolymer depot appeared to be more "tight"[38]. One may expect pRAL-BMA depots to be tighter given that the polymer is more hydrophobic. However, it may be possible that the increased hydrophobicity drives a more rapid demixing during depot formation *in situ*, hence a more porous and less dense depot, and resulting in a greater depot area[208]. After t=10 d, the fluorescence rapidly decreased indicating depot dissolution, and reaching baseline values at t=40 d. Compared to the pRAL injection, pRAL-MSEMA depots exhibited dissolution more rapidly without a 7-day dissolution period. This may suggest that, following drug release, depots of the pRAL-MSEMA allow for water penetration to a greater degree due to the charged carboxylate group following hydrolysis, and thus, rapid dissolution of the depot occurred almost immediately. The more hydrophobic pRAL-BMA depot exhibited slower dissolution, where the fluorescence decreases gradually throughout the study but does not return to baseline values. This was consistent with the slower drug release, and the pendant hydrophobic drugs together with BMA prevented rapid dissoluion. However, future studies are required to definitively assess the state of the depot given the dynamic nature of the physical properties of the polymer.

Altogether, the release of RAL from pRAL-MSEMA, pRAL, and pRAL-BMA subcutaneous drugamer depots elucidated the extent of tunability afforded by rational design in copolymerization to control water penetration and achieve different extents of drug exposure. In the case of RAL, the modification with comonomers allowed for tunability of approximately 40 days. As discussed previously in Chapter 3, the alkyl ester linker was described as the "slower" hydrolytically cleavable linker and selected in the design of the polymer prodrug due to the low

pK_a of RAL (pK_a=6.63±0.02) [161,179]. For drugs containing hydroxyl groups with low pK_a, the copolymerization approach can offer a greater degree of tunability than linker selection. Furthermore, the area under the curve (AUC) differed significantly between different RAL drugamers, which suggested the variable extents of exposure to RAL despite similar dosages (±5.10%). Conversely, the AUC of pRAL-MSEMA and pRAL-BMA had a percentage difference of 38.76%. The difference in RAL exposure could be attributed to the greater hydrophilicity of pRAL-MSEMA due to the MSEMA units within the polymer backbone, which allowed polymer chains to become soluble "prematurely" and were excreted renally. The rapid release of RAL from pRAL-MSEMA may also be influenced by its lower molecular weight (8300 Da) compared to pRAL and pRAL-BMA (24000 and 18000 Da, respectively). Polymers with greater molecular weight have demonstrated decreased solubility [209]. In the case of polymers as depots, the lower molecular weight polymers are more easily shed from the depot. Furthermore, lower molecular weight polymers may have lower degrees of entanglement, thus facilitating greater water penetration and hydrolysis to release RAL [210,211]. However, further studies need to be done to investigate the contribution of molecular weight and entanglement to the release and depot dissolution rate. The "premature" excretion of these drugamers indicated that polymer chains were excreted with some amount of drug still attached to the polymer. On the other hand, pRAL-BMA polymer chains were able to release a greater amount of RAL before becoming sufficiently water-soluble, and thus fewer drug was lost due to "premature" excretion. In summary, the release of RAL from subcutaneous drugarmer depots was tunable by designing different copolymers, which also modulated the extent of exposure of drug.

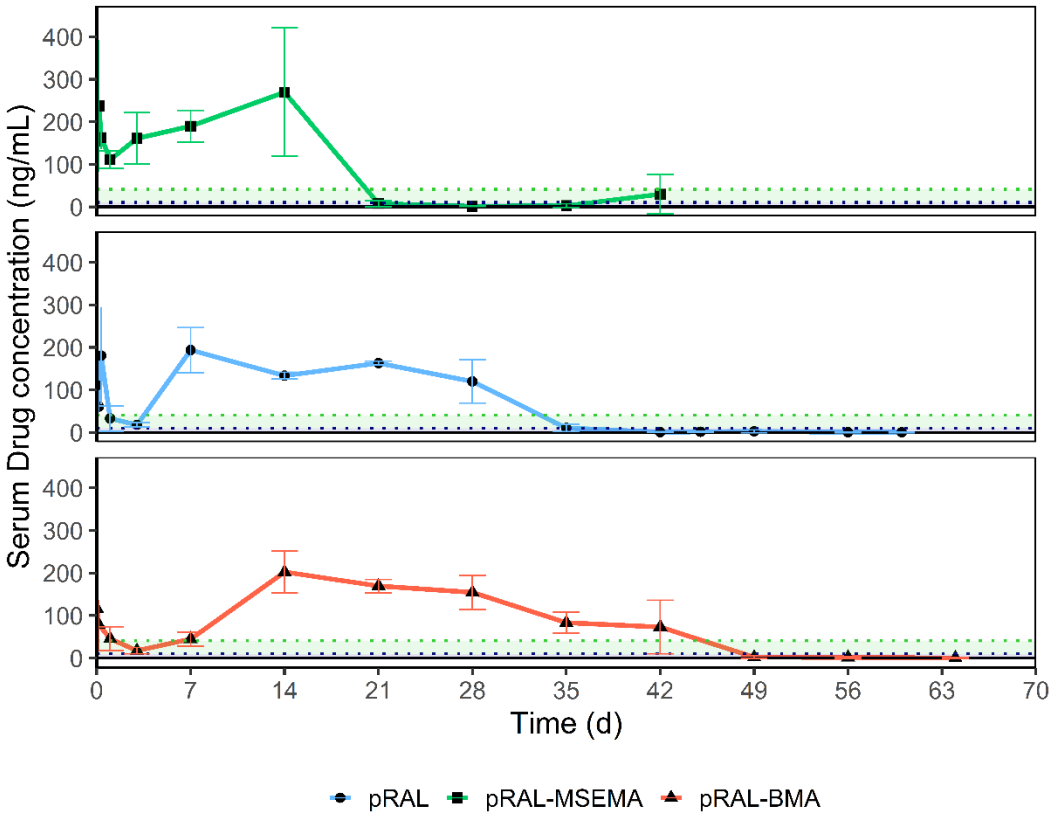

H

Fig 4. 1. Pharmacokinetic profile of single subcutaneous RAL drugamer injections in murine models

Following subcutaneous injection of RAL drugamer formulated in DMSO in the right flank at a dose of equivalent 5 mg of RAL/mouse, serum concentration of RAL was measured via LC-MS/MS to establish PK profile. From top to bottom, the PK curves are pRAL-MSEMA, pRAL, and pRAL-BMA. The dark blue and green dotted lines denote the PA-IC90 and 4 x PA-IC90,

respectively *[42]*

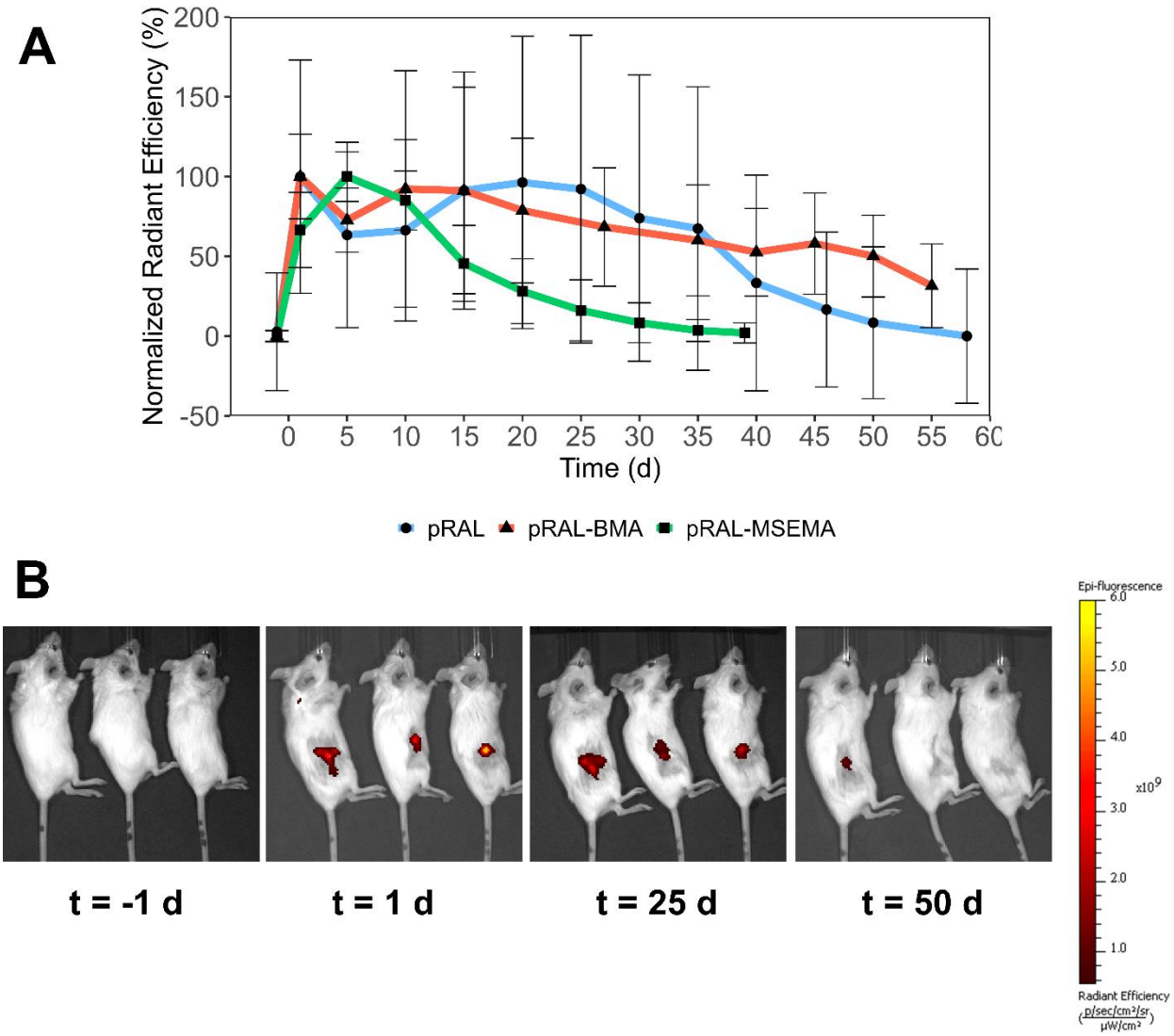

Fig 4. 2. Dissolution kinetics of subcutaneous RAL drugamer depots

(A) Normalized radiant efficiency of various subcutaneous RAL drugamer depots normalized to the max radiant efficiency. (B) Visualization of subcutaneous drugamer depot of mice treated with pRAL (blue solid line shown in **Fig 4.2A**) at selected days (t=-1, 1, 25, and 50 days).

4.4.5. Single ATV homopolymer and ATV-MSEMA copolymer drugamer subcutaneous injectable depot

With the effect of copolymerization strategies on drugamer release profiles established, we next assessed ATV drugamers for a similar trend with different pendant drugs. To evaluate ATV drugamers were designed as ISFIs to sustain release of ATV, and mice were subcutaneously injected with pATV and pATV-MSEMA. ATV release was hypothesized to be slower than RAL due to the pK_a of the hydroxyl group of ATV (pK_a=11.92), making ATV a poor leaving group. Similar to the RAL drugamers, a copolymerization approach was employed to modulate the release rate by tuning the hydrophilicity of the polymer. As expected, ATV release from pATV was significantly slower than RAL, likely due to the ATV being a poor leaving group. Following administration, ATV was detectable and reached a maximum concentration of 2.62 ng/mL. Throughout the study, ATV remained detectable but at low concentration, and was finally undetectable at t=42 d. Notably, the serum concentration of ATV never increased above the PA-IC90 (14 ng/mL), suggesting that an alternative design of the ATV drugamer was necessary to achieve a clinically relevant release profile[212]. To determine whether copolymerization was sufficient in accelerating the release rate, pATV-MSEMA was also administered in a separate cohort of mice. Like pATV, release of ATV from pATV-MSEMA was detectable but significantly below the PA-IC90 (**Fig S16**). Unexpectedly, the inclusion of hydrophilic comonomers in the polymer backbone failed to increase the rate of ATV release.

Although pATV and pATV-MSEMA showed similar release profiles, the depot dissolution kinetics differed significantly. The depot dissolution was longitudinally tracked with IVIS throughout the study and depots of pATV-MSEMA exhibited significantly faster dissolution, while depots of pATV remained intact (shown in **Fig 4.4A**). The dissolution of the

pATV-MSEMA depot was confirmed by analyzing the excised kidneys, wherein fluorescence originating from the drugamer could be detected (shown in **Fig 4.4B**). In contrast, kidneys from pATV-treated mice showed no detectable fluorescence, confirming the persistence of the depot without the shedding of polymer chains. This suggest that pATV-MSEMA dissolution was driven by polymer chain shedding due to the inherent hydrophilicity of the polymer, rather than the increased hydrophilicity following drug release. What likely occurred was pATV-MSEMA polymer chains being shed prior to cleavage of the alkyl ester linkage, which could be cleared renally given the relatively low molecular weight (5800 Da) being less than the glomerular filtration molecular weight cutoff (30000-50000 Da)[204]. This parallels findings with RAL drugamers, where pRAL-MSEMA depots exhibited faster dissolution, but unlike pATV-MSEMA, released the drug prior to chain dissolution.

The lack of ATV release was attributed to the stability of the alkyl ester linkage conjugating the drug to the polymer backbone. This finding was surprising when compared with TAF drugamers, the other case of RAFT polymeric prodrug subcutaneous depots found in literature. Despite the slower release, Ho *et al*. still observed sustained release of drug from homopolymer TAF drugamers even up to 60 days, whereas minimal drug was released from pATV-MSEMA[38]. This difference likely reflects the relative hydrolysis rates of carbamates and carboxylic esters, with carbamate carbonyl carbon being more susceptible to the initial hydroxyl ion or water molecule nucleophilic attack[213,214]. This trend may not be the sole reason for observing TAF release, and may be due to the aromaticity of the amine utilized to form the carbamate linkage that causes greater cleavability. These findings suggest that for antiretrovirals with hydroxyls with high pK_a, the copolymerization approach alone is insufficient to increase the release rate. The IVIS results further supported this conclusion, showing that

while copolymerization enhances water penetration into the depot, it can cause depot dissolution without drug release. Ultimately, the results highlight the need to optimize linker chemistry before applying copolymerization to modulate drug release.

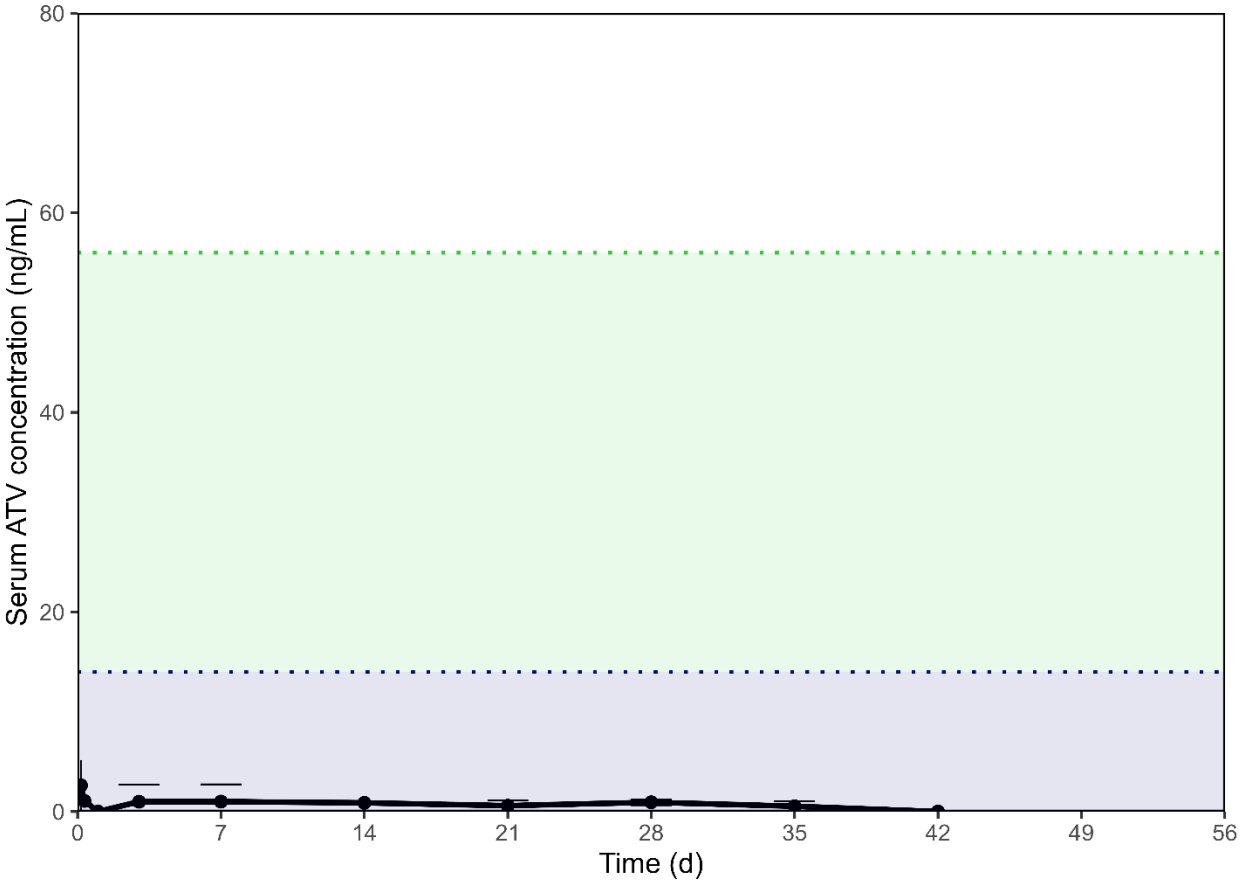

Fig 4. 3. Pharmacokinetic profile of single subcutaneous ATV drugamer injections in murine models

Following subcutaneous injection of pATV formulated in DMSO in the right flank at a dose of equivalent 5 mg of RAL/mouse, serum concentration of ATV was detectable but significantly below the PA-IC90. The dark blue and green dotted lines denote the PA-IC90 and 4 x PA-IC90, respectively [212].

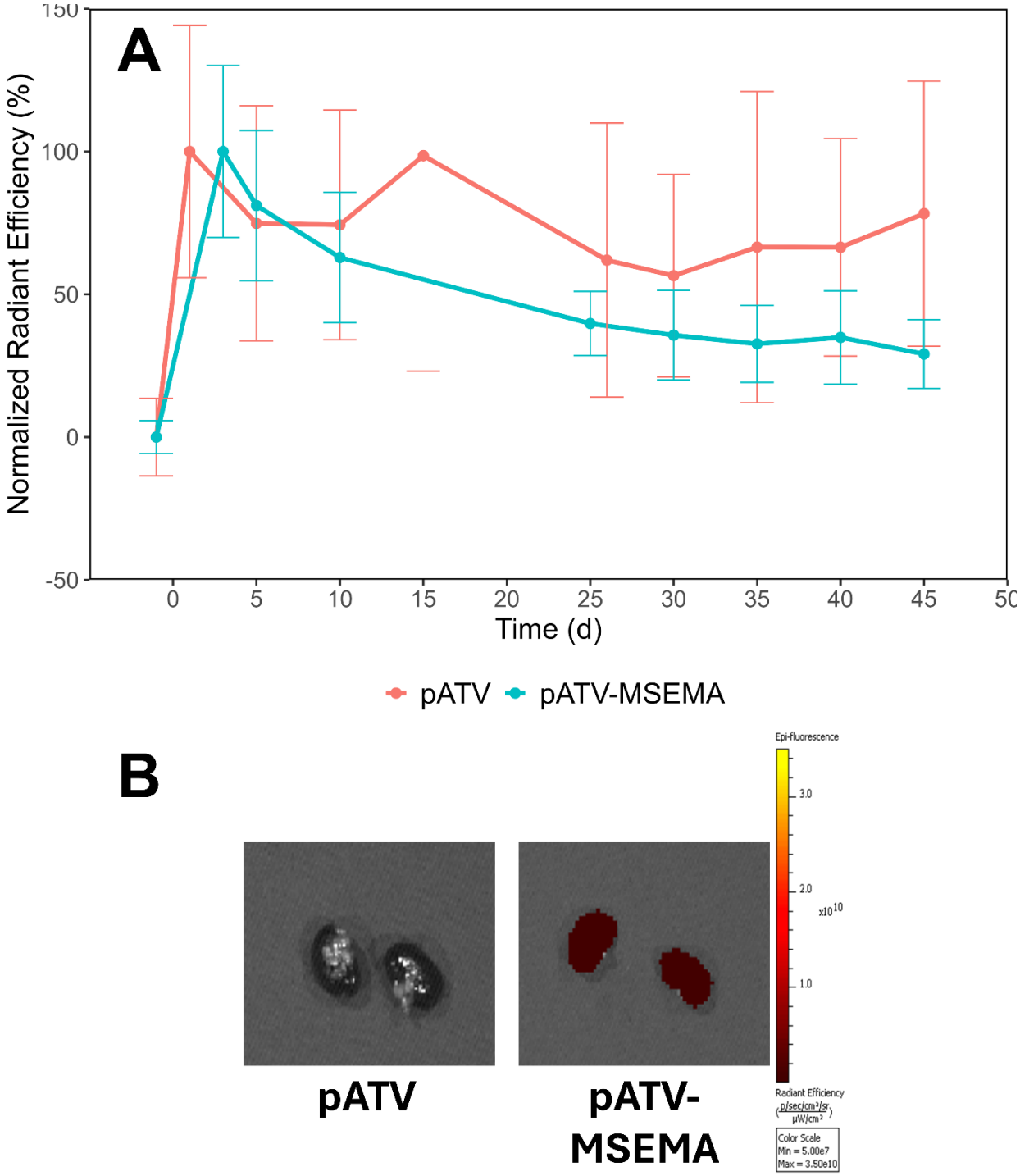

Fig 4. 4. Dissolution kinetics of subcutaneous ATV drugamer depots

(A) Normalized radiant efficiency of subcutaneous drugamer depots of pATV and pATV-MSEMA normalized to the max radiant efficiency. Depots of pATV-MSEMA exhibited faster dissolution. (B) Excised kidneys of mice receiving pATV and pATV-MSEMA injections.

Fluorescence could be detected in the kidney of mice administered with pATV-MSEMA, indicating polymer chains were breaking off from the depot and being cleared renally.

4.4.6. Tolerability and Histological Assessment to Drugamer Injections

Tolerability towards subcutaneous injections of a series of RAL drugamers was assessed by longitudinally tracking the weight changes in mice that received drugamer injections. No weight loss was observed in any of the cohorts. The final weights of each cohort on the day of study termination increased by 20.00%, 14.29%, 15.00%, 10.68% and 19.95% compared with the initial weight for pRAL, pRAL-MSEMA, pRAL-BMA, pATV, and pATV-MSEMA, respectively. The longitudinal tracking of weight is shown on **Fig S14**. These findings suggest that the mice experienced minimal distress following administration of drugamers[215]. Although no direct comparisons between drugamer formulations and weight increase can be made due to mice being sacrificed at different times, the overall increase in weight demonstrated good tolerability.

In addition to the ease of administration without the need for surgical implantation, ARV drugamer polymer chains were designed to be cleared from the injection site after drug has been released. As discussed in section 4.2, the molecular weight of the drugamer decreases significantly after drug release, thus allowing the polymer backbone to be renally cleared. Upon the termination of the study, the injection site was excised and analyzed to observe whether the depot stayed localized in the injection site. By inspection with the naked eye, RAL drugamer depots (all homopolymer and copolymers) were no longer observable, demonstrating the successful clearing of polymers after RAL release. This was supported by the decrease in fluorescence of the injection site observed by IVIS discussed in section 4.4.4, as well as the

fluorescence detected in the excised kidneys emitted by the covalently conjugated rhodamine tags on polymer chains (**Fig S15**).

Histological analysis further assessed the biocompatibility and foreign body response following drugamer injection. The excised injection site was fixed in formalin and stained with hematoxylin and eosin (H&E) and Masson's Trichrome (MT) staining. The subcutis of mice treated with pRAL demonstrated a slight increase in lymphocyte infiltration compared with the sham control (**Fig 4.5A-B**). Similarly, the pRAL-MSEMA-treated and pRAL-BMA subcutis demonstrated comparable levels of lymphocyte infiltration to pRAL (**Fig 4.5C-D**). MT staining revealed the collagen deposition was slightly increased in the subcutis of mice treated with RAL drugamers, as shown by the blue staining. Collagen deposition indicates the final part of the foreign body reaction, suggesting the gradual resolution of inflammation and response to the implant[216,217]. The eventual resolution of foreign body reaction was confirmed in a separate study where mice were subcutaneously injection with pRAL and then sacrificed at t=168 d, where the cumulative release reached the maximum and the drugamer depot dissolution occurred significantly earlier than the study termination date (**Fig 4.5E**). The subcutis from that cohort exhibited significantly less collagen accumulation and histology of the skin obtained by necropsy demonstrated comparable lymphocyte infiltration and collagen deposition to the control, indicating the foreign body reaction to be completely reversible after depot dissolution without persistent local inflammation. For reference, pRAL, pRAL-MSEMA, and pRAL-BMA were sacrificed at t=60 d, t=42 d, and t=63 d, respectively.

Conversely, the histological analysis of ATV drugamer-treated injection sites exhibited a relatively sustained foreign body reaction. By inspection with the naked eye, a tight depot remained in the subcutis of mice treated with pATV. This observation was consistent with the

depot tracking performed with IVIS, confirming minimal depot dissolution. The subcutis of mice treated with pATV-MSEMA had less of the depot localized in one area, which was also consistent with the IVIS data. Histological analysis of pATV-treated subcutis demonstrated significant collagen deposition in the depot (**Fig 4.6B**, depot is indicated by the blue arrow). Furthermore, H&E stains show the formation of foreign body giant cells (**Fig 4.6C**, indicated by black stars), which adhere to and enhance the degradation of the foreign material[216]. The p-ATV-MSEMA-treated subcutis displayed lesser lymphocyte infiltration and collagen deposition, and no foreign body giant cells could be observed, despite some of the depot still remaining. This may be attributed to the greater degree of depot dissolution, which allowed the foreign body reaction to resolve faster. This observation would be consistent with what was observed in RAL drugamers, where dissolution occurred faster and thus foreign body reaction resolved earlier.

In summary, drugamer depots were safe to mice when subcutaneously injected. The absence of sudden weight loss demonstrated good tolerability in mice. Good biocompatibility was further confirmed with histology images with H&E and Masson's Trichrome stains, showing minimal lymphocyte infiltration and collagen deposition. Histology images also confirmed the complete dissolution and clearance of the drugamer depot after the release of RAL. Despite the weight tracking and histology indicating good tolerability, some mice have exhibited ulceration at the site of injection, which may be due to the compression of arteries by the drugamer injection resulting in ischemia and then necrosis[218]. It may be possible to circumvent injection site ulceration by tuning the formulation of the drugamer solution, such as reducing the viscosity to minimize the chance of ischemia. Further studies would be required to optimize the formulation to prevent ulceration at the site of injection. Nevertheless, the ulceration did not alter the behavior of the mice and resolved in a timescale of one or two weeks.

Altogether, drugamer depots were tolerable in mice and did not require further removal after drug was released.

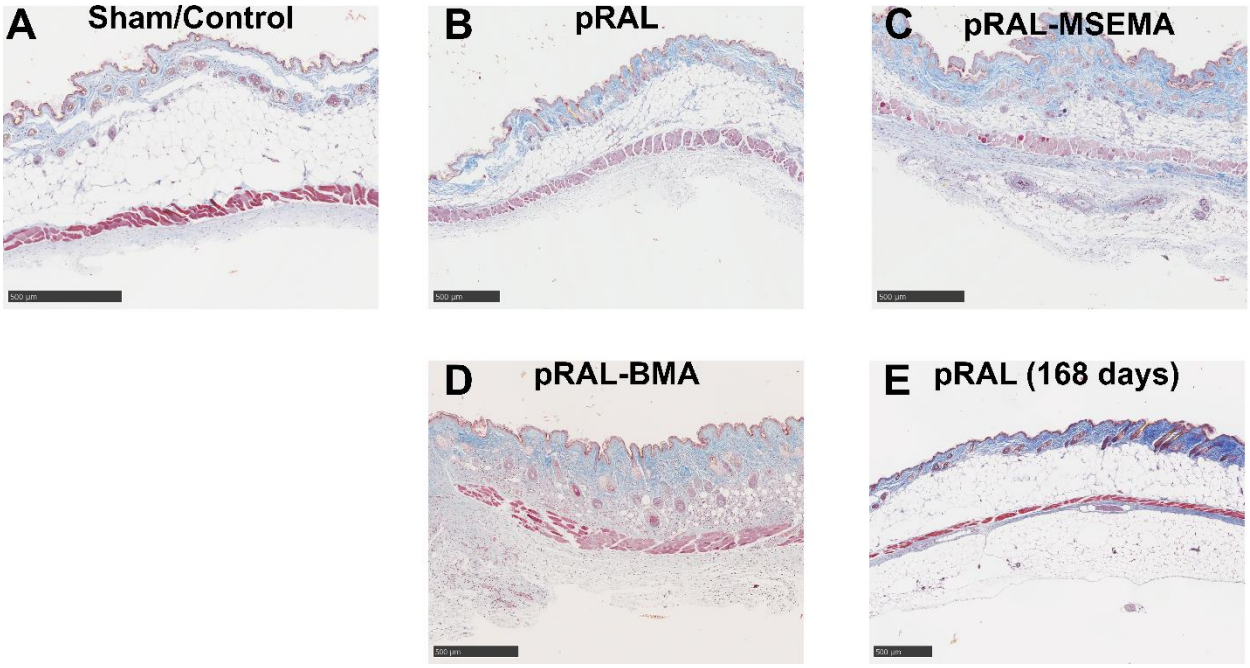

Fig 4. 5. Histological analysis of RAL drugamer injection site with Masson's Trichrome stain

(A) Tissue section for sham control. (B) RAL homopolymer drugamer. (C) RAL-MSEMA copolymer drugamer. (D) RAL-BMA copolymer. (E) RAL homopolymer sacrificed 168 days after drugamer administration. Collagen deposition was stained blue, cell cytoplasm was stained red/pink. All drugamer depots were not found in histology images, indicating successful dissolution and clearance after release of RAL. Histology indicated a slight increase in lymphocyte infiltration and collagen deposition in the subcutis in response to the drugamer depots.

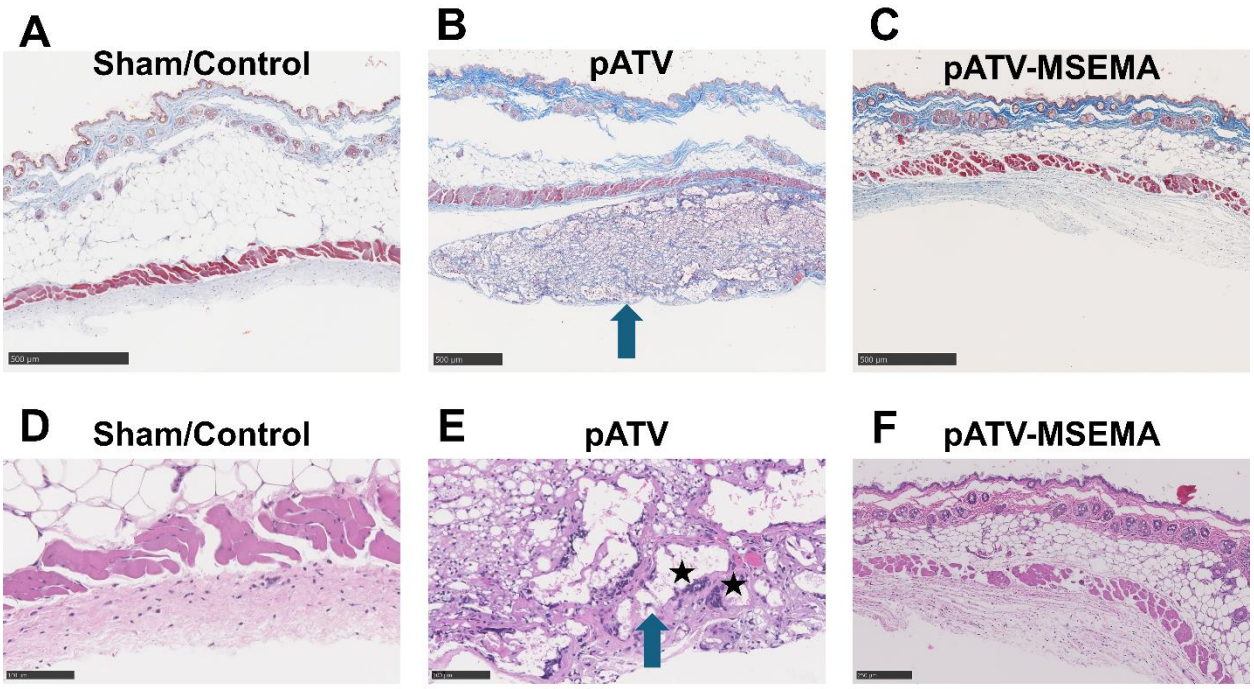

Fig 4. 6. Histological analysis of ATV drugamer injection site indicates persistent foreign body reaction

(A) Tissue section for sham control stained with Masson's Trichrome (MT). (B) ATV homopolymer drugamer stained with MT. (C) ATV-MSEMA copolymer drugamer stained with MT. (D) Tissue section for sham control stained with H&E. (E) ATV homopolymer drugamer stained with H&E. (F) ATV-MSEMA copolymer drugamer stained with H&E. Blue arrows denote the drugamer depot. Black stars denote foreign body giant cells. Histology results indicate significant collagen deposition, lymphocyte infiltration, and giant cell formation following administration of pATV. A lesser foreign body response was observed following pATV-MSEMA administration.

4.5 CONCLUSION

A series of ARV drugamers were evaluated for their ability to achieve sustained release of antiretrovirals using a copolymerization approach. Single subcutaneous injections of RAL

drugamers were administered to mice to establish pharmacokinetic profiles and assess the impact of prodrug monomer and comonomer composition on drug release rates. By tuning the degree of water penetration into the drugamer depot through copolymerization, the release of RAL was successfully modulated over a period of up to 40 days.Compared to TAF drugamers previously studied by Ho et al., RAL drugamers demonstrated relatively faster release, likely due to the superior leaving group ability of RAL. In contrast, ATV, a poor leaving group, exhibited significantly slower release rates. The copolymerization approach used to accelerate ATV release was insufficient, indicating that optimization of linker chemistry is required to achieve clinically relevant release profiles for antiretrovirals with high-pKa hydroxyl groups.

Tolerability studies showed that RAL drugamers were well-tolerated in mice, with no significant weight loss observed. Histological analyses confirmed good biocompatibility, with mild and reversible foreign body responses following depot dissolution and clearance. Although some mice exhibited localized ulceration at the injection site, this resolved within 1–2 weeks without behavioral changes, suggesting the need for further optimization of formulation parameters to prevent ischemia-induced necrosis.

Overall, this work demonstrates the tunability and biocompatibility of drugamer depots for sustained ARV delivery. Future efforts would focus on improving the release of ATV with different linker selections, such as phenyl ester or carbonate linkages. In addition, the release of RAL could be further extended by other chemical modifications to the drugamers, such as the usage of other linkers or larger molecular weight. For one, acetal carbonate or acetal ester linkers could decrease the release rate by minimizing the effect of the phenolic hydroxyl group (pK_a=6.67) on hydrolysis[219]. In addition, the lesser AUC of the more hydrophilic drugamers suggested that drugamers were being shed from the depot with RAL. A drugamer with greater

molecular weight could potentially minimize premature drug loss, given that the solubility of polymers generally decreases as their molecular weight increases[220].

CHAPTER 5: PHARMACOKINETICS OF CO-INJECTIONS OF SUBCUTANEOUS INJECTIONS OF RALTEGRAVIR DRUGAMERS

5.1. ABSTRACT

In the effort to extend the sustained release of RAL from drugamer *in situ* forming depots, RAL drugamers with distinct polymer compositions were co-injected to obtain the summation of their release profiles. Co-injection of distinct drugamers is an alternative strategy of obtaining sustained release without the trial-and-error of tuning release profile by modulating the polymer composition. Co-injection of pRAL-MSEMA and pRAL-BMA extended release of RAL to 42 days above the 4 x PA-IC90 threshold, which was the longer duration than previous dissolution- and diffusion-based DDS. In addition, distinct drugamers could be formulated as a single solution for co-injection. Despite the increased RAL dosage, drugamer depots remained to be well-tolerated by mice, as demonstrated by the comparable collagen deposition and lymphocyte infiltration with single RAL drugamer injection studies. The drugamer formulation combined with co-injection expands the toolbox for sustained delivery of drugs beyond noncovalent LA-DDS and can potentially be applied for PrEP and treatment in other diseases, particularly for drugs with similar release profiles as RAL or with hydroxyl groups with similar pK_a values.

5.2. INTRODUCTION

The potential of RAFT polymer prodrugs to extend the release of other hydrophilic drugs requires functional groups that are amenable to the formation of cleavable linkers. RAFT

polymer prodrugs, or drugamers, have demonstrated sustained release of antiretrovirals for at least 60 days in murine models via subcutaneous *in situ* forming injectables [38]. Sustained delivery achieved by drugamers is desired in the delivery of anti-HIV antiretrovirals by minimizing the dosage frequency to improve drug regimen adherence and patient outcome [62,63,165,221]. Currently, hydrophilic drugs (log P<1.0) make up about a third of small-molecule ARVs FDA-approved for HIV suppression, which could potentially be repurposed for long-acting delivery and expand the number of drug entities used in LA injectables [222]. However, the hydrophilic nature of these ARVs makes high drug encapsulation and sustained delivery with conventional, noncovalent drug carriers difficult [43]. One example of an ARV is RAL, wherein the delivery by noncovalent DDS above the target concentration was sustained for only 18 days[223]. Thus, we aim to use a drugamer approach to sustain the delivery of RAL.

Here, we investigate the RAL was selected given the low octanol-water partition coefficient (logP = 0.58) and a hydroxyl group readily amenable to conjugation[224]. As discussed in section 3.2, RAL offers several clinical advantages. RAL is also an ideal candidate for PrEP regimens because it demonstrates high genital tissue penetration, good tolerability, and minimal drug-drug interactions [34,41,225,226]. The potential of RAL to be used in PrEP alone or in combination with lamivudine has been investigated in a clinical trial due to the high penetration in vaginal and gut tissue [34].

As discussed in Chapter 4, delivery of RAL by subcutaneous injectables offers sustained release up to 28 days. The sustained delivery of RAL could potentially be extended by further modifications to the polymer architecture and composition, but the low pK_a of RAL (pKa=6.67), accelerates release and makes sustained delivery using drugamers challenging, therefore it is unclear how much the release could be extended [105]. Furthermore, the design of polymers

requires significant amount of trial-and-error to obtain the desired properties [227]. In pursuit of alternate strategies to extend the release of RAL, the different RAL drugamers (pRAL, pRAL-MSEMA, and pRAL-BMA) could be co-injected to achieve a summation of their respective release profiles. This strategy capitalizes on the advantages of drugamer approach (high drug loading and sustained release with hydrophilic drugs), while balancing the resources on designing polymers for sustained release. In this section, we investigate the release profile achieved using the co-injection strategy. Furthermore, we explore the effect of formulation on the release profile, as well as the tolerability of co-injections.

5.3. MATERIALS AND METHODS

5.3.1. Materials and reagents

Formulations of drugamer injections were prepared in 0.65 μL microcentrifuge tubes (Corning Costar). Formulation of drugamer injections were prepared with DMSO-*d*6 (Acros Organic). RAL and RAL-d6 standards (Alsachim, Inc.) were used for LC-MS/MS analysis. Millipore water, acetonitrile (ACN, Fisher Scientific), formic acid (Fisher Scientific), and methanol (MeOH, Fisher Scientific) were used to prepare mobile phases for LC-MS/MS analysis. Solvents used for LC-MS/MS were all Optima LC/MS grade. ACN (Fisher Scientific) was used for the extraction of serum to prepare samples for LC-MS/MS analysis. Polyvinyledene fluoride (PVDF) membrane syringe filters (Fisher Scientific) were used to prepare samples for LC-MS/MS analysis.

5.3.1. Animal procedures and ethics statement

Ethics statements was described earlier in section 4.3.1. At designated timepoints, blood was collected from mice via tail prick or subcutaneous bleed. Tail prick was employed such that

volume of blood collected stayed below the blood collection limits of 10% of mouse weight within any 2-week period as mandated by the animal protocol. Tail prick samples were obtained by pricking the tail with a $23^{3}/_{4}$ G needle. Volume of blood collected via tail prick were quantified by using a pipette. Blood was then diluted in 15 µL of PBS such that there was sufficient volume of sample for downstream processing. Submental bleeds were performed using 5 mm lancets weekly after the initial 2-week period where tail prick was employed. At the study endpoint, terminal blood collection was performed using cardiac puncture. To isolate serum, all blood samples (diluted and non-diluted) were allowed to clot at 4 °C overnight. Samples were centrifuged at 2.3 kG for 10 min and the supernatant was collected. The supernatant was centrifuged once more at 2.3 kG and the supernatant was collected again to yield the final serum samples for downstream processing and analysis.

5.3.2. Formulation of RAL drugamer injections for co-injections

For co-injections studies where two different RAL drugamers were administered without admixing, drugamer solutions were prepared in the same concentration as described in section 4.3.2. Separate drugamer solutions were subsequently injected at opposite flanks of the mice. For co-formulated injections of the pRAL and pRAL-MSEMA (CoF), drugamer solutions of the pRAL homopolymer and pRAL-MSEMA copolymer were prepared as described above. Subsequently, a coformulation of the two drugamer solutions was obtained by mixing a 1:1 volumetric ratio of the RAL homopolymer and RAL-MSEMA copolymer together.

5.3.3. Co-injection of subcutaneous injections of RAL drugamers

Female 6-8 week old BALB/cJ mice were anesthetized using isoflurane delivered via a precision gas vaporizer. The injection site, the right flank, was shaved and sterilized by swabbing

with an alcohol prep pad. For co-injection studies of where two different RAL drugamers were administered without admixing, 30 μL of one drugamer solution was administered subcutaneously into the left flank, and another 30 μL of a different drugamer solution was administered into the right flank.

To determine the accurate dosage of drugamers in each mouse, microcentrifuge tubes containing drugamer solutions were weighed prior to the addition of the drugamer solution, before, and after the subcutaneous injections. The change in weight equated to percentage of the solution injected, which could be used to calculate the total mass of drugamer injected in mice. The drug dosage per animal could be calculated given the drug wt% of the drugamer, and a summary of RAL dosage is shown in **Table S2**.

5.3.4. In vivo *imaging of drugamer depot and excised organs by IVIS*

After mice were subcutaneously injected with drugamer solutions, mice were anesthetized with isoflurane gas and placed in the IVIS in vivo imaging system (Caliper Xenogen, PerkinElmer). Mice were laid in the prone position such that both the left and right flank could be imaged. Depots were monitored using fluorescent mode (Ex/Em: 500/620 nm). The fluorescence intensity emitted from the depot in each mouse was quantified using Xenogen Living Image software. Mice were imaged prior to treatment to determine the lower and upper bounds of the scale of fluorescence to be used throughout the experiment. The lower bound of the scale of fluorescence (radiant efficiency, $(\frac{p/sec/cm^2/sr}{\frac{\mu W}{cm^2}})$) was determined to be the maximum fluorescence emitted by the mouse fur, while the upper bound of the scale was determined arbitrarily to be 1-2 orders of magnitude greater than the lower bound value. The region of interest of a specific mouse was identified at t=0 d by using an ellipse that encapsulated the drugamer depot, which was a primarily continuous region wherein the fluorescence exceeded the

lower bound of the scale of fluorescence. The total radiant efficiency (TRE) was tracked longitudinally to quantifiably estimate the elimination rate of the drugamer depot. Normalized radiance efficiency was calculated by normalizing the total radiant efficiency to the minimum total radiant efficiency to account for the background signal. The equation (Eq. (5.1)) used to calculate was described by Ho *et al.* and is shown below[38].

$$Normalized\ Radiant\ Efficiency\ (\%) = \frac{TRE_{detected} - TRE_{min}}{TRE_{max} - TRE_{min}} \times 100 \quad (5.1)$$

Depot area is measured by analyzing fluorescence images with ImageJ. To automatically select the area, a threshold analysis was performed. First, the image was scaled given the size of the image (23.1 x 23.1 cm). Then, a copy of the blue channel was created, and a representative area of the depot was manually selected to correspond to a fluorescent region, such that the threshold was identified. Then the thresholded areas were identified by ImageJ by analyzing areas of all sizes (0-Infinity) and circularities (0.00-1.00). Areas were calculated by counting the number of pixels in the region, given each pixel was a known area based on the established scale.

5.3.5 Quantification of Drug Concentration in Serum by LC-MS/MS

The liquid chromatography system comprised of an I-Class Acquity UPLC, Direct Infusion Syringe Pump as the inlet system. Samples were separated using ACQUITY UPLC BEH C18 columns (130 Å, 1.7 µm, 2.1 mm X 50 mm). The LC system was coupled to a Waters Xevo TQ-S tandem quadrupole mass spectrometer with a Micromass Zspray™ Atmospheric Pressure Ionisation (API) Source. Data analysis was conducted using MassLynx® software (v4.1).

Stock solutions of RAL and RAL-*d*6 were prepared at 1 mg/mL in DMSO. RAL-*d*6 was selected as the internal standard. Working solutions of RAL and RAL-*d*6 were prepared at

10000, 1000, 10, 1 ng/mL and 10000, 1000, 15 ng/mL, respectively. Calibration standards were prepared by diluting working solutions in appropriate volumes of neat ACN to obtain a calibration range of 0.1-100 ng/mL of RAL and a fixed concentration of 10 ng/mL of RAL-*d*6. Quality control standards (QCs) were prepared at 3.33 (low), 33.33 (medium), and 333.33 (high) ng/mL of RAL in neat ACN. Spiked serum QCs were prepared with the addition of blank serum to neat ACN resulting in the final concentration of 33.33 ng/mL of RAL. Samples were prepared within 72 hours prior to analysis and stored at -20 °C until analysis.

Mobile phase A was composed of 10 mM of formic acid in ultrapure water and mobile phase B was composed of 10 mM formic acid in 50:50 ACN: MeOH. Solvents were prepared before each set of analyses. The flow rate of the mobile phase was fixed at 0.5 mL/min. Injection volumes were fixed at 2 μL. The mobile phase gradient was initially fixed at 98% A:2% B for 1 minute. Over the next 5 minutes, the ratio of mobile phase B was increased such that the ratio was 0% A:100% B; this ratio was held for the following 2 minutes. The following mobile phase method was to minimize carryover in between analysis of different samples. Over the following 0.10 minute, the ratio of B was decreased such that the ratio of mobile phase was 98% A:2% B. The ratio of B was increased once more such that the ratio of mobile phase was 0% A:100% B over 1 minute, and then held for 1 minute. This cycle was repeated twice more. Lastly, ratio of mobile phase was returned to 98% A:2% B over 0.10 minute and then held for 1.70 minutes.

The mass spectrometer was operated in positive ion mode. The ionization parameters were as follows: capillary voltage of 3 kV, cone voltage of 40 V, source temperature of 350 ° C, desolvation gas flow of 800 L/h, cone gas flow of 150 L/h, and collision gas flow of 0.15 L/min. The mass spectrometer was engaged in between 2.5-12.1 minutes for each run. The *m/z* transitions and retention times for RAL and RAL-*d*6 were as follows: 445.35→109.10, 4.10 min

and 451.35→115.10, 4.11 min, respectively. The C_{max}, T_{max}, and AUC_{all} were determined by using the PKNCA R package by Denney *et al* [205].

5.3.6. Histological assessment of subcutaneous injection sites

At the termination of the animal study, mice were sacrificed, and the injection site was excised for histological assessment. For single injection studies, the skin distal to the injection site was excised and acted as the control. Following tissue excision, the skin was cut into strips of the subcutaneous space and placed in histology cassettes. The skin was washed twice with PBS and then fixed in formalin overnight. Fixed tissue was embedded in paraffin, sectioned in 4 µm cross-sections of the subcutaneous space, and then stained with Masson's trichrome and hematoxylin and eosin (H&E) stains. Sectioning, embedding, and staining were conducted by the Histology and Imaging Core at the University of Washington.

5.4. RESULTS AND DISCUSSION

5.4.1. Co-injection of separate and mixed solution of RAL and RAL-MSEMA drugamer subcutaneous injection depots

To combine the advantages of the pRAL and pRAL-MSEMA drugamer, mice were subcutaneously injected with both polymers to investigate whether their pharmacokinetic profiles could be superimposed to achieve a summation for extended release. Two study arms were conducted to investigate the feasibility of formulating the homopolymer and copolymer as one single solution. In one arm (CoS) of the study, mice were injected with pRAL in the right flank (5 mg of RAL) and pRAL-MSEMA in the left flank (5 mg of RAL). In the other arm (CoF), pRAL and pRAL-MSEMA were formulated as one single solution (dosage of 5 mg of RAL from

the homopolymer and 5 mg of copolymer) and injected into both side flanks of the mice. The design of the study was summarized in **Fig 5.1**.

Both arms of the animal study exhibited similar pharmacokinetic curves, with comparable T_{max}, C_{max}, and AUC_{all}, and none of the differences being significantly different. Pharmacokinetic curves of the two arms of study is shown in **Fig. 5.2**. Both arms exhibited a T_{max}=14 d, a C_{max} of 585.59 and 446. 44 ng/mL (CoS and CoF, respectively), and AUC_{all} of 8628 and 7902 d ng mL^{-1} (CoS and CoF, respectively). In both arms of the animal study, serum RAL concentrations were above the target concentration immediately upon administration and persisted above the target concentration for 28 days, dropping below the target thereafter.

The hypothesis that the hydrophilicity of pRAL-MSEMA in the CoF drugamer solution would drive greater water influx and result in a greater C_{max} was not supported by the data. Instead, the C_{max} in the CoF was slightly lower than in the CoS arm, although the difference was not significant. In the CoS arm, mice are subcutaneously injected with the pRAL and pRAL-MSEMA at separate injection sites, one would expect to see a true summation of the two pharmacokinetic curves of the individual drugamers. The difference in C_{max} might be more aptly attributed to the frequency of blood samples taken, as the "true" T_{max} might occur sometime in between t=7-14 d. However, what is more likely is the faster depot clearance in the CoF arm contributing to the lower C_{max}. The depots in the CoF study arm might have greater water penetration, and resulting in a faster clearing of the depot, and thus why the experimental C_{max} of CoF is less than C_{max} of CoS. Similarly to the what was observed in section 4.4.4, polymer chains that still contain conjugated RAL might have also been shed from the depot earlier, as the hydrodynamic radius may be sufficiently small to be cleared by renal clearance [204]. This hypothesis was in agreement with the IVIS data, wherein the fluorescence intensities of the

depots of CoF began to decrease at t=15-20 d (**Fig S17**), while the fluorescence intensity of the pRAL depot of CoS began to decline at t=35 d. This hypothesis may also explain the slight decrease in the AUC of the CoF arm. This suggests that the depot formation and elimination were different when drugamers were injected as separate or a coformulation, but the resulting pharmacokinetic profile and parameters would not be significantly different.

Co-injection of RAL homopolymer drugamer with RAL-MSEMA copolymer drugamer combined the advantages of delivery of the two polymers, and sustained release of RAL above the target concentration without a window of "lag" in release for 28 days. In addition, *in vivo* studies investigating the differences in drug delivery of RAL with injections of separate solutions versus co-formulation of two different drugamers demonstrated that pharmacokinetic curves obtained are not significantly different. It may be possible to administer subcutaneous injections of different copolymers as one single injection to obtain the same pharmacokinetic curve. This approach addresses user concerns highlighted in a survey study performed by Simoni *et al.*, where individuals living with HIV (PLWH) have indicated receiving more than a single injection per clinic visit to be "deal breakers" in selecting long-acting injectables as treatment [40]. In summary, the co-injection strategy effectively combined the unique advantages of pRAL and pRAL-MSEMA and explored the potential of a single-injection approach for sustained RAL delivery.

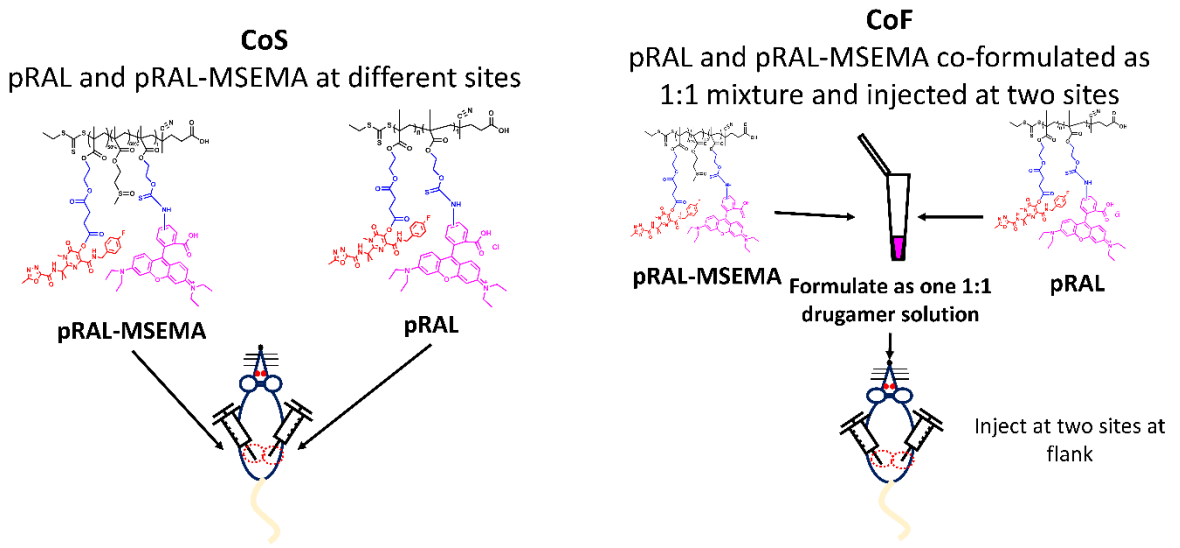

Fig 5. 1. Separate arms of the co-injection of pRAL and pRAL-MSEMA drugamers

(A) In one arm (CoS), mice were subcutaneously injected with two different RAL drugamers in each side flank. (B) In another arm (CoF), two different RAL drugamers were formulated as one single solution and mice were subcutaneously injected in each side flank.

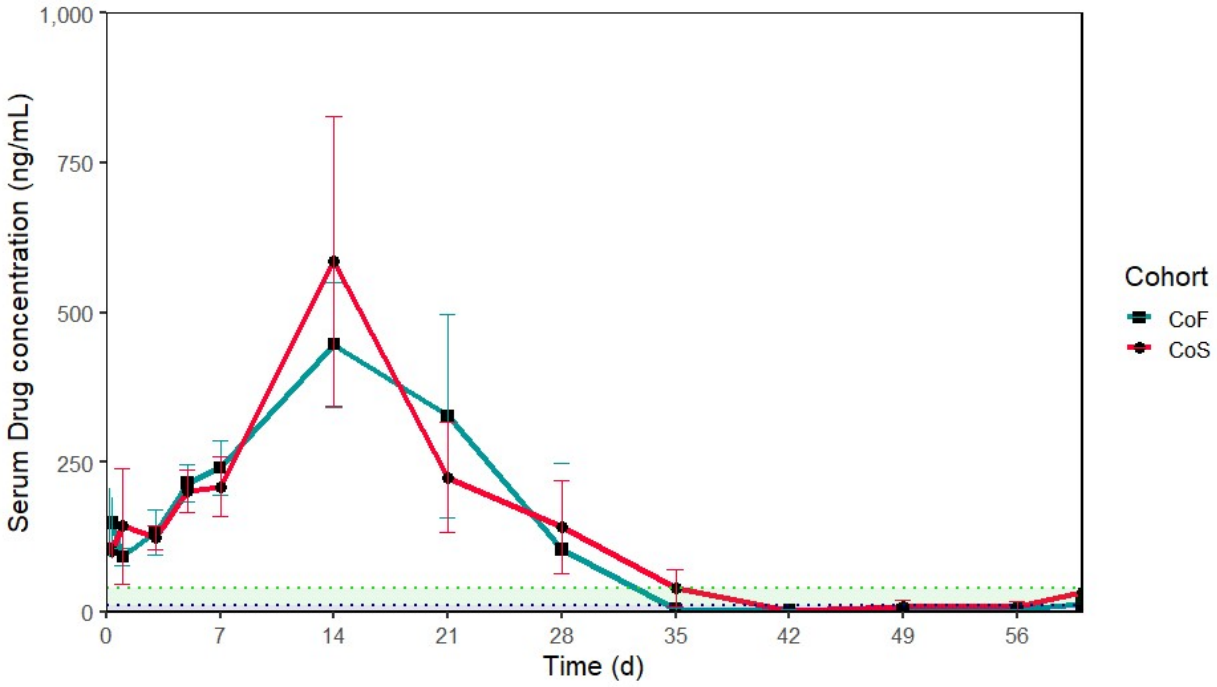

Fig 5. 2. Co-injection of RAL homopolymer and RAL-MSEMA copolymer drugamer

Both arms of the study demonstrated sustained release above the target concentration for 28 days after administration. The red curve represents CoS, in which mice were received separate injections of different RAL drugamers. The cyan curve represents CoF, in which mice received injections of a co-formulated mixture of RAL homopolymer and copolymer drugamers.

5.4.2. Co-injection of RAL-MSEMA and RAL-BMA drugamer subcutaneous injection depots

In the effort to achieve the longest duration of RAL release, mice were subcutaneously administered with pRAL-MSEMA and pRAL-BMA at opposite flanks of mice. It was hypothesized that separate depots of pRAL-MSEMA and pRAL-BMA could achieve a summation of their respective release profiles and extend the overall duration of RAL release due to the staggered release profile. To inject depots of similar surface area and release profiles as the depots of single drugamer injection studies, mice were administered 5 mg each of pRAL-MSEMA and pRAL-BMA at the left and right flank, respectively (referred to as MBRAL). A summary of the treatment and expected outcome is shown below (**Fig 5.3**).

Co-injection of pRAL-MSEMA and pRAL-BMA combined the advantages of delivery of the two polymers with different degrees of hydrophilicity and sustained release of RAL above the target concentration without a window of "lag" in release for 42 days (**Fig 5.4**). The serum concentration of RAL reached a maximum value at t=14 d with a C_{max}=282.61 ng/mL. With the effective RAL dosage being doubled, the extent of exposure of RAL through co-injection was also approximately doubled (AUC_{all}=7239 ng d mL^{-1}, versus 3415 and 5057 ng d mL^{-1} for pRAL-MSEMA and pRAL-BMA, respectively). The formation of separate drugamer depots was confirmed by IVIS, wherein the fluorescence emitted by separate depots was localized in two distinct areas. In addition, the longitudinal tracking of the separate depots supported the mechanism behind sustained release (as shown in **Fig 5.5**). The similar dissolution kinetics were

attributed to keeping the dosage of RAL per injection site at 5 mg, which was the same as single injections, and resulted in similar depot formation. The fluorescence of the pRAL-MSEMA depot sharply decreased at t=15 d, whereas the fluorescence of the pRAL-BMA depot did not sharply decrease until t=45 d, which indicated the separate depots dissolving at different rates. This demonstrated that the release of RAL was primarily from pRAL-MSEMA for the first 14 days of release, while the remaining 28 days of release were attributed to pRAL-BMA.

To our knowledge, the duration of RAL release achieved in this work is the longest that has been observed due to the novel ways of modulating release implemented in this paper. Previous efforts in sustaining release above the 4 x PA-IC90 observed release for 18 days with long-acting nanosuspension formulation administered subcutaneously. Moreover, the duration of release achieved in MBRAL exceeded previous dissolution- and diffusion-based DDS developed previously in-house while simultaneously eliminating the initial lag of RAL release (as shown in **Fig S18**) [93]. By utilizing a polymeric prodrug approach, the duration of release above the 4 x PA-IC90 was extended to more than twice as long. As discussed in the previous subsection, copolymerization with different comonomers can extend the release of RAL, but only within a range of 14 days. Thus, the co-injection strategy was employed to further extend the duration of release by achieving a summation of the release profiles of different RAL copolymer drugamers. The choice to administer pRAL-MSEMA and pRAL-BMA was due to the least amount of overlap in the windows of RAL release, which was validated to achieve the longest duration of release. The design of future drugamers with drugs with low pK_a can consider the usage of both copolymerization and co-injection to extend the longest duration of release.

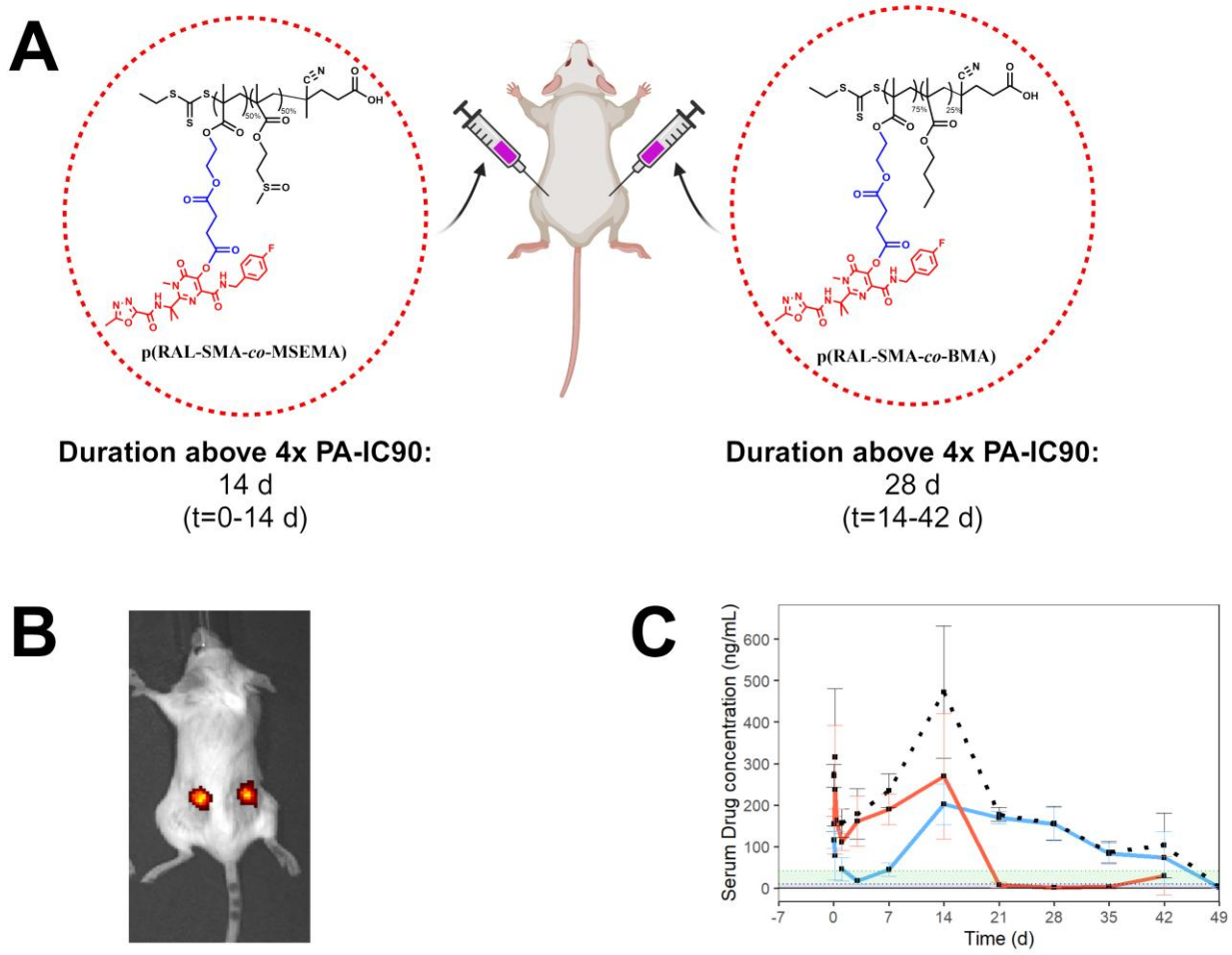

Fig 5. 3. Summary of dual injection of pRAL-MSEMA and pRAL-BMA

(A) Mice were subcutaneously administered pRAL-MSEMA at their left flank, and pRAL-BMA at their right flank. (B) Visualization of a mouse that received subcutaneous co-injection of RAL drugamers at opposite flanks. Depots were shown as the red and yellow areas. (C) Summation of release profiles of pRAL-MSEMA and pRAL-BMA is shown as the black dashed line. The summation of release profiles predict release profile for the co-injection study. Individual release profiles are shown in red and blue for pRAL-MSEMA and pRAL-BMA, respectively. Image created with BioRender.com.

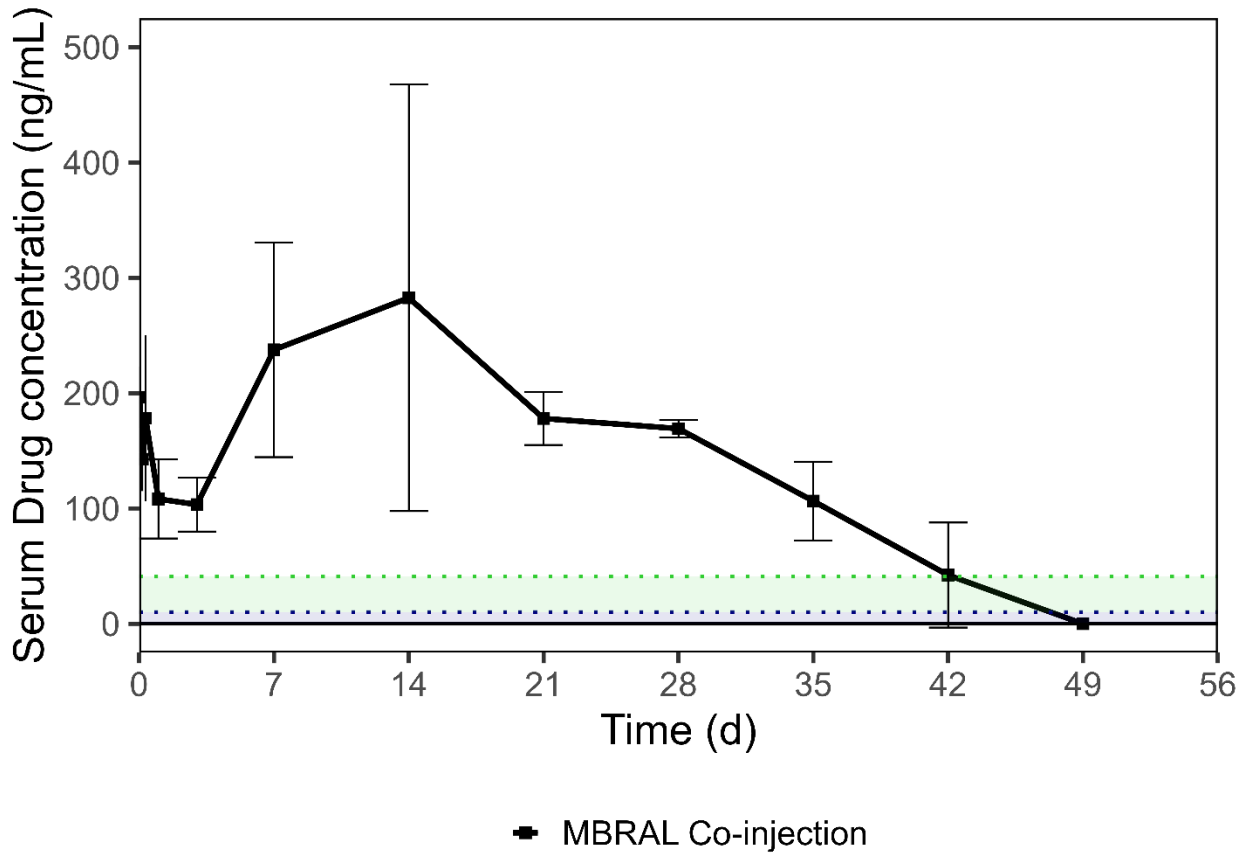

Fig 5. 4. Pharmacokinetic profile of co-injection of pRAL-MSEMA and pRAL-BMA in murine models

(A) Separate subcutaneous injections of pRAL-MSEMA and pRAL-BMA formulated in DMSO were administered with dosages of equivalent 5 mg of RAL in each flank, totaling 10 mg/mouse. Serum concentration of RAL was measured *via* LC-MS/MS to establish release profile

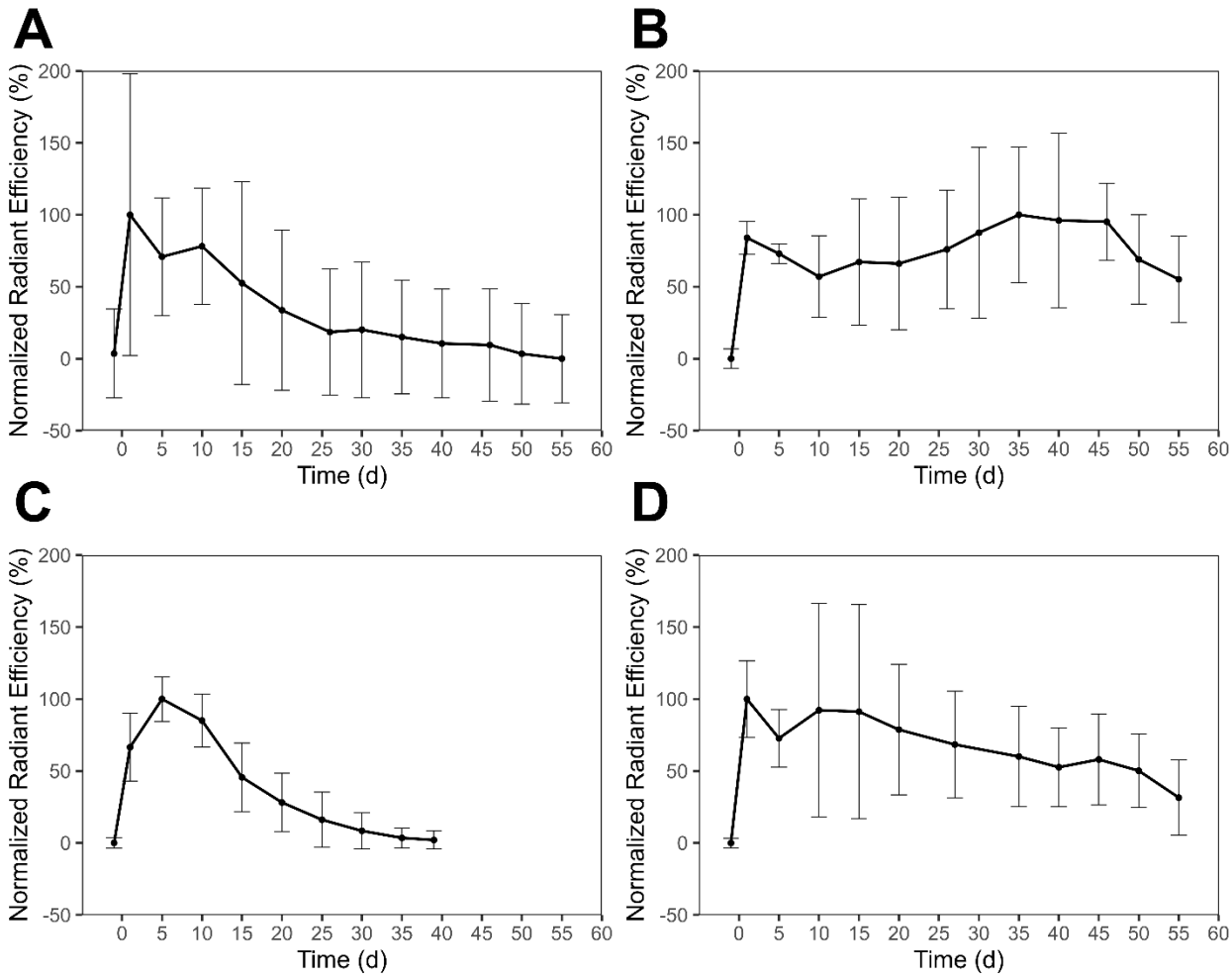

Fig 5. 5. Comparison of dissolution kinetics of co-injection versus single injections of pRAL-MSEMA and pRAL-BMA

(A) Depot of pRAL-MSEMA in MBRAL cohort. (B) Depot of pRAL-BMA in MBRAL cohort. (C) Depot of pRAL-MSEMA in single injection study (discussed in section 4.4.4). (D) Depot of pRAL-BMA in single injection study (discussed in section 4.4.4).

5.4.3. Tolerability and histological assessment to drugamer co-injections

Tolerability towards the co-injections of RAL drugamers was assessed by tracking weight changes and histological analyses after animal sacrifice. Similar to single injections of RAL drugamers, mice receiving co-injections of RAL drugamers did not experience weight loss

throughout the study, and the final weight increase at study termination was 18.87%, 18.97%, and 18.64% in the CoS, CoF, and MBRAL cohorts, respectively. The longitudinal tracking of weight is shown in **Fig S14**. As discussed in section 4.4.6, the weight increase suggest that mice experienced minimal distress to the increased dosage of RAL [215].

Histological analyses of excised injection sites demonstrated comparable foreign body response to co-injections as single injections of RAL drugamers. Upon visual inspection of the injection site, the depot was no longer observable, which was similar to what was observed in single injections. This observation was supported by the comparison of depot dissolution kinetics by IVIS (**Fig 5.5**), which indicated that dissolution kinetics were similar to single injections. Moreover, collagen deposition due to drugamer co-injection was comparable to single injections, as exhibited by Masson's trichrome stains of excised injection sites demonstrated an increase in collagen deposition in all injection sites (**Fig S19**). H&E stains of injection sites also did not indicate a slight elevation in lymphocyte infiltration, but not any greater than that of single injections (**Fig 5.6**). In the MBRAL injection site administered with pRAL-BMA (**Fig 5.6G**), lymphocyte infiltration was greater than the other histological images. This was expected due to the slower dissolution of the pRAL-BMA depot, and thus less time was allowed for the subcutis to return to basal state (**Fig 5.6A**). Despite this, these findings indicate that co-injections did not elicit a greater foreign body response than single injections, while significantly extending the sustained release of RAL.

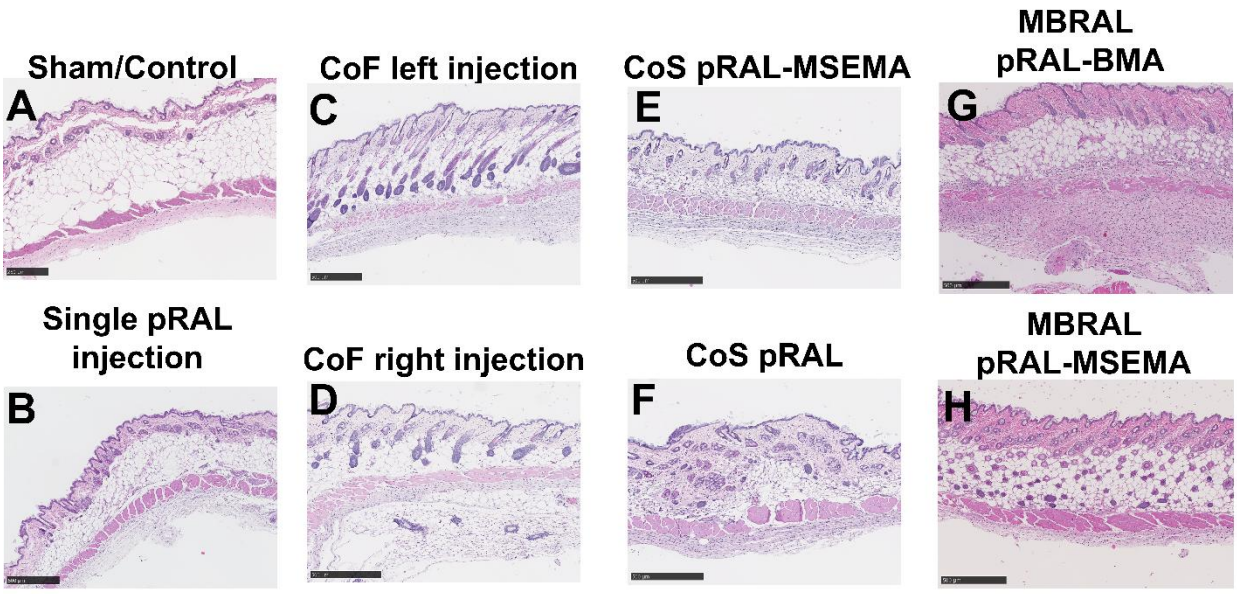

Fig 5. 6. Histological assessment of injection sites in co-injection studies stained with Masson's Trichrome stain

Injection sites were excised and stained with Masson's Trichrome. (A) Sham control. (B) Injection site from single injection of pRAL. (C-D) The left and right injection site of the CoF cohort, respectively. (E) CoS injection site of pRAL-MSEMA. (F) CoS injection site of pRAL. (G) MBRAL injection site of pRAL-BMA. (H) MBRAL injection site of pRAL-MSEMA. Co-injections exhibited slight increase in lymphocyte infiltration, particularly the MBRAL injection site administered with pRAL-BMA.

5.5. CONCLUSION

In this work, we developed RAL drugamers capable of sustained and tunable release of RAL *via* ISFIs, achieving the longest reported in the literature to date. Our findings demonstrated that the release rate of drugs can be tuned not only by controlling the water penetration into the depot but also by co-injection of distinct RAL drugamers. Co-injection of pRAL-MSEMA and pRAL-BMA extended release of RAL to 42 days above the 4 x PA-IC90 threshold, which was

the longer duration than previous dissolution- and diffusion-based DDS. Moreover, our results suggest that different drugamers could potentially be formulated together as a single solution and administered as a single subcutaneous injection.

Future work on the delivery of ARV drugamers should focus on further extending release of drugs and translating co-injection strategies to other drugs. To further extend the release of RAL, strategies such as alternative linkers and modification of polymer molecular weight can be employed [219,220]. When combined with the co-injection strategy, new RAL copolymer drugamers may potentially extend release beyond 42 days. Additionally, formulation strategies should be investigated to determine if co-injections can be administered as one single injection to satisfy the critical needs of potential users. For individuals living with HIV (PLWH), receiving more than a single injection per clinic visit to be "deal breakers" in selecting long-acting injectables as treatment [40]. However, syringeability and depot formation studies would need to be conducted, as these factors impact drug release [39,228].

Subcutaneously administered RAL drugamers can potentially be used as HIV PrEP or co-delivered with other ARVs for treatment. Injection volumes of RAL drugamers in humans could potentially less than that of LA-CAB and LA-RPV (3 mL), as shown in the allometric dosage calculation in **Appendix A, Section S3** [229]. In addition, our results demonstrate that the drugamer formulation strategy could be applied to other hydrophilic drugs to achieve a longer duration of release provided the presence of functional groups amenable for conjugation to cleavable linkers, such as some nucleoside reverse transcriptase inhibitors or tetracycline antibiotics. The drugamer formulation expands the toolbox for sustained delivery of drugs beyond noncovalent LA-DDS and can potentially be applied for PrEP and treatment in other diseases. However, careful consideration must be undertaken in the design of the drugamer to

achieve the target release rate, as our findings indicated the release rate being dependent upon the chemically modifiable functional group. In addition to the promise of the drugamer strategy, our results highlight that a similar release profile could be expected of drugs with hydroxyl groups with similar pK_a values.

APPENDIX A: SUPPORTING MATERIALS FOR CHAPTER 3-5

S1. Stability testing of ATV-SMA in polar aprotic solvents to determine polymerization conditions

The stability of ATV-SMA was measured using the same equipment as described in subsection 3.3.4. ATV-SMA was dissolved in DMF or DMSO and incubated at a water bath at 45 °C to determine the stability of ATV-SMA over time. At t=0, 1, 2, 12, 18, 24, 135 h, 10 µL of the incubated solution was drawn up and prepared for HPLC analysis by diluting with 90 µL of acetonitrile. Samples were eluted with a gradient flow of 38:62 acetonitrile:25 mM KH_2PO_4 to 73:27 acetonitrile:25 mM KH_2PO_4 over 8 min at 1 mL/min, then held at 38:62 acetonitrile:25 mM KH_2PO_4 for the remaining time for a total elution time of 20 min while measuring the absorbance at 300 nm.

S2. Determination of target concentration of RAL

The primary objective of the antiretroviral drugamer is to provide sustained pre-exposure prophylactic effect. In order to determine whether the RAL-drugamer is capable of achieving this effect, we identified the target serum concentration of RAL in which the subject can be protected from HIV infection. In other words, we must identify the serum concentration of RAL in mice that would provide pre-exposure prophylactic effect while considering the allometric scaling of the basal metabolic rate between mice and human. Akkina *et al.* employed humanized mouse (BALB/c-Rag2$^{-/-}$γc$^{-/-}$(RAG-hu)) to demonstrate pre-exposure prophylaxis against HIV-1 vaginal transmission [230]. Akkina *et al.* administered RAL daily by oral gavage (3.28 mg per 20 g mouse, calculated by using interspecies allometric scaling factor of 12.3) for one week and induced vaginal viral challenge on the 4th day. Humanized mice dosed with RAL (n=6) were fully protected from HIV-1 viral challenge. The trough plasma concentration of RAL was

determined to be 3.6 ng/mL [231]. However, Kovarova *et al.* also developed long-acting formulations of RAL and noted viral rebound in HIV-challenged humanized mice despite plasma concentration above 3.6 ng/mL [223]. Viral rebound was also observed in some mice in which plasma concentration of RAL was above the PA-IC90 value (10.22 ng/mL). Hence, the target concentration of RAL drugamers was determined to be 4x PA-IC90 (40.88 ng/mL) for a greater confidence in delivering a protective concentration. 4x PA-IC90 has also been used as the "target" for long-acting cabotegravir [232].

S3. Allometric scaling calculations for prediction of RAL drugamer solution formulation for humans

In order to predict the potential volume of subcutaneous injections of drugamers in humans, allometric scaling is performed to extrapolate the dosage of RAL drugamers. Allometric scaling calculations were performed according to the protocol developed by Nair *et al* [233]. The human equivalent dosage (HED) was calculated with **Eq (S1)**. The reference body weights of mice and humans are 0.02 and 60, respectively. The exponent in **Eq (S1)** was applied to account for body surface area and metabolic rate differences. The animal dose was determined to be 250 mg/kg given the reference weight of mice.

$$HED\ \left(\frac{mg}{kg}\right) = Animal\ dose\ \left(\frac{mg}{kg}\right) \times \left(\frac{Weight_{animal}[kg]}{Weight_{human}[kg]}\right)^{(1-0.67)} \quad (S1)$$

HED was calculated to be 17.38 mg/kg. Using the reference weight of humans provided by Nair *et al.*, human dosages were calculated to be 1068.17 mg of RAL. For a RAL drugamer subcutaneous injection to be less than 3 mL, RAL drugamers must be formulated at concentrations of 477.29, 686.31, and 580.94 mg/mL for pRAL, pRAL-MSEMA, and pRAL-BMA, respectively.

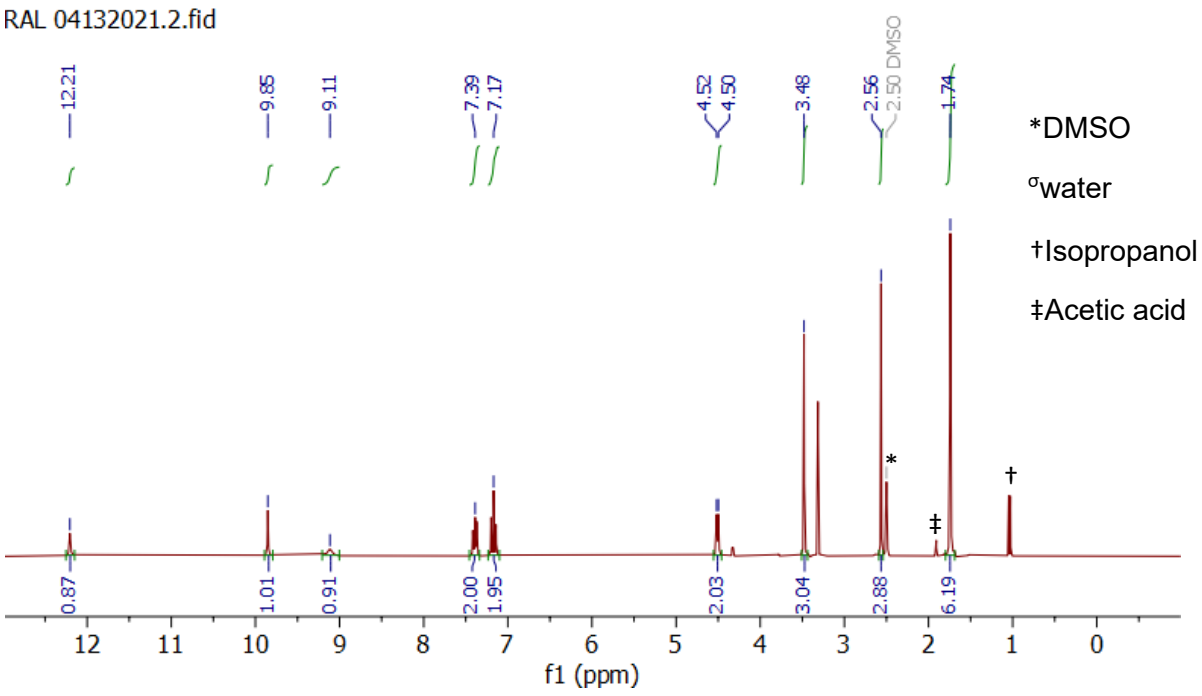

Fig S1. ^{1}H-NMR (300.1 MHz) of purified RAL in DMSO-*d*6

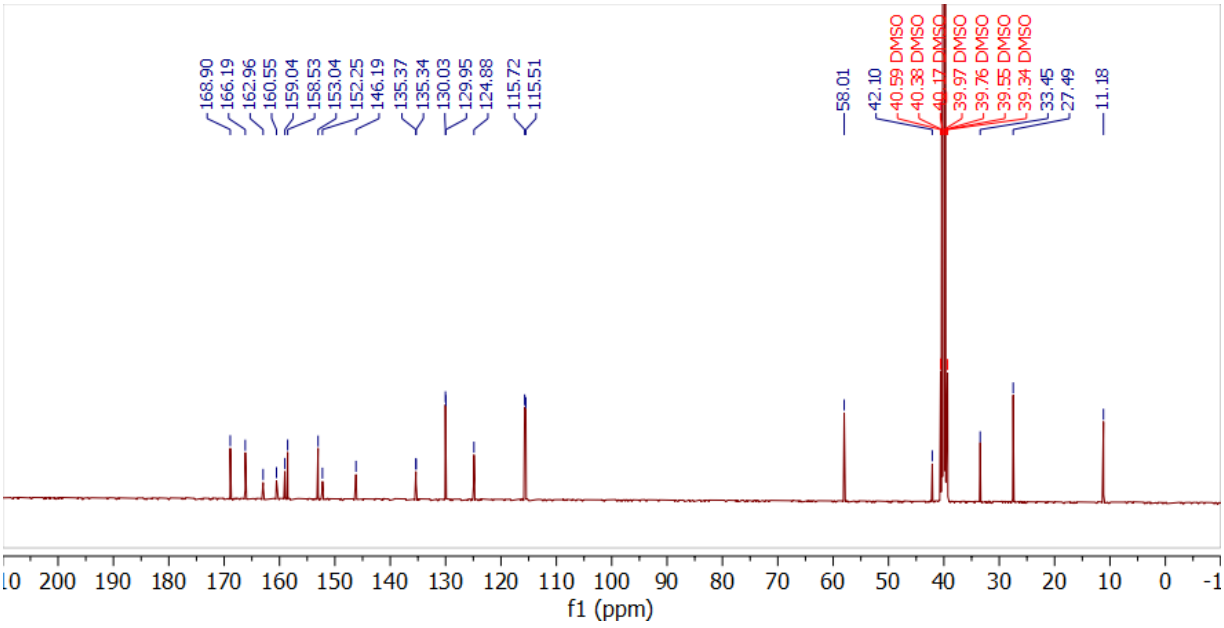

Fig S2. ^{13}C-NMR (101 MHz) of purified RAL in DMSO-*d*6

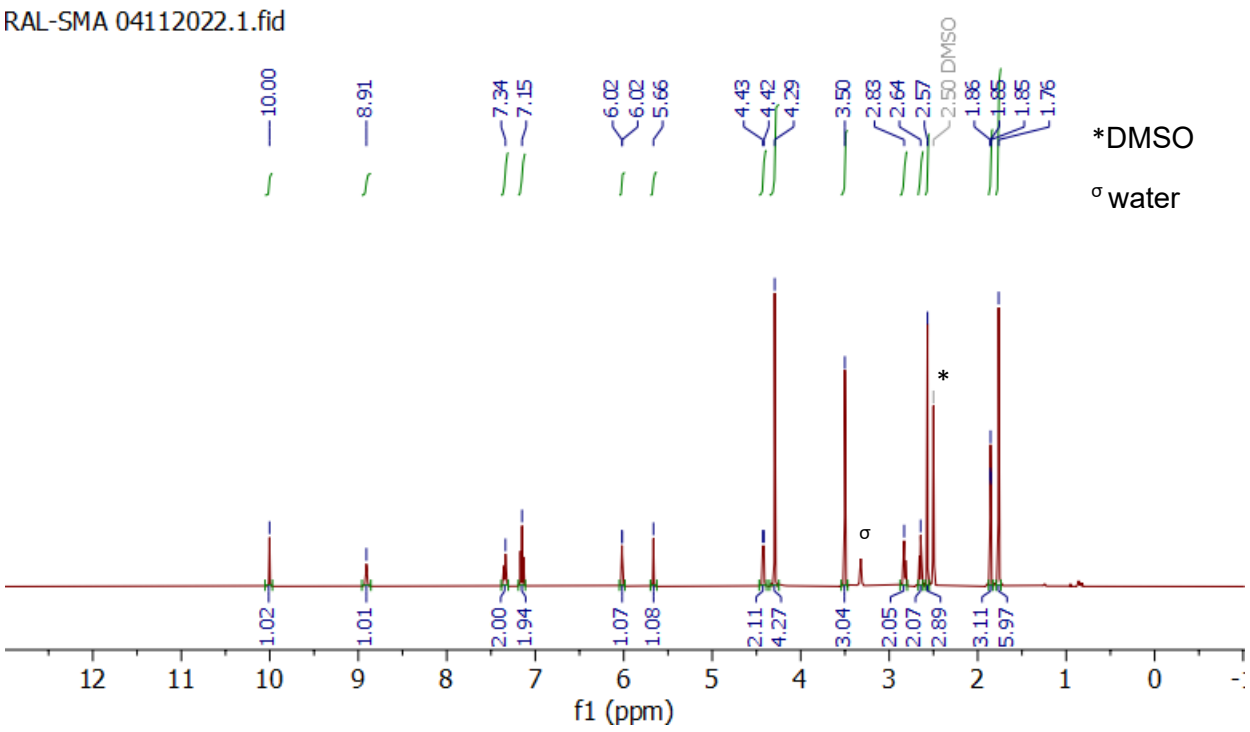

Fig S3. ^{1}H-NMR (500 MHz) of RAL-SMA in DMSO-*d*6

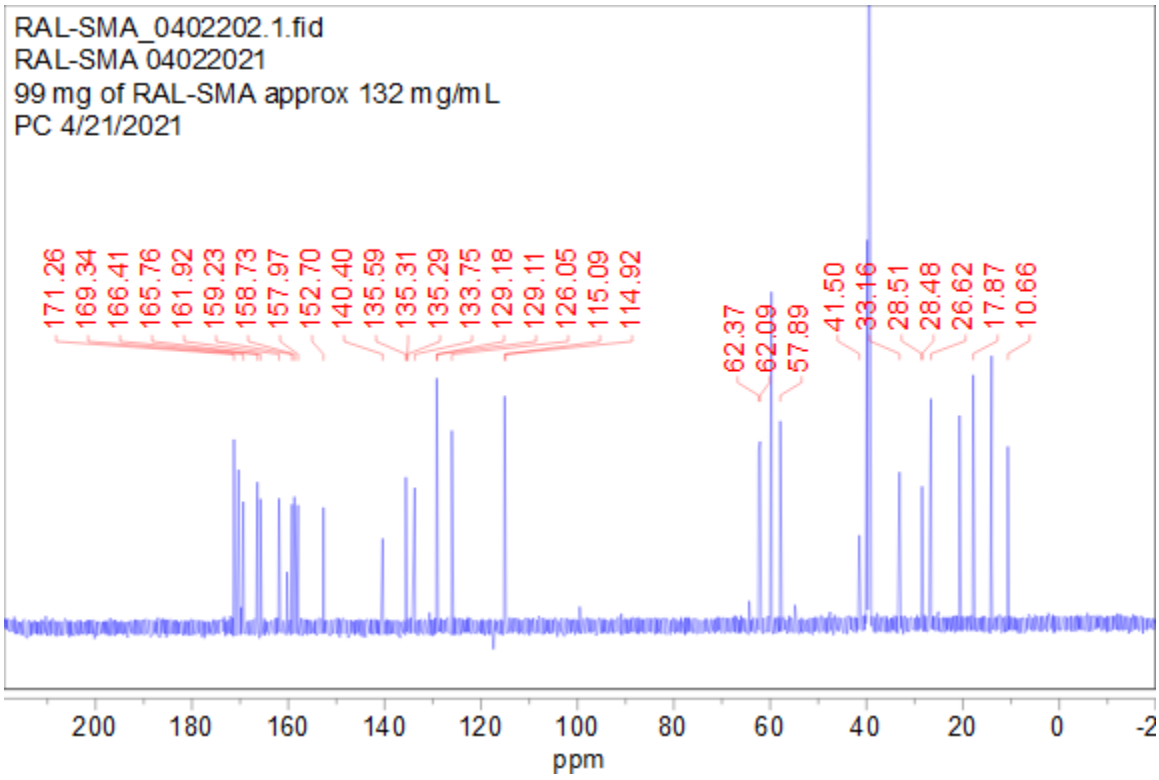

Fig S4. ^{13}C-NMR (126 MHz) of RAL-SMA in DMSO-*d*6

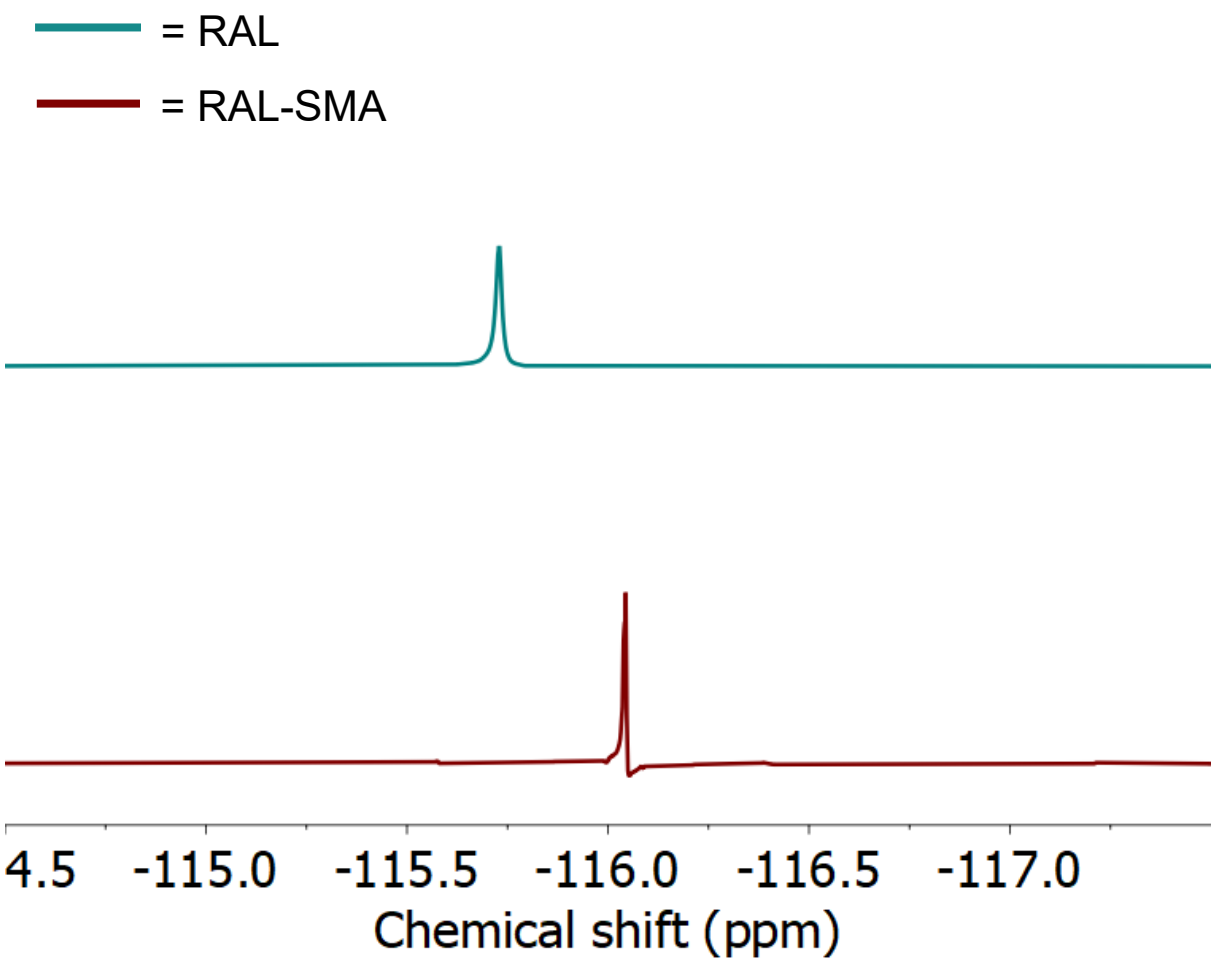

Fig S5. Stacked ^{19}F-NMR spectrum of RAL and RAL-SMA.

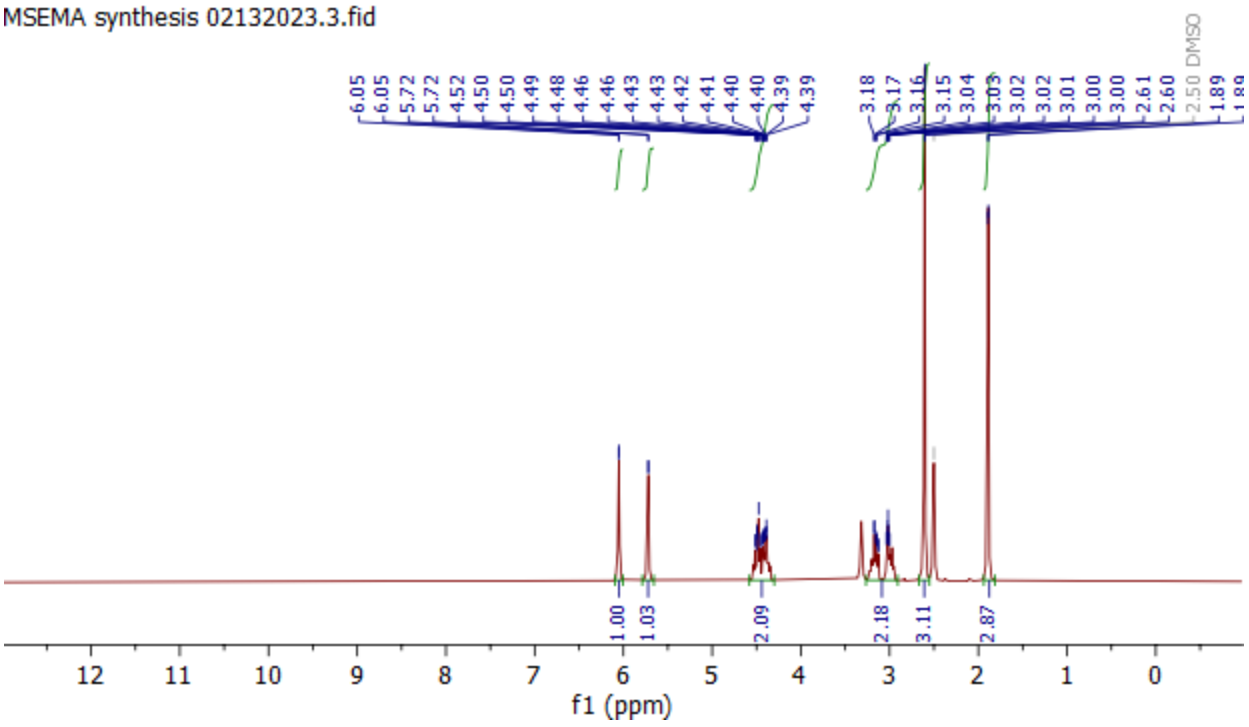

Fig S6. ^{1}H-NMR (300 MHz) of MSEMA in DMSO-d6.

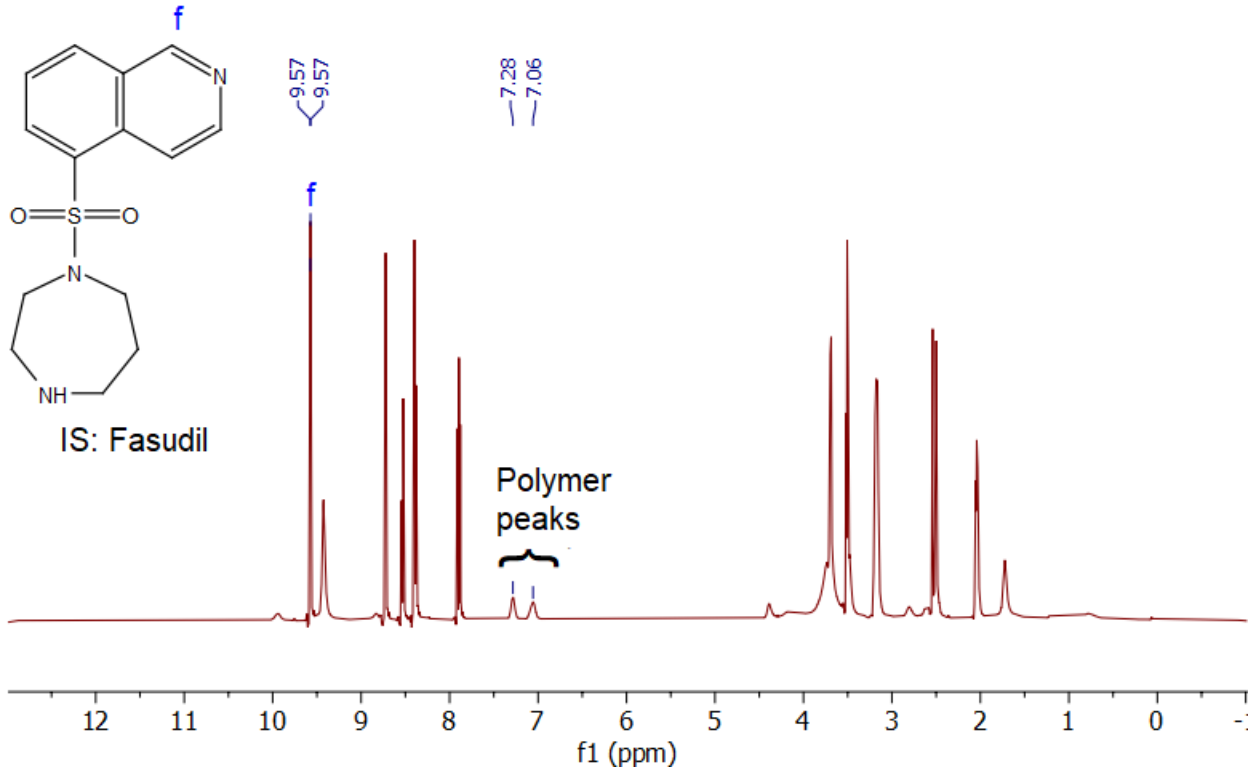

Fig S7. [1]H-NMR spectra of RAL homopolymer spiked with Fasudil as the internal standard

The ratio of proton signals of the RAL homopolymer peaks (δ=7.06, 7.28 ppm, 4H, denoted by the brackets) to the fasudil peak (δ=9.57 ppm, 1H) was used to determine drug loading. The same method was used to determine the drug loading of other drugamers.

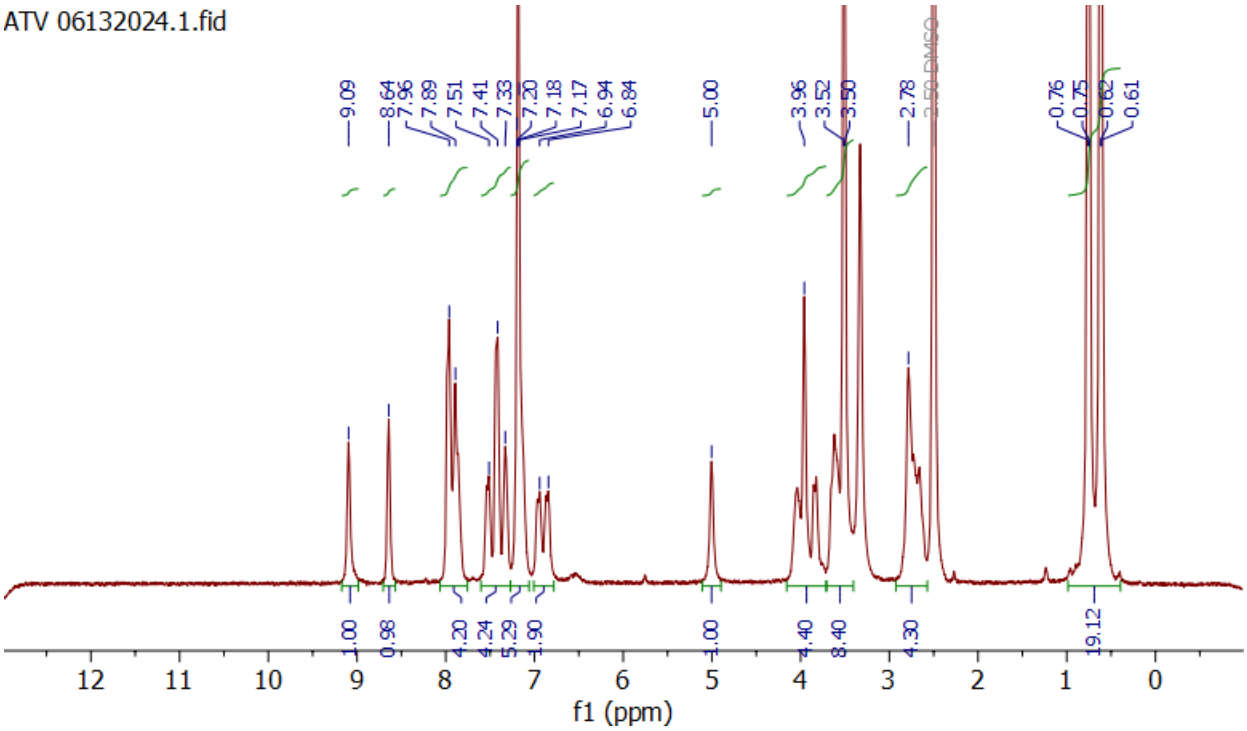

Fig S8. [1]H-NMR (300 MHz) of ATV in DMSO-*d*6

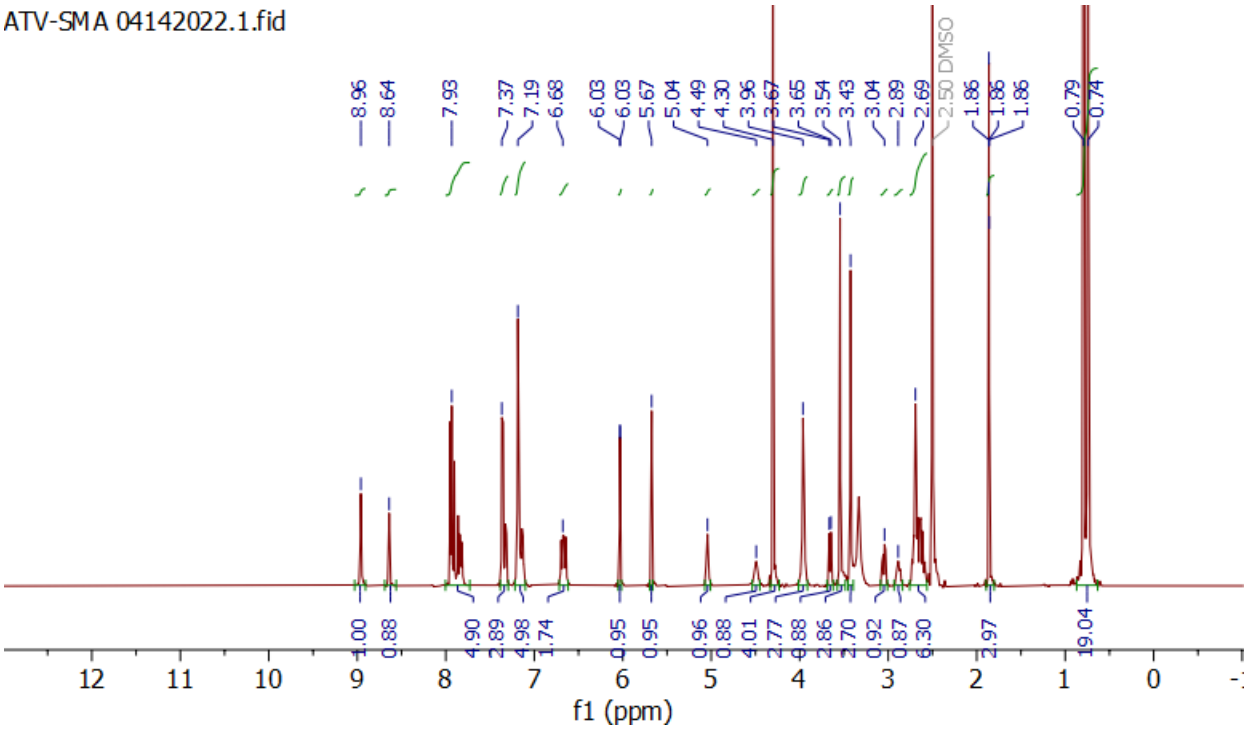

Fig S9. ^{1}H-NMR (300 MHz) of ATV-SMA in DMSO-*d*6

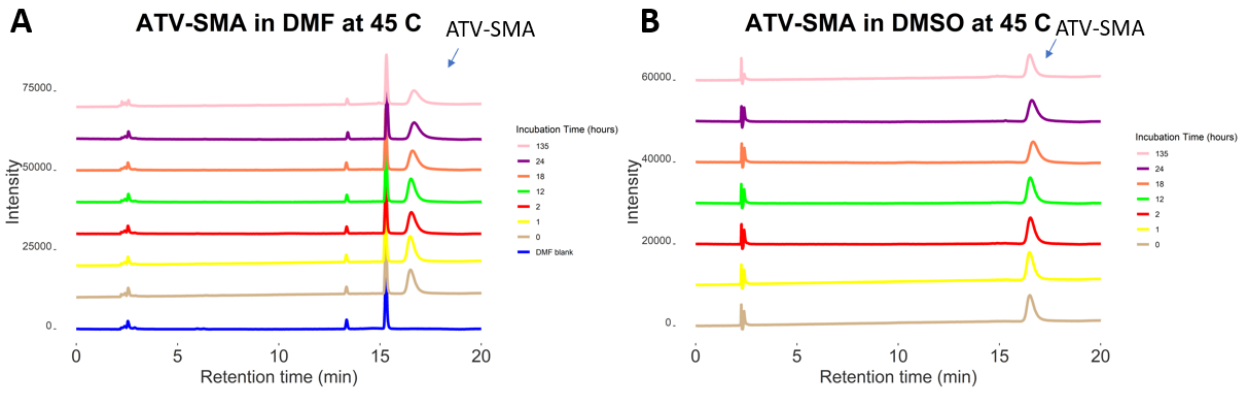

C

DMF 45 C

Time (h)	Hydrolysis (%)
0	0
1	-6.90247
2	0.762793
12	-2.38413
18	2.561578
24	7.931965
135	22.62033

DMSO 45 C

Time (h)	Hydrolysis (%)
0	0
1	-4.48323
2	N/A
12	0.266881
18	5.299314
24	3.725212
135	19.42423

c

Table S1. Cloud points of RAL drugamer solutions prepared in DMSO

	Polymer Solution Concentration (mg/mL)	Water (wt%)	DMSO (wt%)	Polymer (wt%)

pRAL	300.00	9.14	71.39	19.47
	75.00	17.35	77.38	5.28
	37.50	18.60	78.71	2.68
	9.38	23.15	76.20	0.65
	4.69	36.93	62.80	0.27
pRAL-MSEMA	300.00	17.85	64.55	17.60
	75.00	22.14	72.89	4.97
	37.50	29.43	68.24	2.33
	9.38	32.24	67.19	0.57
	4.69	46.55	53.23	0.23
pRAL-BMA	300.00	4.47	75.06	20.47
	75.00	16.98	77.72	5.30
	37.50	16.51	80.74	2.75
	9.38	20.12	79.20	0.68
	4.69	19.93	79.73	0.34

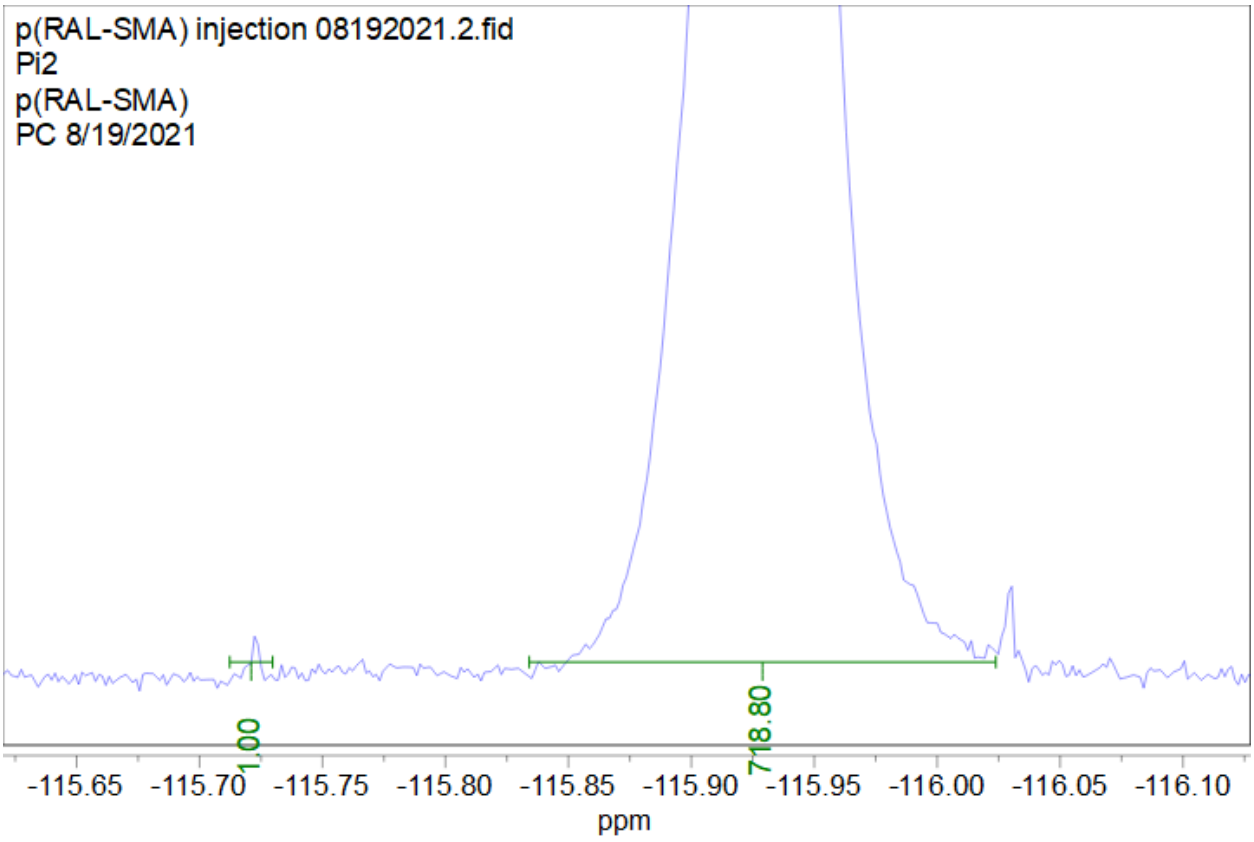

Fig S10. Investigation of premature hydrolysis of pRAL prior to subcutaneous administration

The degree of hydrolysis of RAL drugamers was assessed by taking the ^{19}F-NMR spectra immediately after subcutaneous injection of the drugamer in mice. The significantly larger, upfield peak corresponds to the fluorine signal from the RAL that is still conjugated to the polymer backbone in pRAL. The small, downfield peak corresponds to free RAL that may have hydrolyzed off of the backbone during the formulation step. In this sample, premature hydrolysis was determined to be 0.13%, thus it was concluded that minimal hydrolysis occurred during the formulation step.

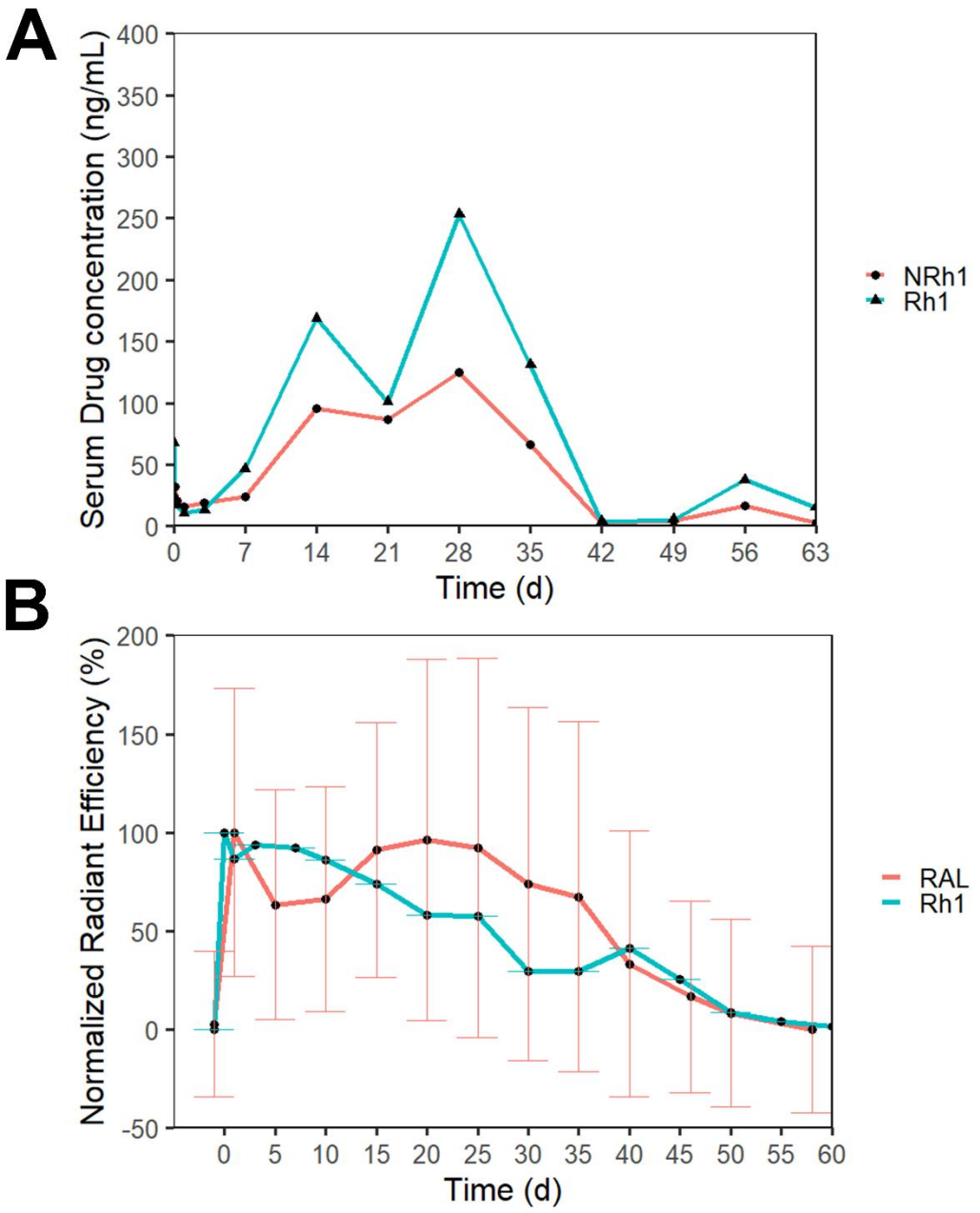

Fig S11. Study of effect of rhodamine unit on release profile of RAL drugamers

(A) One female BALB/cJ mouse was subcutaneously administered RAL homopolymer drugamer tagged with one rhodamine unit per chain (denoted as Rh1). Another mouse was subcutaneously administered the same dosage of RAL homopolymer drugamer without the rhodamine tag (denoted as NRh1). Release curves were compared and rhodamine was determined not to inhibit

the release of RAL. (B) The longitudinal tracking of the radiant efficiency of Rh1 compared with a separate cohort of mice subcutaneously injected with RAL homopolymer drugamers with one rhodamine unit per chain (denoted as RAL). The fluorescence data demonstrated the depot dissolution kinetics of the two cohorts were comparable.

Fig S 12. Representative image of depot area measurement by ImageJ

Fluorescence images of mice subcutaneously injected with pRAL at t=1 d analyzed with ImageJ to measure the "tightness" of depot.

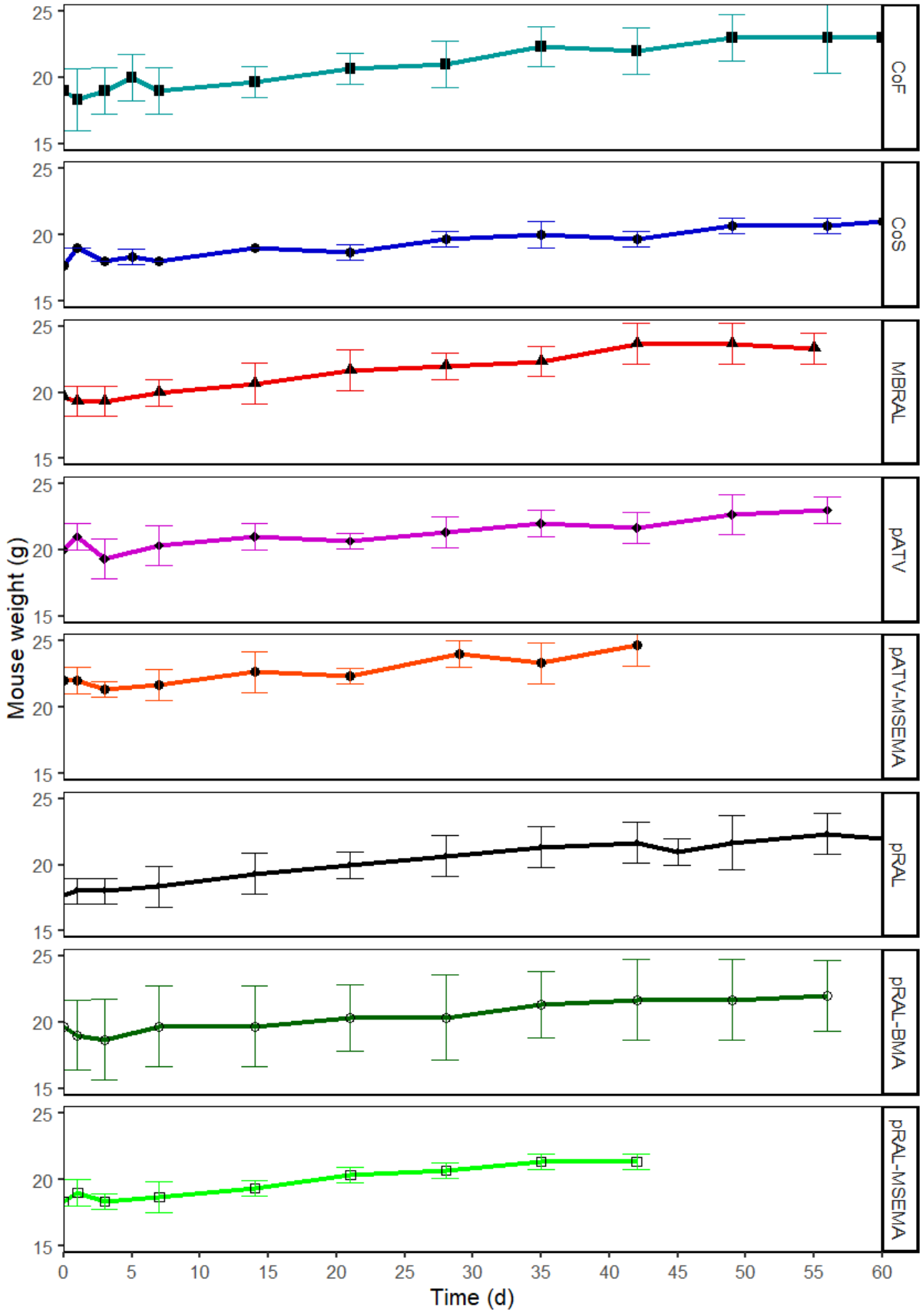
Mouse weight (g)
Time (d)
CoF
CoS
MBRAL
pATV
pATV-MSEMA
pRAL
pRAL-BMA
pRAL-MSEMA
25
20
15
0
5
10
15
20
25
30
35
40
45
50
55
60

Fig S13. Longitudinal tracking of mice weight post-administration of drugamers

Mice were weighed prior to administration of single injection and co-injection drugamers and every time blood was collected. The facet labels on the right refers to the separate cohorts. Following administration, mice weight steadily increases, indicating good tolerability towards ARV drugamers.

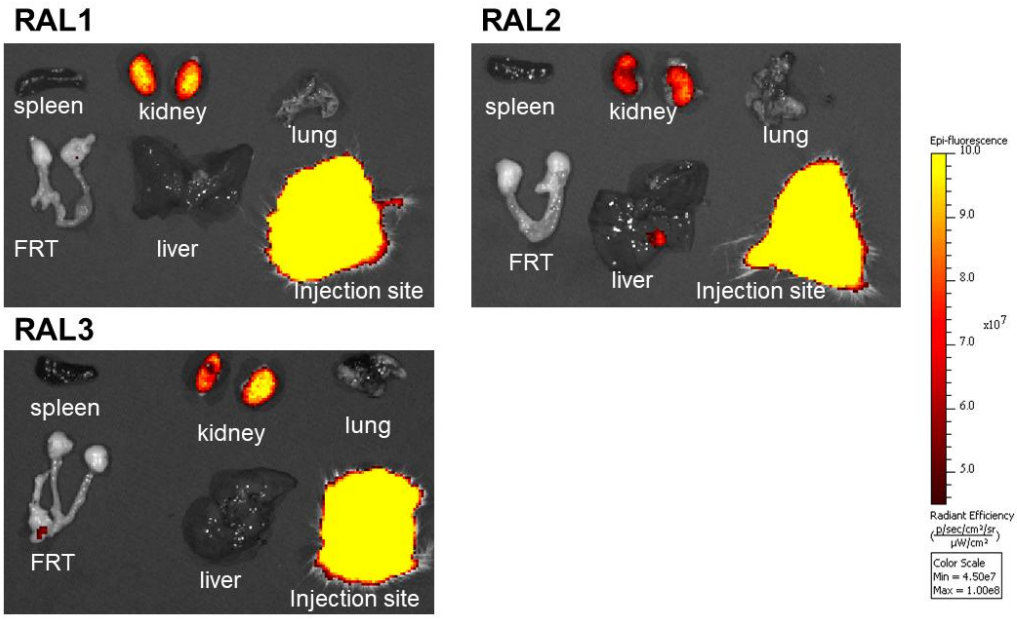

Fig S14. IVIS images of excised organs of mice that were administered pRAL

The spleen, kidney, lung, female reproductive tract (FRT), liver, and skin (injection site) were excised and imaged by IVIS. Fluorescence was detected in the injection site, due to rhodamine staining the injection site, which is visible by the naked eye. Fluorescence was also detected in the kidney, due to polymers being cleared by renal clearance after cleavage of RAL.

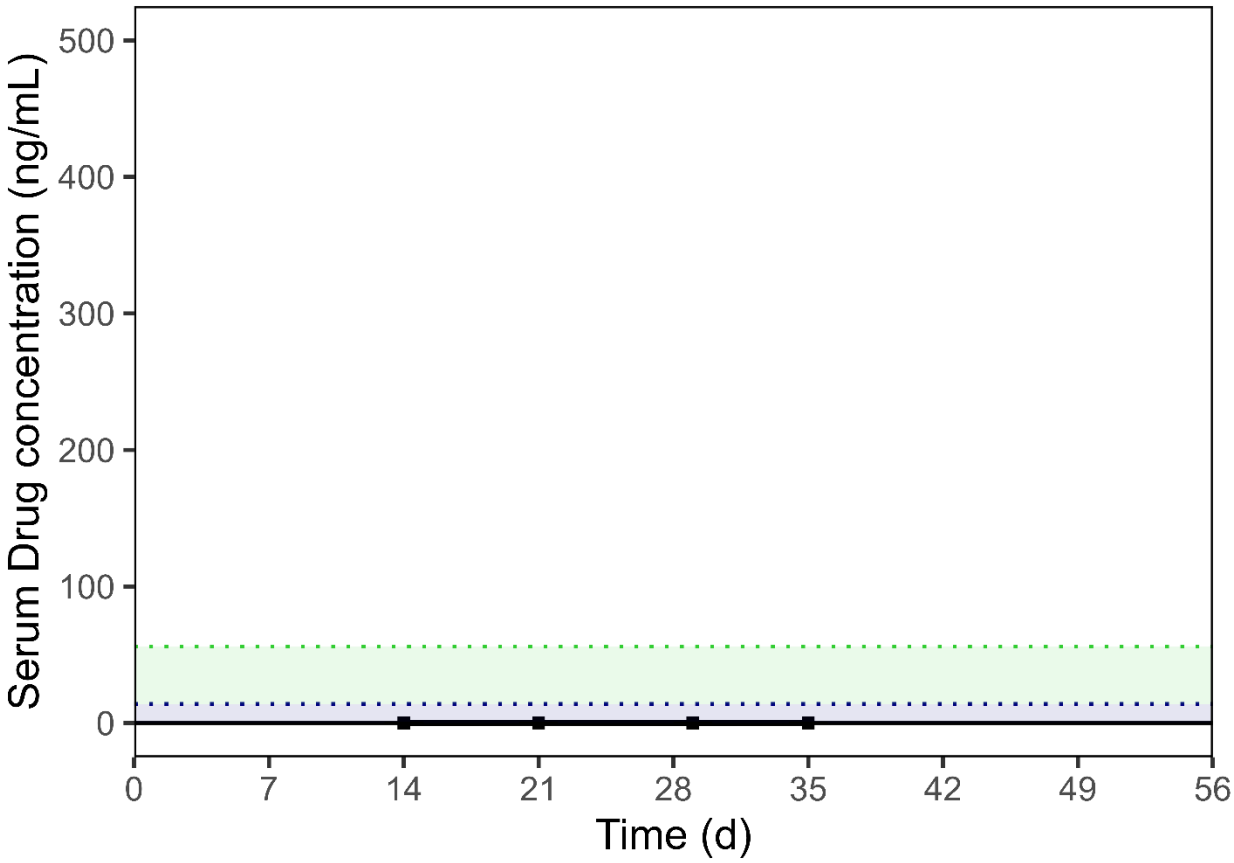

Fig S15. Pharmacokinetic profile of single subcutaneous pATV-MSEMA injections in murine models

ATV was detectable but not quantifiable. Due to ATV not being quantifiable over t=14-35 d, serum concentrations of ATV were not measured for other timepoints.

Table S2. Co-injection RAL dosage

Study	**Left Depot RAL Dosage (mg)**	**Right Depot RAL Dosage (mg)**	**Total RAL Dosage (mg)**
CoF	5.48±0.24	4.76±0.32	9.62 ±0.57
CoS	4.50±0.29 [a]	5.05±0.14 [b]	9.55 ±0.25
MBRAL	4.73±0.39 [c]	4.84±0.22 [a]	9.56 ±0.45

[a] pRAL-MSEMA depot
[b] pRAL depot
[c] pRAL-BMA depot

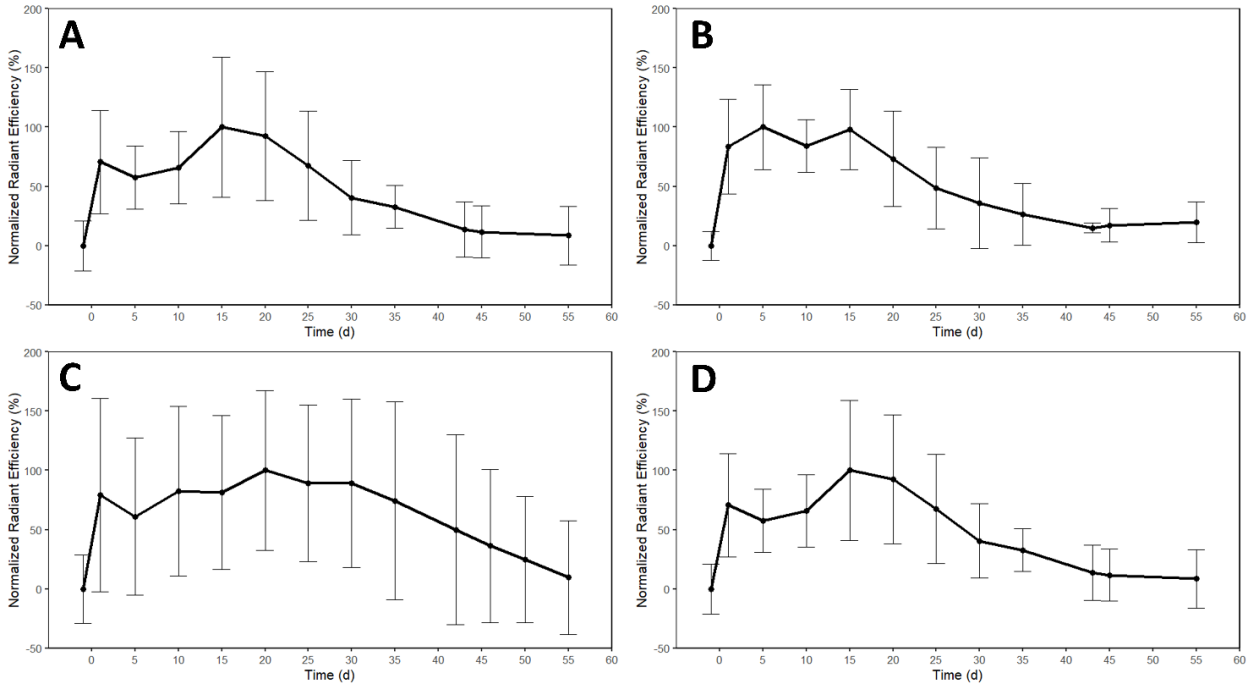

Fig S16. Longitudinal fluorescence tracking of depot of co-injection of pRAL and pRAL-MSEMA

(A-B) Longitudinal tracking of depot of CoF arm. (A) Left flank depot. (B) Right flank depot. (C-D) Longitudinal tracking of depot of CoS arm. (C) RAL homopolymer depot. (D) RAL-MSEMA copolymer depot.

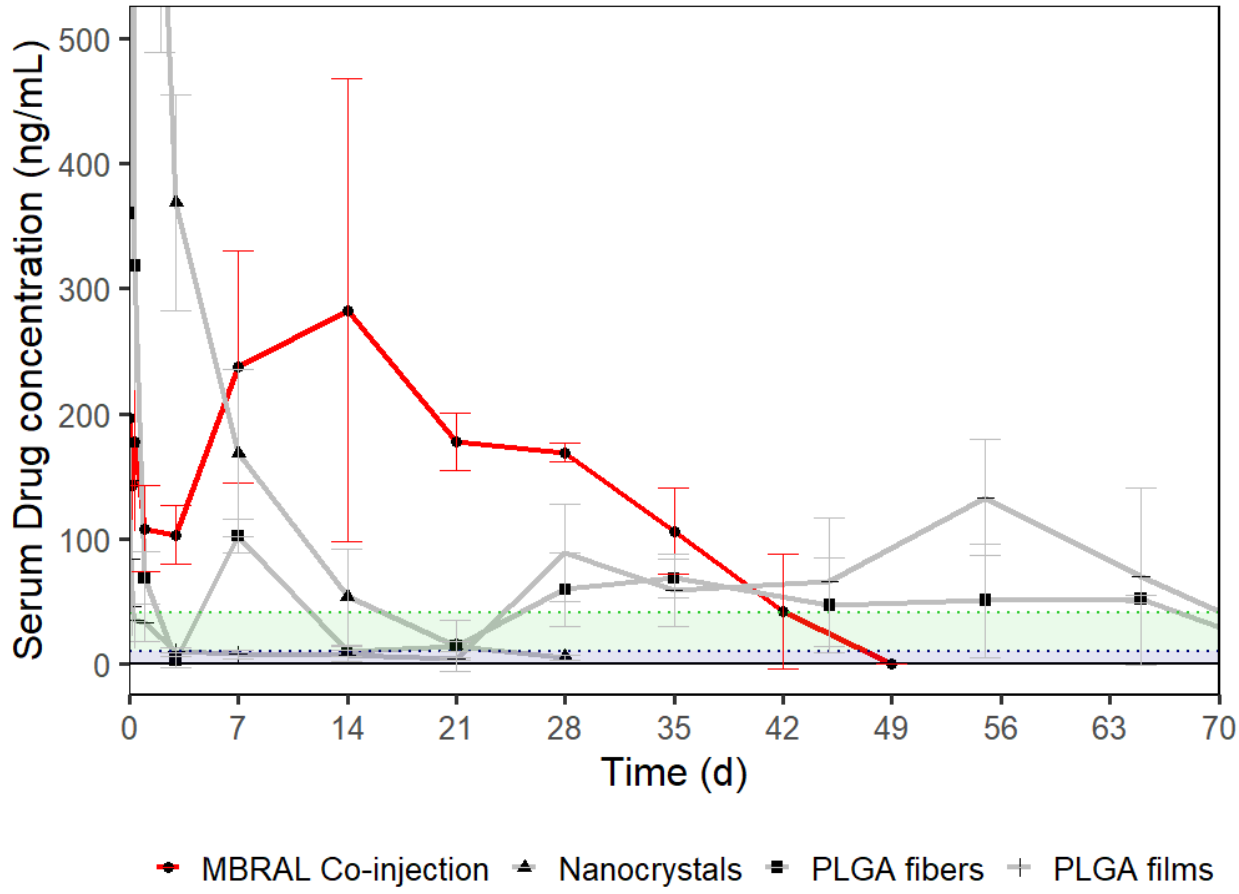

Fig S17. Comparison of co-injection pharmacokinetic curves with diffusion- and dissolution-based DDS

Co-injections of pRAL-MSEMA and pRAL-BMA (MBRAL) achieved the longest duration of release of 42 days. Release from co-injections of RAL drugamers exhibited longer durations than diffusion- and dissolution-based DDS previously developed by Hernandez *et al* [93].

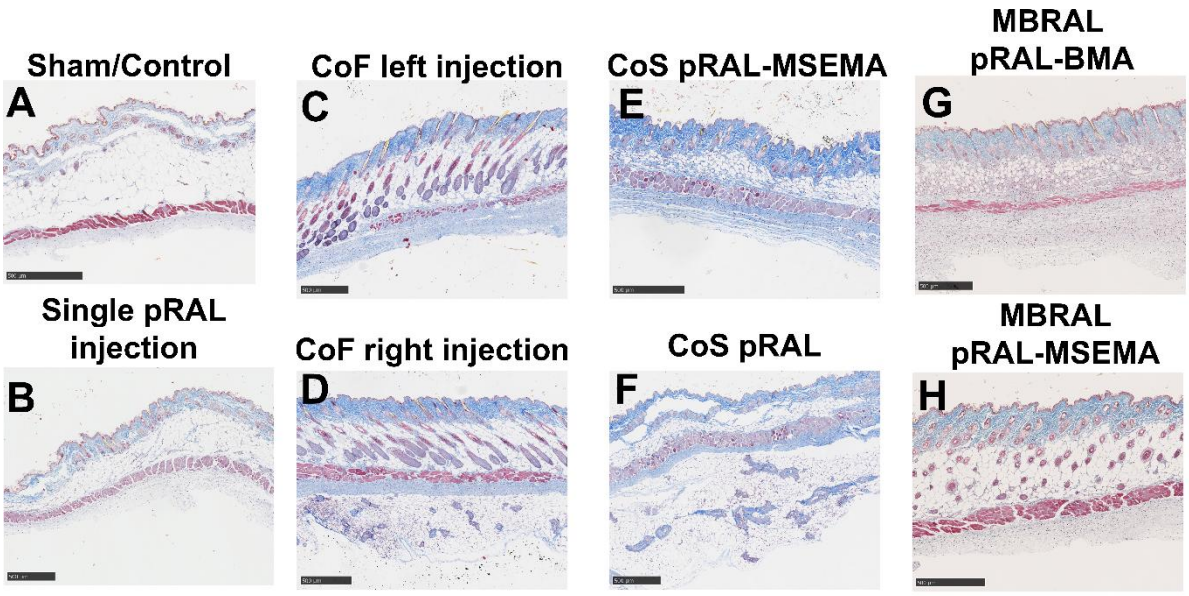

Fig S18. Histological assessment of injection sites in co-injection studies stained with Masson's Trichrome stain

Injection sites were excised and stained with Masson's Trichrome. (A) Sham control. (B) Injection site from single injection of pRAL. (C-D) The left and right injection site of the CoF cohort, respectively. (E) CoS injection site of pRAL-MSEMA. (F) CoS injection site of pRAL. (G) MBRAL injection site of pRAL-BMA. (H) MBRAL injection site of pRAL-MSEMA.

BIBLIOGRAPHY

[1] C.D. Holtzer, M. Roland, The Use of Combination Antiretroviral Therapy in HIV-Infected Patients, Annals of Pharmacotherapy 33 (1999) 198–209. https://doi.org/10.1345/aph.18145.

[2] P. Arashiro, C.G. Maciel, F.P.R. Freitas, G.S.R. Koch, J.C.P. da Cunha, A.R. Stolf, A.M.M. Paniago, M.J. de Medeiros, C.D.B. Santos-Pinto, E.F. de Oliveira, Adherence to antiretroviral therapy in people living with HIV with moderate or severe mental disorder, Sci Rep 13 (2023) 3569. https://doi.org/10.1038/s41598-023-30451-z.

[3] J.Z. Li, S. Gallien, H. Ribaudo, A. Heisey, D.R. Bangsberg, D.R. Kuritzkes, Incomplete adherence to antiretroviral therapy is associated with higher levels of residual HIV-1 viremia, AIDS 28 (2014). https://journals.lww.com/aidsonline/fulltext/2014/01140/incomplete_adherence_to_antiretroviral_therapy_is.4.aspx.

[4] V.D. Lima, J. Geller, D.R. Bangsberg, T.L. Patterson, M. Daniel, T. Kerr, J.S.G. Montaner, R.S. Hogg, The effect of adherence on the association between depressive symptoms and mortality among HIV-infected individuals first initiating HAART, AIDS 21 (2007). https://journals.lww.com/aidsonline/fulltext/2007/05310/the_effect_of_adherence_on_the_association_between.11.aspx.

[5] M. Martin, S. Vanichseni, P. Suntharasamai, U. Sangkum, P.A. Mock, M. Leethochawalit, S. Chiamwongpaet, M.E. Curlin, S. Na-pompet, A. Warapronmongkholkul, S. Kittimunkong, R.J. Gvetadze, J.M. McNicholl, L.A. Paxton, K. Choopanya, The impact of adherence to preexposure prophylaxis on the risk of HIV infection among people who inject drugs, AIDS 29 (2015) 819–824. https://doi.org/10.1097/QAD.0000000000000613.

[6] E. Quiros-Roldan, C. Torti, G. Lapadula, N. Ladisa, V. Micheli, A. Patroni, M. Cusato, P. Pierotti, V. Tirelli, M.C. Uccelli, S. Di Giambenedetto, F. Castelnuovo, F. Gargiulo, N. Manca, G. Carosi, T.R.-M.S. Group, Adherence And Plasma Drug Concentrations Are Predictors of Confirmed Virologic Response after 24-Week Salvage Highly Active Antiretroviral Therapy, AIDS Patient Care STDS 21 (2007) 92–99. https://doi.org/10.1089/apc.2005.0037.

[7] P.K. Drain, A.R. Bardon, J.M. Simoni, T.R. Cressey, P. Anderson, D. Sevenler, A.O. Olanrewaju, M. Gandhi, C. Celum, Point-of-care and Near Real-time Testing for Antiretroviral Adherence Monitoring to HIV Treatment and Prevention, Curr HIV/AIDS Rep 17 (2020) 487–498. https://doi.org/10.1007/s11904-020-00512-3.

[8] J.R. Castillo-Mancilla, J.-H. Zheng, J.E. Rower, A. Meditz, E.M. Gardner, J. Predhomme, C. Fernandez, J. Langness, J.J. Kiser, L.R. Bushman, P.L. Anderson, Tenofovir, Emtricitabine, and Tenofovir Diphosphate in Dried Blood Spots for Determining Recent and Cumulative Drug Exposure, AIDS Res Hum Retroviruses 29 (2013) 384–390. https://doi.org/10.1089/aid.2012.0089.

[9] A.O. Olanrewaju, B.P. Sullivan, A.R. Bardon, T.J. Lo, T.R. Cressey, J.D. Posner, P.K. Drain, Pilot evaluation of an enzymatic assay for rapid measurement of antiretroviral drug concentrations, Virol J 18 (2021) 77. https://doi.org/10.1186/s12985-021-01543-x.

[10] D. Bukenya, B.N. Mayanja, S. Nakamanya, R. Muhumuza, J. Seeley, What causes non-adherence among some individuals on long term antiretroviral therapy? Experiences of individuals with poor viral suppression in Uganda, AIDS Res Ther 16 (2019) 2. https://doi.org/10.1186/s12981-018-0214-y.

[11] A. Owen, S. Rannard, Strengths, weaknesses, opportunities and challenges for long acting injectable therapies: Insights for applications in HIV therapy, Adv Drug Deliv Rev 103 (2016) 144–156. https://doi.org/https://doi.org/10.1016/j.addr.2016.02.003.

[12] V. Agrahari, S.M. Anderson, M.M. Peet, A.P. Wong, O.N. Singh, G.F. Doncel, M.R. Clark, Long-acting HIV pre-exposure prophylaxis (PrEP) approaches: recent advances, emerging technologies, and development challenges, Expert Opin Drug Deliv 19 (2022) 1365–1380. https://doi.org/10.1080/17425247.2022.2135699.

[13] J.M. Baeten, T. Palanee-Phillips, E.R. Brown, K. Schwartz, L.E. Soto-Torres, V. Govender, N.M. Mgodi, F. Matovu Kiweewa, G. Nair, F. Mhlanga, S. Siva, L.-G. Bekker, N. Jeenarain, Z. Gaffoor, F. Martinson, B. Makanani, A. Pather, L. Naidoo, M. Husnik, B.A. Richardson, U.M. Parikh, J.W. Mellors, M.A. Marzinke, C.W. Hendrix, A. van der Straten, G. Ramjee, Z.M. Chirenje, C. Nakabiito, T.E. Taha, J. Jones, A. Mayo, R. Scheckter, J. Berthiaume, E. Livant, C. Jacobson, P. Ndase, R. White, K. Patterson, D. Germuga, B. Galaska, K. Bunge, D. Singh, D.W. Szydlo, E.T. Montgomery, B.S. Mensch, K. Torjesen, C.I. Grossman, N. Chakhtoura, A. Nel, Z. Rosenberg, I. McGowan, S. Hillier, Use of a Vaginal Ring Containing Dapivirine for HIV-1 Prevention in Women, New England Journal of Medicine 375 (2016) 2121–2132. https://doi.org/10.1056/NEJMoa1506110.

[14] Global HIV & AIDS statistics - Fact sheet, UNAIDS (2023). https://www.unaids.org/en/resources/fact-sheet.

[15] T.D. Leong, J. Nel, L. Jamieson, R. Osih, H. Dawood, H. Subedar, M. McCaul, L.F. Johnson, K. Cohen, A Review and Economic Analysis of the Dapivirine Vaginal Ring as HIV Pre-Exposure Prophylaxis for Women, to Inform South African Public-Sector Guidelines, JAIDS Journal of Acquired Immune Deficiency Syndromes 97 (2024). https://journals.lww.com/jaids/fulltext/2024/11010/a_review_and_economic_analysis_of_the_dapivirine.8.aspx.

[16] E.T. Montgomery, J. Stadler, S. Naidoo, A.W.K. Katz, N. Laborde, M. Garcia, K. Reddy, L.E. Mansoor, J. Etima, C. Zimba, M. Chitukuta, L. Soto-Torres, Reasons for nonadherence to the dapivirine vaginal ring, AIDS 32 (2018) 1517–1525. https://doi.org/10.1097/QAD.0000000000001868.

[17] E.T. Overton, G. Richmond, G. Rizzardini, H. Jaeger, C. Orrell, F. Nagimova, F. Bredeek, M. García Deltoro, S. Swindells, J.F. Andrade-Villanueva, A. Wong, M.-A. Khuong-

Josses, R. Van Solingen-Ristea, V. van Eygen, H. Crauwels, S. Ford, C. Talarico, P. Benn, Y. Wang, K.J. Hudson, V. Chounta, A. Cutrell, P. Patel, M. Shaefer, D.A. Margolis, K.Y. Smith, S. Vanveggel, W. Spreen, Long-acting cabotegravir and rilpivirine dosed every 2 months in adults with HIV-1 infection (ATLAS-2M), 48-week results: a randomised, multicentre, open-label, phase 3b, non-inferiority study, The Lancet 396 (2020) 1994–2005. https://doi.org/https://doi.org/10.1016/S0140-6736(20)32666-0.

[18] C. Trezza, S.L. Ford, W. Spreen, R. Pan, S. Piscitelli, Formulation and pharmacology of long-acting cabotegravir, Curr Opin HIV AIDS 10 (2015).

[19] R.J. Landovitz, B.S. Hanscom, M.E. Clement, H. V Tran, E.G. Kallas, M. Magnus, O. Sued, J. Sanchez, H. Scott, J.J. Eron, C. del Rio, S.D. Fields, M.A. Marzinke, S.H. Eshleman, D. Donnell, M.A. Spinelli, R.M. Kofron, R. Berman, E.M. Piwowar-Manning, P.A. Richardson, P.A. Sullivan, J.P. Lucas, P.L. Anderson, C.W. Hendrix, A. Adeyeye, J.F. Rooney, A.R. Rinehart, M.S. Cohen, M. McCauley, B. Grinsztejn, Efficacy and safety of long-acting cabotegravir compared with daily oral tenofovir disoproxil fumarate plus emtricitabine to prevent HIV infection in cisgender men and transgender women who have sex with men 1 year after study unblinding: a secondary anal, Lancet HIV 10 (2023) e767–e778. https://doi.org/10.1016/S2352-3018(23)00261-8.

[20] R.J. Landovitz, B.S. Hanscom, M.E. Clement, H. V Tran, E.G. Kallas, M. Magnus, O. Sued, J. Sanchez, H. Scott, J.J. Eron, C. del Rio, S.D. Fields, M.A. Marzinke, S.H. Eshleman, D. Donnell, M.A. Spinelli, R.M. Kofron, R. Berman, E.M. Piwowar-Manning, P.A. Richardson, P.A. Sullivan, J.P. Lucas, P.L. Anderson, C.W. Hendrix, A. Adeyeye, J.F. Rooney, A.R. Rinehart, M.S. Cohen, M. McCauley, B. Grinsztejn, Efficacy and safety of long-acting cabotegravir compared with daily oral tenofovir disoproxil fumarate plus emtricitabine to prevent HIV infection in cisgender men and transgender women who have sex with men 1 year after study unblinding: a secondary anal, Lancet HIV 10 (2023) e767–e778. https://doi.org/10.1016/S2352-3018(23)00261-8.

[21] NIH Statement on Preliminary Efficacy Results of Twice-Yearly Lenacapavir for HIV Prevention in Cisgender Women, NIH (2024). https://www.niaid.nih.gov/news-events/nih-statement-preliminary-efficacy-results-twice-yearly-lenacapavir-hiv-prevention?utm_campaign=+61149283&utm_content=&utm_medium=email&utm_source=govdelivery&utm_term=.

[22] C. Trezza, S.L. Ford, W. Spreen, R. Pan, S. Piscitelli, Formulation and pharmacology of long-acting cabotegravir, Curr Opin HIV AIDS 10 (2015). https://journals.lww.com/co-hivandaids/Fulltext/2015/07000/Formulation_and_pharmacology_of_long_acting.7.aspx.

[23] I. Usach, R. Martinez, T. Festini, J.-E. Peris, Subcutaneous Injection of Drugs: Literature Review of Factors Influencing Pain Sensation at the Injection Site, Adv Ther 36 (2019) 2986–2996. https://doi.org/10.1007/s12325-019-01101-6.

[24] K.K. Scarsi, Chasing the cabotegravir tail: implications for prevention, Lancet HIV 7 (2020) e451–e453. https://doi.org/10.1016/S2352-3018(20)30165-X.

[25] SUNLENCA® [PRODUCT MONOGRAPH], (2022).

[26] D.H. Surve, A.B. Jindal, Recent advances in long-acting nanoformulations for delivery of antiretroviral drugs, Journal of Controlled Release 324 (2020) 379–404. https://doi.org/https://doi.org/10.1016/j.jconrel.2020.05.022.

[27] E.D. Weld, C. Flexner, Long-acting implants to treat and prevent HIV infection, Curr Opin HIV AIDS 15 (2020) 33–41. https://doi.org/10.1097/COH.0000000000000591.

[28] L. Pinzi, N. Bisi, G. Rastelli, How drug repurposing can advance drug discovery: challenges and opportunities, Frontiers in Drug Discovery 4 (2024). https://doi.org/10.3389/fddsv.2024.1460100.

[29] J.M. Baeten, T. Palanee-Phillips, E.R. Brown, K. Schwartz, L.E. Soto-Torres, V. Govender, N.M. Mgodi, F. Matovu Kiweewa, G. Nair, F. Mhlanga, S. Siva, L.-G. Bekker, N. Jeenarain, Z. Gaffoor, F. Martinson, B. Makanani, A. Pather, L. Naidoo, M. Husnik, B.A. Richardson, U.M. Parikh, J.W. Mellors, M.A. Marzinke, C.W. Hendrix, A. van der Straten, G. Ramjee, Z.M. Chirenje, C. Nakabiito, T.E. Taha, J. Jones, A. Mayo, R. Scheckter, J. Berthiaume, E. Livant, C. Jacobson, P. Ndase, R. White, K. Patterson, D. Germuga, B. Galaska, K. Bunge, D. Singh, D.W. Szydlo, E.T. Montgomery, B.S. Mensch, K. Torjesen, C.I. Grossman, N. Chakhtoura, A. Nel, Z. Rosenberg, I. McGowan, S. Hillier, Use of a Vaginal Ring Containing Dapivirine for HIV-1 Prevention in Women, New England Journal of Medicine 375 (2016) 2121–2132. https://doi.org/10.1056/NEJMoa1506110.

[30] U.M. Parikh, C.A. Koss, J.W. Mellors, Long-Acting Injectable Cabotegravir for HIV Prevention: What Do We Know and Need to Know about the Risks and Consequences of Cabotegravir Resistance?, Curr HIV/AIDS Rep 19 (2022) 384–393. https://doi.org/10.1007/s11904-022-00616-y.

[31] B.L. Jilek, M. Zarr, M.E. Sampah, S.A. Rabi, C.K. Bullen, J. Lai, L. Shen, R.F. Siliciano, A quantitative basis for antiretroviral therapy for HIV-1 infection, Nat Med 18 (2012) 446–451. https://doi.org/10.1038/nm.2649.

[32] M.L. Cottrell, K.B. Patterson, H.M.A. Prince, A. Jones, N. White, R. Wang, A.D.M. Kashuba, Effect of HIV Infection and Menopause Status on Raltegravir Pharmacokinetics in the Blood and Genital Tract, Antivir Ther 20 (2014) 795–803. https://doi.org/10.3851/IMP2968.

[33] C. Barau, C. Delaugerre, J. Braun, N. de Castro, V. Furlan, I. Charreau, L. Gérard, C. Lascoux-Combe, J.-M. Molina, A.-M. Taburet, High Concentration of Raltegravir in Semen of HIV-Infected Men: Results from a Substudy of the EASIER-ANRS 138 Trial, Antimicrob Agents Chemother 54 (2009) 937–939.

[34] C. Herrera, J. Lwanga, M. Lee, S. Mantori, A. Amara, L. Else, S.D. Penchala, D. Egan, E. Challenger, L. Dickinson, M. Boffito, R. Shattock, S. Khoo, J. Fox, Pharmacokinetic/pharmacodynamic investigation of raltegravir with or without

lamivudine in the context of HIV-1 pre-exposure prophylaxis (PrEP), Journal of Antimicrobial Chemotherapy 76 (2021) 2129–2136. https://doi.org/10.1093/jac/dkab136.

[35] J.L. Hernandez, S.-T. Chien, M.-A. Doan, I.T. Suydam, K.A. Woodrow, Antiretroviral (ARV) Properties Dictate Long-Acting Release and Tissue Partitioning Behaviors in Multidrug Subcutaneous Implants, ACS Biomater Sci Eng (2024). https://doi.org/10.1021/acsbiomaterials.4c01290.

[36] S.-T. Chien, I.T. Suydam, K.A. Woodrow, Prodrug approaches for the development of a long-acting drug delivery systems, Adv Drug Deliv Rev 198 (2023) 114860. https://doi.org/https://doi.org/10.1016/j.addr.2023.114860.

[37] S. Perrier, 50th Anniversary Perspective: RAFT Polymerization—A User Guide, Macromolecules 50 (2017) 7433–7447. https://doi.org/10.1021/acs.macromol.7b00767.

[38] D.-K. Ho, C. LeGuyader, S. Srinivasan, D. Roy, V. Vlaskin, T.E.J. Chavas, C.L. Lopez, J.M. Snyder, A. Postma, J. Chiefari, P.S. Stayton, Fully synthetic injectable depots with high drug content and tunable pharmacokinetics for long-acting drug delivery, Journal of Controlled Release 329 (2021) 257–269. https://doi.org/https://doi.org/10.1016/j.jconrel.2020.11.030.

[39] M. Parent, C. Nouvel, M. Koerber, A. Sapin, P. Maincent, A. Boudier, PLGA in situ implants formed by phase inversion: Critical physicochemical parameters to modulate drug release, Journal of Controlled Release 172 (2013) 292–304. https://doi.org/https://doi.org/10.1016/j.jconrel.2013.08.024.

[40] J.M. Simoni, K. Beima-Sofie, Z.H. Mohamed, J. Christodoulou, K. Tapia, S.M. Graham, R. Ho, A.C. Collier, Long-Acting Injectable Antiretroviral Treatment Acceptability and Preferences: A Qualitative Study Among US Providers, Adults Living with HIV, and Parents of Youth Living with HIV, AIDS Patient Care STDS 33 (2019) 104–111. https://doi.org/10.1089/apc.2018.0198.

[41] C.R. Trezza, A.D.M. Kashuba, Pharmacokinetics of Antiretrovirals in Genital Secretions and Anatomic Sites of HIV Transmission: Implications for HIV Prevention, Clin Pharmacokinet 53 (2014) 611–624. https://doi.org/10.1007/s40262-014-0148-z.

[42] M. Kovarova, M.D. Swanson, R.I. Sanchez, C.E. Baker, J. Steve, R.A. Spagnuolo, B.J. Howell, D.J. Hazuda, J. Victor Garcia, A long-acting formulation of the integrase inhibitor raltegravir protects humanized BLT mice from repeated high-dose vaginal HIV challenges, Journal of Antimicrobial Chemotherapy 71 (2016) 1586–1596. https://doi.org/10.1093/jac/dkw042.

[43] Q. Li, X. Li, C. Zhao, Strategies to Obtain Encapsulation and Controlled Release of Small Hydrophilic Molecules, Front Bioeng Biotechnol 8 (2020) 437.

[44] L.-G. Bekker, C. Beyrer, N. Mgodi, S.R. Lewin, S. Delany-Moretlwe, B. Taiwo, M.C. Masters, J. V Lazarus, HIV infection, Nat Rev Dis Primers 9 (2023) 42. https://doi.org/10.1038/s41572-023-00452-3.

[45] UN Joint Programme on HIV/AIDS (UNAIDS), The Gap Report, 2014.

[46] T.D. Frank, A. Carter, D. Jahagirdar, M.H. Biehl, D. Douwes-Schultz, S.L. Larson, M. Arora, L. Dwyer-Lindgren, K.M. Steuben, H. Abbastabar, L.J. Abu-Raddad, D.M. Abyu, M. Adabi, O.M. Adebayo, V. Adekanmbi, O.O. Adetokunboh, A. Ahmadi, K. Ahmadi, E. Ahmadian, E. Ahmadpour, M.B. Ahmed, C.G. Akal, F. Alahdab, N. Alam, S.B. Albertson, B.T.T. Alemnew, K.A. Alene, V. Alipour, N. Alvis-Guzman, S. Amini, Z. Anbari, N.H. Anber, M. Anjomshoa, C.A.T. Antonio, J. Arabloo, O. Aremu, H.A. Areri, E.T. Asfaw, A.F. Ashagre, D. Asmelash, A.A. Asrat, E.F.G.A. Avokpaho, A. Awasthi, N. Awoke, M.A. Ayanore, S. Azari, A. Badawi, M. Bagherzadeh, M. Banach, A. Barac, T.W. Bärnighausen, S. Basu, N. Bedi, M. Behzadifar, B.B. Bekele, S.A. Belay, Y.B. Belay, Y.M. Belayneh, A. Berhane, A.G. Bhat, K. Bhattacharyya, B. Biadgo, A. Bijani, M.S. Bin Sayeed, H. Bitew, A. Blinov, K.A. Bogale, H.A. Bojia, S.B.N. Burugina Nagaraja, Z.A. Butt, L. Cahuana-Hurtado, J.C. Campuzano Rincon, F. Carvalho, V.K. Chattu, D.J. Christopher, D.-T. Chu, R. Crider, T. Dahiru, L. Dandona, R. Dandona, A. Daryani, J. das Neves, J.-W. De Neve, L. Degenhardt, F.M. Demeke, A.B. Demis, D.B. Demissie, G.T. Demoz, K. Deribe, D. Des Jarlais, G.P. Dhungana, D. Diaz, S. Djalalinia, H.P. Do, L.P. Doan, H. Duber, M. Dubey, E. Dubljanin, E.E. Duken, B. Duko Adema, A. Effiong, A. Eftekhari, M. El Sayed Zaki, S.I. El-Jaafary, Z. El-Khatib, A. Elsharkawy, A.Y. Endries, S. Eskandarieh, O. Eyawo, F. Farzadfar, B. Fatima, N. Fentahun, E. Fernandes, I. Filip, F. Fischer, M.O. Folayan, M. Foroutan, T. Fukumoto, N. Fullman, A.L. Garcia-Basteiro, R.T. Gayesa, K.B. Gebremedhin, G.G.G. Gebremeskel, K.K. Gebreyohannes, G.A. Gedefaw, B.K. Gelaw, H.A. Gesesew, B. Geta, K.E. Gezae, K. Ghadiri, A. Ghashghaee, T.T.G. Ginindza, H.C. Gugnani, R.A. Guimarães, M.T. Haile, G.B. Hailu, A. Haj-Mirzaian, A. Haj-Mirzaian, S. Hamidi, S. Handanagic, D.W. Handiso, L.K. Hanfore, A. Hasanzadeh, H. Hassankhani, H.Y. Hassen, S.I. Hay, A. Henok, C.L. Hoang, H.D. Hosgood, M. Hosseinzadeh, M. Hsairi, S.E. Ibitoye, B. Idrisov, K.S. Ikuta, O.S. Ilesanmi, S.S.N. Irvani, C.J. Iwu, K.H. Jacobsen, S.L. James, E. Jenabi, R.P. Jha, J.B. Jonas, Z. Jorjoran Shushtari, A. Kabir, Z. Kabir, R. Kadel, A. Kasaeian, B. Kassa, G.M. Kassa, T.D. Kassa, G.A. Kayode, M.M. Kebede, A.T. Kefale, A.P. Kengne, Y.S. Khader, M.A. Khafaie, N. Khalid, E.A. Khan, G. Khan, J. Khan, Y.-H. Khang, K. Khatab, S. Khazaei, A.T. Khoja, A.A. Kiadaliri, Y.J. Kim, A. Kisa, S. Kisa, S. Kochhar, H. Komaki, P.A. Koul, A. Koyanagi, B. Kuate Defo, G.A. Kumar, M. Kumar, D. Kuupiel, D.K. Lal, J.J.-H. Lee, T.L. Lenjebo, C.T. Leshargie, E.R.K. Macarayan, E.R. Maddison, H. Magdy Abd El Razek, C. Magis-Rodriguez, P.W. Mahasha, M. Majdan, A. Majeed, R. Malekzadeh, N. Manafi, C.C. Mapoma, F.R. Martins-Melo, A. Masaka, E.N.L. Mayenga, V. Mehta, G.G. Meles, H.G. Meles, A. Melese, M. Melku, P.T.N. Memiah, Z.A. Memish, A.T. Mena, W. Mendoza, D.T. Mengistu, G. Mengistu, T.J. Meretoja, T. Mestrovic, T.R. Miller, B. Moazen, B. Mohajer, A. Mohamadi-Bolbanabad, K.A. Mohammad, Y. Mohammad, A. Mohammad Darwesh, N. Mohammad Gholi Mezerji, M. Mohammadi, R. Mohammadibakhsh, M. Mohammadoo-Khorasani, J.A. Mohammed, S. Mohammed, F. Mohebi, A.H. Mokdad, Y. Moodley, M. Moossavi, G. Moradi, M. Moradi-Lakeh, M.M. Moschos, T.B. Mossie, S.M. Mousavi, K.F. Muchie, A.G. Muluneh, M.K. Muriithi, G. Mustafa, S. Muthupandian, A.J. Nagarajan, G. Naik, F. Najafi, J. Nazari, D.E. Ndwandwe, C.T. Nguyen, H.L.T. Nguyen,

S.H. Nguyen, T.H. Nguyen, D.N.A. Ningrum, M.R. Nixon, C.A. Nnaji, M. Noroozi, J.J. Noubiap, M. Nourollahpour Shiadeh, M.S. Obsa, E.A. Odame, R. Ofori-Asenso, F.A. Ogbo, A. Okoro, O. Oladimeji, A.T. Olagunju, T.O. Olagunju, S. Olum, K.O.A. Oppong Asante, E. Oren, S.S. Otstavnov, M. PA, J.R. Padubidri, S. Pakhale, A.H. Pakpour, S.K. Patel, K. Paulos, V.C.F. Pepito, E.K. Peprah, B. Piroozi, A. Pourshams, M. Qorbani, M. Rabiee, N. Rabiee, A. Radfar, A. Rafay, A. Rafiei, F. Rahim, A. Rahimi-Movaghar, V. Rahimi-Movaghar, S. ur Rahman, C.L. Ranabhat, S. Rawaf, C. Reis, V. Renjith, M.A. Reta, M.S. Rezai, C.M. Rios González, E.M. Roro, A. Rostami, S. Rubino, S. Saeedi Moghaddam, S. Safari, R. Sagar, M.A. Sahraian, M.R.R. Salem, Y. Salimi, J.A. Salomon, E.Z. Sambala, A.M. Samy, B. Sartorius, M. Satpathy, M. Sawhney, M. Sayyah, A.E. Schutte, S.G. Sepanlou, S. Seyedmousavi, H. Shabaninejad, A.A. Shaheen, M.A. Shaikh, S.A. Shallo, M. Shamsizadeh, H. Sharifi, K. Shibuya, J. Il Shin, R. Shirkoohi, D.A.S. Silva, D.G.A. Silveira, J.A. Singh, M.M.M. Sisay, M. Sisay, S. Sisay, A.E. Smith, A. Sokhan, R. Somayaji, S. Soshnikov, D.J. Stein, M.B. Sufiyan, B.F. Sunguya, B.L. Sykes, B.T. Tadesse, D.B. Tadesse, K.S. Tamirat, N. Taveira, S.W. Tekelemedhin, H.D. Temesgen, F.H. Tesfay, M.Y. Teshale, S. Thapa, K.G. Tlaye, S.M. Topp, M.R. Tovani-Palone, B.X. Tran, K.B. Tran, I. Ullah, B. Unnikrishnan, O.A. Uthman, Y. Veisani, S.K. Vladimirov, F.W. Wada, Y. Waheed, K.G. Weldegwergs, G.T.T. Weldesamuel, R. Westerman, T. Wijeratne, H.F. Wolde, D.Z. Wondafrash, T.E. Wonde, B.Y. Wondmagegn, A.G. Yeshanew, M.T. Yilma, E.M. Yimer, N. Yonemoto, M. Yotebieng, Y. Youm, C. Yu, Z. Zaidi, A. Zarghi, Z.M. Zenebe, T.A. Zewale, A. Ziapour, S. Zodpey, M. Naghavi, S.E. Vollset, H. Wang, S.S. Lim, H.H. Kyu, C.J.L. Murray, Global, regional, and national incidence, prevalence, and mortality of HIV, 1980–2017, and forecasts to 2030, for 195 countries and territories: a systematic analysis for the Global Burden of Diseases, Injuries, and Risk Factors Study 2017, Lancet HIV 6 (2019) e831–e859. https://doi.org/10.1016/S2352-3018(19)30196-1.

[47] S. Gregson, E. Gonese, T.B. Hallett, N. Taruberekera, J.W. Hargrove, B. Lopman, E.L. Corbett, R. Dorrington, S. Dube, K. Dehne, O. Mugurungi, HIV decline in Zimbabwe due to reductions in risky sex? Evidence from a comprehensive epidemiological review, Int J Epidemiol 39 (2010) 1311–1323. https://doi.org/10.1093/ije/dyq055.

[48] A.T. Haase, Perils at mucosal front lines for HIV and SIV and their hosts, Nat Rev Immunol 5 (2005) 783–792. https://doi.org/10.1038/nri1706.

[49] K. Govender, S. Beckett, T. Reddy, R.G. Cowden, C. Cawood, D. Khanyile, A.B.M. Kharsany, G. George, A. Puren, Association of HIV Intervention Uptake With HIV Prevalence in Adolescent Girls and Young Women in South Africa, JAMA Netw Open 5 (2022) e228640.

[50] R.V. Luckheeram, R. Zhou, A.D. Verma, B. Xia, CD4+T Cells: Differentiation and Functions, J Immunol Res 2012 (2012) 925135. https://doi.org/https://doi.org/10.1155/2012/925135.

[51] S.G. Deeks, J. Overbaugh, A. Phillips, S. Buchbinder, HIV infection, Nat Rev Dis Primers 1 (2015) 15035. https://doi.org/10.1038/nrdp.2015.35.

[52] D.M. Tebit, N. Ndembi, A. Weinberg, M.E. Quiñones-Mateu, Mucosal Transmission of Human Immunodeficiency Virus, Curr HIV Res 10 (2012) 3–8.

[53] K.K. Ariën, V. Jespers, G. Vanham, HIV sexual transmission and microbicides, Rev Med Virol 21 (2011) 110–33.

[54] T. Dragic, V. Litwin, G.P. Allaway, S.R. Martin, Y. Huang, K.A. Nagashima, C. Cayanan, P.J. Maddon, R.A. Koup, J.P. Moore, W.A. Paxton, HIV-1 entry into CD4+ cells is mediated by the chemokine receptor CC-CKR-5, Nature 381 (1996) 667–673. https://doi.org/10.1038/381667a0.

[55] J.D. Roberts, K. Bebenek, T.A. Kunkel, The Accuracy of Reverse Transcriptase from HIV-1, Science (1979) 242 (1988) 1171–1173. https://doi.org/10.1126/science.2460925.

[56] A.S. Perelson, A.U. Neumann, M. Markowitz, J.M. Leonard, D.D. Ho, HIV-1 Dynamics in Vivo: Virion Clearance Rate, Infected Cell Life-Span, and Viral Generation Time, Science (1979) 271 (1996) 1582–1586. https://doi.org/10.1126/science.271.5255.1582.

[57] M.S. Cohen, Y.Q. Chen, M. McCauley, T. Gamble, M.C. Hosseinipour, N. Kumarasamy, J.G. Hakim, J. Kumwenda, B. Grinsztejn, J.H.S. Pilotto, S. V Godbole, S. Chariyalertsak, B.R. Santos, K.H. Mayer, I.F. Hoffman, S.H. Eshleman, E. Piwowar-Manning, L. Cottle, X.C. Zhang, J. Makhema, L.A. Mills, R. Panchia, S. Faesen, J. Eron, J. Gallant, D. Havlir, S. Swindells, V. Elharrar, D. Burns, T.E. Taha, K. Nielsen-Saines, D.D. Celentano, M. Essex, S.E. Hudelson, A.D. Redd, T.R. Fleming, Antiretroviral Therapy for the Prevention of HIV-1 Transmission, New England Journal of Medicine 375 (2016) 830–839. https://doi.org/10.1056/NEJMoa1600693.

[58] R.T. Davey, N. Bhat, C. Yoder, T.-W. Chun, J.A. Metcalf, R. Dewar, V. Natarajan, R.A. Lempicki, J.W. Adelsberger, K.D. Miller, J.A. Kovacs, M.A. Polis, R.E. Walker, J. Falloon, H. Masur, D. Gee, M. Baseler, D.S. Dimitrov, A.S. Fauci, H.C. Lane, HIV-1 and T cell dynamics after interruption of highly active antiretroviral therapy (HAART) in patients with a history of sustained viral suppression, Proceedings of the National Academy of Sciences 96 (1999) 15109–15114. https://doi.org/10.1073/pnas.96.26.15109.

[59] T.-W. Chun, J.S. Justement, D. Murray, C.W. Hallahan, J. Maenza, A.C. Collier, P.M. Sheth, R. Kaul, M. Ostrowski, S. Moir, C. Kovacs, A.S. Fauci, Rebound of plasma viremia following cessation of antiretroviral therapy despite profoundly low levels of HIV reservoir: implications for eradication, AIDS 24 (2011) 2803–2808.

[60] M.F. Kearney, A. Wiegand, W. Shao, J.M. Coffin, J.W. Mellors, M. Lederman, R.T. Gandhi, B.F. Keele, J.Z. Li, Origin of Rebound Plasma HIV Includes Cells with Identical Proviruses That Are Transcriptionally Active before Stopping of Antiretroviral Therapy, J Virol 90 (2016) 1369–1376.

[61] E.J. Mills, J.B. Nachega, D.R. Bangsberg, S. Singh, B. Rachlis, P. Wu, K. Wilson, I. Buchan, C.J. Gill, C. Cooper, Adherence to HAART: A systematic Review of Developed and Developing Nation Patient-Reported Barriers and Facilitators, PLoS Med 3 (2006) e438.

[62] Y. Yu, D. Luo, X. Chen, Z. Huang, M. Wang, S. Xiao, Medication adherence to antiretroviral therapy among newly treated people living with HIV, BMC Public Health 18 (2018) 825. https://doi.org/10.1186/s12889-018-5731-z.

[63] F. Altice, O. Evuarherhe, S. Shina, G. Carter, A.C. Beaubrun, Adherence to HIV treatment regimens: systematic literature review and meta-analysis, Patient Prefer Adherence 13 (2019) 475–490.

[64] S.A. Iacob, D.G. Iacob, G. Jugulete, Improving the Adherence to Antiretroviral Therapy, a Difficult but Essential Task for a Successful HIV Treatment—Clinical Points of View and Practical Considerations , Frontiers in Pharmacology 8 (2017).

[65] S. Kanters, J.J.H. Park, K. Chan, M.E. Socias, N. Ford, J.I. Forrest, K. Thorlund, J.B. Nachega, E.J. Mills, Interventions to improve adherence to antiretroviral therapy: a systematic review and network meta-analysis, Lancet HIV 4 (2017) e31–e40. https://doi.org/10.1016/S2352-3018(16)30206-5.

[66] K.L. Scarsi, S. Swindells, The Promise of Improved Adherence with Long-Acting Antiretroviral Therapy: What Are the Data?, J Int Assoc Provid AIDS Care Jan-Dec (2021) 20.

[67] B. Winner, J.F. Peipert, Q. Zhao, C. Buckel, T. Madden, J.E. Allsworth, G.M. Secura, Effectiveness of Long-Acting Reversible Contraception, New England Journal of Medicine 366 (2012) 1998–2007.

[68] P. Teichner, A. Cutrell, R. D'Amico, D. Dorey, S. Griffith, C.M. Harrington, J. Huang, K.J. Hudson, D. Margolis, J. Mrus, J. Polli, W. Spreen, P. Williams, R. Van Solingen-Ristea, M.S. Shaefer, 884. Patient Adherence to Long-Acting Injectable Cabotegravir + Rilpivirine Through 48 Weeks of Maintenance Therapy in the Phase 3 ATLAS and FLAIR Studies, Open Forum Infect Dis 6 (2019) S20.

[69] R.J. Landovitz, D. Donnell, M.E. Clement, B. Hanscom, L. Cottle, L. Coelho, R. Cabello, S. Chariyalertsak, E.F. Dunne, I. Frank, J.A. Gallardo-Cartagena, A.H. Gaur, P. Gonzales, H. V Tran, J.C. Hinojosa, E.G. Kallas, C.F. Kelley, M.H. Losso, J.V. Madruga, K. Middelkoop, N. Phanuphak, B. Santos, O. Sued, J. Valencia Huamaní, E.T. Overton, S. Swaminathan, C. del Rio, R.M. Gulick, P. Richardson, P. Sullivan, E. Piwowar-Manning, M. Marzinke, C. Hendrix, M. Li, Z. Wang, J. Marrazzo, E. Daar, A. Asmelash, T.T. Brown, P. Anderson, S.H. Eshleman, M. Bryan, C. Blanchette, J. Lucas, C. Psaros, S. Safren, J. Sugarman, H. Scott, J.J. Eron, S.D. Fields, N.D. Sista, K. Gomez-Feliciano, A. Jennings, R.M. Kofron, T.H. Holtz, K. Shin, J.F. Rooney, K.Y. Smith, W. Spreen, D. Margolis, A. Rinehart, A. Adeyeye, M.S. Cohen, M. McCauley, B. Grinsztejn, Cabotegravir for HIV Prevention in Cisgender Men and Transgender Women, New

England Journal of Medicine 385 (2021) 595–608. https://doi.org/10.1056/NEJMoa2101016.

[70] R.J. Landovitz, B.S. Hanscom, M.E. Clement, H. V Tran, E.G. Kallas, M. Magnus, O. Sued, J. Sanchez, H. Scott, J.J. Eron, C. del Rio, S.D. Fields, M.A. Marzinke, S.H. Eshleman, D. Donnell, M.A. Spinelli, R.M. Kofron, R. Berman, E.M. Piwowar-Manning, P.A. Richardson, P.A. Sullivan, J.P. Lucas, P.L. Anderson, C.W. Hendrix, A. Adeyeye, J.F. Rooney, A.R. Rinehart, M.S. Cohen, M. McCauley, B. Grinsztejn, Efficacy and safety of long-acting cabotegravir compared with daily oral tenofovir disoproxil fumarate plus emtricitabine to prevent HIV infection in cisgender men and transgender women who have sex with men 1 year after study unblinding: a secondary anal, Lancet HIV 10 (2023) e767–e778. https://doi.org/10.1016/S2352-3018(23)00261-8.

[71] S. Delany-Moretlwe, J.P. Hughes, P. Bock, S.G. Ouma, P. Hunidzarira, D. Kalonji, N. Kayange, J. Makhema, P. Mandima, C. Mathew, E. Spooner, J. Mpendo, P. Mukwekwerere, N. Mgodi, P.N. Ntege, G. Nair, C. Nakabiito, H. Nuwagaba-Biribonwoha, R. Panchia, N. Singh, B. Siziba, J. Farrior, S. Rose, P.L. Anderson, S.H. Eshleman, M.A. Marzinke, C.W. Hendrix, S. Beigel-Orme, S. Hosek, E. Tolley, N. Sista, A. Adeyeye, J.F. Rooney, A. Rinehart, W.R. Spreen, K. Smith, B. Hanscom, M.S. Cohen, M.C. Hosseinipour, A. Asmelash, A. Sehurutshi, A. Baguma, A. Marais, B. Kawoozo, B.P. Malinga, B.G. Mirembe, B. Okech, B. Esterhuizen, C. Murombedzi, D. Gadama, E. Hwengwere, E. Roos, E.S. Magada, E. Shava, E. Piwowar-Manning, E. Tahuringana, F.G.S. Muhlanga, F. Conradie, F. Angira, G. Nanyonjo, G. Kistnasami, H. Mvula, I. Naidoo, J. Horak, J. Jere, J. Moodley, K. Shin, K. Nel, K. Bokoch, L. Birungi, L. Emel, M. Monametsi, M. Sibanda, M. Mutambanengwe, M. Chitukuta, M. Matimbira, M. Bhondai-Mhuri, N. Sibisi, N. Morar, N. Mudzonga, P. Natureeba, P. Richardson, P. Musara, P. Macdonald, R. Nkambule, R. Mosime, R. White, R. Berhanu, R. Ncube-Sihlongonyane, R. Sekabira, S. Siva, S. Pillay, S. Govender, S. Bamweyana, S. Nzimande, S. Innes, S. Dadabhai, T. Samandari, T. Tembo, T. Lungu Mabedi, T. Chirenda, T. Chidemo, V. Mudhune, V. Naidoo, W. Samaneka, Y. Agyei, Y. Musodza, Y. Fourie, Z. Gaffoor, Cabotegravir for the prevention of HIV-1 in women: results from HPTN 084, a phase 3, randomised clinical trial, The Lancet 399 (2022) 1779–1789. https://doi.org/10.1016/S0140-6736(22)00538-4.

[72] K. Meyers, Y. Wu, H. Qian, T. Sandfort, X. Huang, J. Xu, J. Zhang, W. Xia, D. Glidden, H. Wu, H. Shang, Interest in Long-Acting Injectable PrEP in a Cohort of Men Who have Sex with Men in China, AIDS Behav 22 (2018) 1217–1227. https://doi.org/10.1007/s10461-017-1845-z.

[73] E.E. Tolley, S. Li, S.Z. Zangeneh, M. Atujuna, P. Musara, J. Justman, S. Pathak, L.-G. Bekker, S. Swaminathan, J. Stanton, J. Farrior, N. Sista, Acceptability of a long-acting injectable HIV prevention product among US and African women: findings from a phase 2 clinical Trial (HPTN 076), J Int AIDS Soc 22 (2019) e25408. https://doi.org/https://doi.org/10.1002/jia2.25408.

[74] S. Adepu, S. Ramakrishna, Controlled Drug Delivery Systems: Current Status and Future Directions, Molecules 26 (2021) 5905.

[75] W. Li, J. Tang, D. Lee, T.R. Tice, S.P. Schwendeman, M.R. Prausnitz, Clinical translation of long-acting drug delivery formulations, Nat Rev Mater 7 (2022) 406–420. https://doi.org/10.1038/s41578-021-00405-w.

[76] A. Butreddy, R.P. Gaddam, N. Kommineni, N. Dudhipala, C. Voshavar, PGLA/PLA-Based Long-Acting Injectable Depot Microspheres in Clinical Use: Production and Characterization Overview for Protein/Peptide Delivery, Int J Mol Sci 22 (2021) 8884.

[77] P. Darney, A. Patel, K. Rosen, L.S. Shapiro, A.M. Kaunitz, Safety and efficacy of a single-rod etonogestrel implant (Implanon): results from 11 international clinical trials, Fertil Steril 91 (2009) 1646–53.

[78] Nexplanon® (Etonogestrel) Implant Prescribing Information, (n.d.). https://www.merck.com/product/usa/pi_circulars/n/nexplanon/nexplanon_pi.pdf.

[79] E.D. Weld, C. Flexner, Long-acting implants to treat and prevent HIV infection, Curr Opin HIV AIDS 15 (2020) 33–41. https://doi.org/10.1097/COH.0000000000000591.

[80] J.W. McBride, P. Boyd, N. Dias, D. Cameron, R.E. Offord, O. Hartley, V.L. Kett, R.K. Malcolm, Vaginal rings with exposed cores for sustained delivery of the HIV CCR5 inhibitor 5P12-RANTES, J Control Release 298 (2019) 1–11. https://doi.org/10.1016/j.jconrel.2019.02.003.

[81] M.T.C. Mc Crudden, E. Larrañeta, A. Clark, C. Jarrahian, A. Rein-Weston, S. Lachau-Durand, N. Niemeijer, P. Williams, C. Haeck, H.O. McCarthy, D. Zehrung, R.F. Donnelly, Design, formulation and evaluation of novel dissolving microarray patches containing a long-acting rilpivirine nanosuspension, Journal of Controlled Release 292 (2018) 119–129. https://doi.org/https://doi.org/10.1016/j.jconrel.2018.11.002.

[82] R.P. Matthews, X. Zang, S.E. Barrett, A. Koynov, A. Goodey, T. Heimbach, V.L. Weissler, C. Leyssens, T. Reynders, Z. Xu, S. Rottey, R. Vargo, M.N. Robertson, S.A. Stoch, M. Iwamoto, A Randomized, Double-Blind, Placebo-Controlled, Phase 1 Trial of Radiopaque Islatravir-Eluting Subdermal Implants for Pre-exposure Prophylaxis Against HIV-1 Infection, JAIDS Journal of Acquired Immune Deficiency Syndromes 92 (2023).

[83] J. Chen, K. Walters, P. Ashton, Correlation of in vitro-in vivo release rates for sustained release nevirapine implants in rats, Journal of Controlled Release 101 (2005) 357–8.

[84] C.Y.X. Chua, P. Jain, A. Ballerini, G. Bruno, R.L. Hood, M. Gupte, S. Gao, N. Di Trani, A. Susnjar, K. Shelton, L.R. Bushman, M. Folci, C.S. Filgueira, M.A. Marzinke, P.L. Anderson, M. Hu, P. Nehete, R.C. Arduino, K.J. Sastry, A. Grattoni, Transcutaneously refillable nanofluidic implant achieves sustained level of tenofovir diphosphate for HIV pre-exposure prophylaxis, Journal of Controlled Release 286 (2019) 315–325.

[85] S.E. Barrett, R.S. Teller, S.P. Forster, L. Li, M.A. Mackey, D. Skomski, Z. Yang, K.L. Fillgrove, G.J. Doto, S.L. Wood, J. Lebron, J.A. Grobler, R.I. Sanchez, Z. Liu, B. Lu, Extended-Duration MK-8591-Eluting Implant as a Candidate for HIV Treatment and Prevention, Antimicrob Agents Chemother 62 (2018) 1–13.

[86] J. Li, D.J. Mooney, Designing hydrogels for controlled drug delivery, Nat Rev Mater 1 (2016) 16071. https://doi.org/10.1038/natrevmats.2016.71.

[87] BIKTARVY™ [PRODUCT MONOGRAPH], (2018).

[88] A.T. Podany, K.K. Scarsi, M.M. Pham, C. V Fletcher, Comparative Clinical Pharmacokinetics and Pharmacodynamics of HIV-1 Integrase Strand Transfer Inhibitors: An Updated Review, Clin Pharmacokinet 59 (2020) 1085–1107.

[89] S. Mandal, P.K. Prathipati, S.W. Sunagawa, C.J. Destache, A Concept Evaluation Study of a New Combination Bictegravir plus Tenofovir Alafenamide Nanoformulation with Prolonged Sustained-Drug-Release Potency for HIV-1 Preexposure Prophylaxis, Antimicrob Agents Chemother 65 (2021) e02320-20.

[90] P. Rogueda, Novel hydrofluoroalkane suspension formulations for respiratory drug delivery, Expert Opin Drug Deliv 2 (2005) 625–638. https://doi.org/10.1517/17425247.2.4.625.

[91] A.A. Date, C.J. Destache, A review of nanotechnological approaches for the prophylaxis of HIV/AIDS, Biomaterials 34 (2013) 6202–6228. https://doi.org/https://doi.org/10.1016/j.biomaterials.2013.05.012.

[92] A. Wiesner, P. Zagrodzki, M. Jamrozik, J. Korchowiec, M. Marcinkowska, P. Paśko, Chemometrics as a valuable tool for evaluating interactions between antiretroviral drugs and food, Br J Clin Pharmacol 89 (2023) 2977–2991. https://doi.org/https://doi.org/10.1111/bcp.15796.

[93] J.L. Hernandez, S.-T. Chien, M.-A. Doan, I.T. Suydam, K.A. Woodrow, Antiretroviral (ARV) Properties Dictate Long-Acting Release and Tissue Partitioning Behaviors in Multidrug Subcutaneous Implants, ACS Biomater Sci Eng (2024). https://doi.org/10.1021/acsbiomaterials.4c01290.

[94] E.J. Torres-Martinez, J.M. Cornejo Bravo, A. Serrano Medina, G.L. Pérez González, L.J. Villarreal Gómez, A Summary of Electrospun Nanofibers as Drug Delivery System: Drugs Loaded and Biopolymers Used as Matrices, Curr Drug Deliv 15 (2018) 1360–1374. https://doi.org/10.2174/1567201815666180723114326.

[95] J. Rautio, H. Kumpulainen, T. Heimbach, R. Oliyai, D. Oh, T. Järvinen, J. Savolainen, Prodrugs: design and clinical applications, Nat Rev Drug Discov 7 (2008) 255–270. https://doi.org/10.1038/nrd2468.

[96] E.J. Eisenberg, G.-X. He, W.A. Lee, METABOLISM OF GS-7340, A NOVEL PHENYL MONOPHOSPHORAMIDATE INTRACELLULAR PRODRUG OF PMPA, IN BLOOD,

Nucleosides Nucleotides Nucleic Acids 20 (2001) 1091–1098. https://doi.org/10.1081/NCN-100002496.

[97] B.H. McCarberg, R.L. Barkin, Long-Acting Opioids for Chronic Pain: Pharmacotherapeutic Opportunities to Enhance Compliance, Quality of Life, and Analgesia, Am J Ther 8 (2001).

[98] P. Trucillo, Drug Carriers: Classification, Administration, Release Profiles, and Industrial Approach, Processes 9 (2021). https://doi.org/10.3390/pr9030470.

[99] K. Kita, C. Dittrich, Drug delivery vehicles with improved encapsulation efficiency: taking advantage of specific drug–carrier interactions, Expert Opin Drug Deliv 8 (2011) 329–342. https://doi.org/10.1517/17425247.2011.553216.

[100] Q. Li, X. Li, C. Zhao, Strategies to Obtain Encapsulation and Controlled Release of Small Hydrophilic Molecules, Front Bioeng Biotechnol 8 (2020) 437.

[101] M. Shah, Y.K. Agrawal, K. Garala, A. Ramkishan, Solid Lipid Nanoparticles of a Water Soluble Drug, Ciprofloxacin Hydrochloride, Indian J Pharm Sci 74 (2012) 434–442.

[102] Y. Mirchandani, V.B. Patravale, B. S., Solid lipid nanoparticles for hydrophilic drugs, Journal of Controlled Release 335 (2021) 457–464. https://doi.org/https://doi.org/10.1016/j.jconrel.2021.05.032.

[103] F. Ramazani, W. Chen, C.F. van Nostrum, G. Storm, F. Kiessling, T. Lammers, W.E. Hennick, R.J. Kok, Strategies for encapsulation of small hydrophilic and amphiphilic drugs in PLGA microscpheres: state-of-the-art and challenges, Int J Pharm 499 (2016) 358–367.

[104] B. Ghosh, S. Biswas, Polymeric micelles in cancer therapy: State of the art, Journal of Controlled Release 332 (2021) 127–147. https://doi.org/https://doi.org/10.1016/j.jconrel.2021.02.016.

[105] R.L. Creighton, I.T. Suydam, M.E. Ebner, W.E. Afunugo, A.M. Bever, S. Cao, Y. Jiang, K.A. Woodrow, Sustained Intracellular Raltegravir Depots Generated with Prodrugs Designed for Nanoparticle Delivery, ACS Biomater Sci Eng 5 (2019) 4013–4022. https://doi.org/10.1021/acsbiomaterials.9b00658.

[106] I. Vhora, N. Khatri, A. Misra, Chapter 8 - Applications of Polymers in Parenteral Drug Delivery, in: A. Misra, A.B.T.-A. of P. in D.D. (Second E. Shahiwala (Eds.), Elsevier, 2021: pp. 221–261. https://doi.org/https://doi.org/10.1016/B978-0-12-819659-5.00008-2.

[107] G. Giacalone, H. Hillaireau, E. Fattal, Improving bioavailability and biodistribution of anti-HIV chemotherapy, European Journal of Pharmaceutical Sciences 75 (2015) 40–53. https://doi.org/https://doi.org/10.1016/j.ejps.2015.04.011.

[108] V. Agostoni, R. Anand, S. Monti, S. Hall, G. Maurin, K. Horcajada, Patricia; Serre, Christian; Bouchemal, R. Gref, Impact of phosphorylation on the encapsulation of

nucleoside analogues within porous iron(iii) metal–organic framework MIL-100(Fe) nanoparticles, J Mater Chem B 1 (2013) 4231–4242.

[109] K. Gallicano, J. Sahai, E. Ormsby, D.W. Cameron, A. Pakuts, I. McGilveray, Pharmacokinetics of zidovudine after the initial single dose and during chronic-dose therapy in HIV-infected patients, Br J Clin Pharmacol 36 (1993) 128–131.

[110] J. Balzarini, P. Herdewijn, E. De Clercq, Differential Patterns of Intracellular Metabolism of 2′,3′-Didehydro-2′,3′-dideoxythymidine and 3′-Azido-2′,3′-dideoxythymidine, Two Potent Anti-human Immunodeficiency Virus Compounds, Journal of Biological Chemistry 264 (1989) 6127–6133. https://doi.org/https://doi.org/10.1016/S0021-9258(18)83322-1.

[111] M.L. Forrest, J.A. Yáñez, C.M. Remsberg, Y. Ohgami, G.S. Kwon, N.M. Davies, Paclitaxel Prodrugs with Sustained Release and High Solubility in Poly(ethylene glycol)-b-poly(ε-caprolactone) Micelle Nanocarriers: Pharmacokinetic Disposition, Tolerability, and Cytotoxicity, Pharm Res 25 (2008) 194–206. https://doi.org/10.1007/s11095-007-9451-9.

[112] H. Wang, H. Xie, J. Wu, X. Wei, L. Zhou, X. Xu, S. Zheng, Structure-Based Rational Design of Prodrugs To Enable Their Combination with Polymeric Nanoparticle Delivery Platforms for Enhanced Antitumor Efficacy, Angewandte Chemie International Edition 53 (2014) 11532–11537. https://doi.org/https://doi.org/10.1002/anie.201406685.

[113] B.B. Ward, B. Huang, A. Desai, X.-M. Cheng, M. Vartanian, H. Zong, X. Shi, T.P. Thomas, A.E. Kotlyar, A. Van Der Spek, P.R. Leroueil, J.R. Baker, Sustained Analgesia Achieved Through Esterase-Activated Morphine Prodrugs Complexed with PAMAM Dendrimer, Pharm Res 30 (2013) 247–256. https://doi.org/10.1007/s11095-012-0869-3.

[114] R. Pignatello, T. Musumeci, A.C.E. Graziano, D. Lo Furno, P. Varamini, F.M. Mansfeld, V. Cardile, I. Toth, A study on liposomal encapsulation of a lipophilic prodrug of LHRH, Pharm Dev Technol 21 (2016) 664–671. https://doi.org/10.3109/10837450.2015.1041045.

[115] X. Zhang, M. Cao, J. Xing, M. Zheng, F. Liu, P. Dong, X. Tian, H. Xu, L. Zhang, H. Gu, L. Yang, R. Li, M. Ji, N. Gu, Identification, characterization, and synthesis of process-related impurities in antiproliferative agent TQ-B3203, J Liq Chromatogr Relat Technol 39 (2016) 488–496. https://doi.org/10.1080/10826076.2016.1196216.

[116] J. Xing, X. Zhang, Z. Wang, H. Zhang, P. Chen, G. Zhou, C. Sun, N. Gu, M. Ji, Novel lipophilic SN38 prodrug forming stable liposomes for colorectal carcinoma therapy, Int J Nanomedicine 14 (2019) 5201–5213.

[117] Y. Shi, A. Lu, X. Wang, Z. Belhadj, J. Wang, Q. Zhang, A review of existing strategies for designing long-acting parenteral formulations: Focus on underlying mechanisms, and future perspectives, Acta Pharm Sin B 11 (2021) 2396–2415. https://doi.org/https://doi.org/10.1016/j.apsb.2021.05.002.

[118] C. Brough, R.O. Williams, Amorphous solid dispersions and nano-crystal technologies for poorly water-soluble drug delivery, Int J Pharm 453 (2013) 157–166. https://doi.org/https://doi.org/10.1016/j.ijpharm.2013.05.061.

[119] W. Nernst, Theorie der Reaktionsgeschwindigkeit in heterogenen Systemen, 47U (1904) 52–55. https://doi.org/doi:10.1515/zpch-1904-4704.

[120] E. Brunner, Reaktionsgeschwindigkeit in heterogenen Systemen, 47U (1904) 56–102. https://doi.org/doi:10.1515/zpch-1904-4705.

[121] J.-U.A.H. Junghanns, R.H. Muller, Nanocrystal technology, drug delivery and clinical applications, Int J Nanomedicine 3 (2008) 295–309.

[122] T.A. Kulkarni, A.N. Bade, B. Sillman, B.L.D. Shetty, M.S. Wojtkiewicz, N. Gautam, J.R. Hilaire, S. Sravanam, A. Szlachetka, B.G. Lamberty, B.M. Morsey, H.S. Fox, Y. Alnouti, J.M. McMillan, R.L. Mosley, J. Meza, P.L. Domanico, T.-Y. Yue, G. Moore, B.J. Edagwa, H.E. Gendelman, A year-long extended release nanoformulated cabotegravir prodrug, Nat Mater 19 (2020) 910–920. https://doi.org/10.1038/s41563-020-0674-z.

[123] B.S. Reddy, G. Harish, Md.F. Ul-Haq, FORMULATION AND IN-VITRO CHARACTERISATION OF SOLID-SELF NANOEMULSIFYING DRUG DELIVERY SYSTEM (s-SNEDDS) OF RILPIVIRINE, Int J Pharm Sci Res 7 (2016) 3117–3129.

[124] H. Jaeger, E.T. Overton, G. Richmond, G. Rizzardini, J.F. Andrade-Villanueva, R. Mngqibisa, A.O. Hermida, A. Thalme, E. Belonosova, F. Ajana, P.D. Benn, Y. Wang, K.J. Hudson, C.M. Español, S.L. Ford, H. Crauwels, D.A. Margolis, C.L. Talarico, K.Y. Smith, V. van Eygen, R. Van Solingen-Ristea, S. Vanveggel, W.R. Spreen, Long-acting cabotegravir and rilpivirine dosed every 2 months in adults with HIV-1 infection (ATLAS-2M), 96-week results: a randomised, multicentre, open-label, phase 3b, non-inferiority study, Lancet HIV 8 (2021) e679–e689. https://doi.org/10.1016/S2352-3018(21)00185-5.

[125] D.H. Surve, A.B. Jindal, Recent advances in long-acting nanoformulations for delivery of antiretroviral drugs, Journal of Controlled Release 324 (2020) 379–404. https://doi.org/https://doi.org/10.1016/j.jconrel.2020.05.022.

[126] P. Chue, J. Chue, A critical appraisal of paliperidone long-acting injection in the treatment of schizoaffective disorder, Ther Clin Risk Manag 12 (2016) 109–116.

[127] R. Emsley, S. Kilian, Efficacy and safety profile of paliperidone palmitate injections in the management of patients with schizophrenia: an evidence-based review, Neuropsychiatr Dis Treat 14 (2018) 205–223.

[128] M.L. Hard, R.J. Mills, B.M. Sadler, R.Z. Turncliff, L. Citrome, Aripiprazole Lauroxil: Pharmacokinetic Profile of This Long-Acting Injectable Antipsychotic in Persons With Schizophrenia, J Clin Psychopharmacol 37 (2017).

[129] L.P.H. Yang, Oral Paliperidone, CNS Drugs 25 (2011) 523–538. https://doi.org/10.2165/11207440-000000000-00000.

[130] N. Gettu, A. Saadabadi, Aripiprazole, StatsPearl, StatsPearls Publishing, 2022.

[131] M.T. Morris, S.P. Tarpada, Long-Acting Injectable Paliperidone Palmitate: A Review of Efficacy and Safety, Psychopharmacol Bull 47 (2017) 42–52.

[132] M.L. Hard, R.J. Mills, B.M. Sadler, A.Y. Wehr, P.J. Weiden, L. von Moltke, Pharmacokinetic Profile of a 2-Month Dose Regimen of Aripiprazole Lauroxil: A Phase I study and a Population Pharmacokinetic Model, CNS Drugs 31 (2017) 617–624.

[133] M. Markovic, S. Deodhar, J. Machhi, P. Yeapuri, M. Saleh, B. J. Edagwa, R.L. Mosley, H.E. Gendelman, Prodrug Therapies for Infectious and Neurodegenerative Diseases, Pharmaceutics 14 (2022). https://doi.org/10.3390/pharmaceutics14030518.

[134] C. Anastasi, G. Quelever, S. Burlet, C. Garino, F. Souard, J.-L. Kraus, New Antiviral Nucleaoside Prodrugs Await Application, Curr Med Chem 10 (2003) 1825–1843.

[135] GlaxoSmithKline. Ziagen (abacavir), (2003).

[136] D. Singh, J. McMillan, J. Hilaire, N. Guatam, D. Palandri, Y. Alnouti, H.E. Gendelman, B. Edagwa, Development and characterization of a long-acting nanoformulated abacavir prodrug, Nanomedicine (Lond). 11 (2016) 1913–1927.

[137] S. Deodhar, B. Sillman, A.N. Bade, S.N. Avedissian, A.T. Podany, J.M. McMillan, N. Gautam, B. Hanson, B.L. Dyavar Shetty, A. Szlachetka, M. Johnston, M. Thurman, D.J. Munt, A.K. Dash, M. Markovic, A. Dahan, Y. Alnouti, A. Yazdi, B.D. Kevadiya, S.N. Byrareddy, S.M. Cohen, B. Edagwa, H.E. Gendelman, Transformation of dolutegravir into an ultra-long-acting parenteral prodrug formulation, Nat Commun 13 (2022) 3226. https://doi.org/10.1038/s41467-022-30902-7.

[138] D.A. Cobb, N. Smith, S. Deodhar, A.N. Bade, N. Gautam, B.L.D. Shetty, J. McMillan, Y. Alnouti, S.M. Cohen, H.E. Gendelman, B. Edagwa, Transformation of tenofovir into stable ProTide nanocrystals with long-acting pharmacokinetic profiles, Nat Commun 12 (2021) 5458. https://doi.org/10.1038/s41467-021-25690-5.

[139] D. Soni, A.N. Bade, N. Gautam, J. Herskovitz, I.M. Ibrahim, N. Smith, M.S. Wojtkiewicz, B.L. Dyavar Shetty, Y. Alnouti, J. McMillan, H.E. Gendelman, B.J. Edagwa, Synthesis of a long acting nanoformulated emtricitabine ProTide, Biomaterials 222 (2019) 119441. https://doi.org/https://doi.org/10.1016/j.biomaterials.2019.119441.

[140] M.G. Banoub, A.N. Bade, Z. Lin, D. Cobb, N. Guatam, B.L. Dyavar Shetty, M. Wojtkiewicz, Y. Alnouti, J. McMillan, H.E. Gendelman, B. Edagwa, Synthesis and characterization of Long Acting darunavir Prodrugs, Mol Pharm 17 (2020) 155–166.

[141] D.A. Margolis, J. Gonzalez-Garcia, H.-J. Stellbrink, J.J. Eron, Y. Yazdanpanah, D. Podzamczer, T. Lutz, J.B. Angel, G.J. Richmond, B. Clotet, F. Gutierrez, L. Sloan, M.S. Clair, M. Murray, S.L. Ford, J. Mrus, P. Patel, H. Crauwels, S.K. Griffith, K.C. Sutton, D. Dorey, K.Y. Smith, P.E. Williams, W.R. Spreen, Long-acting intramuscular cabotegravir and rilpivirine in adults with HIV-1 infection (LATTE-2): 96-week results of a

randomised, open-label, phase 2b, non-inferiority trial, The Lancet 390 (2017) 1499–1510. https://doi.org/https://doi.org/10.1016/S0140-6736(17)31917-7.

[142] M. Markowitz, I. Frank, R.M. Grant, K.H. Mayer, R. Elion, D. Goldstein, C. Fisher, M.E. Sobieszczyk, J.E. Gallant, H. Van Tieu, W. Weinberg, D.A. Margolis, K.J. Hudson, B.S. Stancil, S.L. Ford, P. Patel, E. Gould, A.R. Rinehart, K.Y. Smith, W.R. Spreen, Safety and tolerability of long-acting cabotegravir injections in HIV-uninfected men (ECLAIR): a multicentre, double-blind, randomised, placebo-controlled, phase 2a trial, Lancet HIV 4 (2017) e331–e340. https://doi.org/https://doi.org/10.1016/S2352-3018(17)30068-1.

[143] H.E. Gendelman, J. McMillan, A. Bade, B. Edagwa, B. Kevadiya, The Promise of Long Acting Antiretroviral Therapies: From Need to Manufacture, Trends Microbiol 27 (2019) 593–606.

[144] J.R. Hilaire, A.N. Bade, B. Sillman, N. Gautam, J. Herskovitz, B.L. Dyavar Shetty, M.S. Wojtkiewicz, A. Szlachetka, B.G. Lamberty, S. Sravanam, H.S. Fox, Y. Alnouti, P.K. Dash, J.M. McMillan, B.J. Edagwa, H.E. Gendelman, Creation of a long-acting rilpivirine prodrug nanoformulation, Journal of Controlled Release 311–312 (2019) 201–211. https://doi.org/https://doi.org/10.1016/j.jconrel.2019.09.001.

[145] A.S. Nowacek, R.L. Miller, J. McMillan, G. Kanmogne, M. Kanmogne, R.L. Mosley, Z. Ma, S. Graham, M. Chaubal, J. Werling, B. Rabinow, H. Dou, H.E. Gendelman, NanoART synthesis, characterization, uptake, release and toxicology for human monocyte-macrophage drug delivery, Nanomedicine (Lond). 4 (2009) 903–917.

[146] D.P. Gnanadhas, P.K. Dash, B. Sillman, A.N. Bade, Z. Lin, D.L. Palandri, N. Guatam, Y. Alnouti, H.A. Gelbard, J. McMillan, R.L. Mosley, B. Edagwa, H.E. Gendelman, S. Gorantla, Autophagy facilitates macrophage depots of sustained-release nanoformulated antiretroviral drugs, J Clin Invest 127 (2017) 857–873.

[147] P. Puligujja, J. McMillan, L. Kendrick, T. Li, S. Balkundi, N. Smith, R.S. Veerubhotla, B.J. Edagwa, A. V Kabanov, T. Bronich, H.E. Gendelman, X.-M. Liu, Macrophage folate receptor-targeted antiretroviral therapy facilitates drug entry, retention, antiretroviral activities and biodistribution for reduction of human immunodeficiency virus infections, Nanomedicine 9 (2013) 1263–1273. https://doi.org/https://doi.org/10.1016/j.nano.2013.05.003.

[148] Y. Zhong, B.J. Zeberl, X. Wang, J. Luo, Combinatorial approaches in post-polymerization modification for rational development of therapeutic delivery systems, Acta Biomater 73 (2018) 21–37. https://doi.org/https://doi.org/10.1016/j.actbio.2018.04.010.

[149] S. Dragojevic, J.S. Ryu, D. Raucher, Polymer-Based Prodrugs: Improving Tumor Targeting and the Solubility of Small Molecule Drugs in Cancer Therapy, Molecules 20 (2015) 21750–21769.

[150] J. Nicolas, Drug-Initiated Synthesis of Polymer Prodrugs: Combining Simplicity and Efficacy in Drug Delivery, Chemistry of Materials 28 (2016) 1591–1606. https://doi.org/10.1021/acs.chemmater.5b04281.

[151] A.A.A. Smith, M.B.L. Kryger, B.M. Wohl, P. Ruiz-Sanchis, K. Zuwala, M. Tolstrup, A.N. Zelikin, Macromolecular (pro)drugs in antiviral research, Polym Chem 5 (2014) 6407–6425. https://doi.org/10.1039/C4PY00624K.

[152] K. Yang, Z. Yang, G. Yu, Z. Nie, R. Wang, X. Chen, Polyprodrug Nanomedicines: An Emerging Paradigm for Cancer Therapy, Advanced Materials 34 (2022) 2107434. https://doi.org/https://doi.org/10.1002/adma.202107434.

[153] F. Greco, M.J. Vicent, Combination therapy: Opportunities and challenges for polymer–drug conjugates as anticancer nanomedicines, Adv Drug Deliv Rev 61 (2009) 1203–1213. https://doi.org/https://doi.org/10.1016/j.addr.2009.05.006.

[154] J.K. Stille, Step-growth polymerization, J Chem Educ 58 (1981) 862. https://doi.org/10.1021/ed058p862.

[155] A. Shakil, F.Y. Hern, C. Liu, K. Temburnikar, P. Chambon, N. Liptrott, T.O. McDonald, M. Neary, A. Owen, C. Freel Meyers, S.P. Rannard, Linear and branched polymer prodrugs of the water-soluble nucleoside reverse-transcriptase inhibitor emtricitabine as structural materials for long-acting implants, J Mater Chem B 10 (2022) 4395–4404. https://doi.org/10.1039/D2TB00825D.

[156] U. Hasegawa, A.J. van der Vlies, C. Wandrey, J.A. Hubbell, Preparation of Well-Defined Ibuprofen Prodrug Micelles by RAFT Polymerization, Biomacromolecules 14 (2013) 3314–3320. https://doi.org/10.1021/bm4009149.

[157] F. Joubert, L. Martin, S. Perrier, G. Pasparakis, Development of a Gemcitabine-Polymer Conjugate with Prolonged Cytotoxicity against a Pancreatic Cancer Cell Line, ACS Macro Lett 6 (2017) 535–540. https://doi.org/10.1021/acsmacrolett.7b00160.

[158] B.D. Fairbanks, P.A. Gunatillake, L. Meagher, Biomedical applications of polymers derived by reversible addition – fragmentation chain-transfer (RAFT), Adv Drug Deliv Rev 91 (2015) 141–152. https://doi.org/https://doi.org/10.1016/j.addr.2015.05.016.

[159] M. Rogošić, H.J. Mencer, Z. Gomzi, Polydispersity index and molecular weight distributions of polymers, Eur Polym J 32 (1996) 1337–1344. https://doi.org/10.1016/S0014-3057(96)00091-2.

[160] B.D. Fairbanks, P.A. Gunatillake, L. Meagher, Biomedical applications of polymers derived by reversible addition – fragmentation chain-transfer (RAFT), Adv Drug Deliv Rev 91 (2015) 141–152. https://doi.org/https://doi.org/10.1016/j.addr.2015.05.016.

[161] D. Das, S. Srinivasan, A.M. Kelly, D.Y. Chiu, B.K. Daugherty, D.M. Ratner, P.S. Stayton, A.J. Convertine, RAFT polymerization of ciprofloxacin prodrug monomers for the

controlled intracellular delivery of antibiotics, Polym Chem 7 (2016) 826–837. https://doi.org/10.1039/C5PY01704A.

[162] F.-Y. Su, S. Srinivasan, B. Lee, J. Chen, A.J. Convertine, T.E. West, D.M. Ratner, S.J. Skerrett, P.S. Stayton, Macrophage-targeted drugamers with enzyme-cleavable linkers deliver high intracellular drug dosing and sustained drug pharmacokinetics against alveolar pulmonary infections, Journal of Controlled Release 287 (2018) 1–11. https://doi.org/https://doi.org/10.1016/j.jconrel.2018.08.014.

[163] T.E.J. Chavas, F.-Y. Su, S. Srinivasan, D. Roy, B. Lee, L. Lovelace-Macon, G.F. Rerolle, E. Limqueco, S.J. Skerrett, D.M. Ratner, T.E. West, P.S. Stayton, A macrophage-targeted platform for extending drug dosing with polymer prodrugs for pulmonary infection prophylaxis, Journal of Controlled Release 330 (2021) 284–292. https://doi.org/https://doi.org/10.1016/j.jconrel.2020.11.031.

[164] A. Dart, D. Roy, V. Vlaskin, E. Limqueco, N.M. Lowe, S. Srinivasan, D.M. Ratner, M. Bhave, P. Stayton, P. Kingshott, A nanofiber based antiviral (TAF) prodrug delivery system, Biomaterials Advances 133 (2022) 112626. https://doi.org/https://doi.org/10.1016/j.msec.2021.112626.

[165] J.B. Nachega, K.K. Scarsi, M. Gandhi, R.K. Scott, L.M. Mofenson, M. Archary, S. Nachman, E. Decloedt, E.H. Geng, L. Wilson, A. Rawat, J.W. Mellors, Long-acting antiretrovirals and HIV treatment adherence, Lancet HIV 10 (2023) e332–e342. https://doi.org/https://doi.org/10.1016/S2352-3018(23)00051-6.

[166] J. Radzio-Basu, O. Council, M. Cong, S. Ruone, A. Newton, X. Wei, J. Mitchell, S. Ellis, C.J. Petropoulos, W. Huang, W. Spreen, W. Heneine, J.G. García-Lerma, Drug resistance emergence in macaques administered cabotegravir long-acting for pre-exposure prophylaxis during acute SHIV infection, Nat Commun 10 (2019) 2005. https://doi.org/10.1038/s41467-019-10047-w.

[167] D. Das, J. Chen, S. Srinivasan, A.M. Kelly, B. Lee, H.-N. Son, F. Radella, T.E. West, D.M. Ratner, A.J. Convertine, S.J. Skerrett, P.S. Stayton, Synthetic Macromolecular Antibiotic Platform for Inhalable Therapy against Aerosolized Intracellular Alveolar Infections, Mol Pharm 14 (2017) 1988–1997. https://doi.org/10.1021/acs.molpharmaceut.7b00093.

[168] F.-Y. Su, S. Srinivasan, B. Lee, J. Chen, A.J. Convertine, T.E. West, D.M. Ratner, S.J. Skerrett, P.S. Stayton, Macrophage-targeted drugamers with enzyme-cleavable linkers deliver high intracellular drug dosing and sustained drug pharmacokinetics against alveolar pulmonary infections, Journal of Controlled Release 287 (2018) 1–11. https://doi.org/10.1016/J.JCONREL.2018.08.014.

[169] J.-F. Mouscadet, L. Tchertanov, Raltegravir: molecular basis of its mechanism of action, Eur J Med Res 14 (2009) 5–16.

[170] P. Rivas, J. Morello, C. Garrido, S. Rodríguez-Nóvoa, V. Soriano, Role of atazanavir in the treatment of HIV infection, Ther Clin Risk Manag 5 (2009) 99–116. https://doi.org/10.2147/tcrm.s12187324.

[171] L. Martín-Carbonero, V. Soriano, Long-Term Use of Atazanavir in the Treament of HIV-Infected patients, Clin Med Insights Ther 4 (2012) CMT.S5764. https://doi.org/10.4137/CMT.S5764.

[172] H.N. Son, S. Srinivasan, J.Y. Yhee, D. Das, B.K. Daugherty, G.Y. Berguig, V.G. Oehle, S.H. Kim, K. Kim, I.C. Kwon, P.S. Stayton, A.J. Convertine, Chemotherapeutic copolymers prepared via the RAFT polymerization of prodrug monomers, Polym Chem 7 (2016) 4494–4505. https://doi.org/10.1039/C6PY00756B.

[173] J.K. Twibanire, T.B. Grindley, Efficient and Controllably Selective Preparation of Esters Using Uronium-Based Coupling Agents, Org Lett 13 (2011) 2988–2991. https://doi.org/10.1021/ol201005s.

[174] S.C. Story, J. V Aldrich, Side-product formation during cyclization with HBTU on a solid support, Int J Pept Protein Res 43 (1994) 292–296.

[175] S.-Y. Han, Y.-A. Kim, Recent development of peptide coupling reagents in organic synthesis, Tetrahedron 60 (2004) 2447–2467. https://doi.org/https://doi.org/10.1016/j.tet.2004.01.020.

[176] R.B. Grubbs, R.H. Grubbs, 50th Anniversary Perspective: Living Polymerization—Emphasizing the Molecule in Macromolecules, Macromolecules 50 (2017) 6979–6997. https://doi.org/10.1021/acs.macromol.7b01440.

[177] C.L. Moad, G. Moad, Fundamentals of reversible addition–fragmentation chain transfer (RAFT), 3 (2021) 3–17. https://doi.org/doi:10.1515/cti-2020-0026.

[178] S. Broekmans, F. Dobbels, K. Milisen, B. Morlion, S. Vanderschueren, Medication adherence in patients with chronic non-malignant pain: Is there a problem?, European Journal of Pain 13 (2009) 115–123. https://doi.org/https://doi.org/10.1016/j.ejpain.2008.02.010.

[179] S.J. Benkovic, A.J. Kirby, R.J.E. Talbot, Comprehensive Chemical Kinetics Volume 10 Ester Formation and Hydrolysis and Related Reactions, Elsevier Publishing Company, Amsterdam-Longdon-New York, 1972.

[180] V-70, FUJIFILM Wako Chemicals (n.d.). https://specchem-wako.fujifilm.com/us/oil-soluble-azo-initiators/V-70.htm (accessed May 12, 2024).

[181] N.I. Paton, W. Stöhr, A. Arenas-Pinto, M. Fisher, I. Williams, M. Johnson, C. Orkin, F. Chen, V. Lee, A. Winston, M. Gompels, J. Fox, K. Scott, D.T. Dunn, Protease inhibitor monotherapy for long-term management of HIV infection: a randomised, controlled, open-label, non-inferiority trial, Lancet HIV 2 (2015) e417–e426. https://doi.org/10.1016/S2352-3018(15)00176-9.

[182] Atazanavir, Drugbank (2023). https://go.drugbank.com/drugs/DB01072.

[183] C.A.G.N. Montalbetti, V. Falque, Amide bond formation and peptide coupling, Tetrahedron 61 (2005) 10827–10852. https://doi.org/https://doi.org/10.1016/j.tet.2005.08.031.

[184] S. Li, M. Omi, F. Cartieri, D. Konkolewicz, G. Mao, H. Gao, S.E. Averick, Y. Mishina, K. Matyjaszewski, Cationic Hyperbranched Polymers with Biocompatible Shells for siRNA Delivery, Biomacromolecules 19 (2018) 3754–3765. https://doi.org/10.1021/acs.biomac.8b00902.

[185] Y. Zhou, P. Wu, J. Wu, J.C. Doverspike, Q. Zhang, J. Shao, C. Xi, Y. Liu, M.E. Meyerhoff, Delivering nitric oxide with poly(n-butyl methacrylate) films doped with S-nitroso-N-acetylpenicillamine, Polymer (Guildf) 228 (2021) 123943. https://doi.org/https://doi.org/10.1016/j.polymer.2021.123943.

[186] T. Pilgrim, S. Windecker, Drug-eluting stent technology: progress beyond the polymer, Eur Heart J 35 (2014) 1991–1995. https://doi.org/10.1093/eurheartj/ehu224.

[187] J.C. Townsend, P. Rideout, D.H. Steinberg, Everolimus-eluting stents in interventional cardiology, Vasc Health Risk Manag 8 (2012) 393–405. https://doi.org/10.2147/VHRM.S23388.

[188] Z. Ge, S. Liu, Functional block copolymer assemblies responsive to tumor and intracellular microenvironments for site-specific drug delivery and enhanced imaging performance, Chem. Soc. Rev 42 (2013) 7289–7325.

[189] Q. Zhang, N.R. Ko, J.K. Oh, Recent advances in stimuli-responsive degradable block copolymer micelles: synthesis and controlled drug delivery applications, Chem. Commun. 48 (2012) 7542–7552.

[190] J.K. Kim, S.Y. Yang, Y. Lee, Y. Kim, Functional nanomaterials based on block copolymer self-assembly, Prog Polym Sci 35 (2010) 1325–1349. https://doi.org/https://doi.org/10.1016/j.progpolymsci.2010.06.002.

[191] L. Fical, M. Khalikova, H.K. Vlčková, I. Lhotská, Z. Hadysová, I. Vokřál, L. Červený, F. Švec, L. Nováková, Determination of Antiviral Drugs and Their Metabolites Using Micro-Solid Phase Extraction and UHPLC-MS/MS in Reversed-Phase and Hydrophilic Interaction Chromatography Modes, Molecules 26 (2021) 2123.

[192] R.R.S. Thakur, H.L. McMillan, D.S. Jones, Solvent induced phase inversion-based in situ forming controlled release drug delivery implants, Journal of Controlled Release 176 (2014) 8–23. https://doi.org/https://doi.org/10.1016/j.jconrel.2013.12.020.

[193] E. V. Capela, J.H.P.M. Santos, I. Boal-Palheiros, J.A.P. Coutinho, S.P.M. Ventura, M.G. Freire, A simple approach for the determination and characterization of ternary phase diagrams of aqueous two-phase systems composed of water, polyethylene glycol and sodium carbonate, Chem Eng Educ 53 (2019) 112–120.

[194] L. Keshavarz, M.A. Khansary, S. Shirazian, Phase diagram of ternary polymeric solutions containing nonsolvent/solvent/polymer: Theoretical calculation and experimental validation, Polymer (Guildf) 73 (2015) 1–8. https://doi.org/https://doi.org/10.1016/j.polymer.2015.07.027.

[195] H. Choi, H. Liang, Wettability and spontaneous penetration of a water drop into hydrophobic pores, J Colloid Interface Sci 477 (2016) 176–180. https://doi.org/https://doi.org/10.1016/j.jcis.2016.05.029.

[196] C.I. Nkanga, A. Fisch, M. Rad-Malekshahi, M.D. Romic, B. Kittel, T. Ullrich, J. Wang, R.W.M. Krause, S. Adler, T. Lammers, W.E. Hennink, F. Ramazani, Clinically established biodegradable long acting injectables: An industry perspective, Adv Drug Deliv Rev 167 (2020) 19–46. https://doi.org/https://doi.org/10.1016/j.addr.2020.11.008.

[197] X. Wang, D.J. Burgess, Drug release from in situ forming implants and advances in release testing, Adv Drug Deliv Rev 178 (2021) 113912. https://doi.org/https://doi.org/10.1016/j.addr.2021.113912.

[198] M. Lizambard, T. Menu, M. Fossart, C. Bassand, K. Agossa, O. Huck, C. Neut, F. Siepmann, In-situ forming implants for the treatment of periodontal diseases: Simultaneous controlled release of an antiseptic and an anti-inflammatory drug, Int J Pharm 572 (2019) 118833. https://doi.org/https://doi.org/10.1016/j.ijpharm.2019.118833.

[199] S. Juvekar, H. Kathpalia, Solvent removal precipitation based in situ forming implant for controlled drug delivery in periodontitis, Journal of Controlled Release 251 (2017) 75–81. https://doi.org/https://doi.org/10.1016/j.jconrel.2017.02.022.

[200] W.J. Lorman, Sublocade: The Once-Monthly Buprenorphine Injectable, J Addict Nurs 29 (2018) 139 PM-29864061–140. https://doi.org/10.1097/JAN.0000000000000223.

[201] Y. Chen, L. Jiang, R. Wang, M. Lu, Q. Zhang, Y. Zhou, Z. Wang, G. Lu, P. Liang, H. Ran, H. Chen, Y. Zheng, Injectable smart phase-transformation implants for highly efficient in vivo magnetic-hyperthermia regression of tumors, Adv Mater 26 (2014) 7468–7473. https://doi.org/10.1002/adma.201402509.

[202] A. Krogmann, L. Peters, L. von Hardenberg, K. Bödeker, V.B. Nöhles, C.U. Correll, Keeping up with the therapeutic advances in schizophrenia: a review of novel and emerging pharmacological entities, CNS Spectr 24 (2019) 38–69. https://doi.org/DOI: 10.1017/S109285291900124X.

[203] S.R. Benhabbour, M. Kovarova, C. Jones, D.J. Copeland, R. Shrivastava, M.D. Swanson, C. Sykes, P.T. Ho, M.L. Cottrell, A. Sridharan, S.M. Fix, O. Thayer, J.M. Long, D.J. Hazuda, P.A. Dayton, R.J. Mumper, A.D.M. Kashuba, J. Victor Garcia, Ultra-long-acting tunable biodegradable and removable controlled release implants for drug delivery, Nat Commun 10 (2019) 4324. https://doi.org/10.1038/s41467-019-12141-5.

[204] A. Ruggiero, C.H. Villa, E. Bander, D.A. Rey, M. Bergkvist, C.A. Batt, K. Manova-Todorova, W.M. Deen, D.A. Scheinberg, M.R. McDevitt, Paradoxical glomerular filtration

of carbon nanotubes, Proc Natl Acad Sci U S A 107 (2010) 12369–12374. https://doi.org/10.1073/pnas.0913667107.

[205] W. Denney, S. Duvvuri, C. Buckeridge, Simple, Automatic Noncompartmental Analysis: The PKNCA R Package, J Pharmacokinet Pharmacodyn 42 (2015) 11–107, S65.

[206] P.D. Graham, K.J. Brodbeck, A.J. McHugh, Phase inversion dynamics of PLGA solutions related to drug delivery, Journal of Controlled Release 58 (1999) 233–245. https://doi.org/https://doi.org/10.1016/S0168-3659(98)00158-8.

[207] C.U. Correll, E. Kim, J.K. Sliwa, W. Hamm, S. Gopal, M. Mathews, R. Venkatasubramanian, S.R. Saklad, Pharmacokinetic Characteristics of Long-Acting Injectable Antipsychotics for Schizophrenia: An Overview, CNS Drugs 35 (2021) 39–59.

[208] A.K. Hołda, I.F.J. Vankelecom, Understanding and guiding the phase inversion process for synthesis of solvent resistant nanofiltration membranes, J Appl Polym Sci 132 (2015). https://doi.org/https://doi.org/10.1002/app.42130.

[209] R.Y. Lochhead, Chapter 3 - Basic Physical Sciences for the Formulation of Cosmetic Products, in: K. Sakamoto, R.Y. Lochhead, H.I. Maibach, Y.B.T.-C.S. and T. Yamashita (Eds.), Elsevier, Amsterdam, 2017: pp. 39–76. https://doi.org/https://doi.org/10.1016/B978-0-12-802005-0.00003-3.

[210] S. Kempe, K. Mäder, In situ forming implants — an attractive formulation principle for parenteral depot formulations, Journal of Controlled Release 161 (2012) 668–679. https://doi.org/https://doi.org/10.1016/j.jconrel.2012.04.016.

[211] A.K. Pandya, L.K. Vora, C. Umeyor, D. Surve, A. Patel, S. Biswas, K. Patel, V.B. Patravale, Polymeric in situ forming depots for long-acting drug delivery systems, Adv Drug Deliv Rev 200 (2023) 115003. https://doi.org/https://doi.org/10.1016/j.addr.2023.115003.

[212] K. Gausi, H. Mugerwa, M. Siccardi, M.C. Montanha, M. Lamorde, L. Wiesner, A. D'Avolio, H. McIlleron, E. Wilkins, A. De Nicolò, G. Maartens, S. Khoo, C. Kityo, P. Denti, C. Waitt, Pharmacokinetics and Safety of Twice-daily Ritonavir-boosted Atazanavir With Rifampicin, Clinical Infectious Diseases 78 (2023) 1246–1255.

[213] L.W. Dittert, T. Higuchi, Rates of Hydrolysis of Carbamate and Carbonate Esters in Alkaline Solution, J Pharm Sci 52 (1963) 852–857. https://doi.org/https://doi.org/10.1002/jps.2600520908.

[214] G.D. Cooper, B. Williams, Hydrolysis of Simple Aromatic Esters and Carbonates, J Org Chem 27 (1962) 3717–3720. https://doi.org/10.1021/jo01057a529.

[215] D.B. Morton, P.H.M. Griffiths, Guidelines on the recognition of pain, distress and discomfort in experimental animals and an hypothesis for assessment, Veterinary Record 116 (1985) 431–436.

[216] J.M. Anderson, A. Rodriguez, D.T. Chang, FOREIGN BODY REACTION TO BIOMATERIALS, Semin Immunol 20 (2008) 86–100.

[217] M. Kastellorizios, N. Tipnis, D.J. Burgess, Foreign Body Reaction to Subcutaneous Implants BT - Immune Responses to Biosurfaces, in: J.D. Lambris, K.N. Ekdahl, D. Ricklin, B. Nilsson (Eds.), Springer International Publishing, Cham, 2015: pp. 93–108.

[218] E. Senel, Nicolau syndrome as an avoidable complication, J Family Community Med 19 (2012) 52–53.

[219] A.M. Walji, R.I. Sanchez, S.-D. Clas, R. Nofsinger, M. de Lera Ruiz, J. Li, A. Bennet, C. John, D.J. Bennett, J.M. Sanders, C.N. Di Marco, S.H. Kim, J. Balsells, S.S. Ceglia, Q. Dang, K. Manser, B. Nissley, J.S. Wai, M. Hafey, J. Wang, G. Chessen, A. Templeton, J. Higgins, R. Smith, Y. Wu, J. Grobler, P.J. Coleman, Discovery of MK-8970: An Acetal Carbonate Prodrug of Raltegravir with Enhanced Colonic Absorption, ChemMedChem 10 (2015) 245–252. https://doi.org/https://doi.org/10.1002/cmdc.201402393.

[220] A. Eckelt, J. Eckelt, B. Wolf, Solubility of Polymers, in: Encyclopedia of Polymer Science and Technology, 2011. https://doi.org/https://doi.org/10.1002/0471440264.pst345.

[221] Y. Jiang, X. Gao, O.N. Singh, W. Zhang, V. Agrahari, M.M. Peet, M.R. Clark, G.F. Doncel, A.K. Banga, Pharmacokinetics of a weekly transdermal delivery system of tenofovir alafenamide in hairless rats, Int J Pharm 582 (2020) 119342. https://doi.org/https://doi.org/10.1016/j.ijpharm.2020.119342.

[222] FDA-Approved HIV Medicines, NIH (2023). https://hivinfo.nih.gov/understanding-hiv/fact-sheets/fda-approved-hiv-medicines.

[223] M. Kovarova, M.D. Swanson, R.I. Sanchez, C.E. Baker, J. Steve, R.A. Spagnuolo, B.J. Howell, D.J. Hazuda, J.V. Garcia, A long-acting formulation of the integrase inhibitor raltegravir pro(1) Kovarova, M.; Swanson, M. D.; Sanchez, R. I.; Baker, C. E.; Steve, J.; Spagnuolo, R. A.; Howell, B. J.; Hazuda, D. J.; Garcia, J. V. A Long-Acting Formulation of the Integrase Inhibit, J Antimicrob Chemother 71 (2016) 1586–1596. https://doi.org/10.1093/jac/dkw042.

[224] D.M. Moss, M. Siccardi, M. Murphy, M.M. Piperakis, S.H. Khoo, D.J. Back, A. Owen, Divalent metals and pH alter raltegravir disposition in vitro, Antimicrob Agents Chemother 56 (2012) 3020–3026. https://doi.org/10.1128/aac.06407-11.

[225] K.K. Pandey, Raltegravir in HIV-1 infection: Safety and Efficacy in Treatment-naïve Patients, Clin Med Rev Ther 4 (2011) 13–30.

[226] M.L. Rizk, H. Robert, C.G. Hoyee, H. Mike, R.E. G., C. Xiaoyan, Raltegravir Has a Low Propensity To Cause Clinical Drug Interactions through Inhibition of Major Drug Transporters: an In Vitro Evaluation, Antimicrob Agents Chemother 58 (2014) 1294–1301. https://doi.org/10.1128/aac.02049-13.

[227] T.K. Patra, Data-Driven Methods for Accelerating Polymer Design, ACS Polymers Au 2 (2022) 8–26. https://doi.org/10.1021/acspolymersau.1c00035.

[228] Q. Zhang, M.A. Fassihi, R. Fassihi, Delivery Considerations of Highly Viscous Polymeric Fluids Mimicking Concentrated Biopharmaceuticals: Assessment of Injectability via Measurement of Total Work Done "WT," AAPS PharmSciTech 19 (2018) 1520–1528. https://doi.org/10.1208/s12249-018-0963-x.

[229] The switch to every-2-month CABENUVA...It starts with you, ViiV Healthcare (2024).

[230] C.P. Neff, T. Ndolo, A. Tandon, Y. Habu, R. Akkina, Oral Pre-Exposure Prophylaxis by Anti-Retrovirals Raltegravir and Maraviroc Protects against HIV-1 Vaginal Transmission in a Humanized Mouse Model, PLoS One 5 (2010) e15257.

[231] M. Veselinovic, K.-H. Yang, C. Sykes, L. Remling-Mulder, A.D.M. Kashuba, R. Akkina, Mucosal tissue pharmacokinetics of the integrase inhibitor raltegravir in a humanized mouse model: Implications for HIV pre-exposure prophylaxis, Virology 489 (2016) 173–178. https://doi.org/https://doi.org/10.1016/j.virol.2015.12.014.

[232] M.E. Clement, R. Kofron, R.J. Landovitz, Long-acting Injectable Cabotegravir for the Prevention of HIV Infection, Curr Opin HIV AIDS 15 (2020) 19–26.

[233] A.B. Nair, S. Jacob, A simple practice guide for dose conversion between animals and human, J Basic Clin Pharm 7 (2016) 27–31. https://doi.org/10.4103/0976-0105.177703.